ISSN 1854-6250

APEM journal

Advances in Production Engineering & Management

Volume 14 | Number 1 | March 2019

University of Maribor

Published by CPE
apem-journal.org

Advances in Production Engineering & Management

Identification Statement

APEM journal

ISSN 1854-6250 | Abbreviated key title: **Adv produc engineer manag** | Start year: 2006
ISSN 1855-6531 (on-line)

Published quarterly by **Chair of Production Engineering (CPE)**, **University of Maribor**
Smetanova ulica 17, SI – 2000 Maribor, Slovenia, European Union (EU)

Phone: 00386 2 2207522, Fax: 00386 2 2207990
Language of text: English

University of Maribor

APEM homepage: apem-journal.org
University homepage: www.um.si

APEM Editorial

Subscription Rate: 120 EUR for 4 issues (worldwide postage included); 30 EUR for single copies (plus 10 EUR for postage); for details about payment please contact: info@apem-journal.org
Cover and interior design: Miran Brezocnik
Printed: Tiskarna Koštomaj, Celje, Slovenia
Subsidizer: The journal is subsidized by Slovenian Research Agency

Advances in Production Engineering & Management is indexed and abstracted in the **WEB OF SCIENCE** (maintained by **Clarivate Analytics**): **Science Citation Index Expanded**, **Journal Citation Reports** – Science Edition, **Current Contents** – Engineering, Computing and Technology • **Scopus** (maintained by **Elsevier**) • **Inspec** • **EBSCO**: Academic Search Alumni Edition, Academic Search Complete, Academic Search Elite, Academic Search Premier, Engineering Source, Sales & Marketing Source, TOC Premier • **ProQuest**: CSA Engineering Research Database – Cambridge Scientific Abstracts, Materials Business File, Materials Research Database, Mechanical & Transportation Engineering Abstracts, ProQuest SciTech Collection • **TEMA** (**DOMA**) • The journal is listed in **Ulrich's** Periodicals Directory and **Cabell's** Directory

University of Maribor
Chair of Production Engineering (CPE)

Advances in Production Engineering & Management

Volume 14 | Number 1 | March 2019 | pp 1–138

Contents

Journal homepage: apem-journal.org

ISSN 1854-6250 (print)
ISSN 1855-6531 (on-line)

Scope and topics

Advances in Production Engineering & Management (*APEM journal*) is an interdisciplinary refereed international academic journal published quarterly by the *Chair of Production Engineering* at the *University of Maribor*. The main goal of the *APEM journal* is to present original, high quality, theoretical and application-oriented research developments in all areas of production engineering and production management to a broad audience of academics and practitioners. In order to bridge the gap between theory and practice, applications based on advanced theory and case studies are particularly welcome. For theoretical papers, their originality and research contributions are the main factors in the evaluation process. General approaches, formalisms, algorithms or techniques should be illustrated with significant applications that demonstrate their applicability to real-world problems. Although the *APEM journal* main goal is to publish original research papers, review articles and professional papers are occasionally published.

Fields of interest include, but are not limited to:

Additive Manufacturing Processes
Advanced Production Technologies
Artificial Intelligence in Production
Assembly Systems
Automation
Big Data in Production
Computer-Integrated Manufacturing
Cutting and Forming Processes
Decision Support Systems
Deep Learning in Manufacturing
Discrete Systems and Methodology
e-Manufacturing
Evolutionary Computation in Production
Fuzzy Systems
Human Factor Engineering, Ergonomics
Industrial Engineering
Industrial Processes
Industrial Robotics
Intelligent Manufacturing Systems
Joining Processes
Knowledge Management
Logistics in Production
Machine Learning in Production
Machine Tools
Machining Systems
Manufacturing Systems
Materials Science, Multidisciplinary
Mechanical Engineering
Mechatronics
Metrology in Production
Modelling and Simulation
Numerical Techniques
Operations Research
Operations Planning, Scheduling and Control
Optimisation Techniques
Project Management
Quality Management
Risk and Uncertainty
Self-Organizing Systems
Statistical Methods
Supply Chain Management
Virtual Reality in Production

APEM journal
Advances in Production Engineering & Management
Volume 14 | Number 1 | March 2019 | pp 5–14
https://doi.org/10.14743/apem2019.1.307
ISSN 1854-6250
Journal home: apem-journal.org
Original scientific paper

An integrated optimization of quality control chart parameters and preventive maintenance using Markov chain

Farahani, A.[a], **Tohidi, H.**[b,*], **Shoja, A.**[c]

[a]Department of Industrial Engineering, Roudehen Branch, Islamic Azad University, Roudehen, Iran
[b]Department of Industrial Engineering, South Tehran Branch, Islamic Azad University, Tehran, Iran
[c]Department of Mathematics and Statistic, Roudehen Branch, Islamic Azad University, Roudehen, Iran

ABSTRACT

Manufacturing costs are reduced significantly with the integrated optimization of preventive maintenance and quality control. In this paper, a new mixed integer non-linear programming model is presented. This model determines the optimal preventive maintenance interval and the optimal parameters of the ($\bar{X}$) control chart, including the sampling interval and the sample size and the control limit. The production system is considered in the form of a continuous time Markov chain. Formulation of the production process of a machine in the form of a continuous time Markov chain is a breakthrough in the integrated modeling of repair and quality. The goal is to reduce costs per unit time. It is assumed that preventive maintenance can be carried out at several levels either perfect or imperfect. The duration of corrective and preventive maintenance is not negligible. Considering the length of time for maintenance, this model is closer to the real production environment. A numerical example is used to illustrate this new model. Sensitivity analysis was performed to determine the effect of the model parameters on optimal decisions. This analysis further shows the relationship between preventive maintenance and statistical quality control as well as the performance of the new model.

ARTICLE INFO

Keywords:
Maintenance;
Optimization;
Chart control;
Non-linear model;
Markov chain

**Corresponding author:*
H_tohidi@azad.ac.ir
(Tohidi, H.)

Article history:
Received 10 December 2017
Revised 22 November 2018
Accepted 3 December 2018

1. Introduction

The performance of a production system essentially depends on the performance of the floor of the workshop. The operating policies of the floor of the workshop include maintenance scheduling, quality control and production scheduling. These three aspects of operational planning are mutually reinforcing. Therefore, their integrated optimization considerably improves the performance of the system [1].

Production planning, quality and maintenance are the main elements of a production system. Many researchers believe that models that optimize each of these elements independently do not provide an optimal global solution for the whole production system. Accordingly, the literature has grown in the field of integrated models [2].

Pandey *et al*. [3] review articles that optimize quality and maintenances simultaneously. Hadidi *et al*. [2] referred to the list of articles that optimize integrated the maintenances and quality control.

Pandey *et al*. [4] present an article on simultaneous optimization of maintenance planning, quality control and production planning. In this study, a model was first developed to integrate maintenance planning and decision-making related to quality control of the process. Then, with

attention to the preventive maintenance interval, the sequence of production batches with minimization of the production schedule delay was performed.

In another paper, Pandey *et al*. [5] present an integrated model for optimizing the preventive maintenance interval and control chart parameters using the Taguchi loss function.

Liu *et al*. [6] consider a $\bar{X}$ control chart for a two-unit production system that operates in series. This system is described using the continuous time Markov chain. In this paper, it is assumed that the system is controlled by a $\bar{X}$ control chart to avoid cost of failure and an optimization model has been developed to obtain optimal control chart parameters for minimizing maintenance costs. When the control chart gives an out-of-control signal, a complete inspection is performed if this inspection indicates the partial failure of each system unit, it should immediately be replaced as a part of preventive maintenance, and if the system stops, that is, a unit of the system is in a state of failure. In this paper, the length of maintenance is considered negligible. Xiang [7] provide an article on determining the optimal parameters of the $\overline{\mathrm{X}}$ control chart and preventive maintenance in the form of a discrete time Markov chain. In this model, the length of time for preventive and corrective maintenance is negligible.

Zhang *et al*. [8] integrated a $\overline{\mathrm{X}}$ control chart with a repair plan. This paper proposes a delayed maintenance policy. This policy takes a delay time to detect after an alarm from the control chart.

Yin *et al*. [9] provide an integrated model for statistical quality control and maintenance decisions based on a delay control policy. This mathematical model is solved to minimize the expected cost.

Tambe and Kulkarni [1] have provided an article to optimize the maintenance and quality program with the constraint on schedule, availability, and repair time and detection time for a single-machine production system and a Simulated Annealing algorithm and a Genetic algorithm are used to solve the model. Bouslah *et al*. [10] propose an integrated production, preventive maintenance, and quality control system for a production system, which is subject to deterioration in quality and reliability. The main objective of this study is to optimize the production, inventory level, parameters of the sampling plan and the overall repair level, minimizing the total cost imposed simultaneously. Tambe and Kulkarni [11] have presented an approach to integrate planning of repairs, quality control and production planning. The purpose of this study is to examine the benefits of the integration of these three issues with regard to the overall expected cost of the system. Lu *et al*. [12] presented an integrated model in which the process improvement with PM decisions in a single-machine production system was performed simultaneously.

Nourelfath *et al*. [13] optimize production, maintenance and quality policies for a complete process in a multi-period multi-product production system with limited production size. Shrivastava *et al*. [14] presented an integrated model for optimizing preventive maintenance and quality control policies with CUSUM chart. Zhong *et al*. [15] provide an integrated model for optimizing control chart parameters and maintenance times in the supply chain.

Ardakan *et al*. [16] presented a hybrid model for combining control charts and preventive maintenance (PM) systems to quickly diagnose out-of-control modes and this model reduces system control costs. In this paper a multivariate control chart (MEWMA) is used to control process changes. Khrueasom and Pongpullponsak [17] provide an integrated model for determining the parameters of the control charts of EWMA and Kolmogorov-Smirnov, with regard to repair management. Salmasnia *et al*. [18] provide an integrated model for determining the size of economic production, statistical process control, and repair, in a system, with a number of reasonable causes for failure and Particle Mass Optimization algorithms are used to minimize the total cost expected for each production cycle, according to the limitations of statistical quality. Zhong and Ma [19] provide an integrated model for statistical process control and maintenance. This paper optimizes Shewhart individual-residual ($Z_x - Z_e$) control chart and repair parameters for two-step dependent processes, with the goal of minimizing the total cost of repair, inspection and quality.

In an article, Beheshti Fakher *et al*. [20] propose integrated production planning, incomplete repairs and process inspection in a multi-machine system. Rasay *et al*. [21] presented an integrated model that coordinates the decisions on designing the chi-square chart and the planning

of maintenance, and an independent maintenance model is also presented for assessing the integrated model, and the performance of these two the model is compared with each other.

The purpose of this paper is to consider a mixed integer nonlinear programming model for simultaneous optimization of preventive maintenance and quality policies in a jobshop system in the form of a continuous time Markov chain. In this model, the process has an in control state and several out of control modes which are invisible. In out of control states, the percentage of manufactured parts is inconsistent. The failure mode is directly visible and detected immediately. Preventive maintenance is carried out at several levels, which can be perfect such that the process is turned into a state of in control or can be performed imperfect, in which case the process is converted with a probability to a state that is not worse before, but corrective maintenance is perfect and the process is then turned into a state of in control. Different modes of machine and sampling and various levels of preventive maintenance and corrective maintenance and false alarm are considered as nodes of a continuous time Markov chain.

It is assumed that the duration of stay in various machine modes and the various levels of preventive maintenance and corrective maintenance and inspection for false alarm is an exponential random variable. However, the duration of stay in different modes of the machine until entering sampling mode and the duration of stay in sampling mode is a hyper exponential random variable. This model determines the optimal preventive maintenance interval and $\overline{X}$ control chart parameters for each machine at the time of production of each product, so that the cost per unit time is minimized.

This paper is close to article [7]. In that paper, a discrete-time Markov chain is proposed for the integrated optimization of $\overline{X}$ control chart and preventive maintenance. In [7], the length of time for preventive and corrective maintenance is negligible and, as stated in the article itself, such a hypothesis is not feasible in practical situations. In the present study, the length of time for corrective and preventive maintenance is considered, so that the proposed model is closer to the reality of production systems. According to review articles by Pandey *et al*. [3] and Hadidi *et al*. [2], as well as reviewing the literature presented in this paper and the search, the following points can be cited as the innovation of this research. (1) All process modes including in control mode and out-of-control modes, and sampling mode and preventive maintenance at various levels, and corrective maintenance and inspection for false alarm, are considered as a continuous time Markov chain. (2) The duration of preventive and corrective repairs is not zero and the duration of their execution is exponential random variable.

The rest of the article is presented as follows. Section 2 describes the problem and provides an integrated planning model for preventive maintenance and $\overline{X}$ control chart. In section 3, a numerical example is solved and sensitivity analysis is performed. In the end, section 4 will present a summary of the paper and conclusions and future suggestions.

2. Description of proposed non-linear model

A jobshop system is considered. In this system, several machines work in series at the stations. In order for the production line machines to work together on balance, at some workstations several machines work in parallel to provide a specific production rate. The failure of each of the machines reduces a certain percentage of line production. A component of each machine is considered as one piece that must be preventive maintenance done on it. The length of time until the failure of each machine follows exponential distribution. Two failure modes are considered for each machine. The first one is that the machine breaks down, and the production of the same moment stops, and the machine cannot continue to work. The second is that machine failure can reduce the process quality of the machine, which is due to a change in the average of the process. Therefore, the cost of a breakdown of the first mode includes the cost of stopping the line, the cost of repair work and the fixed cost of repair and the cost of set up. The second failure mode affects the product in terms of quality and increases the production rate of the defective product until the failure has been discovered and the production is stopped, so the cost of defect product includes quality costs.

In this paper, it is assumed that the quality of each process can be assessed by measuring a qualitative key characteristic of the output of that process. It is also assumed that this qualitative characteristic is a random variable with a certain mean and standard deviation. When the process is in control, the average of this variable is within the control limit. This average can be out of limit due to machine failure or some other external causes such as environmental effects, operator error, use the wrong tool, etc. After this happens, the process is considered out of control. In this case, it is assumed that the inspection of the machine is carried out without stopping the process and the cause of the failure is determined. If the cause is due to machine failure, the machine will be stopped and repairs will be done.

From the above, it is obvious that machine failure and repair affects the quality of the process. Therefore, the optimization of preventive maintenance and the economic design of the control chart should be carried out simultaneously. The operation of each machine on each product is considered as a process. For each process, a controlled state (mode 1) and several (f $-$ 1) modes out of the control $i = 2, 3, .., f - 1$ are considered. Mode f is a failure mode. A $\bar{X}$ control chart is used to evaluate and control the process. The distribution of the qualitative feature of the process is supposed to follow the normal distribution. When the process is in control, the mean of the process is $\mu = \mu_0$ and the standard deviation of the process is $\sigma = \sigma_0$.

The occurrence of the assignable cause causes the change in the mean of the process, but the process variance does not change. In this case $\mu_i = \mu_0 + \delta_i \sigma$ and $2 \leq i \leq f$. The average of the process increases as the machine worsens so that $0 < \delta_1 < \delta_2 < \cdots < \delta_{f-1}$.

In this paper, preventive maintenance can be carried out at several levels; either perfect or imperfect is considered. The imperfect preventive maintenance is defined as the condition of the machine that is being repaired is not worse than the previous one, but the machine may not be turned into in control state, but the perfect preventive maintenance turns the machine into in control state (mode 1). Different modes of the machine (process) include in control mode and several out of control modes, failure mode and sampling mode, and different levels of preventive maintenance and corrective maintenance and false alarm. These modes are nodes of a continuous time Markov chain.

We now describe the integrated model of $\bar{X}$ control chart and preventive maintenance. First, we introduce sets, indices, parameters, and variables, and then objective function and a set of constraints are introduced.

Sets:

M	Set of machines
P	Set of products
I	Set of machine states
L	Set of preventive maintenance levels

Indicators:

m	Machine
p	Product
i	Machine mode
s	Sampling mode
l	Preventive maintenance level mode
f	Corrective maintenance, failure mode
ins	False alarm mode

Parameters:

ais_{imp}	The probability of transferring the mode of the machine (process) m during the production of the product p from the state i to the state s, so that the mod s is the sampling mode.
asi_{imp}	The probability of transferring the machine mode (process) m when producing the product p from the state s to the state i.

asl_{lmp} The probability of transferring the mode of the machine (process) m during the production of the product p from s to state l such that the state l is a level of preventive maintenance.

ali_{limp} The probability of transferring the mode of the machine (process) m during the production of the product p from state l to state i so that the state l is a level of preventive maintenance.

λij_{ijmp} Machine arrival rate (process) m when producing product p from i mode to j mode so that j mode is worse than i.

λli_{limp} Machine arrival rate (process) m during production of product p from preventive maintenance of level l to mode i.

λins_{mp} Machine arrival rate (process) m during production of Product p from inspection mode of false alarm to in control mode.

λf_{mp} Machine arrival rate (process) m during production of product p from failure mode to in control state.

θs_{mp} The length of time to check a sample taken from the product p machine (process) m.

δ_{mp} The magnitude of quality shift of the process mean of the machine (process) m during the production of the product p .

ci_{imp} The cost of each unit time when the machine (process) m is in the state of i during the production of the product p.

cl_{lmp} The cost of each unit time when the machine (process) m is at the level l of the preventive maintenance during production of the product p.

ccm_{mp} The cost of each unit time when the machine (process) m is in the corrective maintenance mode when producing the product p.

$cstop_{mp}$ The cost of each unit time of stopping the machine (process) m during the production of the product p, which is imposed on the production line during both the preventive maintenance and corrective maintenance, which is, in fact, the cost of losing output per unit of time.

cf_{mp} The fixed cost of each sampling of the machine (process) m during the production of the product p.

cv_{mp} The variable cost of each sampling unit of the machine (process) m during the production of the product p.

$cins_{mp}$ The cost of each unit of time for inspection of the machine (process) m during the production of the product p due to the false alarm.

Variables:

α_{mp} Type 1 error for machine (process) m when producing product p.

πi_{imp} The percentage of production time that the machine (process) m is in state i when produces the product p.

πl_{lmp} The percentage of production time that the machine (process) m during production of the product p is in the level of l preventive maintenance.

πf_{mp} The percentage of production time that the machine (process) m is in the corrective maintenance mode when producing the product p.

πins_{mp} The percentage of production time that machine (process) m is in the inspection mode for false alarm when production of product p.

πs_{mp} The percentage of production time that the machine (process) m is in sampling mode when production of product p.

λIS_{pm} The machine arrival rate (Process) m from operating modes i (machine modes) to sampling mode s when producing product p.

n_{mp} The number of samples taken from the machine (process) m during the production of the product p at each sampling time.

k_{mp} The amount of standard deviations allowed for the machine (process) m during the production of the product p at each sampling time.

β_{mp} The probability of the second type of machine error (process) m during the production of the product p at each sampling time.

h_{mp} The sampling interval of the machine (process) m at during the production of the product p.

τ_{mp} The preventive maintenance interval of the machine (process) m at the time of production of the product p.

The objective function is of cost type, therefore, should be minimized.

$$Min\ Z = \sum_{m=1}^{M}\sum_{p=1}^{P}\sum_{i=1}^{f-1} ci_{imp}\pi i_{imp} + \sum_{m=1}^{M}\sum_{p=1}^{P} cstop_{mp}\pi f_{mp} + \sum_{m=1}^{M}\sum_{p=1}^{P}\sum_{l=1}^{L} cstop_{mp}\pi l_{lmp} + \sum_{m=1}^{M}\sum_{p=1}^{P}\sum_{l=1}^{L} cl_{lmp}\pi l_{lmp} + \sum_{m=1}^{M}\sum_{p=1}^{P} ccm_{mp}\pi f_{mp} + \sum_{m=1}^{M}\sum_{p=1}^{P} cins_{mp}\pi ins_{mp} + \sum_{m=1}^{M}\sum_{p=1}^{P} cf_{mp}\pi s_{mp} + \sum_{m=1}^{M}\sum_{p=1}^{P} cv_{mp}n_{mp}\pi s_{mp} \quad (1)$$

Constraints:

Equations of equilibrium are written for each node (state). Eq. 2 is the equilibrium equation of the node in-control (node one).

$$\sum_{l=1}^{L} ali_{limp}\lambda li_{limp}\pi l_{lmp} + \lambda ins_{mp}\pi ins_{mp} + 2\left[\left((1-\alpha_{mp})\lambda IS_{mp}\right)\left(\frac{1}{\theta s_{mp}n_{mp}}\right)\right]\pi s_{mp} + \lambda f_{mp}\pi f_{mp} - \sum_{j=2}^{f}\lambda ij_{ijmp}\pi i_{imp} - (f-1)ais_{imp}\lambda IS_{mp} = 0 \quad i=1, \quad \forall m\in M, \forall p\in P \quad (2)$$

Eq. 3 is equilibrium equations for out-of-control nodes other than failure mode.

$$\sum_{l=1}^{L} ali_{limp}\lambda li_{limp}\pi l_{lmp} + 2asi_{imp}\left[\left(\beta_{mp}\lambda IS_{mp}\right) + \left(\frac{1}{\theta s_{mp}n_{mp}}\right)\right]\pi s_{mp} + \sum_{j=1}^{j=i-1}\lambda ij_{jimp}\pi i_{jmp} - \sum_{j=i+1}^{f}\lambda ij_{ijmp}\pi i_{imp} - (f-1)ais_{imp}\lambda IS_{mp} = 0 \quad i=2,\dots,f-1, \quad \forall m\in M, \forall p\in P \quad (3)$$

Eq. 4 is equilibrium equation for failure node (corrective maintenance).

$$\sum_{i=1}^{f-1}\lambda ij_{ijmp}\pi i_{imp} - \lambda f_{mp}\pi f_{mp} = 0 \quad j=f, \quad \forall m\in M, \forall p\in P \quad (4)$$

Eq. 5 is equilibrium equation for sampling node.

$$(f-1)\sum_{i=1}^{f-1} ais_{imp}\lambda IS_{mp}\pi i_{imp} - 2\left[\left((1-\alpha_{mp})\lambda IS_{mp}\right) + \left(\frac{1}{\theta s_{mp}n_{mp}}\right)\right]\pi s_{mp} - 2\left[(\alpha_{mp}\lambda IS_{mp}) + \left(\frac{1}{\theta s_{mp}n_{mp}}\right)\right]\pi s_{mp} - 2\sum_{i=2}^{i=f-1} asi_{imp}\left[(\beta_{mp}\lambda IS_{mp}) + \left(\frac{1}{\theta s_{mp}n_{mp}}\right)\right]\pi s_{mp} - 2\sum_{l=1}^{L}(asl_{lmp})\left[\left((1-\beta_{mp})\lambda IS_{mp}\right) + \left(\frac{1}{\theta s_{mp}n_{mp}}\right)\right]\pi s_{mp} = 0 \quad \forall m\in M, \quad \forall p\in P \quad (5)$$

Eq. 6 is equilibrium equation for nodes of various levels of preventive maintenance.

$$2(asl_{lmp})\left[\left((1-\beta_{mp})\lambda IS_{mp}\right)+\left(\frac{1}{\theta s_{mp}n_{mp}}\right)\right]\pi s_{mp}-\sum_{i=1}^{f-1} ali_{limp}\lambda li_{limp}\pi l_{lmp}=0 \qquad (6)$$

$$\forall m\in M,\quad \forall p\in P,\quad l\in L$$

Eq. 7 is equilibrium equation for inspection node (false alarm).

$$2\left[(a_{mp}\lambda IS_{mp})+\left(\frac{1}{\theta s_{mp}n_{mp}}\right)\right]\pi s_{mp}-\lambda ins_{mp}\pi ins_{mp}=0 \quad \forall m\in M,\ \forall p\in P \qquad (7)$$

Eq. 8 calculates the sampling interval.

$$h_{mp}=\frac{1}{\lambda IS_{mp}} \quad \forall m\in M,\quad \forall p\in P \qquad (8)$$

Eq. 9 calculates the preventive maintenance interval.

$$\tau_{mp}=\left(\frac{1}{(1-\beta_{mp})(\lambda IS_{mp})}\right)+\left(\frac{1}{\theta_{mp}n_{mp}}\right) \quad \forall m\in M,\ \forall p\in P \qquad (9)$$

Now, Eq. 10, which is necessary to obtain the percentage of process time remaining in each of the modes.

$$\sum_{i=1}^{f-1}\pi i_{imp}+\sum_{l=1}^{L}\pi l_{lmp}+\pi f_{mp}+\pi ins_{mp}+\pi s_{mp}=1 \quad \forall m\in M,\quad \forall p\in P \qquad (10)$$

Eq. 11 calculates the probability of type I error.

$$\alpha_{mp}=2\phi(-k_{mp}) \quad \forall m\in M,\quad \forall p\in P \qquad (11)$$

$\phi(x)$ is the cumulative distribution function of normal distribution. Eq. 12 calculates the probability of type II error.

$$\beta_{mp}=\phi(k_{mp}-\delta_{mp}\sqrt{n_{mp}})-\phi(-k_{mp}-\delta_{mp}\sqrt{n_{mp}}) \quad \forall m\in M,\quad \forall p\in P \qquad (12)$$

It should be noted that the duration of stay in different modes of the machine (process) up to entering the sampling mode, $f-1$ type hyper exponential random variable, is considered. Because of failure mode, there is no input for sampling mode. The duration until the exit from the sampling mode is also considered to be a hyper exponential random variable of type 4. Because after the sampling, the process is detected either in-control or out-of- control, then the probability of entering the in control mode is 0.5 and the probability of entering the out-of-control modes is 0.5. Also, with the probability α, the process enters the false alarm state, and with the probability β, it is not specified out-of-control of the process, and enters from the sampling mode into out-of-control modes. In addition, with the probability $1-\alpha$, enters the in-control state and, with the probability $1-\beta$, enters the preventive maintenance state. The duration of stay in each machine mode (process), as well as the duration of stay in a failure mode, and preventive maintenance and inspection for false alarm, is an exponential random variable.

3. Results and discussion: Case studies and sensitivity analysis

In order to validate and evaluate the proposed model, a numerical example is presented here, and then a sensitivity analysis is performed to examine the effect of model parameters on optimal solutions.

Consider a manufacturing system that includes a machine that produces a product by the machine. The process of controlling the machine is performed by the $\bar{X}$ control chart. The process of this machine involves various machine (process) modes and failure mode, which, if the process

is in a state of failure, corrective maintenance transform the process into a in control state. All modes of the machine (process) and failure mode, preventive maintenance mode, and sampling mode and false alarm mode are considered in the form of a continuous time Markov chain. In the jobshop production system, for each machine and product, a format of the continuous time Markov chain should be considered and solved. In the numerical example presented, a machine is considered to produce a product. . The machine has four modes: the in control mode (mode 1), the out of control modes (mode 2 and 3) and the mode of failure (mode 4). We know that the process state, in the absence of maintenance, only goes to worse condition. A preventive maintenance level is considered. The costs, the arrival rates and the probability of transfers and other assumed parameters, for this example, are presented in Tables 1-4.

To solve the nonlinear model presented in section 2, taking into account the above parameters, a program is written in GAMS software (version 24.9.1). The optimal solution obtained using the BARON solver is $Z^* = 94.108,\ h_{11}^* = 134,\ \tau_{11}^* = 2014,\ n_{11}^* = 5,\ k_{11}^* = 2.3$. It should be noted that the unit of time in this example is in minutes.

Sensitivity analysis was performed to observe the effect of model parameters on an optimal solution. The parameters we are interested in examining their impact are the cost of preventive maintenance, the cost of corrective maintenance and the magnitude of the changes.

The sensitivity analysis parameters are presented in Table 5. The results of the sensitivity analysis are summarized in Table 6.

As we see, the change in magnitude δ_{11} affects the value k_{11}. As δ_{11} increases, k_{11} also increases. And it is logical that larger process changes necessarily require a larger control limit.

Table 1 The exit rates between each mode (node)

λij_{0111}	λij_{0211}	λij_{0311}	λij_{1211}	λ_{ij1311}	λ_{ij2311}	λl_{111}	λf_{11}	λins_{11}
0.00025	0.000166	0.000125	0.0002	0.00011	0.000222	0.0222	0.00555	0.05

Table 2 The probability of transition between each mode (node)

ais_{011}	ais_{111}	ais_{211}	asi_{111}	asi_{211}	asi_{311}	ali_{1011}	ali_{1111}	ali_{1211}
0.0001	0.2999	0.7	0.3	0.3	0.4	0.6	0.3	0.1

Table 3 The costs

ci_{011}	ci_{111}	ci_{211}	ccm_{11}	cl_{111}	cf_{11}	cv_{11}	$cins_{11}$	$cstop_{11}$
0	100	200	2000	200	20	5	50	1000

Table 4 Other parameters

δ_{11}	θs_{11}
1.5	20

Table 5 Changes ccm_{11} and cl_{111} and δ_{11} for sensitivity analysis

Different states	ccm_{11}	cl_{111}	δ_{11}
State1	1000		
State2	4000		
State3		100	
State4		400	
State5			1
State6			3

Table 6 Sensitivity analysis results

Different states	Z^*	h_{11}^*	τ_{11}^*	n_{11}^*	k_{11}^*
State1	71.220	143	2023	3	1.85
State2	139.748	119	1999	5	2.25
State3	92.610	126	2006	3	1.67
State4	96.983	150	2030	4	2.3
State5	108.999	130	1930	3	1.98
State6	82.409	156	1680	3	2.9

As shown in Table 6, the cost of preventive maintenance affects both the sampling interval and the preventive maintenance interval and the sample size. As the cost of preventive maintenance is reduced, the sampling interval and the preventive maintenance interval and the sample size increases to ensure the performance of the production system.

When the cost of corrective maintenance increases, the sampling interval and the preventive maintenance interval decreases, but the sample size increases.

From Table 6, we can see that the relationship between the cost changes of model parameters and the optimal cost derived from the integrated model is not linear. By changing the cost parameters, the model variables that are related to repair and statistical quality control are changed so that the total cost of the integrated model is minimized. Therefore, this analysis shows that a potential cost reduction is done by applying an integrated model for determining repair and quality control policies. In today's competitive environments, cost reduction plays an important role in the performance of the production system.

Changing non-cost parameters of the model also affected the optimal cost of the integrated model. This is also due to changes in the model variables, which simultaneously changed the variables related to repairs and quality control.

The analysis results show that the change in input parameters affects both the preventive maintenance policy and the statistical process control policy, and simultaneously optimizes repair and quality control policies by minimizing the total cost of both policies. Moreover, these results indicate the dependence between these two policies.

4. Conclusion

This paper presents an integrated model for optimizing statistical process control policies (sampling interval, sample size and control limit) and preventive maintenance (the preventive maintenance interval). The information obtained from the quality control charts was used to decide on the preventive maintenance interval. The proposed model was modeled in the form of a continuous time Markov chain, and the model was optimized with the cost-per-unit time scale.

A numerical example is done to clarify the problem, and the sensitivity analysis shows the dependence between preventive maintenance and statistical process control.

The contribution of this paper was to develop an integrated model to optimize preventive maintenance policy and statistical process control policy, which was modeled in the form of a continuous time Markov chain considering the length of time for preventive maintenance and corrective maintenance. The goal was to reduce costs per unit time.

In this model, the duration of preventive maintenance and duration of corrective maintenance are not zero. Considering the length of time for corrective and preventive maintenance, this model is consistent with the reality of the production system. In addition, this assumption makes this model applicable to industrial environments, because in most cases, the duration of corrective and preventive maintenance is not negligible. This issue has not been considered in the literature on the integrated consideration of preventive maintenance and quality control of the process in the form of a Markov chain. This research gap was considered in this article. According to the results and findings of this research, it is possible in future researches to introduce production planning policies in this model. Considering the simultaneous optimization of production planning, preventive maintenance and statistical quality control is an interesting topic for future research.

References

[1] Tambe, P.P., Kulkarni, M.S. (2015). A superimposition based approach for maintenance and quality plan optimization with production schedule, availability, repair time and detection time constraints for a single machine, *Journal of Manufacturing Systems*, Vol. 37, Part 1, 17-32, doi: 10.1016/j.jmsy.2015.09.009.

[2] Hadidi, L.A., Al-Turki, U.M., Rahim, A. (2011). Integrated models in production planning and scheduling, maintenance and quality: A review, *International Journal of Industrial and Systems Engineering*, Vol. 10, No. 1, 21-50, doi: 10.1504/IJISE.2012.044042.

[3] Pandey, D., Kulkarni, M.S., Vrat, P. (2010). Joint consideration of production scheduling, maintenance and quality policies: A review and conceptual framework, *International Journal of Advanced Operations Management*, Vol. 2, No. 1-2, 1-24, doi: 10.1504/IJAOM.2010.034583.
[4] Pandey, D., Kulkarni, M.S., Vrat, P. (2011). A methodology for joint optimization for maintenance planning, process quality and production scheduling, *Computers & Industrial Engineering*, Vol. 61, No. 4, 1098-1106, doi: 10.1016/j.cie.2011.06.023.
[5] Pandey, D., Kulkarni, M.S., Vrat, P. (2012). A methodology for simultaneous optimisation of design parameters for the preventive maintenance and quality policy incorporating Taguchi loss function, *International Journal of Production Research*, Vol. 50, No. 7, 2030-2045, doi: 10.1080/00207543.2011.561882.
[6] Liu, L., Yu, M., Ma, Y., Tu, Y. (2013). Economic and economic-statistical designs of an $\bar{X}$ control chart for two-unit series systems with condition-based maintenance, *European Journal of Operational Research*, Vol. 226, No. 3, 491-499, doi: 10.1016/j.ejor.2012.11.031.
[7] Xiang, Y. (2013). Joint optimization of $\bar{X}$ control chart and preventive maintenance policies: A discrete-time Markov chain approach, *European Journal of Operational Research*, Vol. 229, No. 2, 382-390, doi: 10.1016/j.ejor.2013.02.041.
[8] Zhang, G., Deng, Y., Zhu, H., Yin, H. (2015). Delayed maintenance policy optimisation based on $\bar{X}$ control chart, *International Journal of Production Research*, Vol. 53, No. 2, 341-353, doi: 10.1080/00207543.2014.923948.
[9] Yin, H., Zhang, G., Zhu, H., Deng, Y., He, F. (2015). An integrated model of statistical process control and maintenance based on the delayed monitoring, *Reliability Engineering & System Safety*, Vol. 133, 323-333, doi: 10.1016/j.ress.2014.09.020.
[10] Bouslah, B., Gharbi, A., Pellerin, R. (2016). Joint economic design of production, continuous sampling inspection and preventive maintenance of a deteriorating production system, *International Journal of Production Economics*, Vol. 173, 184-198, doi: 10.1016/j.ijpe.2015.12.016.
[11] Tambe, P.P., Kulkarni, M.S. (2016). Selective maintenance optimization under schedule and quality constraints, *International Journal of Quality & Reliability Management*, Vol. 33, No. 7, 1030-1059, doi: 10.1108/IJQRM-10-2014-0153.
[12] Lu, B., Zhou, X., Li, Y. (2016). Joint modeling of preventive maintenance and quality improvement for deteriorating single-machine manufacturing systems, *Computers & Industrial Engineering*, Vol. 91, 188-196, doi: 10.1016/j.cie.2015.11.019.
[13] Nourelfath, M., Nahas, N., Ben-Daya, M. (2016). Integrated preventive maintenance and production decisions for imperfect processes, *Reliability Engineering & System Safety*, Vol. 148, 21-31, doi: 10.1016/j.ress.2015.11.015.
[14] Shrivastava, D., Kulkarni, M.S., Vrat, P. (2016). Integrated design of preventive maintenance and quality control policy parameters with CUSUM chart, *The International Journal of Advanced Manufacturing Technology*, Vol. 82, No. 9-12, 2101-2112, doi: 10.1007/s00170-015-7502-7.
[15] Zhong, J., Ma, Y., Tu, Y.L. (2016). Integration of SPC and performance maintenance for supply chain system, *International Journal of Production Research*, Vol. 54, No. 19, 5932-5945, doi: 10.1080/00207543.2016.1189104.
[16] Ardakan, M.A., Hamadani, A.Z., Sima, M., Reihaneh, M. (2016). A hybrid model for economic design of MEWMA control chart under maintenance policies, *The International Journal of Advanced Manufacturing Technology*, Vol. 83, No. 9-12, 2101-2110, doi: 10.1007/s00170-015-7716-8.
[17] Khrueasom, P., Pongpullponsak, A. (2017). The integrated model of the Kolmogorov–Smirnov distribution-free statistic approach to process control and maintenance, *Journal of King Saud University-Science*, Vol. 29, No. 2, 182-190, doi: 10.1016/j.jksus.2016.04.005.
[18] Salmasnia, A., Abdzadeh, B., Namdar, M. (2017). A joint design of production run length, maintenance policy and control chart with multiple assignable causes, *Journal of Manufacturing Systems*, Vol. 42, 44-56, doi: 10.1016/j.jmsy.2016.11.003.
[19] Zhong, J., Ma, Y. (2017). An integrated model based on statistical process control and maintenance for two-stage dependent processes, *Communications in Statistics-Simulation and Computation*, Vol. 46, No. 1, 106-126, doi: 10.1080/03610918.2014.957841.
[20] Beheshti Fakher, H., Nourelfath, M., Gendreau, M. (2017). A cost minimisation model for joint production and maintenance planning under quality constraints*, International Journal of Production Research*, Vol. 55, No. 8, 2163-2176, doi: 10.1080/00207543.2016.1201605.
[21] Rasay, H., Fallahnezhad, M.S., Mehrjerdi, Y.Z. (2017). An integrated model for economic design of chi-square control chart and maintenance planning, *Communications in Statistics – Theory and Methods*, Vol. 47, No. 12, 2892-2907, doi: 10.1080/03610926.2017.1343848.

APEM journal
Advances in Production Engineering & Management
Volume 14 | Number 1 | March 2019 | pp 15–26
https://doi.org/10.14743/apem2019.1.308
ISSN 1854-6250
Journal home: apem-journal.org
Original scientific paper

Determination of nano-roughness for micro-objects by measuring the van der Waals force

Bratina, B.[a,*], **Šafarič, J.**[a], **Uran, S.**[a], **Šafarič, R.**[a]

[a]Faculty of Electrical Engineering and Computer Science, University of Maribor, Maribor, Slovenia

ABSTRACT

3D printing or assembly techniques in the micro/nano-world enable production of micro-parts for building small machines or structures for biomedicine applications, such as cultivation of living cells in the field of Tissue Engineering. Micro-sized assembly requires automated manipulation procedures and methods for determination of suitable objects for assembly. The latter is possible by van der Waals force measurement and determination of distance at the van der Waals peak between two objects in contact. They are dependent not only on the Hamaker coefficients of the materials in contact and their geometries, but also on the nano-roughness asperities and crystal structure asperities of the contact surfaces. A method is presented for measuring van der Waals` force and determining micro-objects' (sizes between 10-100 μm) distances between materials in contact at the van der Waals peak in the presence of nano-roughness and crystal structure roughness. The proposed model was validated by experimental lab results between various materials and shapes (glass and polystyrene beads, metallic wires).

ARTICLE INFO

Keywords:
Micro-object;
Surface roughness;
Nano-roughness;
Van der Waals force;
Distance at van der Waals peak

**Corresponding author:*
bozidar.bratina@um.si
(Bratina, B.)

Article history:
Received 14 September 2018
Revised 18 February 2019
Accepted 24 February 2019

1. Introduction

3D printing is becoming an essential part of rapid prototyping in Research and Development Departments. Today, classic and novel printing technologies enable printing of almost everything that can be designed. Also, the variety of printing materials and composites is increasing on the market (plastics, imitation wood, metals, etc.), which also makes possible prototyping of high end industrial products (jet engine blades, high-temperature and high-pressure rocket engine combustion chambers [1], airplane parts, etc.). However, additive manufacturing on a small scale, such as micro/ nano level 3D printing, presents one of the challenges. Scientists have developed many different deposition and hardening techniques (electron beam lithography, multiphoton polymerization, etc.), which enable printing of small objects to a micron level [2]. These 3D printing technologies have in common operating with light sensitive materials, resins, powders as an additive material which can later be treated for hardening. On the other hand, 3D printing can also be managed by using micro/nano-objects assembled into a microstructure layer by layer [3, 4] (micro-machines, gearbox, motor, etc.), or structures with living cells, which could boost the field of Tissue Engineering.

To be able to assemble given micro-objects into a structure, it is essential to have adequate equipment and to master the manipulation of material. Automated assembly procedures with micro/nano-manipulators include sensors to control the assembly process, hence detecting micro-objects for assembly, which are too small for machine vision applications. Therefore, a

method is needed to be able to determine if the object for assembly is adequate or not (dust particle, micro-object not adequate in size or material). In the paper such a method is presented, where micro-object' properties are measured by van der Waals force, and distances at van der Waals peak are determined between materials in contact. Similar measuring methods (atomic force microscope measurements, X-ray method etc.), are performed very rarely due to the expensive equipment used, whereas the presented method is quite simple, and gives similar accuracy results.

Van der Waals force and distance at van der Waals peak

Even on fine polished solid surfaces of materials (glass or polystyrene microbeads, metal wires, etc.), asperities are large in comparison with the size of the crystal structure (atoms or molecules) of the solid materials placed in contact. Most materials used in engineering practice have surface asperities (so-called nano-roughness) greater than few decades of a nano-metre. If two such solid materials are placed in contact, because of the mentioned asperities, the great areas of surfaces will be separated by a distance much greater than the molecular range of action [5]. Previously developed models of van der Waals forces [3] for a one-finger gripper, based on the van der Waals force, demand an accurate calculation of the van der Waals force at the point of contact. The van der Waals force between two objects in contact is dependent on the geometry of the objects, their materials (Hamaker coefficients), and the distance between the objects in contact. This paper focuses on the determination of the distances between objects in contact, with the presence of nano-roughness asperities and crystal structure asperities on both the contact surfaces (distance at van der Waals peak, Fig. 1). An assembly application of micro structures from micro/nano-objects [3] demands characterization of material properties, the identification and manipulation of micro-objects, and assembly techniques. For identification of the geometric features of a micro-sized object (size, diameter in the case of spherical or cylindrical shapes …), measurements of the van der Waals contact forces are necessary, and demand an accurate measurement of the surface roughness of the micro-object. Determining the surface roughness of a micro-object has been proven to be problematic, whereas present methods can only give an inaccurate estimation or calculation of the roughness and, consequently, the van der Waals contact force. Three methods exist for measuring or determining the roughness of micro-sized objects.

The first one, originally described by Rowland and Taylor [6], and later used by Alvarez [7], calculates the distances at van der Waals peak statistically from the distribution of intermolecular distances (Fig. 1) between most of the elements in the periodic system against a so-called oxygen probe. This method is based on the statistical analysis of the intermolecular contacts in X-ray crystal structures for determining the van der Waals radii. However, with this method, only the distances at van der Waals peak between the periodic system elements and the oxygen probe have been determined and published, while the contacts for a variety of other materials (except sulphur and hydrogen probes) have not yet been studied to the knowledge of the authors of this paper. The second method is the so-called analytical method, first described in Rumpf [8], and later used as a modified version by various authors [9-12, 14]. For this method, the square root of the mean square values of the surface roughness is measured with a precise AFM (Atomic Force Microscope), or by the electron beam evaporation method. The different models based on this method assume that the asperities are hemispherical caps on a smooth substrate [8]. Matope *et al*. [13] have suggested that the adhesion (van der Waals) force on surfaces exhibiting asperities should be written as a combination of sphere–sphere and sphere–plane surface interactions in the form:

$$F_{adh} = \frac{A\,R}{6\,H_0^2}\left(\frac{1}{1+58\,R\,rms/\lambda^2}+\frac{1}{(1+1.82\,rms/H_0)^2}\right) \quad (1)$$

where A is the Hamaker coefficient, R is the radius of the micro-sized spherical object, H_0 is the contact distance between the surface and the object, *rms* is the root of mean square values of the micro-object's surface roughness, and λ is the peak-to-peak distance of the asperities of the surface roughness of the micro-object. These models calculate the van der Waals force between

various micro-sized objects (spheres or blunt particles), where the *rms* of the surface roughness is measured on only one side of the materials in contact (usually the plane surface), while the *rms* of the surface roughness of the probe (sphere) is not measured at all.

Instead, the distance $H_0 = 2\text{-}3$ Å ($1\text{Å} = 10^{-10}$ m) is used between the material and the probe (sphere). The drawback of this model is that it gives precise results only for F_{adh}, where the probe has the exact value inside $H_0 = 2\text{-}3$ Å. Moreover, the difference between F_{adh} for the case when $H_0 = 2$ Å or 3 Å, is more than 40 %. So, this method is quite inaccurate. Of course, this model is only suitable for calculating the van der Waals force between a plane surface and a sphere particle. The third method is the so-called computational method, which is in good agreement with our experiments [14]. The drawback of the third method is its complexity (fractal surfaces, Fourier Transforms), which makes it hard to apply, especially for quick estimations of the van der Waals force for specific systems.

Our presented method solves all mentioned drawbacks (distances at van der Waals peak are known only for the elements of the periodic system against an O-probe, the use of only one side of a surface in contact, the distance $H_0 = 2\text{-}3$ Å produces huge errors in order to calculate the van der Waals force, and the complexity of the Eichenlaub's method). The developed method for determining the distance at van der Waals peak in the presence of nano-roughness and the crystal structure roughness of contact surfaces, is valid for arbitrary materials (not only pure elements against an oxygen probe) of micro-sized objects. In addition, it is also suitable for situations where two objects with different geometries have their own surface roughness. The developed surface model can also determine the roughness of the materials' surfaces in contact (distances at van der Waals peak) between micro-objects with materials 1 and 2, if the previously determined roughness between micro-objects with materials 1 and 1 and materials 2 and 2 are known. Moreover, it is simple to use, because its equations rely on only one parameter (distance at van der Waals peak), which is determined easily from the van der Waals force measurements. It is not necessary to use an AFM, beam-electron or other expensive microscopes.

The paper structure is as follows. The second section of the paper presents a description of the method for determining distances at van der Waals peak in the presence of nano-roughness and crystal structure roughness on contact surfaces. The next section describes the laboratory set-up and the set of used equations for calculating the van der Waals force of two micro-sized objects in contact with different geometries, different materials and different roughness of materials. The third section presents experimental results and analysis, and fourth the conclusion of the paper.

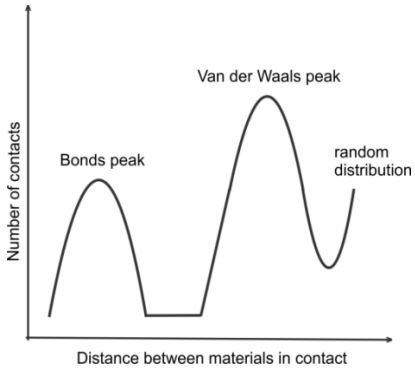

Fig. 1 Scheme for determining the distance between materials in contact at van der Waals peak

2. Materials and methods for surface roughness determination (distance at van der Waals peak)

The determination of the distance at van der Waals peak demands precise measurements of the van der Waals force between two objects in contact. We focused on micro-sized objects of different shapes: Plane surface, cylinder with a radius of 25 μm, and spheres with a radius of 5-50 μm, chosen because of their availability on the market, which gives us the following van der Waals

force measurement pairs: Plane surface-sphere, sphere-sphere, sphere-cylinder and cylinder-cylinder. The other two possible types of measurements, plane surface-plane surface and cylinder-plane surface, are not practical, due to problems with the alignment of both objects. Therefore, our method is based on four practical geometrical pairs. The laboratory set-up hardware was designed for 3D movement of both objects against each other.

2.1 Laboratory set-up and materials used in the experiments

The laboratory set-up is shown in Fig. 2a. The nano-precision 3D manipulator system consists of an optic microscope, a turbo-molecular vacuum pump and a vacuum chamber with nano-precision 3D manipulator (Fig. 2b) inside. The vacuum can be set as low as 2 μbar. Fig. 2b shows the nano-precision 3D manipulator mechanism, with x- and y-axes consisting of magnetic linear incremental encoder sensors that operate as a planar mechanism, and a z-axis with its own linear incremental sensor. Different end-effectors (tools, grippers, etc.) can be mounted on the 3D manipulator tip at the end of the y-axis. The y-axis is placed on a movable cart that moves along the x-axis' linear guide. All three piezo electric motors with sensors are mounted on an aluminium block that serves as a vibration-absorber to limit mechanical disturbances from the environment. The position accuracy of the robotic tip, along a single axis, is ± 3.9 nm in an open loop, while the position control loop of each axis has an accuracy of ± 61 nm. We also used a long distance focus (21 mm) optical microscope for observations of micro-objects up to 3 μm. A more precise description of the lab set-up can be found in [3, 4, 15].

Different micro-sized objects were used in the experiments: Metal wires, glass (SiO_2) and polystyrene beads, glass surfaces and mica surfaces. The glass beads (radius 25-50 μm and 10-30 μm) were purchased from Polysciences, Inc., USA. The polystyrene beads (radius of 30 μm) were purchased from Kisker Biotech GMBH, Germany. The nickel wire (puratronic, radius 25 μm, LOT: E22Z008), palladium wire (hard, radius 25 μm, LOT: L15T030), aluminium wire (hard, radius 25 μm, LOT: G24Z014), silver wire (Premion, radius 25 μm, LOT: 13467) and gold wire (Premion, radius 25 μm, LOT: P21A023) were purchased from Alfa Aesar GmbH, Germany. All the metal wires had 99.99 % trace metals basis. Standard microscope slides (SiO_2) were used for the glass surface plane, purchased from Logitech, UK. The Muscovite mica insulating slides were purchased from EA Elektronika, Slovenia.

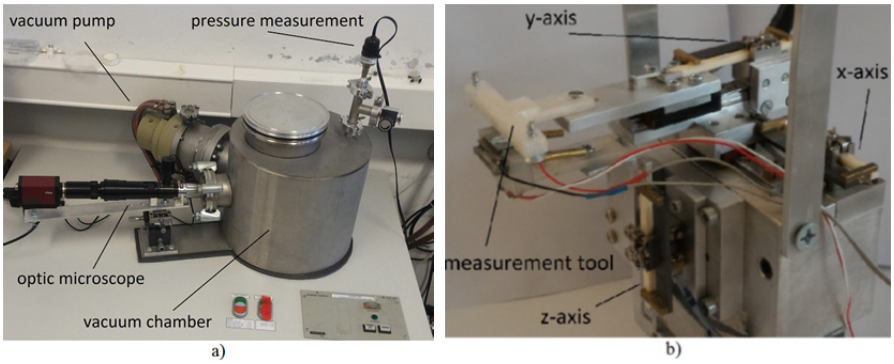

Fig. 2 The nano-precision 3D manipulator system a), and the nano-precision 3D manipulator mechanism b)

2.2 Used methods: Pull-off measurements of the van der Waals force

Small attraction forces, such as the van der Waals forces between micro-sized objects in contact, are often measured using an AFM microscope. However, the presented pull-off method consisted of measuring the attraction force using a spring traverse [16]. Fig. 3 shows a schematic diagram of the four different types of measurements of the van der Waals forces between the geometrically different objects used in our experiments. The attraction force F_{ATR} attracts the micro-sized objects when they have been put into contact. If the lower object is pulled away by the force F with z-axis (Fig. 3), then the traverse starts to deflect with the distance f. The objects are "attached" together during the deflection due to the attraction force, and the objects in contact keep this position until the opposite traverse's elastic force F becomes equal to the attraction force. At that moment, the traverse tears away from the lower object towards a position of equilibrium,

hence, the deflection f is measured. Calculation of the traverse's deflection force F and inertia I_z [17] for a circular cross-section is presented by Eq. 2:

$$F = \frac{3fEI_z}{l_T^3}, \quad I_z = \frac{\pi d^4}{64} \quad \Rightarrow \quad F_{ATR} = F = \frac{3fE\pi d^4}{l_T^3 64} \tag{2}$$

where l_T is the length of the traverse, E is its Young's modulus, and d is its diameter. The measurements of F_{ATR} were conducted in a vacuum chamber with pressure lower than 1 mbar to avoid capillary force effects. The static electric charge on the SiO_2 (amorphous) plane surface was discharged by putting the tip of the traverse into contact with the plane surface for a moment, thus equalising the electrical charges. Both the traverse and the plane were also grounded electrically. Consequently, the capillary and electrostatic forces were avoided.

Fig. 4a shows the measurement tool on the robotic tip with a mounted golden traverse and a glass plane, where the spherical object is glued. Fig. 4b shows the golden traverse touching the spherical glass object. The traverse and the object in Fig. 4b were observed through a microscope (the diameter of the traverse is 50 μm).

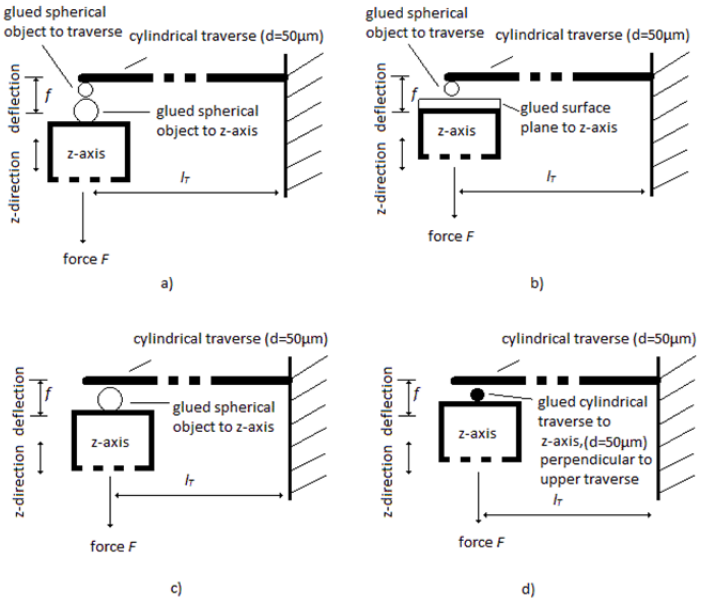

Fig. 3 Schematic diagram of the four methods used for measuring attraction forces: a) Between micro-sized spheres, b) Between micro-sized spheres and the surface plane, c) Between micro-sized spheres and a cylinder and d) Between two perpendicular cylinders

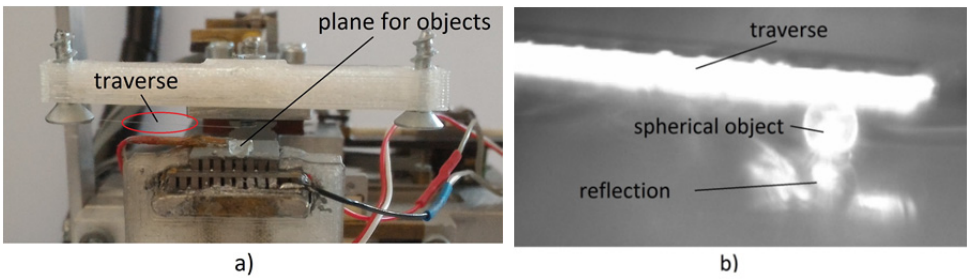

Fig. 4 Measurement tool a), and zoomed view - traverse touching a spherical object b)

2.3 Proposed model for determining the distance at van der Waals peak

Four models were developed for determining (calculating) the distance at van der Waals peak from the measured van der Waals force $F = F_{ATR}$ (Eq. 2) which are presented next. The models for determining the distance at van der Waals peak for the following examples: Sphere-sphere (Fig. 3a), sphere-surface plane (Fig. 3b), and between two perpendicular cylinders (Fig. 3d) are easy to develop from known analytical equations for the van der Waals force between different

geometrical objects [18-20]. The equations used for determining the average contact distance d or the distance at van der Waals peak are as follows:

a) For sphere - sphere geometrical combination:

$$F = \frac{AR_1R_2}{(R_1+R_2)6d^2} \quad \Rightarrow \quad d = \sqrt{\frac{AR_1R_2}{(R_1+R_2)6F}} \tag{3}$$

b) For sphere - surface plane there is an approximate formula:

$$F = \frac{AR}{6d^2} \quad \Rightarrow \quad d = \sqrt{\frac{AR}{6F}} \tag{4}$$

c) And for two infinite perpendicular cylinders of the same radius, there is again an approximate formula:

$$F = \frac{AR_c}{6d^2} \quad \Rightarrow \quad d = \sqrt{\frac{AR_c}{6F}} \tag{5}$$

where A is the Hamaker coefficient, R_1, R_2, R are the radii of the spheres, R_c is the radius of the cylinder, and F is the van der Waals force in contact (F_{ATR}), measured and calculated by Eq. 2. The situation is far more complex in the case when the distance at van der Waals peak is determined between a cylinder and a sphere. We found two sources [19, 21] where the authors claimed that they had developed an analytical expression for the van der Waals force between a sphere and an infinitive cylinder. Unfortunately, the expression used by Montgomery [19] was proven experimentally to be incorrect, due to an imprecise use of the Maclaurin series. Ref. [21] showed promising results when the expression was verified experimentally for the van der Waals force in contact. We have tried, unsuccessfully, to repeat the analytical development of the final result of ref. [21]`s complicated expression, which is written as:

$$F = \frac{AR_s^3\left\{(4+2s+s^2)E\left(\frac{1}{p}\right) - s(1+s)K\left(\frac{1}{p}\right)\right\}}{24c^{5/2}R_c^{3/2}s^2p^{3/2}} \tag{6}$$

where $p = 1+ s/2$, $s = ((d + R_s)^2 - R_s^2)/(2cR_c)$, $c = R_c + R_s + d$, d is the distance between the sphere and the cylinder, R_c is the radius of the cylinder, R_s is the radius of the sphere, K and E are the complete elliptic integrals defined as:

$$E(z) = \int_0^{\pi/2} \sqrt{1 - zsin^2\theta}\, d\theta, \tag{7}$$

$$K(z) = \int_0^{\pi/2} 1/\sqrt{1 - zsin^2\theta}\, d\theta. \tag{8}$$

Instead of Eq. 6 [21] we derived our equation (9) for van der Waals force calculation between an infinite cylinder and a sphere from the same mathematical and physical assumptions. Both Eq. 6 and Eq. 9 were compared between themselves. We can confirm that the original equation derived in [21] is correct, because both equations gave the same numerical results for F when the distance d was used between 0.2 nm to 200 nm. Unfortunately, both Eq. 6 and Eq. 9 are not completely analytical, because it is not possible to derive analytical equations from them for the distance d.

$$F = AR_s^3 \int_{R_s+d}^{R_s+R_c+d} \frac{r(c^2 - r^2 + R_c^2)}{c(-r^2 + (c-R_c)^2)^{1/2}(r^2 - (c+R_c)^2)^{1/2}(r^2 - R_s^2)^{5/2}}\, dr \tag{9}$$

Both equations demand numerical calculation of the complete elliptic integrals or finite integrals. In order to calculate the distance d from the van der Waals force F, the theory of Artificial Neural Network was used to approximate the nonlinear inverse function of Eq. 6 and Eq. 9. The

classical backpropagation learning rule was used for a two-layer feedforward neural network, with one input, one output, ten neurons in a hidden layer, and one neuron in the output layer of the network. The learned Artificial Neural Network serves as a nonlinear calculator for the distance d (distance at van der Waals peak) between a sphere and an infinitive cylinder when the measured van der Waals force F is used, (see Fig. 3c) [22]. The tolerance, between the approximated and reference value of distance at van der Waals peak, after the Artificial Neural Network learning phase (150 iterations), was lower than 0.1 % for all the reference values of distance at van der Waals peak between 0.1 nm to 200 nm. The learning input samples (training vector) consisted of 100 pairs of distance at van der Waals peak and their corresponding values of the van der Waals force F. The Artificial Neural Network was learned in only 100 samples of the training vector. The approximated values of distance at van der Waals peak were also valid and accurate between the mentioned learning points, due to the generalization between data pairs.

2.4 Determining the distance at van der Waals peak when both interacting objects have roughness

The experiments published in [9-12] studied the nano-roughness, distribution of nano-roughness asperities and contact distances in the case where the measurement of an SiO_2 spherical probe roughness was not known, but assumed to be between 2-3 Å. Our newly proposed method takes into account both contact surfaces and their roughness affected by nano-roughness asperities and the crystal structure roughness of the contact surfaces – mentioned as the distance at van der Waals peak. Fig. 5 shows the scheme for describing contact surfaces with nano-roughness asperities and asperities due to the crystal structure of the material. The scheme in Fig. 5a shows the distance at van der Waals peak due to roughness d_{11} between two objects of material 1. Fig. 5b shows the distance at van der Waals peak due to the roughness d_{22} between two objects of material 2, while Fig. 5c presents the distance at van der Waals peak due to the roughness d_{12} between two objects of both materials 1 and 2.

The following equation can be stated hypothetically:

$$d_{12} = \frac{d_{11}}{2} + \frac{d_{22}}{2} \Rightarrow d_{11} = 2d_{12} - d_{22} \Rightarrow d_{22} = 2d_{12} - d_{11}. \tag{10}$$

So, if we can determine distances d_{11} and d_{22}, then we can determine the distance d_{12}, or vice versa. Therefore, if two distances at van der Waals peak are determined, it is possible to calculate a third one. In the following section, the experimental laboratory measurements are presented, proving Eq. 10 and the models for calculating the van der Waals force in contact, described by Eq. 3, Eq. 4, Eq. 5 and Eq. 9.

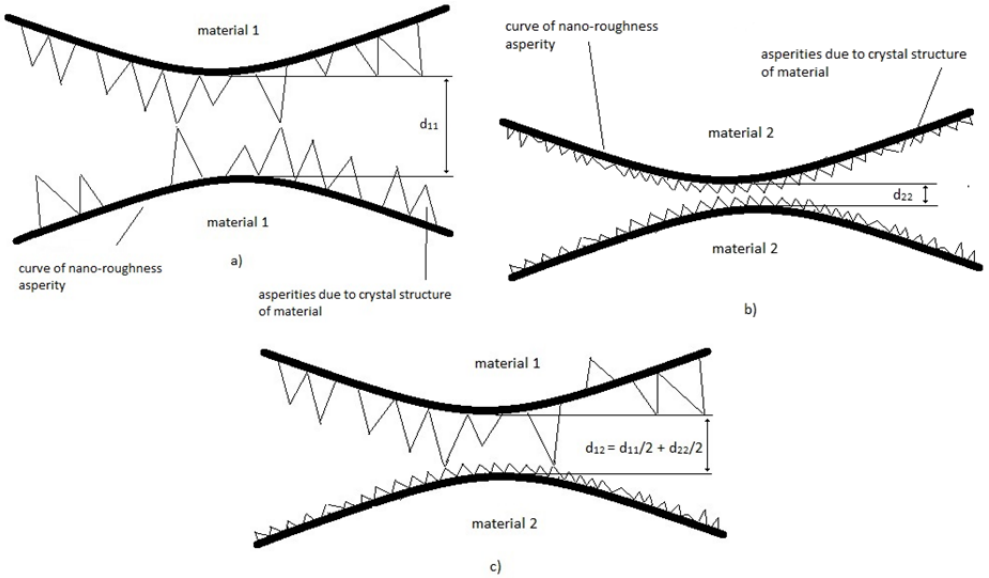

Fig. 5 The scheme of a cross-section of the distance at van der Waals peak due to nano-roughness asperities and the crystal structure asperities of the material in contact

3. Results and discussion

Three different geometries and several different materials of micro-objects were used in the experiments, as described in subsections 2.2 and 2.3: Au cylinder, Ag cylinder, Al cylinder, Ni cylinder, Pd cylinder, polystyrene sphere, SiO_2 sphere, SiO_2 plane and a mica plane.

3.1 Measurements

Thirty-two sets of measurements were done between different combinations of materials and geometries. Every set of measurements was done with twenty repetitions of measurements of deflection *f*. After that, the measurements were eliminated which departed heavily from the average (1-6 measurements out of 20).

The measured van der Waals force F_m (see Eq. 2) and the corresponding Standard Deviations, were calculated from the remaining measurements of deflection. Fig. 6 shows the elimination of the first three measurements of deflection for the measurement between two aluminium cylinders with the same diameter ($d = 50$ μm). The first three are marked with a diamond, while the remaining 17 measurements are marked with a star. Fig. 7, left, presents Hamaker coefficients A_{12} [zJ] between two materials across the vacuum used in measurements and calculations in our models. We used [23] as a source for the Hamaker coefficients between the metals (Ag, Al, Au, Ni, Pd) and the sapphire in a vacuum. We used [24] as a source for the Hamaker coefficients of the polystyrene, SiO_2 and sapphire in a vacuum, and we used [25] as a source for the Hamaker coefficient of mica in a vacuum. Eq. 11 was used to calculate all the Hamaker coefficients Ahmadi [24] presented in Fig. 7, left.

$$A_{12} \approx \sqrt{A_{11}}\sqrt{A_{22}} \tag{11}$$

Fig. 7, right, presents the measured values of van der Waals force F_m [μN] and their Standard Deviations calculated from the measured deflections. The same Fig. 7, right, also presents the calculated van der Waals force F_c [μN] obtained from the contact model of van der Waals forces using Eq. 3, Eq. 4, Eq. 5 and Eq. 9 for control check using calculated van der Waals distance d_c [Å]. The distances at van der Waals peak d_m [Å] between different materials and geometrical appearance were determined from Eq. 3 for the sphere-sphere geometrical combination, from Eq. 4 for the sphere-surface plane geometrical combination, from Eq. 5 for two infinite perpendicular cylinders with the same radius, and from the neural network for a cylinder-sphere combination.

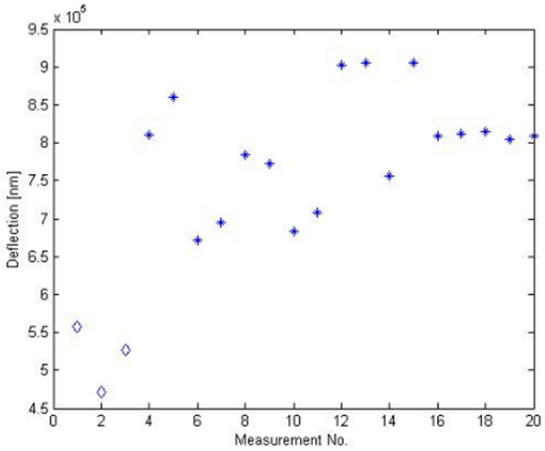

Fig. 6 Elimination of the deflection measurements that deviated significantly from the average value in contact between two aluminium cylinders, both with diameters $d = 50$ μm

Calculated distances at van der Waals peak d_c [Å] were cross-calculated with Eq. 10 from determined distances at van der Waals peak d_{12} or d_{22} or d_{11}. Both distances at van der Waals peak d_m [Å] and d_c [Å] for materials used in the experiment are presented in Fig. 8, left. The absolute value of percentage deviation $|F_d|$ [%] between measured and calculated van der Waals forces F_m and F_c were compared to validate the models for determining the van der Waals force in con

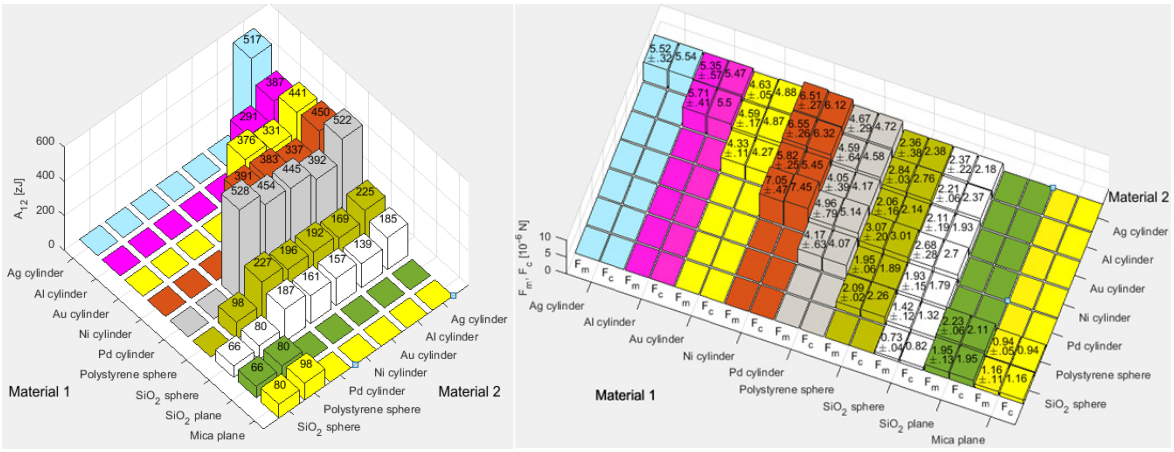

Fig. 7 Hamaker coefficients between materials across the vacuum used in calculations Measured (F_m [μN]), and calculated F_c [μN] van der Waals forces in contact between different materials used in the experiment

tact and presented in Fig. 8, right. So, for example, when material 1 is Ag and material 2 is Ag, the measured van der Waals force F_m with a value of 5.52 ± 0.32 μN was measured (see Fig. 7, right) using the method described by Eq. 2 and Fig. 3d. Then, the value $d_m = d_{11} = 6.25$ Å for the Ag-Ag combination of materials was calculated using Eq. 5 (see Fig. 8, left). The same was done for an Al-Al combination of materials with the value $d_m = d_{22} = 4.62$ Å, and an Ag-Al combination of materials with the value $d_m = d_{12} = 5.52$ Å. After that, using Eq. 10, the value $d_c = d_{12} = d_{11}/2 + d_{22}/2 = 6.25$ Å $/2 + 4.62$ Å $/2 = 5.43$ Å was calculated. The value d_c was used to obtain the calculated van der Waals force $F_c = 5.47$ μN for the case of the Ag-Al combination of materials, using Eq. 5 again (see Fig. 8, right). The values $F_c = 5.47$ μN and $F_m = 5.35 \pm 0.57$ μN for the Ag-Al combination of materials were compared, and, finally, the absolute value of percentage deviation between both values $F_d = 2.6$ % was calculated (see Fig. 8, right). With the same method, the measured and calculated values were cross calculated, and statistical validity was verified for the proposed method and model. This method used Eq. 3, Eq. 4, Eq. 5 and Eq. 9 for calculating van der Waals forces in contact.

Finally, the average values $d_c = d_{11}$ were calculated for material combinations where both materials are the same (Ag-Ag, Al-Al, Au-Au, Ni-Ni, Pd-Pd, Polystyrene-Polystyrene, SiO_2-SiO_2). By using Eq. 10, we calculated all $d_c = d_{11}$ by using all possible combinations of the $d_m = d_{12}$ determined values. For example, to calculate the average $d_c = d_{11} = 6.24$ Å (see Fig. 8, left) for the material combination of Ag-Ag, six determined values of $d_m = d_{12}$ material combinations can be used; Ag-Al ($d_m = d_{12} = 5.52$ Å), Ag-Au ($d_m = d_{12} = 6.30$ Å), Ag-Ni ($d_m = d_{12} = 5.36$ Å), Ag-Pd ($d_m = d_{12} = 6.84$ Å), Ag-Polystyrene ($d_m = d_{12} = 4.34$ Å) and Ag-SiO_2 ($d_m = d_{12} = 4.81$ Å). From the value $d_c = d_{11}$ for the material combination of Ag-Ag, obtained from the material combination of Ag-Al, we get $d_c = d_{11}$ (of Ag-Ag) $= 2\,d_m$ (of Ag-Al) – d_m (of Al-Al), as seen in Eq. 10. In this way, we obtained values $d_c = d_{11}$ for the material combination of Ag-Ag from all five remaining mate-

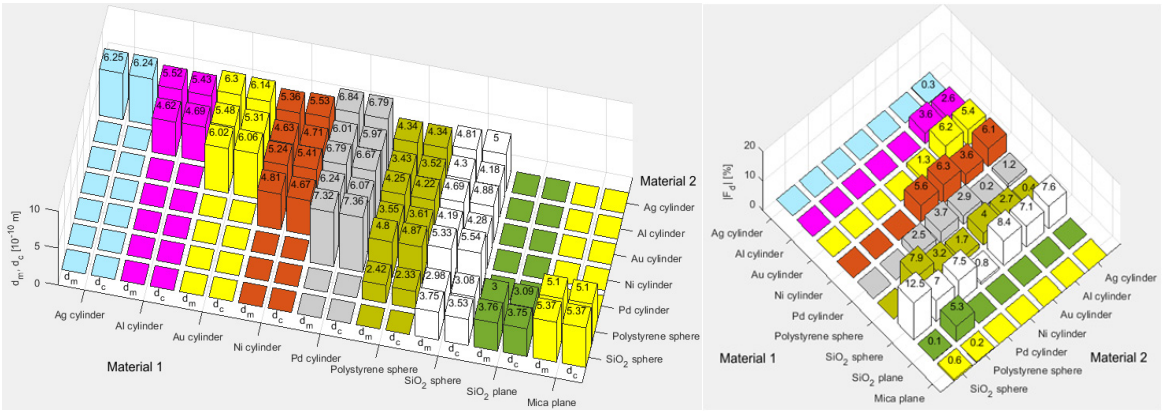

Fig. 8 Determined d_m [Å] and calculated d_c [Å] distances at van der Waals peak and for materials used in the experiment, and Absolute value of percentage deviation $|F_d|$ [%] between F_m and F_c

rial combinations (Ag-Au, Ag-Ni, Ag-Pd, Ag-Polystyrene, Ag-SiO_2). These six values $d_c = d_{11}$ were averaged to achieve a final validation of the determined and calculated value of $d_c = d_{11} = 6.24$ Å for the material combination of Ag-Ag.

3.2 Analysis of the results and discussion

The calculated van der Waals force F_c corresponded with the measured van der Waals force F_m inside the -8.4 % to 12.5 % band. The most inaccurate values are in the column called SiO_2 sphere, the highest F_d [%] gives the experimental measurements between the SiO_2 sphere and the SiO_2 sphere (12.5 %), and between the SiO_2 sphere and the Au cylinder (-8.4 %). The reason for this is that the micro-sized and nano-sized roughness of the SiO_2 spheres was "huge" in comparison with other materials. The asperities of roughness for the SiO_2 spheres were so big that the spherical geometry of the SiO_2 sphere was compromised (see Fig. 9, left). Consequently, the correct radius of the SiO_2 sphere was not determined, and this fact produced a relatively huge error in calculating the distance at van der Waals peak *d* from the measured van der Waals force. Fig. 9 shows the micro-sized and nano-sized irregularities on the surface of some of the used materials in the experiment. We tried to avoid these irregularity problems by repeating the measurements of the deflection *f* in various places. Consequently, we had to move the contact points of measurement by a few micrometres each time. These problems were the source of occasionally scattered data of deflection measurements (Fig. 6), where the first three measurements were eliminated from the set of data used for calculating the average van der Waals force and its Standard Deviation. The next reason for the mistake was, again, the radii of spheres and cylinders used in the experiment. They were determined with an accuracy of ± 1 μm, which can lead to an error in calculating the van der Waals force up to ± 4 %. Another source of errors in the model of the van der Waals force in contact could be the Hamaker coefficients used in the experiments. Different sources give different values for the Hamaker coefficients of the used materials, however, this didn't increase the relative deviation (F_d [%]), but increased the absolute error of the calculated van der Waals forces and the determined distances at van der Waals peak.

Of course, distances at van der Waals peak, determined by [7], (d_{Al}), have to be smaller than our values d_{11}, d_{12} and d_{22}, because he used the crystallographic method to determine these. Therefore, their measurements were "not spoiled" by asperities of nano-roughness and the "roughness of the crystal structure" of the materials used in the experiment. Distances at van der Waals peak determined by our method were always higher than those obtained by Alvarez (distances at van der Waals peak determined for Ag-O is $d_{Ag} = 5.2$ Å, for Al-O is $d_{Al} = 4.0$ Å, for Au-O is $d_{Au} = 4.0$ Å, for Ni-O is $d_{Ni} = 4.1$ Å, for Pd-O $d_{Pd} = 4.2$ Å and for O-O is $d_O = 3.3$ Å; O presents the oxygen probe, such as SiO_2, Al_2O_3, etc) from the source [7] just for comparison with our determined distances at van der Waals peak. The distances at van der Waals peak determined by our method were always higher than those obtained by Alvarez [7]. There is only one exception, where the distance at van der Waals peak was determined and calculated between the Ag cylinder and the SiO_2 sphere. We double checked our force measurements, but the determined values of distances at van der Waals peak were always between 4.8-4.9 Å. We believe that in [7] there is an error in obtaining the distance at van der Waals peak by using the crystallographic method for the Ag-O measurements, because the author claimed that "*Ag-O has a poorly defined peak and larger uncertainty in its position*".

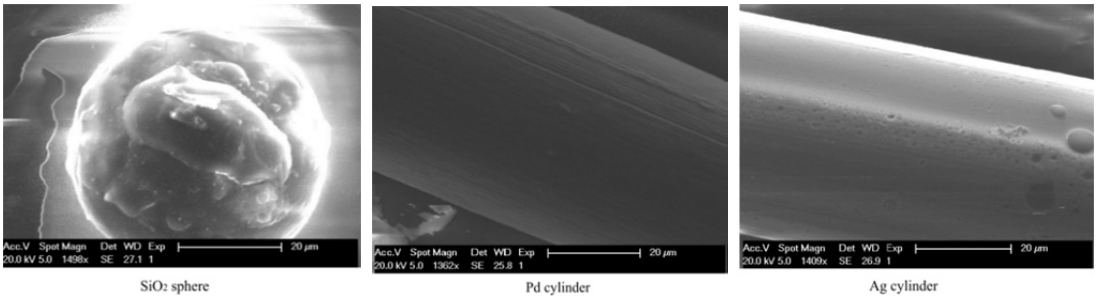

Fig. 9 SEM images of geometrical shapes and roughness of some of the materials used in the experiments

It can also be confirmed by calculating the van der Waals radius for Ag. This can be seen in [27, 28], where van der Waals radius for Ag deviates from [7]. However, other data agree on the majority of other elements of the periodic system. Young's modulus E in Eq. 2 is also an example of an error in measuring the van der Waals force in contact using the pull-off method. Young's modulus for gold varies between 79-80 GPa, which brings measurement error of up to 1 %. For the final experiment, we built a one-layer triangle structure (Fig. 10) by using many micro objects (spheres) scattered on the plane surface. By using the presented method, we were able to determine the proper size of the micro-objects from Hamaker coefficient, geometry, and distance at van der Waals peak, prior to manipulation of the objects. If the measured van der Waals force was not as expected (too small or too big), the object was not suitable to be part of the microstructure.

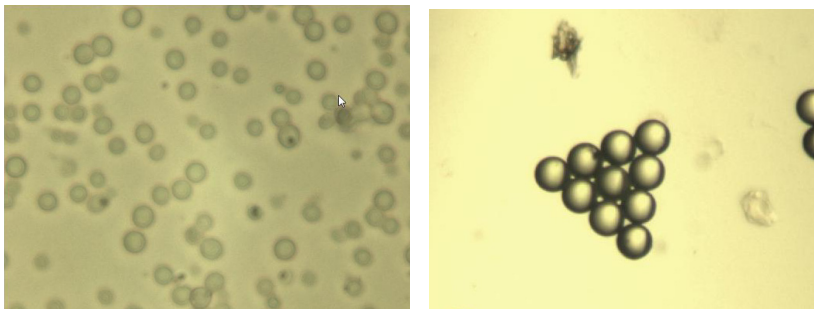

Fig. 10 Scattered micro-objects on the plane (left), and built triangle with cca. 30 μm spheres in diameter

4. Conclusion

The paper presents a method for micro/ nano 3D assembly, where visual information about the objects is not available. By knowing the material type and geometry, a micro-object's properties (e.g. size) can be determined based on van der Waals force measurement and distance at van der Waals peak determination. We present a new model for determining the distance at van der Waals peak and, consequently, measuring the van der Waals force in contact between micro-sized objects, the micro-sized objects being of different materials (metallic wires…), shapes, nano-sized roughness and crystal structure roughness. We have demonstrated experimentally that the distance at van der Waals peak determined with our pull-off method determines the sum of the van der Waals radius, the average impact of nano-sized asperities and the crystal structure roughness of the materials' contact surfaces effectively. Our model for measuring the van der Waals force in contact is more accurate than [13], and easier to use than the methods previously published in [9-12], because they used more sophisticated methods with more expensive equipment (AFM, X-ray devices). An important outcome is the experimental confirmation of Eq. 10, where, if the distances at van der Waals peak are determined between one type of material and a second type of material, we can derive the distance at van der Waals peak for a mixture of both types of material. Consequently, an accurate value of the van der Waals force can be calculated for both materials in contact. The drawback of the presented pull-off method for measuring van der Waals forces in contact is that it is highly sensitive to micro-sized irregularities, e.g. both, or even only one of the materials in contact, have micro-sized irregularities on their surface.

Acknowledgement

This research was partly funded by the Slovenian Research Agency under Grant No. P2-0123(B) Clothing Engineering and Textile Materials.

References

[1] Ngo, T.D., Kashani, A., Imbalzano, G., Nguyen, K.T.Q., Hui, D. (2018). Additive manufacturing (3D printing): A review of materials, methods, applications and challenges, *Composites Part B: Engineering,* Vol. 143, 172-196, doi: 10.1016/j.compositesb.2018.02.012.

[2] Ru, C., Luo, J., Xie, S., Sun, Y. (2014). A review of non-contact micro- and nano-printing technologies, *Journal of Micromechanics and Microengineering*, Vol. 24, No. 5, Article 053001, doi: 10.1088/0960-1317/24/5/053001.

[3] Šafarič, R., Lukman, D. (2014). One-finger gripper based on the variable van der Waals force used for a single nano/micro-sized object, *Journal of Micromechanics and Microengineering*, Vol. 24, 1-13, doi: 10.1088/0960-1317/24/8/085012.

[4] Uran, S., Šafarič, R., Bratina, B. (2017). Reliable and accurate release of micro-sized objects with a gripper that uses the capillary-force method, *Micromachines*, Vol. 8, No. 6, 182, doi: 10.3390/mi8060182.

[5] Kudryavtsev, Y.V., Gelinck, E., Fischer, H.R. (2009). Theoretical investigation of van der Waals forces between solid surfaces at nanoscales. *Surface Science*, Vol. 603, No. 16, 2580-2587, doi:10.1016/j.susc.2009.06.007.

[6] Rowland, R.S., Taylor, R. (1996). Intermolecular nonbonded contact distances in organic crystal structures: Comparison with distances expected from van der Waals radii, *The Journal of Physical Chemistry*, Vol. 100, No. 18, 7384-7391, doi: 10.1021/jp953141.

[7] Alvarez, S. (2013). A cartography of the van der Waals territories, *Dalton Transactions*, Vol. 42, 8617-8636, doi: 10.1039/c3dt50599e.

[8] Rumpf, H. (1990). *Particle Technology*, Chapman and Hall, London, UK.

[9] Rabinovich, Y.I., Adler, J.J., Ata, A., Singh, R.K., Moudgil, B.M. (2000). Adhesion between nanoscale rough surfaces I. Role of asperity geometry, *Journal of Colloid and Interface Science,* Vol. 232, No. 1, 10-16, doi:10.1006/jcis.2000.7167.

[10] Rabinovich, Y.I., Adler, J.J., Ata, A., Singh, R.K., Moudgil, B.M. (2000). Adhesion between nanoscale rough surfaces II. Measurement and comparison with theory, *Journal of Colloid and Interface Science,* Vol. 232, No. 1, 17-24, doi:10.1006/jcis.2000.7168.

[11] Katainen, J., Paajanen, M., Ahtola, E., Pore, V., Lahtinen, J. (2006). Adhesion as an interplay between particle size and surface roughness, *Journal of Colloid and Interface Science*, Vol. 304, No. 2, 524-529, doi: 10.1016/j.jcis.2006.09.015.

[12] Matope, S., van der Merwe, A.F., Nemutudi, R., Nkosi, M., Maaza, M. (2011). Micro-material handling employing E-beam generated topographies of copper and aluminium, *The South African Journal of Industrial Engineering*, Vol. 22, No. 2, 175-188, doi:10.7166/22-2-24.

[13] Matope, S., van der Merwe, A.F., Rabinovich, Y.I. (2013). Silver, copper and aluminium coatings for micro-material handling operations, *The South African Journal of Industrial Engineering*, Vol. 24, No. 2, 69-77, doi: 10.7166/24-2-554.

[14] Eichenlaub, S., Gelb, A., Beaudoin, S. (2004). Roughness models for particle adhesion, *Journal of Colloid and Interface Science,* Vol. 280, No. 2, 289-298, doi:10.1016/j.jcis.2004.08.017.

[15] Škorc, G., Šafarič, R. (2012). Adaptive positioning of MEMS production system with nano-resolution, *Intelligent Automation & Soft Computing,* Vol. 18, No. 4, 381-398, doi: 10.1080/10798587.2012.10643250.

[16] Lambert, P. (2007). *Capillary Forces in Microassembly*, Springer, Boston, USA.

[17] Kraut, B. (2003). *Strojniški priročnik*, Založba Litostroj, (in Slovene), Ljubljana, Slovenia.

[18] Parsegian, V.A. (2006). *Van der Waals Forces,* Cambridge University press, UK.

[19] Montgomery, S.W., Franchek, M.A., Goldschmidt, V.W. (2000). Analytical dispersion force calculation for nontraditional geometries, *Journal of Colloid and Interface Science*, Vol. 227, No. 2, 567-584, doi: 10.1006/jcis.2000.6919.

[20] Visser, J. (1976). Adhesion of colloidal panicles, In: Matijevic, E., Borkovec, M. (eds.), *Surface and Colloid Science*, Vol. 8, John Wiley & Sons, New York, USA, 3-84.

[21] Kirsch, V.A. (2003). Calculation of the van der Waals force between a spherical particle and an infinitive cylinder, *Advances in Colloid and Interface Science*, Vol. 104, No. 1-3, 311-324, doi: 10.1016/S0001-8686(03)00053-8.

[22] Šafarič, R., Rojko, A. (2007). *Inteligentne regulacijske tehnike v mehatroniki*, (in Slovene), Tiskarna tehniških fakultet, Maribor, Slovenia.

[23] Lipkin, D.M., Israelachvili, J.N., Clarke, D.R. (1997). Estimating the metal-ceramic van der Waals adhesion energy, *Philosophical Magazine: A*, Vol. 76, No. 4, 715-728, doi: 10.1080/01418619708214205.

[24] Ahmadi, G. London-van der Waals Force, Clarkson University, from *https://webspace.clarkson.edu/projects/crcd/public_html/me437/downloads/5_vanderWaals.pdf*, accessed January 25, 2018.

[25] Attraction – Dispersion energies (2008), from *http://soft-matter.seas.harvard.edu/index.php/Attraction_-_Dispersion_energies*, accessed January 10, 2018.

[26] Bondi, A. (1966). Van der Waals volumes and radii of metals in covalent compounds, *The Journal of Physical Chemistry*, Vol. 70, No. 9, 3006-3007, doi: 10.1021/j100881a503.

[27] Batsanov, S.S. (2001). Van der Waals radii of elements, *Inorganic Materials*, Vol. 37, No. 9, 871-885, doi: 10.1023/A:1011625728803.

APEM journal
Advances in Production Engineering & Management
Volume 14 | Number 1 | March 2019 | pp 27–38
https://doi.org/10.14743/apem2019.1.309
ISSN 1854-6250
Journal home: apem-journal.org
Original scientific paper

Cutting performance of solid ceramic and carbide end milling tools in machining of nickel based alloy Inconel 718 and stainless steel 316L

Grguraš, D.[a,*], **Kern, M.**[a], **Pušavec, F.**[a]

[a]University of Ljubljana, Faculty of Mechanical Engineering, Laboratory for Machining, Ljubljana, Slovenia

ABSTRACT

Machining of nickel based alloys is in most of the times affected via high mechanical and thermal loads, causing high wear tendency of carbide tools, even at relatively low cutting speeds. On the other hand, ceramic as a cutting material, is more chemically stable and retains its hardness even at higher temperatures (> 800 °C) when machining difficult-to-cut materials. Therefore, to increase productivity, as an alternative to carbide tools, full body ceramic milling tools are proposed. In this paper, high speed milling process, using full body ceramic end milling tools, was analysed in parallel to carbide tools. Tool life of ceramic tools was compared with tool life of more widely used carbide tools when milling two different difficult-to-cut materials, i. e. nickel based alloy Inconel 718 and austenitic stainless steel 316L, under different cooling lubrication conditions. In addition, surface integrity and cost analysis were taken into account. Results are showing that ceramic milling tools are increasing material removal rate and productivity. However, the overall efficiency of ceramic tools can still be economically questionable.

ARTICLE INFO

Keywords:
Milling;
Ceramic end mill;
Carbide end mill;
Inconel 718;
Stainless steel 316L;
Productivity

**Corresponding author:*
damir.grguras@fs.uni-lj.si
(Grguraš, D.)

Article history:
Received 22 August 2018
Revised 4 March 2019
Accepted 5 March 2019

1. Introduction

Nowadays, we are increasingly focused on the sustainability of machining processes, trying to avoid conventional machining where oil based cooling lubrication fluids (oilCLFs) are used. Those are increasing manufacturing expenses and are known to be one of the contaminants in environment, as well are harmful to human's health. Therefore, significantly cleaner and more environmentally friendly machining process would be dry machining. However, lack of cooling and lubricating effect, especially when machining difficult-to-cut materials, can reflect in high temperatures in the cutting zone, which shorten tool life and decrease productivity. In such cases, one of the options to increase productivity is to use other cooling lubrication techniques, such as cryogenics [1], or different tool materials, as ceramic, which can withstand higher temperatures then widely used carbide tools.

Ceramic, as a cutting material, appeared relatively early (in 1935, USA), but its use was not economically justified until the 1960s. Ceramics main advantage is that it is stable even at high temperatures and in such retains its hardness (high compressive strength), has a good wear resistance and is chemically stable at elevated temperatures. To manufacture ceramic end milling tools, sintering manufacturing process is used. The fine-grained powder is pressed under high pressure and bounded at temperatures between 1200-1800 °C. Properties of the ceramic tools depend of the composition, the density of the structure, size and distribution of the grain

and the sintering temperature. Due to these unique ceramic properties, ceramic tools are mainly used for machining of difficult-to-cut materials, primarily thinking of titanium and nickel based alloys that are unable to be machined with carbide tools without oilCLFs [2, 3]. An additional advantage of ceramic tools is that the cutting speed is three to ten times higher as at carbide tools, which contributes to a higher material removal rate (MRR) and consequently higher productivity [4]. However, researches [5] marked poor resistance of ceramic tools to dynamic mechanical stress, as main disadvantage of these tools.

Narutaki *et al*. [6] were observing tool wear of three different ceramic tools when turning Inconel 718. They realized, if they use lower cutting speeds (100-300 m/min), best durability offers ceramic Al_2O_3 with added silicon carbide. If, however, the cutting speed is raised to a 500 m/min, more durable tool turns to be Al_2O_3 with added TiC. They have explained this by diffusivity tests and temperature measurements. When machining with high cutting speeds, flank face has reached 1250-1300 °C, while the melting point of the Inconel 718 is 1550 °C. At such high temperature, diffusion is evident; when using ceramic tool with added SiC, diffusion of nickel from the workpiece material into the tool occurs. When using Si_3N_4 ceramics, silicon passes into Inconel 718 and chromium backwards into the tool. They marked Al_2O_3-TiC tool as most stable tool in such working conditions. Kitagawa *et al*. [7] also came to the same conclusion.

Performances of ceramic tools reinforced with SiC, when milling Inconel 718, were researched by Elbestawi *et al*. [8]. They noticed three types of tool wear: (i) abrasion on the flank face, (ii) notch wear and (iii) the cavity on the rake face. Notch wear was the main reason for the tool failure when milling at full depth, with cutting speeds from 200 to 400 m/min. When milling with higher cutting speeds (400-700 m/min) and a smaller depth of cut, flank wear and wear on the secondary edge were the most dominant.

Li *et al*. [9] have analysed performance of SiAlON ceramic tools (Si_3N_4-Al_2O_3) when turning Inconel 718. For SiAlON ceramic tools notch wear with minimal damage of the cutting edge at low cutting speed (120 m/min) is noticeable. That begins to change at 240 m/min. When the speed is increased to 300 m/min, it is already possible to see a decrease in the notch formation and increase in flank wear.

From most of published scientific researches, it has been observed that removable ceramic cutting tools – inserts were used. There are only a few scientific studies in which full body ceramic cutting tools were used. The reason for this lies in the complex manufacturing processes of ceramic rods and in complex grinding processes to manufacture full body ceramic tools. Some improvements on this field are presented in a paper of Uhlmann and Hubert [10], where proved that the nature of these ceramic cutting tools heavily depends on its composition.

Celik *et al*. [11] investigated wear mechanisms of solid SiAlON ceramic tools when milling Inconel 718. They showed that there were present severe adhesion of workpiece and formation of diffusion layer due to chemical interaction of the tool flank face and the workpiece. Additionally, high operating temperature of the tools (>1000 °C) was observed. It was found that thermal expansion coefficient of the diffusion layer on the tool is lower than expansion coefficient of the tools material. Therefore, thermal micro cracks were formed causing tool wear.

Wang and Liu [12] made another study on full body ceramic tools, where they investigated cutting performances of different solid ceramic end milling tools in comparison with carbide tool in machining hardened AISI H13 steel. They came to conclusion that cutting forces of ceramic end milling tools are lower than that of the carbide tool, mainly due to low chemical activity of ceramic with workpiece material. Overall, Ti(C, N) ceramic end milling tools present best cutting performance considering cutting forces, surface quality and tool life.

Many industrial applications demand machining process to be carried out in tight and narrow pockets and this can be only done with usage of solid end milling tools. According to the above presented review on the state of the art, it can be found that most of the studies were performed on the Inconel 718, as workpiece material, and with usage of ceramic cutting inserts, as a cutting tool. Moreover, there is a lack of studies using full body ceramic tools. To fulfil that gap, authors performed preliminary experiments [13] using full body ceramic milling tools in machining of Inconel 718, where they confirmed their suitability for milling of Inconel 718. Their cutting performance, when machining other workpiece materials, and their cost efficiency, in comparison

to conventional carbide tools, were still questionable. Thus in this paper, full body ceramic end milling tools were used to machine two difficult-to-cut materials, i. e. nickel based alloy Inconel 718 and austenitic stainless steel (SS) 316L, under different cooling lubrication conditions. Focus is placed on analysis of tool wear, tool life, workpiece surface and nevertheless, the productivity and costs.

2. Materials and methods

2.1 Workpiece materials

Difficult-to-cut nickel based alloy Inconel 718 and austenitic stainless steel (SS) 316L in the form of rods, with a diameter of 50 mm and a length of 200 mm, were used as a workpiece materials. Physical properties of both materials are presented in Table 1. Properties as high melting point, heat and wear resistance and high hardness at room temperature, are causing difficulties in machining operations.

Nickel based alloy Inconel 718 is used in the most demanding operating conditions, in the presence of high pressures and high temperatures. Inconel 718 is often used in gas turbines for turbine blades in turbo-compressors as the rotor, in the nuclear power plants, in racing cars, weapons, the high temperature heat exchangers, etc. Machining of Inconel 718 with conventional machining processes with oil CLFs is difficult, due to remarkable strain hardening [16]. Thus, when machining Inconel 718, aggressive strategy is what we are looking for in order to increase the temperature to cause material softening that improves machining performances. In this manner, ceramic tools can be used due to their high temperature resistance [17-19].

Stainless steels are chromium-nickel alloys and can be divided into three basic groups: martensitic steels, ferritic steels, and austenitic steels [20]. Most stainless steels are austenitic and are non-magnetic and cannot be quenched, but they can be welded. Moreover, they are also classified as difficult-to-cut alloys. Austenitic stainless steel 316L, also used in this research, is due to its properties widely used in the food, aerospace and pharmaceutical industry [21].

Table 1 Physical properties of nickel alloy Inconel 718 and stainless steel 316L [14, 15]

Physical property	Inconel 718	SS 316L
Density [g/cm^3]	8.2	7.9
Hardness [HRc]	36	25-39
Tensile strength [MPa]	1240	485
Thermal conductivity [W/m·K]	11.4	15
Specific heat [J/kg·K]	435	500
Melting point [°C]	1260-1336	1375-1400

2.2 Cutting tools and cutting parameters

Ceramic tools have unique physical and mechanical properties, such as high hardness and low chemical reactivity with steels and many other materials. Consequently, they can be used to machine difficult-to-cut materials that are hard to be carried out with traditional tool materials. Thus, in this work, the solid ceramic end mills are compared with widely used carbide cutting tools. 6 edge flat Kennametal EADE (0600A6ARF) solid ceramic end milling tools, based on Si-AlON ceramic with CVD alumina coating and grade KYS40, were chosen. They have optimised geometry for roughing nickel based high temperature alloys and are not suitable for finishing applications. Chosen carbide tools were 5 edge Kennametal HARVI II series (UCDE0600A5ASA) KC643 grade, PVD coated with fine grain grade AlTiN coat. Diameter *D* of the tools was 6 mm.

First experiments were carried out on machining Inconel 718 with ceramic end milling tools using cutting parameters as proposed by manufacturer. However, tool breakage occurred related to the failures of cutting edges and/or tool stems, as shown in Fig 1.

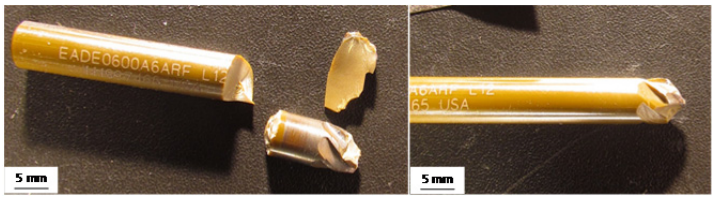

Fig. 1 Failure of cutting edges (left) and tool stem (right)

Table 2 Cutting parameters

	Workpiece material	Teeth per tool, z [/]	Rotational speed of the tool, n [min^{-1}]	Cutting speed, v_c [m/min]	Depth of cut, a_p [mm]	Width of cut, a_e [mm]	Feed speed, v_f [mm/min]	Feed per tooth, f_z [mm/tooth]
Ceramic tool	Inconel 718 and SS 316L	6	31830	600	0.375	4.0	4583	0.024
Carbide tool	Inconel 718	5	2122	40	9.00	1.8	202	0.019
	SS 316L	5	4244	80	9.00	1.8	615	0.029

With further experiments, we came to conclusion that tools failed due to mechanical overload in radial direction because of too big depth of cut (a_p = 4.5 mm) and small width of cut (a_e = 0.6 mm). To change the direction of mechanical loads, from radial to axial direction, milling strategy was changed. Depth of cut was reduced and width of cut was increased without affecting the MRR, consequently milling strategy was changed from side to face milling. New cutting parameters for ceramic tools were determined in collaboration with the tool manufacturer and are shown in the Table 2. Cutting parameters for carbide tools, also shown in Table 2, were given by the manufacturer.

2.3 Execution of experiments

Milling of nickel based alloy Inconel 718 and stainless steel 316L were performed under different cooling lubrication conditions: in a dry, with minimal quantity lubrication (MQL), and with a blast of air in the case of ceramic tools and, in the case of carbide tools, flooding with emulsion. The third scenario represents the reference scenario for both.

As a machining strategy on a high speed machining center Sodick MC 430 L, spiral strategy towards the center of the workpiece (Fig. 2) was chosen. Thus, continuous machining without interruptions and consequentially with less temperature fluctuations, which can result in tool damage, has been assured. The machining surface of workpiece rod was top end surface, which was clamped as shown in Fig. 2. One spiral milling from the outer diameter to the center of the round represents one level. After every level of removed material, the wear of the cutting tool was measured. The measurement were executed on 3D measuring device Alicona InfiniteFocus SL, where flank wear values were determined reaching the criteria VB = 0.3 mm or VB_{max} = 0.6 mm. Thus, tool life was obtained. Moreover, workpiece surface was analysed over energy-dispersive X-ray spectroscopy (EDX) using the scanning electron microscope (SEM) Jeol JSM 5610. Chips were also analysed. In addition, to get justification of the process from financial point of view, cost analysis was carried out.

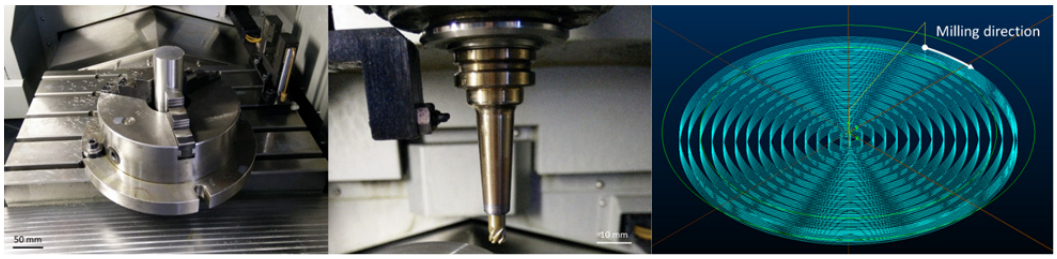

Fig. 2 Workpiece clamping (left), shrink-fit ceramic tool clamping (middle), spiral milling strategy (right) [13]

3. Results and discussion

3.1 Tool life and tool wear mechanisms

During the experiments, the flank wear of end milling tools were measured with 3D measuring device Alicona InfiniteFocusSL. Tool life shown in Fig. 3 was recorder when the flank wear of the tools reached VB = 0.3 mm or VB_{max} = 0.6 mm. However, this requirement was not always reached. In case fracture of the cutting tool/edge has been observed, this has also been treated as end of the tool life.

In the experiments, where carbide tools were used for machining SS 316L, cooling and lubrication conditions had major influence on the tool life. Tool life in dry machining was only 25.9 min, while in MQL and flood conditions tool life was prolonged to more than 375 min (for both conditions equally). In all of the experiments, no significant flank wear could be noticed. Before the cutting edge breakage, no flank wear was noticed, minor damages of cutting edge occurred, i.e. chipping (Fig. 4). Tool life of carbide tools, when machining Inconel 718, was significantly shorter in comparison to those used for machining SS 316L. Due to strain hardening of Inconel 718, breakage of the cutting edge is the main reason for tool failure. Best result of 6.0 min was achieved when flooding was used, while in dry the tool life reached 2.3 min and with MQL 3.8 min.

In the experiments, where ceramic tools were used for machining SS 316L, flank wear was evident. In dry conditions, the main wear mechanism was diffusion, the threshold of tool life was achieved in 1.2 min. When air-blast and MQL were used, tool life was longer (4.8 min and 4.4 min, respectively). As the tool wear increased, the amount of BUE also increased, influencing the cutting geometry in the cutting zone. Main wear mechanism was diffusion (also confirmed in [11]), chipping of the cutting edge was also present, unlike when machining Inconel 718, where this was the main wear mechanism (Fig 5). Because of chipping, geometry of the cutting edge changed, what resulted in chips being welded on the cutting edge (BUE). As a consequence, severe deformation of the workpiece material occurred, which resulted in even more severe material strain hardening. This normally increases forces applied to the end milling tool and loads on the cutting edge. Additionally, the flow of the workpiece material also changes, what was evident by the fact that there was much more chip side flow present. In dry condition, the tool life equals 3.1 min, when using air-blast it was 3.2 min, and when using MQL, it was only 0.8 min (due to breakage of the cutting tooth). Thus, it can be concluded that carbide tools have significantly shorter tool life when machining nickel-based alloy in comparison with stainless steel. This difference is not so significant when using ceramic cutting tools.

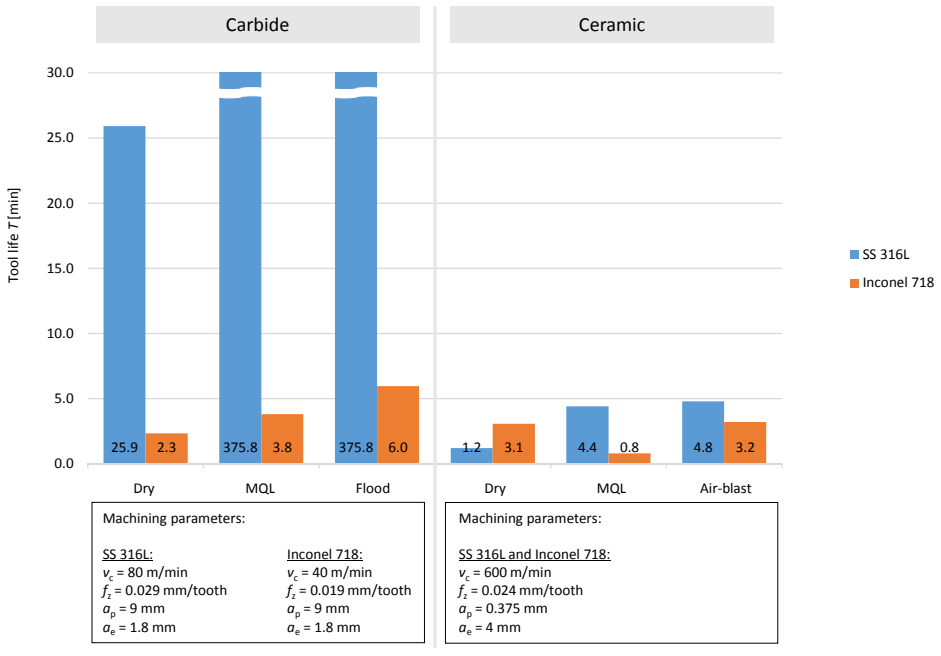

Fig. 3 Tool life achieved when milling Inconel 718 and SS 316L with ceramic and carbide tools

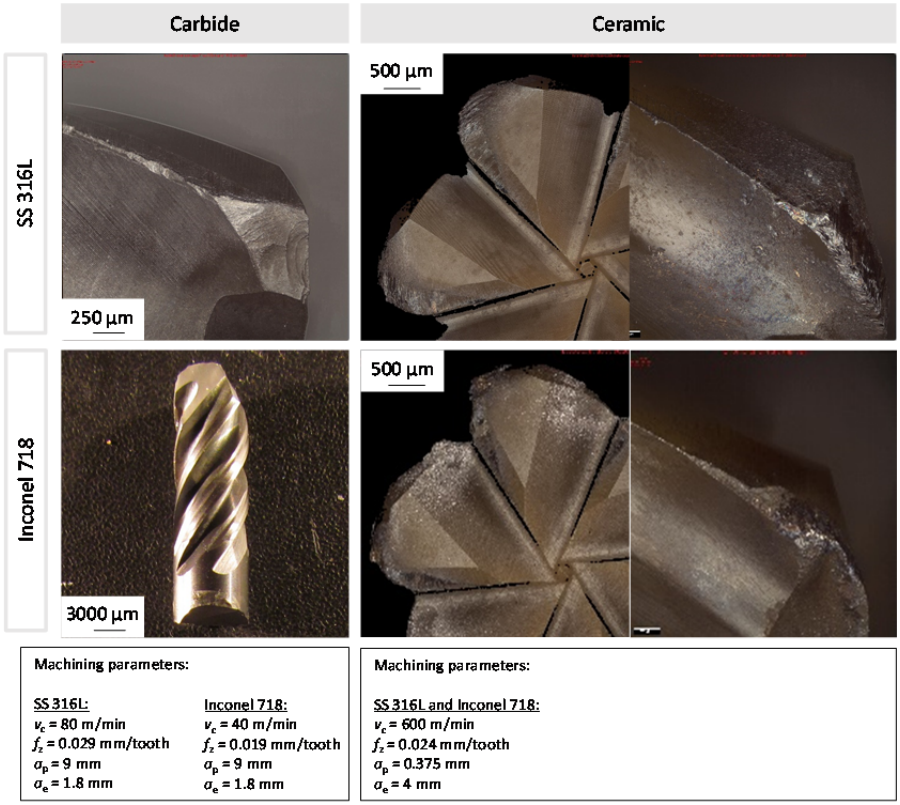

Fig. 4 Wear mechanisms of ceramic (with air-blast) and carbide tools (with flood) when milling Inconel 718 and SS 316L

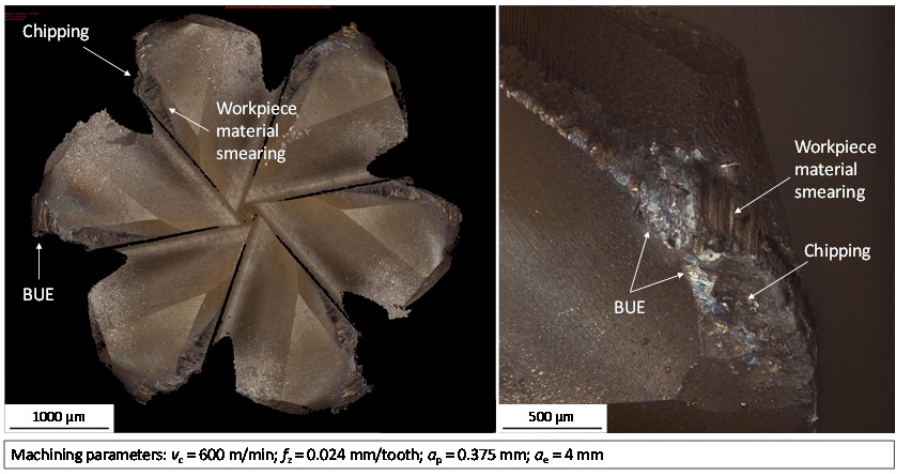

Fig. 5 Wear morphology for ceramic end milling tool (when dry machining Inconel 718) [13]

Furthermore, using scanning electron microscope (SEM) images of new and worn ceramic end milling tool were taken and analysed, as shown in Fig. 6. On different locations of the tool, energy-dispersive X-ray spectroscopy (EDX) was performed to get chemical characterization or elemental analysis of specimen's analysed section. When new ceramic end milling tool was analysed, EDX spectrum showed that it consists mainly of the Si, Al, O elements, which was anticipated, as this are the main elements of SiAlON ceramics. When worn out ceramic end milling tool was analysed, EDX analysis was performed on 3 different sections of the specimen. As it can be seen from the Fig. 6, the first section with label 1, contains Cr, Ni, Fe and other elements that fit into the chemical composition of Inconel 718 alloy. This means that workpiece material was smeared over the tool surface (also shown in Fig. 5). Under this layer of workpiece material, diffusion is taking place. This layer has different thermal expansion coefficient as material of the tool, what means that during temperature fluctuations tool expands differently as main material.

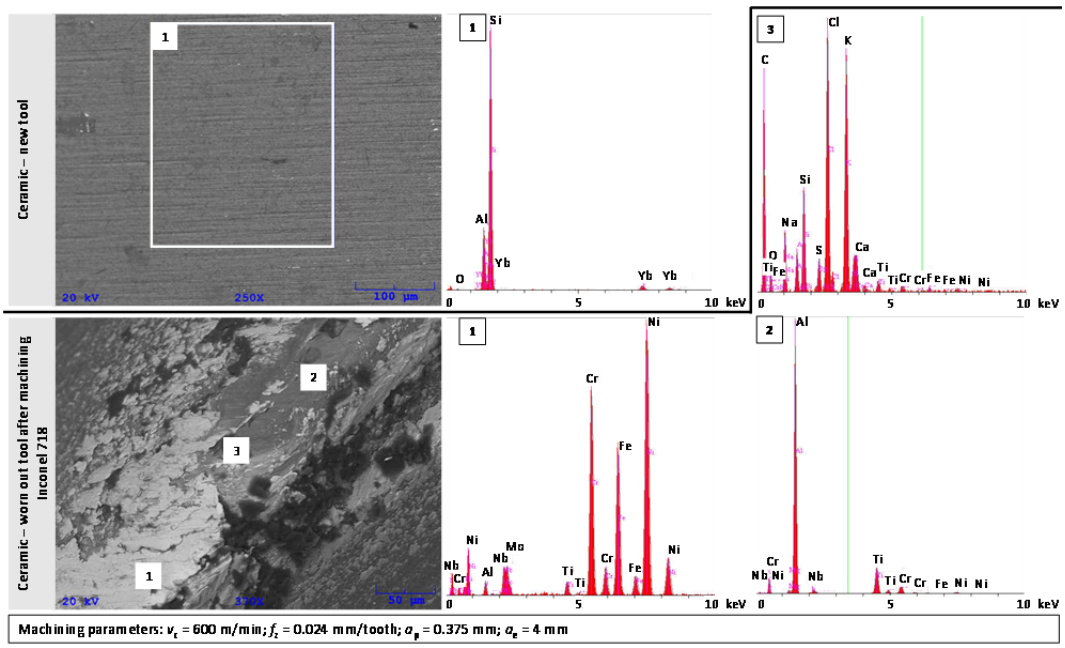

Fig. 6 SEM-EDX analysis of ceramic tool; new tool and worn out tool after machining Inconel 718

This result in the occurrence of micro cracks on the cutting tool and its edges. Spectrum analysis of section 2 in Fig. 6 showed that this is the area of the tool where the surface of the tool already chipped away during milling and consists out of elements that are found in used ceramic material. Section 3 consists of C, CL, K and other elements which are not main components neither of workpiece or tool material. Darker spots in Fig. 6 are impurities that have been left on the tool after the machining process, during the transportation and handling with the specimen.

Ceramic tools achieved longer tool life than carbide tools only for dry machining of Inconel 718. Based on tool life alone, it seems that ceramic performance was lower than that of the carbide tools. However, ceramic tools used in this research have optimized geometry for roughing and therefore, are not suitable for finishing applications. Therefore, volume of removed work-

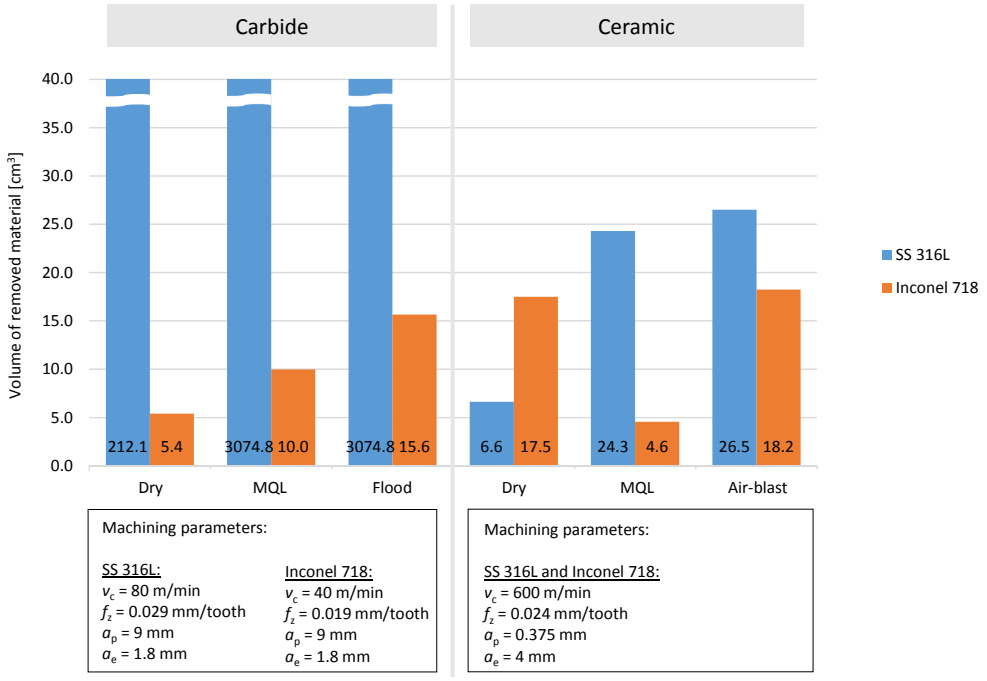

Fig. 7 Volume of removed material when milling Inconel 718 and SS 316L with ceramic and carbide tools

piece material (productivity) was taken into consideration. Fig. 7 shows volume of removed material that each tool removes in its lifetime. In all the experiments, where SS 316L was used, carbide tools outperformed ceramic end milling tools. On the contrary, when machining Inconel 718, ceramic tools in two experiments (out of six) removed more material then carbide tools. Ceramic tools in dry machining of Inconel 718 removed 17.5 cm^3 and 18.2 cm^3 when air-blast was used. The highest amount removed with carbide tools was 15.6 cm^3, in flood cooling lubrication conditions. The results show that ceramic end milling tools are capable of removing more workpiece material, regardless of their shorter lifetime. This is possible due to their much higher material removal rate.

3.2 Workpiece surface analysis

Fig. 8 is showing SEM and EDX images/results of SS 316L before and after machining, where two different structures were found. EDX spectroscopy showed that structure with label 1 is small ceramic particle, part of the tool, which chipped away during machining. Other darker structures (with label 2) are made primarily from carbon, what indicates some organic dirt/impurities.

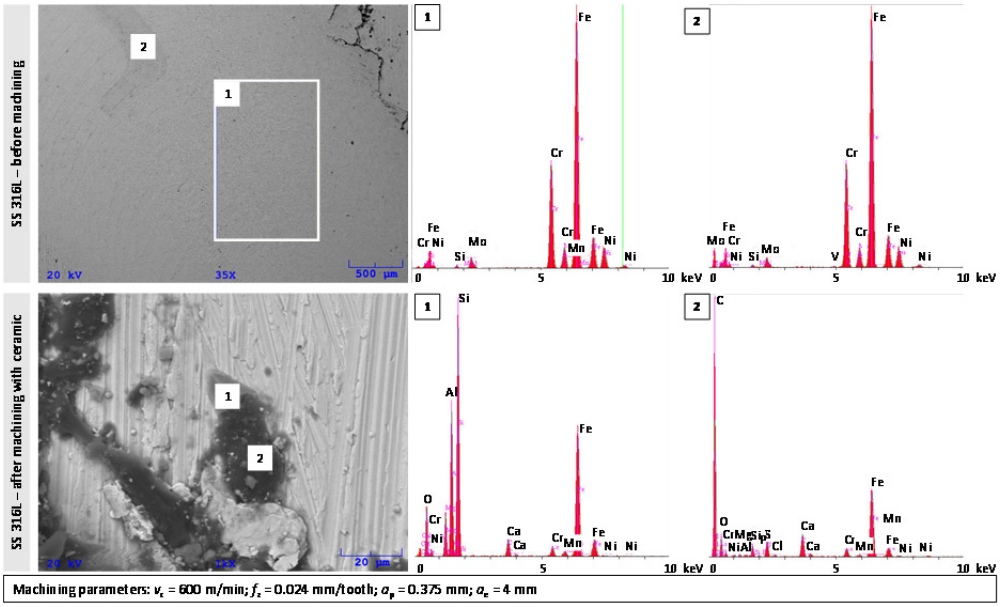

Fig. 8 SEM-EDX analysis of SS 316L; before and after machining with ceramic tool

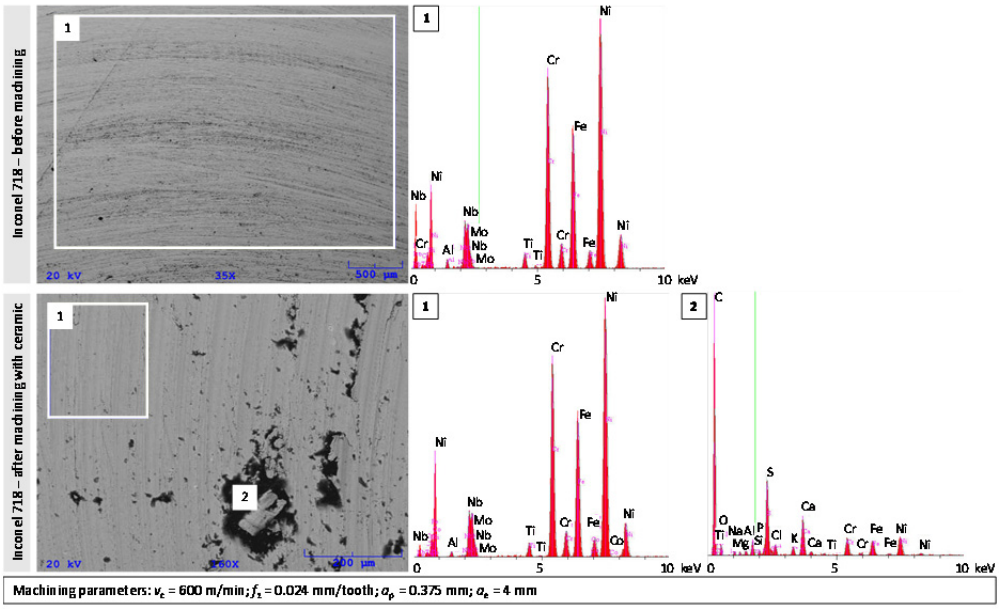

Fig. 9 SEM-EDX analysis of Inconel 718; before and after machining with ceramic tool

These two structures (small ceramic structures and dirt) can only be found on the parts of the machined workpiece surface where the material side-flow appeared during machining process.

EDX analysis of Inconel 718 workpiece (Fig. 9), before and after machining, showed that in machined surface many imperfections can be found. In these recesses, different dirt/impurities are stuck which mainly consists out of carbon.

3.3 Chip shapes

During the milling experiments, chips were collected for further analysis and comparison. The chips formed at different experiments are shown in Fig. 10. In all the experiments, where workpiece (SS 316L and/or Inconel 718) was machined with carbide tools, either with a new or worn out tool, no major differences in chip thickness, width and all in all appearance was noticed. Their length was 9.00 mm, width 0.54 mm and their thickness was 0.096 mm. The only difference that can be observed between chips are some scratch marks on the chips produced while machining with worn tool. After further analysis, it was seen that the tool's cutting edge was damaged, via noticed chipping of the cutting edge.

In experiments, where ceramic end milling tools were used, the cutting speed was much higher than for carbide tools. Consequentially, temperature in the cutting zone was also higher. This plays an important role in cutting performance [22]. If the temperature in the cutting zone is lower than softening temperature of the work material, then it is easier for this material to strain harden [23]. Therefore, beneficial in those machining application is to reach the cutting temperature that is higher than critical temperature, reducing the cutting forces and prolonging the tool life. The observations from this are consistent with results presented in [24]. With other words, cutting temperature plays a very important role in cutting of Inconel 718 and, at the same time, it influences the chip formation. In experiments, where ceramic end milling tools were used, chips were small, in shape of dust and small particles, regardless of workpiece material machined. With the progression of tool wear, chips were getting smaller and a few elementary curled swirl chips occurred. During milling, these chips were formed from side flow material.

From the cooling lubrication point of view, regardless of the strategy that was used in both cases, when carbide or ceramic tools were used, there was no significant difference in form of chips (dry, air-blast, MQL or flood) observed.

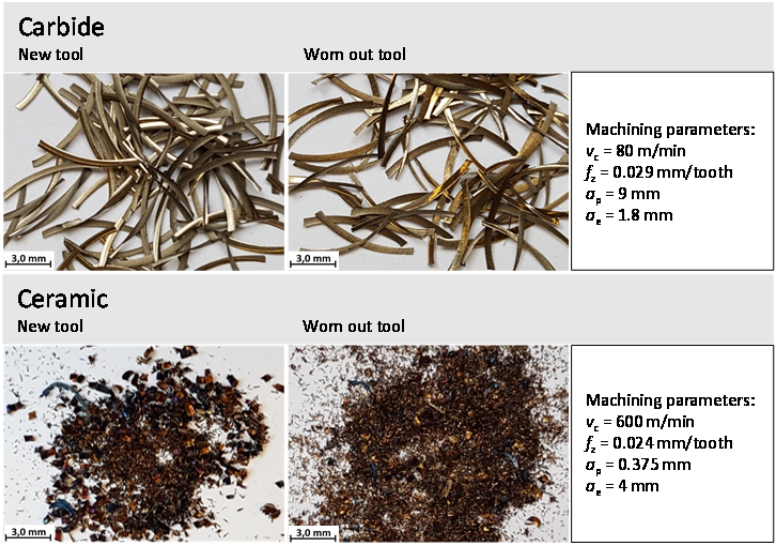

Fig. 10 Chip shapes formed when milling SS 316L with ceramic and carbide tools (dry conditions)

3.4 Cost analysis

Selection of tools in industrial applications is not only performed based on tools' performance, but also on its costs. In this research, total manufacturing cost for using ceramic or carbide tools were calculated. C_{total} is defined by Eq. 1, where C_{tool} is the total tooling cost, C_{change} is the total cost of tool changes, and $C_{\text{machining}}$ is the cost of machining time required. All three costs are nor-

malized in the way that present expenses required to remove 1 cm³ of workpiece material. In this way, the productivity (MRR), as well as costs, can be compared between different tool performances. With this omitted is the problem with presenting results in relation to different MRR values of processes. C_{tool} can be written as Eq. 2, where C_{tool} is the cost of the tool and V_{total} is the volume of removed material with single tool. For calculations, cost of 93 € per ceramic tool and 44.2 € per carbide tool were considered. C_{change} can be calculated using Eq. 3, where $C_{\text{machining}}$ is the cost of machining per unit time, including machining labour cost, i.e. 40 €/h and t_{change} that represents the time to change a single tool (that includes a collection of non-machining time, set to 5 min). $C_{\text{machining}}$ can be calculate by Eq. 4, where MRR is material removal rate given by Eq. 5, where T presents the tool life.

$$C_{\text{total}} = C_{\text{tool}} + C_{\text{change}} + C_{\text{machining}} \tag{1}$$

$$C_{\text{tool}} = c_{\text{tool}}/V_{\text{total}} \tag{2}$$

$$C_{\text{change}} = \frac{c_{\text{machining}} \cdot t_{\text{change}}}{60} \Big/ V_{\text{total}} \tag{3}$$

$$C_{\text{machining}} = c_{\text{machining}}/(\text{MRR} \cdot 60) \tag{4}$$

$$\text{MRR} = V_{\text{total}}/T \tag{5}$$

Cost analyses were performed and compared for experiments where longest tool life have been achieved. Results presented in Fig. 11 are showing that regardless of workpiece material, ceramic tools are more expensive than carbide tools. In experiments, where carbide tools were used for machining SS 316L (in flood conditions), the main expenses were machining costs. Tool costs and tool changing costs were insignificant due to long tool life. On the contrary, in other three experiments, tool life results were significantly shorter, which reflected in tool costs as the main expense. Regarding productivity, ceramic milling tools are offering 115 % higher MRR than carbide tools only when machining Inconel 718. However, there are still 39 % higher overall expenses of ceramics over carbide tools, as saved time due to higher productivity has less impact on total machining costs than purchase price of the tool.

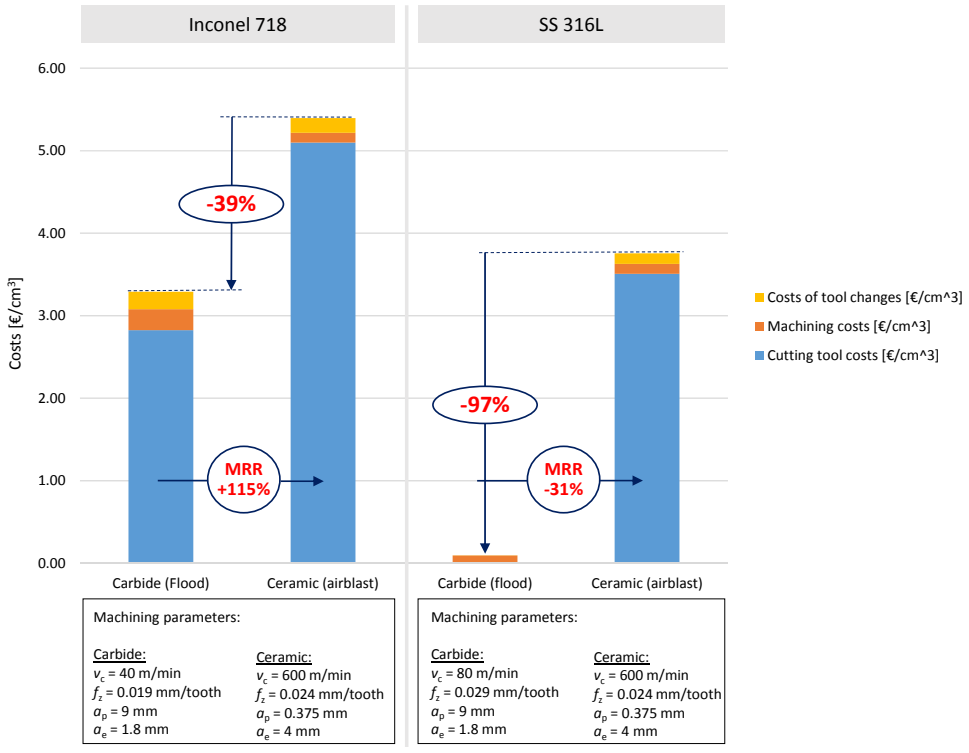

Fig. 11 Cost analysis when milling Inconel 718 and SS 316L with ceramic and carbide tools

4. Conclusion

This research comparatively investigates the cutting performance of solid ceramic end milling tools in machining of nickel based alloy Inconel 718 and austenitic stainless steel 316L, under different cooling lubrication conditions. Main objective was to determine machining performance of solid ceramic end milling tools in comparison with solid carbide tools, as most of the studies were done using interchangeable cutting inserts. Tool wear, tool life, workpiece surface and chip shapes and machining costs were analyzed. From the results concluded can be that:

- Ceramic end milling tools have the longest tool life in dry milling conditions, i.e. 3.1 min (dry) or 3.2 min (air-blast). In addition, air blasting can improve chip evacuation and therefore, can prolong tool life of the ceramic tools. Furthermore, carbide tools should be used only in wet cooling and lubrication conditions (flooding with emulsion).
- Main tool wear mechanism, using ceramic tools, is chipping of the cutting edge. This wear is especially pronounced when using MQL, which indicates that ceramic tools are prone to brittle fracturing when they are exposed to fast temperature changes.
- Carbide tools with appropriate cooling and lubrication outperforms ceramic tools when machining SS 316L. It can be seen, that carbide tools in comparison with ceramic tools, had longer tool life and removed more material, which resulted also in a lower overall costs.
- Ceramic tools provide better cutting performance in comparison with carbide tools only when machining of nickel based alloy Inconel 718 is performed dry. Moreover, ceramic end milling tools, which are offering higher MRR, removed more material in lifetime (18.2 cm^3) than carbide tools (15.6 cm^3). However, it is still questionable, if these differences are sufficient to cover the 39 % higher overall expenses of ceramics over carbide tools.

Acknowledgement

The authors gratefully acknowledge the support of the Slovenian Research agency (ARRS) for founding the research project L2-8184 and research program P2-0266. Authors also express their gratitude to the Kennametal Tools (USA) and prof. dr. Borut Kosec from Faculty of Natural Sciences and Engineering, Ljubljana (SLO) for their support.

References

[1] Jawahir, I.S., Attia, H., Biermann, D., Duflou, J., Klocke, F., Meyer, D., Newman, S.T., Pusavec, F., Putz, M., Rech, J., Schulze, V., Umbrello, D. (2016). Cryogenic manufacturing processes, *CIRP Annals – Manufacturing Technology*, Vol. 65, No. 2, 713-736, doi: 10.1016/j.cirp.2016.06.007.

[2] Kopač, J., Soković, M. (1993). *Machining technique – Modern cutting tools,* (in Slovene), University of Maribor, Faculty of Mechanical Engineering, Ljubljana, Slovenia.

[3] Čuš, F. (1996). *Machining technique,* (in Slovene), University of Maribor, Faculty of Mechanical Engineering, Maribor, Slovenia.

[4] Aruna, M., Dhanalakshmi, V., Mohan, S. (2010). Wear analysis of ceramic cutting tools in finish turning of Inconel 718, *International Journal of Engineering Science and Technology,* Vol. 2, No. 9, 4253-4262.

[5] Arunachalam, R., Mannan, M.A. (2000). Machinability of nickel-based high temperature alloys, *Machining Science and Technology*, Vol. 4, No. 1, 127-168, doi: 10.1080/10940340008945703.

[6] Narutaki, N., Yamane, Y., Hayashi, K., Kitagawa, T., Uehara, K. (1993). High speed machining of Inconel 718 with ceramic tools, *CIRP Annals,* Vol. 42, No. 1, 103-106, doi: 10.1016/S0007-8506(07)62402-0.

[7] Kitagawa, T., Kubo, A., Maekawa, K. (1997). Temperature and wear of cutting tools in high speed machining of Inconel and Ti-6Al-6V-2Sn, *Wear*, Vol. 202, No. 2, 142-148, doi: 10.1016/S0043-1648(96)07255-9.

[8] El-Bestawi, M.A., El-Wardany, T.I., Yan, D., Tan, M. (1993). Performance of whisker-reinforced ceramic tools in milling nickel-based alloy, *CIRP Annals,* Vol. 42, No. 1, 99-102, doi: 10.1016/S0007-8506(07)62401-9.

[9] Li, L., He, N., Wang, M., Wang, Z.G. (2002). High speed cutting of Inconel 718 with coated carbide and ceramic inserts, *Journal of Materials Processing Technology*, Vol. 129, No. 1-3, 127-130, doi: 10.1016/S0924-0136(02)00590-3.

[10] Uhlmann, E., Hübert, C. (2011). Tool grinding of end mill cutting tools made from high performance ceramics and cemented carbides, *CIRP Annals,* Vol. 60, No. 1, 359-362, doi: 10.1016/j.cirp.2011.03.106.

[11] Çelik, A., Sert Alağaç, M., Turan, S., Kara, A., Kara, F. (2017). Wear behavior of solid SiAlON milling tools during high speed milling of Inconel 718, *Wear*, Vol. 378-379, 58-67, doi: 10.1016/j.wear.2017.02.025.

[12] Wang, B., Liu, Z. (2016). Cutting performance of solid ceramic end milling tools in machining hardened AISI H13 steel, *International Journal of Refractory Metals and Hard Materials*, Vol. 55, 24-32, doi: 10.1016/j.ijrmhm.2015.11.004.
[13] Grguraš, D., Kern, M., Pušavec, F. (2018). Suitability of the full body ceramic end milling tools for high speed machining of nickel based alloy Inconel 718, *Procedia CIRP*, Vol. 77, 630-633, doi: 10.1016/j.procir.2018.08.190.
[14] BSSA. Chemical compositions of AISI (ASTM/ASME) and UNS austenitic stainless steel grades, from *http://www.bssa.org.uk/topics.php?article=183*, accessed January 16, 2018.
[15] ESPI Metals. Inconel 718, from *http://www.espimetals.com/index.php/technical-data/91-inconel-718*, accessed January 16, 2018.
[16] Krajewska-Śpiewak, J., Gawlik, J., Piekoszewski, W.; Stachura, K. (2018). Identification of residual stresses in a surface layer of Ti6AL4V and inconel 718 after process of peripheral milling, *Tehnički Vjesnik – Technical Gazette*, Vol. 25, No. 1, 88-91, doi: 10.17559/TV-20160531085315.
[17] Ozcelik, B., Oktem, H., Kurtaran, H. (2005). Optimum surface roughness in end milling Inconel 718 by coupling neural network model and genetic algorithm, *The International Journal of Advanced Manufacturing Technology,* Vol. 27, No. 3-4, 234-241, doi: 10.1007/s00170-004-2175-7.
[18] Choudhury, I.A., El-Baradie, M.A. (1998). Machinability of nickel-base super alloys: Machinability of nickel-base super alloys: A general review, *Journal of Materials Processing Technology*, Vol. 77, No. 1-3, 278-284, doi: 10.1016/S0924-0136(97)00429-9.
[19] Maiyar, L.M., Ramanujam, R., Venkatesan, K., Jerald, J. (2013). Optimization of machining parameters for end milling of Inconel 718 super alloy using Taguchi based grey relational analysis, *Procedia Engineering*, Vol. 64, 1276-1282, doi: 10.1016/j.proeng.2013.09.208.
[20] Kaladhar, M., Subbaiah, K.V., Rao, C.H.S. (2012). Machining of austenitic stainless steels – A review, *International Journal of Machining and Machinability of Materials*, Vol. 12, No. 1-2, 178-192, doi: 10.1504/IJMMM.2012.048564.
[21] Ravani Acciai. Austenitic stainless steel – AISI 316L, from *http://www.ravaniacciai.it/aisi 316l/listtables sl 101.aspx*, accessed January 16, 2018.
[22] Motorcu, A.R., Kuş, A., Arslan, R., Tekin, Y., Ezentaş, R. (2013). Evaluation of tool life – Tool wear in milling of Inconel 718 superalloy and the investigation of effects of cutting parameters on surface roughness with Taguchi method, *Tehnički Vjesnik – Technical Gazette*, Vol. 20, No. 5, 765-774.
[23] Alkali, A., Ginta, T.L., Abdulrani, A.M., Fawad, H., Danish, M. (2016). Study on the machinability of 316L stainless steel using flame assisted machining, *Journal of Engineering and Applied Sciences*, Vol. 11, No. 14, 8743-8749.
[24] Liao, Y.S., Lin, H.M., Wang, J.H. (2008). Behaviors of end milling Inconel 718 superalloy by cemented carbide tools, *Journal of Materials Processing Technology*, Vol. 201, No. 1-3, 460-465, doi: 10.1016/j.jmatprotec. 2007.11.176.

APEM journal
Advances in Production Engineering & Management
Volume 14 | Number 1 | March 2019 | pp 39–50
https://doi.org/10.14743/apem2019.1.310
ISSN 1854-6250
Journal home: apem-journal.org
Original scientific paper

Two-stage product design selection by using PROMETHEE and Taguchi method: A case study

Crnjac, M.[a,*], **Aljinovic, A.**[a], **Gjeldum, N.**[a], **Mladineo, M.**[a]

[a]University of Split, Faculty of Electrical Engineering, Mechanical Engineering and Naval Architecture, Split, Croatia

ABSTRACT

The main goal of this paper was to introduce the methodology for product design selection. The proposed methodology combines two classical methods to find the most appropriate design for the new product, through a reduced number of alternatives (product variants) and experiments for the selection process. In the first stage, the multi-criteria decision-making method, PROMETHEE was used for selecting the most suitable design, according to the chosen preferences and criteria. In the second stage, the Taguchi method was used in order to define the most appropriate parameters for selected suitable design. The fundamental scientific contribution of this paper refers to a benefit introduced by combining these methods. This benefit is related to the reduction of product development time which has a significant effect on manufacturing process time due to the high market pressure. The proposed methodology was applied to find the appropriate table design for CNC milling machine located in the Lean Learning factory. However, this is just one case study to present the proposed methodology which can be applied for other optimization of other product designs. Before applying the proposed methodology for this case study, the methodology is validated on a simple example.

ARTICLE INFO

Keywords:
Learning factory;
Lean manufacturing;
Design optimization;
PROMETHEE method;
Taguchi method;

**Corresponding author:*
mcrnjac@fesb.hr
(Crnjac, M.)

Article history:
Received 9 October 2018
Revised 25 February 2019
Accepted 27 February 2019

1. Introduction

Decision-making support in production is very important because it increases the competitiveness of companies. The digitalization introduction into the production system brings better support for decision-making. This is especially expressed during the development process of a new product. Embedded in 3D software, which is widely used for product design, there is also a very popular function of the Finite Element Method (FEM) simulation. During the development period of a new product, the methodology is very important because of the consequences that can affect cost and quality. Simulation helps to visualize how will the new product "behave" in its environment under the influence of different environmental factors. The step where it is necessary to choose the optimal design of that product represents the step of decision-making. This step means that the decision-maker identifies and selects an alternative from the set of alternatives (new product variants) based on its own preferences. Usually, there are several criteria to deal with, thus creating the multi-criteria problem and requiring multi-objective optimization.

However, product design is a very complex problem, since the criteria are very often mutually conflicting, resulting with engineering trade-off when some product properties are deliberately weakened in favour of some more important property. It means that the decision-makers preferences are known and that enables solving product design problems with some of the Multi-Criteria-Decision-Making (MCDM) methods. MCDM is a discipline that includes mathematics,

management, informatics, psychology, social science and economics. To solve the problem of choice and ranking, PROMETHEE method is often used [1]. MCDM methods are very popular in different areas, especially in operation research and logistics [2-4]. Avikal *et al.* [5] integrated Fuzzy Analytic Hierarchy Process (AHP) and PROMETHEE method in order to select tasks for assignment to the disassembly line. Fuzzy AHP was used to calculate the weights of each selected criterion while the PROMETHEE method was used for ranking the tasks. Peko *et al.* [6] showed the conduction of three different methods (AHP, Fuzzy AHP and PROMETHEE) to choose an appropriate additive manufacturing process. By comparing the results of each method, it is apparent that all methods gave the same rank of observed alternatives. Vinodh *et al.* [7] used PROMETHEE evaluation to select the best sustainable manufacturing concepts. There are three sustainability orientations according to production methodology, material and product design. They stated that the change of material is the best way to improve sustainability for the observed case. Can and Unuvar [8] present application of Taguchi method which enables reduction of experiments, when searching for the optimal parameters in the drilling process. On the other hand, Chang and Chen [9] integrated Taguchi method and TOPSIS algorithm to enhance the attractiveness of the product form.

Another example of using the Taguchi method in product design development is given by Oztekin *et al.* [10]. The method is used to determine the combination of product properties to find a design which takes consumer emotions into consideration. All of the above studies are dealing with MCDM methods to solve various problems and some of them used Taguchi method to reduce the number of experiments. This paper combines the strengths of both methods (PROMETHEE and Taguchi) to choose the optimal design.

The multi-objective optimization approach to product design selection is based on complex algorithms for shape optimization or its special case – the topology optimization. These algorithms are searching for the optimal design (shape) by considering, or not considering, some constraints. Usually, they are based on FEM and if the decision-maker preferences are unknown, it takes a dozens of days or weeks till the algorithm proposes the optimal shape or Pareto set of optimal shapes. In this research, that kind of approach is avoided, instead, it uses a different approach based on a priori knowledge [11] about product variants and decision-maker preferences.

The two-stage methodology is proposed for selecting the most appropriate design for the new product. In the first stage, the multi-criteria decision-making method PROMETHEE is used for selecting the most suitable design according to the chosen preferences and criteria. In the second stage, the Taguchi method is used in order to define the most appropriate parameters for selected suitable design (parameters like the diameter of the steel bar, the thickness of the steel tube, etc.). The methodology is developed so it could be applied in the Learning Factory environment, within the "Development of integrative procedure for management of production and service improvement process" (DEPROCIM) project funded by the Unity through Knowledge Fund (UKF).

The Lean Learning Factory (LLF) is the realistic factory environment created in the Laboratory for industrial engineering, at the University of Split, Faculty of Electrical Engineering, Mechanical Engineering and Naval Architecture (FESB). The LLF idea at FESB is to create an environment for research and development to provide knowledge transfer into the economy [12]. Learning factories should ensure appropriate and up-to-date knowledge about innovations [13]. It allows you to simulate various tasks that appear within a real-world manufacturing environment what helps students and industrial participants to gain knowledge faster [14]. The connection between digital models and methods, including simulation and 3D visualization, is done to integrate planning, implementation, control and on-going improvement [15].

This paper is organized as followed. In section 2, the observed problem is described. Section 3 shows steps of proposed methodology for product design selection. Section 4 explores the case study from the Lean Learning factory and emphasizes the advantage of using proposed methodology instead of classical methods. Section 5 sums up the contribution of this paper.

2. Problem description

Within the DEPROCIM project, the improvement of the case study on FESB, as one project goal, required further development of existing milling machine in order to support assembly line with the production of certain parts necessary for assembly. This paper presents modelling and simulation for choosing an optimal table design for the milling machine in the LLF environment, shown in Fig. 1. The compact design will increase the rigidity of the milling machine because the table legs will overtake feed forces necessary for the milling process. Other improvements on this milling machine include steel T-slot plate and improved linear guides.

Three different designs of tables had been taken into consideration. 3D models of each table design are shown in Fig. 2. For all table designs, the material is construction steel (St 44-2). The legs, frame, stiffener and table base are made of tubes with the quadratic cross-section, with thickness 3 mm. The table width, length and height are predefined. There is also the steel T-slot plate which is predefined.

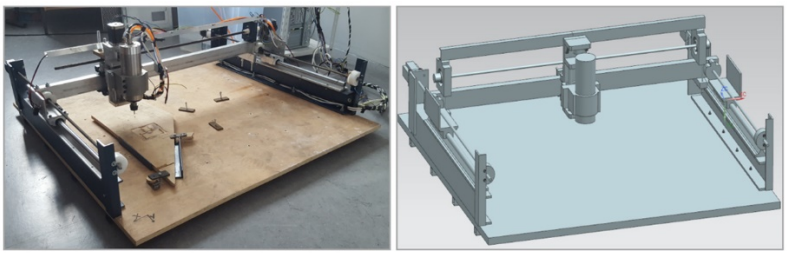

Fig. 1 Milling machine in LLF environment (real image and 3D)

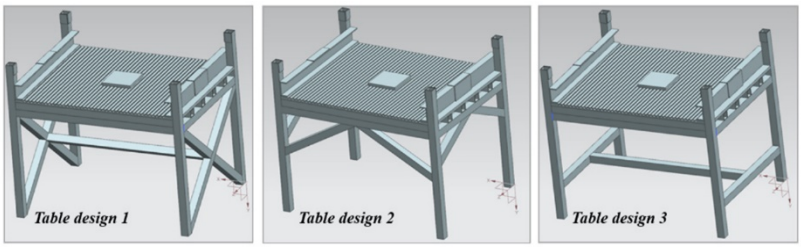

Fig. 2 3D models of Table design 1, 2 and 3

3. Proposed method for product design selection

This study uses the combination of two classic methods for product design selection, PROMETHEE (Preference Ranking Organization Method for Enrichment Evaluations) method and Taguchi method. The PROMETHEE method was used for selecting the most suitable design between proposed ones. The selected design was further used in Taguchi method for evaluation of the most appropriate combination of parameters. In order to gain all the necessary data for the mentioned methods, the first step was the creation of 3D models and their simulation by using the FEM analysis. The idea of FEM is a piecewise approximation. The solution to a complicated problem is obtained by dividing the region of interest into small regions (finite elements) and approximating the solution over each sub-region by a simple function [16]. This method has become popular and it represents a powerful analytical tool for studying different engineering problems [17, 18]. The PROMETHEE method combined with Taguchi method is carried out according to the input criteria provided by decision-maker and simulation results, Fig 3.

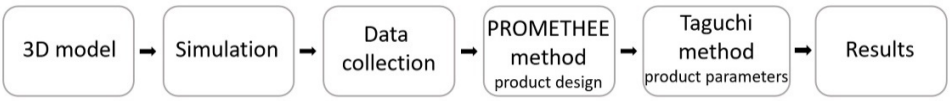

Fig. 3 Methodology for decision making for product design

3.1 PROMETHEE method

The PROMETHEE method is widely used because it has the adaptability to different problems and its implementation is simple [19-21]. This method was developed by J. P. Brans. Input information for the PROMETHEE method is a definition of several important criteria and decision-makers' preferences. It represents the definition of the function of decision-makers' preferences [22]. The function of preferences provides quantitative determination of how decision-maker prefers an alternative a in relation to alternative b. The function of preferences is defined for each criterion and its values may be in the range between 0 and 1. If the function of preferences is low, it means that the indifference between two alternatives is bigger for the decision-maker. If the value of the function of preferences is close to 1, then the preference of one alternative is bigger than the other. Complete preference of one alternative means that the function of preferences is 1. The function *f(a)* represents the assessment of alternative a for specific criteria and alternative a belongs to the set A. If the two alternatives, a and b, are taken from the set A, the relation of preference of the alternative a according to the alternative b is defined by function *P(a,b)*. In this example the function *P(a,b)* is *P(d)* where d represents:

$$d = f(a) - f(b) \tag{1}$$

The function of preferences has six different types. Those types cover most cases in practice and decision-maker should define parameters according to the chosen criteria [23].

3.2 Taguchi method

The founder of the Taguchi method is Genichi Taguchi. His robust design method was applied in the quality field but it can be applied to different problems in many industries. It is also the support for decision making. There are three important design stages in the Taguchi method [24]. System design, which is characterized by definition of the problem and application of knowledge and achievements to develop a prototype that represents the initial state of the product or process features. Parameter design determines the initial states of all features, which will minimize product or process variations. In recent years, Taguchi method has become a powerful tool for improving products and processes [25]. The orthogonal field is selected depending on the number of controlled parameters. The experiments are performed based on the orthogonal field, the data are analysed and the optimal state is identified. Tolerance design determines the tolerance of features, which will minimize product or process variations. P-diagram used as the base model for the Taguchi method is shown in Fig. 4.

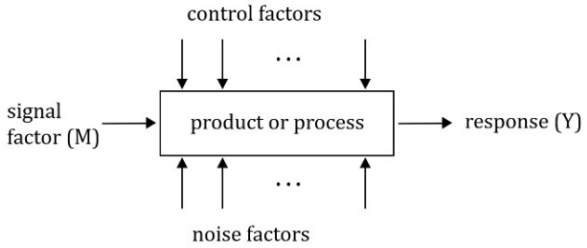

Fig. 4 P-diagram [24]

There is the signal factor and the response, but there are also control and noise factors that affect the process or the product. The main goal of the Taguchi method is to reduce losses of product or process due to deviations from its properties of the desired value. Taguchi defines quality loss as:

$$L(y) = k(y - m)^2 \tag{2}$$

Where y is the quality characteristic of a product, m is the target value for y. The k is constant and represents the coefficient of quality loss. There are four variations of the quadratic loss function: nominal the best, smaller the better, larger the better and asymmetric. This paper uses the smaller the better variation of the loss function.

4. Case study: Results and discussion

To demonstrate the advantages of the proposed methodology that will be used for concrete problem, table design for CNC milling machine, its application on less complex design was introduced in the beginning of this section. Besides the structure complexity, less complex design means a smaller number of overall possible alternatives and thereby, a smaller number of total experiments that need to carry out. In the PROMETHEE method, for the simple example, all alternatives were included in the selection of the design for Taguchi, to show the comparison of the final result obtained with the classic method and proposed methodology.

4.1 Simple example – PROMETHEE method

The basic principles to implement the PROMETHEE method is a pairwise comparison of alternatives evaluated according to determined criteria which have to be maximized or minimized. According to the literature, there are many different criteria for selection. The choice depends on the concrete problem. The aim of this following example is to show the choice of criteria and selection of appropriate design, Fig. 5. For each product design, three criteria (legs, frame and stiffener) were selected. Each of these criteria has two levels: the first level of legs is 40 mm and second 50 mm, criteria frame has 40 mm and 50 mm; criteria stiffener 20 mm and 30 mm respectively. These designs were loaded with force to demonstrate displacements through X, Y and Z-axis. The legs, frame and stiffener are made of tubes with the quadratic cross-section, with 2 mm thickness. The width, height and material of construction are predefined.

Through these combinations of levels, 8 alternatives were generated for each product design. That represents all possible alternatives of variants A and B. The preference functions for each of these criteria are determined according to Fig. 6. For each criterion, despite the determination min or max of function preferences, it was necessary to define the relative importance (the weights). These values of the weight coefficient are present in percentage with the total amount of 100 %. For criteria that have determined linear as preference function, the value of indifference threshold *q* and the value of strict preference threshold *p* are also defined. For each alternative, required data were entered and thus an input matrix was formed, Fig. 6.

Positive outranking flow, *Phi+*, is an aggregated outranking sum of each alternative over the other alternatives, while negative outranking flow, *Phi-*, shows how alternative is dominated by the other alternatives [26]. According to the usage of mentioned outranking flows, it is possible to define two approaches for alternative ranking, PROMETHEE I and PROMETHEE II. PROMETHEE I represents the partial ranking of alternatives and PROMETHEE II represents the full ranking of alternatives.

For this example, the PROMETHEE method was conducted two times. The first approach includes all possible alternatives of design A and design B. It gives their overall ranking, as is shown in Table 1. The best rank belongs to B4 alternative.

The second approach presents the first step of the proposed methodology. Instead of ranking all potential combinations (16 in this case), a selection between two potential designs was made. The analysis shows that B variant should be observed for further optimization, Fig. 7.

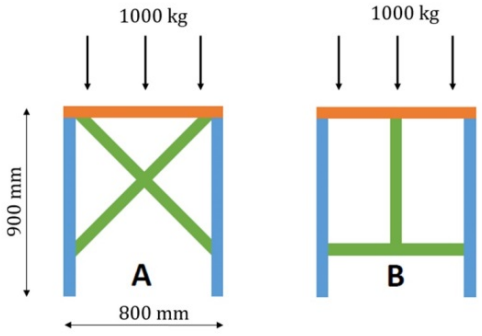

Fig. 5 Variants of product design

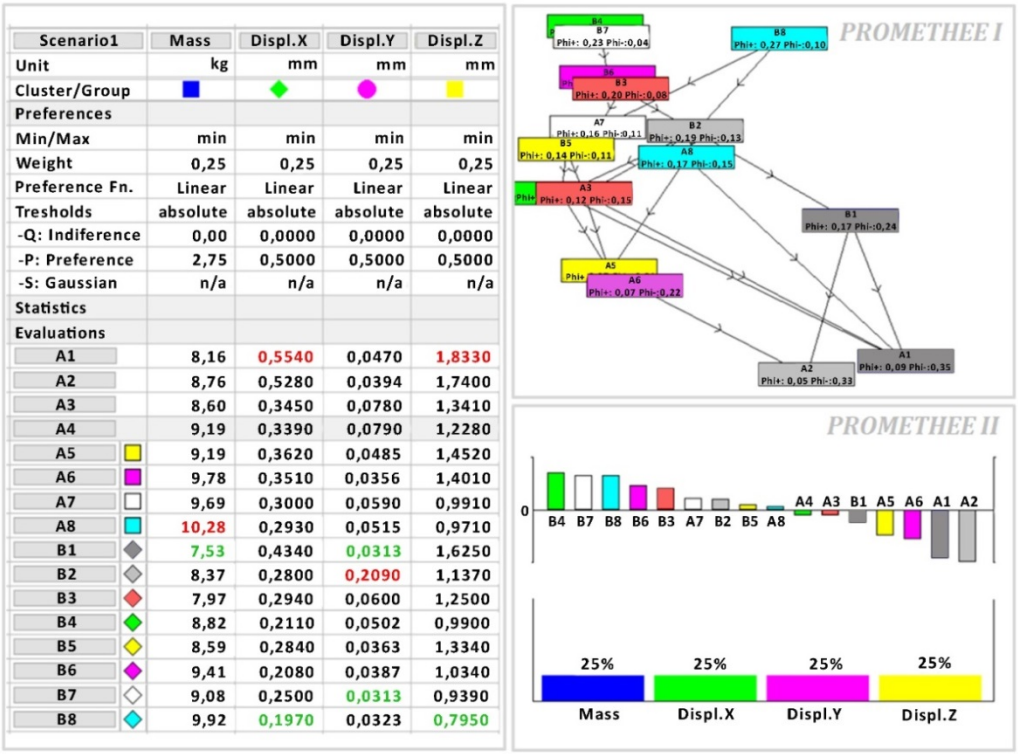

Fig. 6 Input matrix and results according to PROMETHEE I and PROMETHEE II (for all variants)

Table 1 All alternatives of product variants

Alter-native	Legs [mm]	Frame [mm]	Stiffener [mm]	Displ. X [mm]	Displ. Y [mm]	Displ. Z [mm]	Mass [kg]	PROMETHEE rank
A1	40	40	20	0.5540	0.0470	1.8330	8.16	15
A2	40	40	30	0.5280	0.0394	1.7400	8.76	16
A3	40	50	20	0.3450	0.0780	1.3410	8.60	11
A4	40	50	30	0.3390	0.0790	1.2880	9.19	10
A5	50	40	20	0.3620	0.0485	1.4520	9.19	13
A6	50	40	30	0.3510	0.0356	1.4010	9.78	14
A7	50	50	20	0.3000	0.0590	0.9910	9.69	6
A8	50	50	30	0.2930	0.0515	0.9710	10.28	9
B1	40	40	20	0.4340	0.0313	1.6250	7.53	12
B2	40	40	30	0.2800	0.0209	1.3700	8.37	7
B3	40	50	20	0.2940	0.0600	1.2500	7.97	5
B4	40	50	30	0.2110	0.0502	0.9900	8.82	1
B5	50	40	20	0.2840	0.0363	1.3340	8.59	8
B6	50	40	30	0.2080	0.0387	1.0340	9.41	4
B7	50	50	20	0.2500	0.0313	0.9390	9.08	2
B8	50	50	30	0.1970	0.0323	0.7950	9.92	3

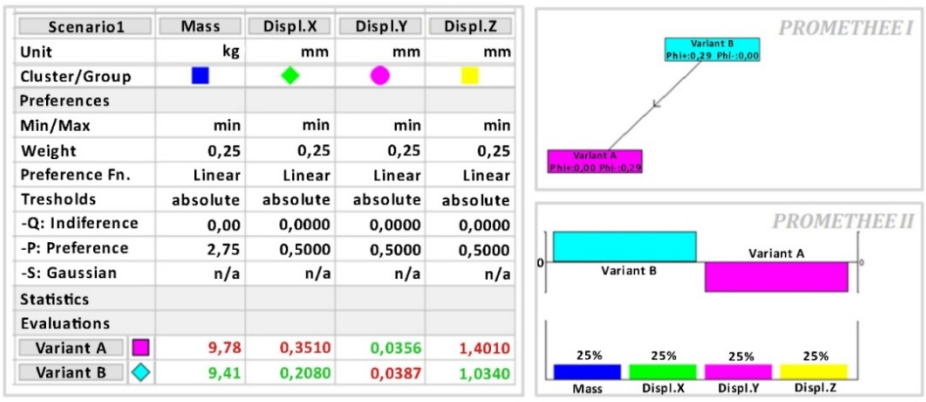

Fig. 7 Input matrix and results according to PROMETHEE I and PROMETHEE II (for two designs)

4.2 Simple example – Taguchi method

In order to create the plan of experiments, it was necessary to define parameters and their levels as it is mentioned before. To reduce the number of experiments, the orthogonal arrays are used in the Taguchi method. It represents the partial plan of experiments. The orthogonal arrays enable the observation of the effect on an individual parameter regardless of the evaluation of the effects of other system parameters. Definition of key parameters and their levels determines an appropriate orthogonal array. For this example, the L4 is chosen as an orthogonal array because there are three key parameters on two different levels which are shown in Fig. 1. Orthogonal array L4 covers 4 experiments, according to the literature [24]. Parameters and their levels were entered in Design Expert 11.0, where Taguchi method is used to find the best combination of parameters according to chosen levels. Data about the given combination for B variant are shown in Table 2.

To conduct the Taguchi method for this example, due to dispersion of response data, it was necessary to include two more experiments to gain a significant model that can be used to navigate the design space. The value of signal to noise ratio for this model is 16.43 and that indicates an adequate signal. The analysis of variance for response displacement Z is shown in Table 3, *F*-value is 36.17 which implies that the model is significant. There is only 2.70 % chance that *F*-value could appear due to noise. *p*-values less than 0.05 indicate that the model factors (A, B, C) are significant.

The main aim during the analysis of responses was the minimization of displacements and mass. For the purposes of analysis, it was necessary to define the importance for each response. According to the conducted FEM analysis, the chosen vertical loads have the greatest influence on the movements in the direction of the Z-axis, hence response displacement Z has the highest importance. The selected combination of parameters for this example is shown in Table 4.

The Taguchi optimum obtained with the proposed methodology is B design with dimensions of 40x50x30 mm. By comparing this final solution with the PROMETHEE solutions in Table 1, in which rang 1 means real optimum design (B4 design), i.e. the most suitable choice, it is obvious that these two methods show the same final solution.

Table 2 The plan of experiments for B variant

Run	Legs [mm]	Frame [mm]	Stiffener [mm]	Displ. X [mm]	Displ. Y [mm]	Displ. Z [mm]	Mass [kg]
1	40	40	20	0.4340	0.0313	1.6250	7,53
2	50	50	20	0.2500	0.0313	0.9390	9,08
3	40	50	30	0.2110	0.0502	0.9900	8,82
4	50	40	30	0.2080	0.0387	1.0340	9,41
5	50	40	20	0.2810	0.0364	1.3320	8,59
6	50	50	30	0.1970	0.0323	0.7950	9,92

Table 3 ANOVA for selected factorial model, response: displacement Z

Source	Sum of squares	df	Mean square	*F*-value	*p*-value	
Model	0.4551	3	0.1517	36.17	0.0270	significant
A-legs	0.1060	1	0.1060	25.28	0.0374	
B-frame	0.1550	1	0.1550	36.97	0.0260	
C-stiffener	0.0807	1	0.0807	19.24	0.0482	
Residual	0.0084	2	0.0042			
Cor Total	0.4635	5				

Table 4 Selected solution

No.	Legs [mm]	Frame [mm]	Stiffener [mm]	Displ. X [mm]	Displ. Y [mm]	Displ. Z [mm]	Mass [kg]	Desirability	
1	40	50	30	0.245	0.050	1.014	8.83	0.242	selected

4.3 Table example – Criteria formation and analysis of the results obtained by PROMETHEE method

According to the presented problem in section 2, the input data necessary to select the best alternative for table design using the PROMETHEE method is defined, as is shown in Fig. 8. For this purpose, five criteria for three variants are observed. As the cost of the table is the most important factor which should fit in the limited budget, the development of three variants of the tables is done in order to get different table shapes for the approximately same cost. Considering that the cost for each table design does not deviate significantly, it is not taken as criteria for the PROMETHEE method. The preference functions for each of the criteria are determined according to [23, 27]. For criteria mass and displacements, the preference function is linear. Linear functions are the best for quantitative criteria (for example: prices, costs, power, etc.). In the case of the small number of levels, on the criterion scale (that is 5-point scale) for qualitative criteria, the usual preference function is recommended and therefore used [22].

For this scenario, criteria are defined according to subjective opinion. In the preference category, it is necessary to define max or min preferences for each criterion, which is the maximum for construction criterion and minimum for the rest. The construction criterion for this case is based on qualitative assessment of the construction strength, with regard to its shape and assembly. In this case, the assembly is not included as individual criterion because this product will be assembled in LLF. Generally, when using this method, the complexity of assembly could be included as a criterion. Through this criterion, it is possible to have an effect on the assembly process, which will reflect on whole manufacturing process efficiency. However, the contribution of this criterion on the assembly process will be affected by the definition of criteria weights, preference functions and its values.

The most suitable solution is the one that acquires the overall preference as close as possible to the value +1 (greatest possible preferences). PROMETHEE I shows the ranking of alternatives at the left side of Fig. 9. The alternative with the highest priority is table design 1 and it has domination above other designs. Table design 2 and 3 are incomparable with each other because table design 2 has the better score on *Phi+* and worse score on *Phi-* and vice versa for table design 3. At the right side of Fig. 9, there is a complete ranking with PROMETHEE II, which confirms our previous statements. The results of partial and complete ranking demonstrate that the table design 1 is the most favourable, with the preferences of +0.1801, hence this alternative is used for further optimization with Taguchi method.

Scenario1	Construction	Mass	Displ.X	Displ.Y	Displ.Z
Unit	5-point	kg	mm	mm	mm
Cluster/Group	◆	●	■	◆	■
Preferences					
Min/Max	max	min	min	min	min
Weight	0,20	0,20	0,20	0,20	0,20
Preference Fn.	Usual	Linear	Linear	Linear	Linear
Tresholds	absolute	absolute	absolute	absolute	absolute
-Q: Indiference	n/a	5,00	0,0000	0,0000	0,0000
-P: Preference	n/a	25,00	0,5000	0,5000	0,5000
-S: Gaussian	n/a	n/a	n/a	n/a	n/a
Statistics					
Minimum	4,00	234,00	0,0062	0,0186	0,0035
Maximum	5,00	244,00	0,0077	0,0215	0,0180
Average	4,33	239,00	0,0070	0,0201	0,0113
Standard Dev.	0,47	4,08	0,0006	0,0012	0,0060
Evaluations					
TableDesign1	very good	244,00	0,0062	0,0201	0,0035
TableDesign2	good	239,00	0,0072	0,0186	0,0123
TableDesign3	good	234,00	0,0077	0,0215	0,0180

Fig. 8 Input matrix for PROMETHEE method

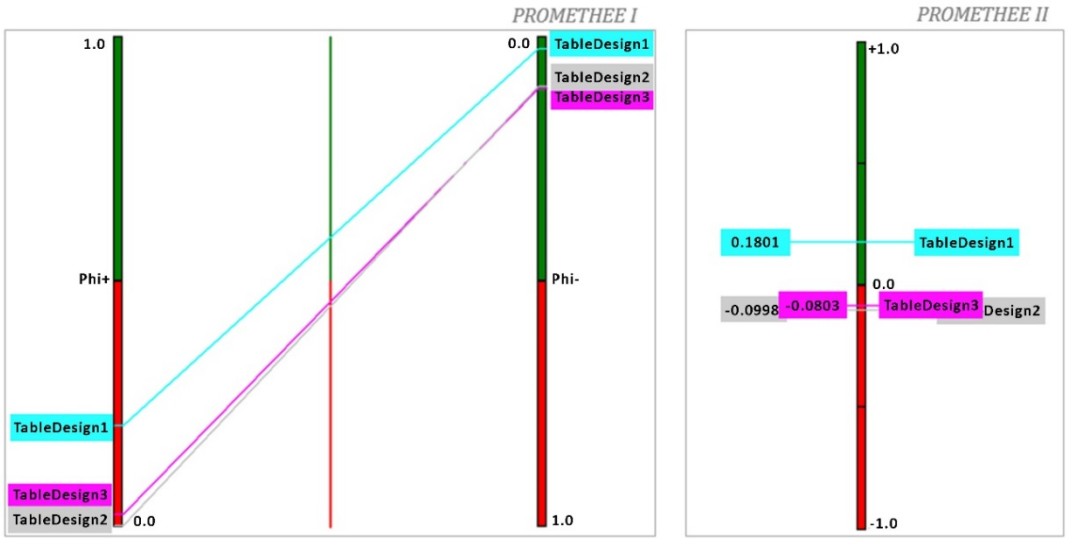

Fig. 9 Partial ranking with PROMETHEE I and complete ranking with PROMETHEE II for the best table design

4.4 Table example – Criteria formation and analysis of the results obtained by Taguchi method

Table design 1 has domination above other designs and its key parameters were defined. The data about experiments are shown in Table 5. For each variant of table design 1, generated by software Design Expert, from 1 to 9, displacement and mass were calculated by using NX Siemens 10.0 software.

To calculate displacement, it was necessary to define loads for table design 1. The loads are shown in Fig. 10 and the fixed constraint is set on the surface of legs that lay on the floor.

Table 5 The plan of experiments from Design Expert 11.0 software

Run	Factor 1: Legs & frame [mm]	Factor 2: Stiffener [mm]	Factor 3: Table base [mm]	Response 1: Displ. X [mm]	Response 2: Displ. Y [mm]	Response 3: Displ. Z [mm]	Response 4: Mass [kg]
1	50	40	50	6.60E-03	2.10E-02	3.93E-03	239.67
2	70	40	40	6.10E-03	2.33E-02	3.56E-03	252.27
3	60	40	60	4.80E-03	1.44E-02	2.99E-03	255.96
4	50	50	60	5.40E-03	1.60E-02	2.83E-03	251.12
5	60	30	50	5.80E-03	1.87E-02	3.74E-03	244.72
6	70	50	50	5.10E-03	1.73E-02	2.55E-03	263.38
7	70	30	60	4.50E-03	1.37E-02	2.72E-03	260.95
8	60	50	40	6.60E-03	2.40E-02	4.23E-03	247.39
9	50	30	40	8.20E-03	2.85E-02	5.52E-03	228.42

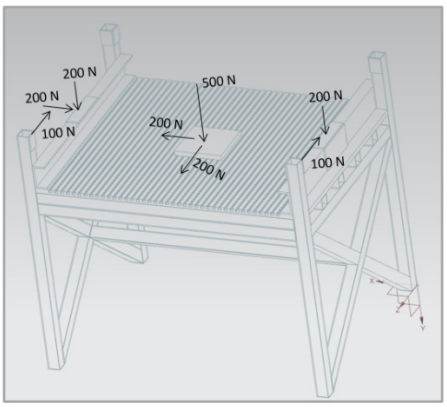

Fig. 10 The load distribution for table design 1

The results of the experiments are analysed and significant parameters are detected. The analysis of variance (ANOVA) verifies the influence on system response when parameters are changing [28]. The ANOVA shows *F*-value 76.88 which means that the model is significant. It is 1.29 % chance that *F*-value could appear because of noise. *p*-values that are less than 0.05 indicate model terms are significant. In this case, legs & frame and table base are significant in model terms. Stiffener has *p*-value that is higher than 0.1, that means that it is not significant in model terms. *S-N ratio* measures the signal to noise ratio which is 24.98. When this ratio is greater than 4, it indicates an adequate signal as it was mentioned in a simple example. The main effect plots are shown in Fig. 11 for displacement Y. It is visible that stiffener is not significant for the model.

The ANOVA for response mass shows *F*-value 14519.51 which means that the model is significant. It is 0.01 % chance that *F*-value could appear because of noise. In this case, legs & frame, stiffener and table base are significant in model terms. *S-N ratio* is 380.858 and it is desirable. It indicates an adequate signal. Displacement and mass were chosen as responses that should be minimum. The importance is higher for the displacement than for the mass. For displacement Y lower limit is 0.0137 mm and the upper limit is 0.0285 mm. For mass, the lower limit is 228.42 kg and the upper limit is 263.38 kg. The optimal solution is found and parameters for table design 1 are: legs & frame 60 mm, stiffener 40 mm, table base 60 mm. For this combination of parameters, displacements and mass are shown in Table 6. The Taguchi method has found 24 solutions. As the optimal solution it gives the combination of parameters under the run 3, which is part of the previous plan of experiments, shown in Table 5.

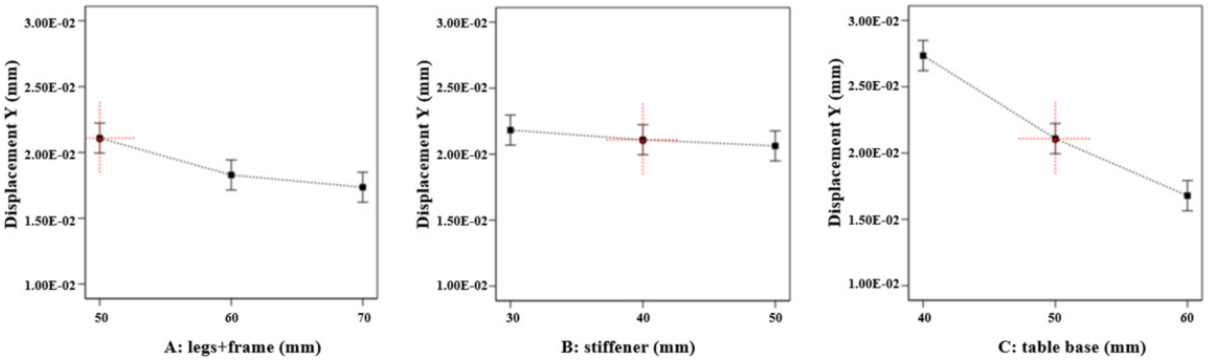

Fig. 11 Main effects for response displacement Y, change of each factor depending on level

Table 6 Solution for the best parameters of table design 1

No.	Legs & Frame [mm]	Stiffener [mm]	Table base [mm]	Displ. X [mm]	Displ. Y [mm]	Displ. Z [mm]	Mass [kg]	Desirability	
1	60	40	60	0.005	0.014	0.003	256	0.579	selected

4.5 Two stage selection of product design using PROMETHEE and Taguchi method: Discussion

The main aim of this paper was to show an advantage of the proposed methodology with an emphasis on the number of experiments that have to be done. Table 7 shows the comparison of differences between classical methods and proposed methodology in terms of the number of variants on the simple example presented in section 4 and the design of table for CNC milling machine. The simple example consists of 2 designs with 3 factors on 2 levels, which means that for the PROMETHEE method it is necessary to prepare 16 variants. If the design of table for CNC milling machine is chosen using the mentioned method, it will be necessary to prepare 81 variants. The simple example was conducted to verify the final result of the proposed methodology with the result obtained by the classical method. It can be seen that the real optimum result from PROMETHEE method coincides with Taguchi optimum gained by the proposed methodology.

Table 7 Comparison of different approaches and number of necessary variants to include in the selection

	Simple example (section 4)	Design for CNC milling machine	
Approach	2 designs, 3 factors, 2 levels	3 designs, 3 factors, 3 levels	Optimum
Classical selection of the best variant – PROMETHEE method	$2 \times 2^3 =$ 16 variants	$3 \times 3^3 =$ 81 variants	real optimum
Classical selection of the best variant – Taguchi method	$2 \times 4 =$ 8 variants	$3 \times 9 =$ 27 variants	Taguchi optimum
Two-stage product design selection using PROMETHEE and Taguchi method	$(2 - 1) + 4 =$ 5 variants (+2)*	$(3 - 1) + 9 =$ 11 variants	Taguchi optimum

* For this example it was necessary to include two more experiments to gain a significant model; detailed explanation is in subsection 4.2

5. Conclusion

The research on how to combine different methods and find an optimal solution is presented in this paper. Today, time is the crucial factor in the design product stage and decision-making support is an important part in manufacturing or research and development process. The longer period of the design phase has effects on the production of a product. This situation is characteristic when it is not clear what properties product should exactly satisfy. Proposed methodology shows the reduction of variants and number of its experiments with help of criteria that should be defined in the beginning in order to reduce search space. It is visible that the number of experiments increases significantly when there is just a small increase in the number of designs, in fact, search space becomes larger. The advantages of the proposed methodology are identified through the comparison of different approaches. Time is saved for the search of appropriate variants and optimum is reached as in the case of the "whole space search". The PROMETHEE method helps to find the best solution according to the decision-makers' selection. Combining it with the Taguchi method, the number of experiments is reduced and it is easy to find out which parameter is significant and how each parameter affects the whole system (product or process). Usage of the strengths of both methods resulted in the two-stage methodology. This new combination of methods mostly contributes in the product design phase while searching for the most appropriate solution according to the "a priori" defined alternatives and criteria.

Acknowledgement

This work has been fully supported by the Unity Through Knowledge Fund (UKF), 1C My First Collaboration Grant, under the project 11/17 Development of integrative procedure for management of production and service improvement process.

References

[1] Ishizaka, A., Nemery, P. (2013). *Multi-criteria decision analysis: Methods and software*, John Wiley & Sons, New Delhi, India, doi: 10.1002/9781118644898.

[2] Govindan, K., Rajendran, S., Sarkis, J., Murugesan, P. (2015). Multi criteria decision making approaches for green supplier evaluation and selection: A literature review, *Journal of Cleaner Production*, Vol. 98, 66-83, doi: 10.1016/j.jclepro.2013.06.046.

[3] Mladineo, M., Veza, I., Gjeldum, N. (2017). Solving partner selection problem in cyber-physical production networks using the HUMANT algorithm, *International Journal of Production Research*, Vol. 55, No. 9, 2506-2521, doi: 10.1080/00207543.2016.1234084.

[4] Mardani, A., Jusoh, A., Zavadskas, E.K. (2015). Fuzzy multiple criteria decision-making techniques and applications – Two decades review from 1994 to 2014, *Expert Systems with Applications*, Vol. 42, No. 8, 4126-4148, doi: 10.1016/j.eswa.2015.01.003.

[5] Avikal, S., Mishra, P.K., Jain, R. (2014). A Fuzzy AHP and PROMETHEE method-based heuristic for disassembly line balancing problems, *International Journal of Production Research*, Vol. 52, No. 5, 1306-1317, doi: 10.1080/00207543.2013.831999.

[6] Peko, I., Gjeldum, N., Bilić, B. (2018). Application of AHP, fuzzy AHP and PROMETHEE method in solving additive manufacturing process selection problem, *Tehnički Vjesnik – Technical Gazette,* Vol. 25, No. 2, 453-461, doi: 10.17559/TV-20170124092906.

[7] Vinodh, S., Girubha, R.J. (2012). PROMETHEE based sustainable concept selection, *Applied Mathematical Modelling*, Vol. 36, No. 11, 5301-5308, doi: 10.1016/j.apm.2011.12.030.
[8] Can, A., Ünüvar, A. (2017). Optimization of process parameters in drilling of SMC composites using Taguchi method, *Tehnički vjesnik – Technical Gazette,* Vol. 24, No. 2, 435-442, doi: 10.17559/TV-20160103215256.
[9] Chang, H.-C., Chen, H.-Y. (2014). Optimizing product form attractiveness using Taguchi method and TOPSIS algorithm: A case study involving a passenger car, *Concurrent Engineering*, Vol. 22, No. 2, 135-147, doi: 10.1177/1063293X13520317.
[10] Oztekin, A., Iseri, A., Zaim, S., Nikov, A. (2013). A Taguchi-based Kansei engineering study of mobile phones at product design stage, *Production Planning & Control*, Vol. 24, No. 6, 465-474, doi: 10.1080/09537287.2011.633575.
[11] Mladineo, M., Celar, S., Celent, L., Crnjac, M. (2018). Selecting manufacturing partners in push and pull-type smart collaborative networks, *Advanced Engineering Informatics*, Vol. 38, 291-305, doi: 10.1016/j.aei.2018.08.001.
[12] Gjeldum, N., Mladineo, M., Veza, I. (2016). Transfer of model of innovative smart factory to Croatian economy using lean learning factory, *Procedia CIRP*, Vol. 54, 158-163, doi: 10.1016/j.procir.2016.06.096.
[13] Abele, E., Metternich, J., Tisch, M., Chryssolouris, G., Sihn, W., ElMaraghy, H., Hummel, V., Ranz, F. (2015). Learning factories for research, education, and training, *Procedia CIRP*, Vol. 32, 1-6, doi: 10.1016/j.procir.2015.02.187.
[14] Prinz, C., Morlock, F., Freith, S., Kreggenfeld, N., Kreimeier, D., Kuhlenkötter, B. (2016). Learning factory modules for smart factories in Industrie 4.0, *Procedia CIRP*, Vol. 54, 113-118, doi: 10.1016/j.procir.2016.05.105.
[15] Herrmann, C., Schmidt, C., Kurle, D., Blume, S., Thiede, S. (2014). Sustainability in manufacturing and factories of the future, *International Journal of Precision Engineering and Manufacturing-Green Technology*, Vol. 1, No. 4, 283-292, doi: 10.1007/s40684-014-0034-z.
[16] Rao, S.S. (2017). *The finite element method in engineering*, (6th edition), Butterworth-Heinemann, Oxford, UK, doi: 10.1016/C2016-0-01493-6.
[17] Özkal, F.M., Cakir, F., Arkun, A.K. (2016). Finite element method for optimum design selection of carport structures under multiple load cases, *Advances in Production Engineering & Management*, Vol. 11, No. 4, 287-298, doi: 10.14743/apem2016.4.227.
[18] Wang, Y., Lu, Y.J., Si, C.D., Sun, T.C. (2017). Finite element analysis for rutting prediction of asphalt concrete pavement under moving wheel load, *International Journal of Simulation Modelling*, Vol. 16, No. 2, 229-240, doi: 10.2507/IJSIMM16(2)4.374.
[19] Sari, T., Timor, M. (2016). Integrated supplier selection model using ANP, Taguchi loss function and PROMETHEE methods, *Journal of Applied Quantitative Methods*, Vol. 11, No. 1, 19-34.
[20] Brans, J.-P., De Smet, Y. (2016). PROMETHEE methods, In: Greco, S., Ehrgott, M., Rui Figueira, J. (eds.), *Multiple Criteria Decision Analysis*, Springer, New York, USA, 187-219, doi: 10.1007/978-1-4939-3094-4.
[21] Behzadian, M., Kazemzadeh, R.B., Albadvi, A., Aghdasi, M. (2010). PROMETHEE: A comprehensive literature review on methodologies and applications, *European Journal of Operational Research*, Vol. 200, No. 1, 198-215, doi: 10.1016/j.ejor.2009.01.021.
[22] Brans, J.-P., Mareschal, B. (2005). PROMETHEE methods, In: Figueira, J., Greco, S., Ehrgott, M. (eds.), *Multiple Criteria Decision Analysis: State of the Art Surveys*, Vol. 78, Springer, New York, USA, 163-186, doi: 10.1007/0-387-23081-5_5.
[23] Brans, J.P., Vincke, Ph. (1985). Note – A preference ranking organization method (The PROMETHEE method for Multiple Criteria Decision-Making), *Management Science*, Vol. 31, No. 6, 647-784, doi: 10.1287/mnsc.31.6.647.
[24] Phadke, M.S. (1995). *Quality engineering using robust design*, Prentice Hall PTR, New Jersey, USA.
[25] Li, Y., Zhu, L. (2017). Optimisation of product form design using fuzzy integral-based Taguchi method, *Journal of Engineering Design*, Vol. 28, No. 7-9, 480-504, doi: 10.1080/09544828.2017.1346239.
[26] Genç, T., Dinçer, S.E. (2013). Visual analysis for multi criteria decision problems by PROMETHEE method and gaia plane: An application, determine the level of regional socio-economic development in Turkey, *Trakya University Journal of Social Science*, Vol. 15, No. 2, 111-130.
[27] Mareschal, B. The PROMETHEE – GAIA FAQ, from *http://www.promethee-gaia.net/,* accessed July 11, 2018.
[28] Cardinal, R.N., Aitken, M.R.F. (2013). *ANOVA for the behavioral sciences researcher*, Psychology Press, New York, USA, doi: 10.4324/9780203763933.

APEM journal
Advances in Production Engineering & Management
Volume 14 | Number 1 | March 2019 | pp 51–64
https://doi.org/10.14743/apem2019.1.311
ISSN 1854-6250
Journal home: apem-journal.org
Original scientific paper

Productivity improvement with parallel adjacent U-shaped assembly lines

Chutima, P.[a,b,*], **Suchanun, T.**[a]

[a]Industrial Engineering, Faculty of Engineering, Chulalongkorn University, Bangkok, Thailand
[b]Academy of Science, The Royal Society of Thailand, Bangkok, Thailand

ABSTRACT

A novel configuration of assembly lines was proposed in this research, namely parallel adjacent U-shaped assembly lines (PAUL). Typically, in a multiple U-line facility, each U-line is designed to work independently which may cause some workstations were not fully functioned. The PAUL aimed at increasing the utilisation of the whole facility by allowing cross-trained workers to work on the opposite legs of the adjacent U-lines (multi-line workstations). This configuration is easier to implement than parallel U-lines due to no restriction in terms of the lengths of U-lines to be paralleled and hidden expenditures that could be incurred in shop floor reconstruction. Since the line balancing of the PAUL is NP-hard and many conflicting objectives need to be optimised simultaneously, the evolutionary meta-heuristic which was the hybridisation of the multi-objective evolutionary algorithm based on decomposition (MOEA/D) and particle swarm optimisation (PSO), namely MOEA/D-PSO, was developed to effectively solve the problem. In addition, the decoding algorithm to convert the solutions obtained from MOEA/D-PSO into the PAUL's configuration was proposed. The performance of MOEA/D-PSO was evaluated against MOEA/D and multi-objective particle swarm optimisation (MOPSO). The experimental results reveal that MOEA/D-PSO outperformed its rival algorithms under the convergence-related performance.

ARTICLE INFO

Keywords:
Assembly line;
U-shaped assembly line;
Parallel adjacent assembly line;
Assembly line balancing;
Productivity improvement;
Multi-objective optimisation;
Evolutionary algorithm (MOEA/D);
Particle swarm optimisation (PSO)

**Corresponding author:*
cparames@chula.ac.th
(Chutima, P.)

Article history:
Received 29 October 2018
Revised 20 December 2019
Accepted 21 January 2019

1. Introduction

Nowadays, manufacturers are encountering shortened product life cycle because of ever-escalating technological innovation, fierce market competition and rapid change in customers' taste. To maintain their competitiveness and survive in heavily competitive businesses, the just-in-time (JIT) philosophy has been adopted to reduce wastes and excessive inventories in production systems. As a result of JIT implementation, the traditional straight-shaped production lines are switched to the U-shaped ones (hereafter called U-lines) to improve their production efficiencies. Moreover, the mixed-model production, another main integral ingredient of JIT, supersedes the mass production of one model of a single product to cope with the swift growth of product varieties in a cost-effective manner.

In view of the production, a U-line offers more options in task-to-workstation assignments since workers are allowed to work on both sides (Front and Back) of the line in crossover workstations apart from regular workstations which are placed only on any single side of the line. This provides a higher opportunity to consolidate more tasks into workstations resulting in higher compact workload, better workload distribution and greater line utilisation. The popular-

ity of U-lines is attributed to lots of benefits gained from production volume flexibility, operator flexibility, less number of workstations, no special material handling equipment needed, less space requirement, greater workplace visibility, increased communication and teamwork, multi-skilled workers, lower inventory, easier production planning and better quality control [1].

In most manufacturing companies which adopt JIT, after a period of production, they may notice that their current capacities are not enough to fulfil increasing demands because their businesses are flourishing and extra orders are received continuously. These orders may be the same products previously offered or even new products never been done before. The simplest way to deal with this problem is to add more duplicated or newly designed lines into the system. Since the planning and operations of these lines are conducted independently as if they cannot interact with others, the system as a whole comprising many unrelated lines is normally underutilised.

Recently, Gökçen *et al*. [2] proposed a new line configuration, namely parallel lines, where one or more straight-lines are allowed to work simultaneously under common resources (e.g. workers or equipment) through multi-line workstations to increase the capacity of the system without the cost of additional lines. This concept was further adapted to fit in the environment of U-lines by Küçükkoç and Zhang [3], namely parallel U-shaped lines (PUL), where two U-lines are placed in parallel to one another to take advantages of multi-line workstations which bestride between both adjacent U-lines.

Although the concept of the PUL is theoretically sound, a number of practical issues could be uncovered as follows. First, the application of this configuration is limited only when the lengths of both adjacent U-lines are more or less the same. If the outer U-line is much longer than the inner U-line and multi-line workstations are located between the Bottoms of both lines, the workers who work in these workstations have to walk back and forth between two legs of the lines in a long distance. This makes multi-line workers unhappy because their jobs are more tired than those working in other places and perhaps they would refuse to work in such workstations.

In contrast, if the inner U-line is much longer than the outer U-line, there will be no multi-line workstation at the Bottoms of both lines since no Bottom of the outer line is existed. Without the Bottom of the outer line, two legs (Front and Back) of the outer line are split apart and hence material transfers between these legs need a great help from material handling equipment or floating workers bringing about additional operational costs.

Second, in order to reconfigure the system according to the PUL, in case of two U-lines are originally working independently, the lines must be reorganised by moving one U-line to encompass with the other. The cost of line relocation may be quite excessive, particularly when heavy machines are parts of the workstations and the foundation on the shop floor for machinery placement needs further reconstruction.

In this paper, an alternative layout of multiple U-lines is proposed, namely parallel adjacent U-lines (PAUL). This layout has no limitation as of the PUL and it is much easier to implement in practice since less machinery movement is required. The PAUL's environment comprises two or more U-lines adjacently located as ubiquitously found in industry. Instead of treating each U-line as an independent entity, multi-line workers are allowed to handle tasks on both legs of the adjacent U-lines, i.e. Front of one U-line and Back of the other U-line (Fig. 1). As a result, the underutilised capacity of independent lines on some workstations, if any, could be unleashed by implementing the PAUL. To our best knowledge, this novel configuration has never been addressed in literature before.

To systematically form the PAUL so that the production is flown smoothly, the disparity of workloads among workers should be minimised to minimise the unused capacity of the lines. This problem is known as the PAUL balancing problem (PAULBP). In this paper, we assume that each U-line of the PAUL produces mixed-model products to reflect real-life applications. In addition, many conflicting objectives are optimised simultaneously. Because the problem is NP-hard, evolutionary algorithms seem to be an effective solution technique. As a result, the multi-objective evolutionary algorithm based on decomposition (MOEA/D) hybridised with particle swarm optimisation (PSO) is proposed to solve the PAULBP.

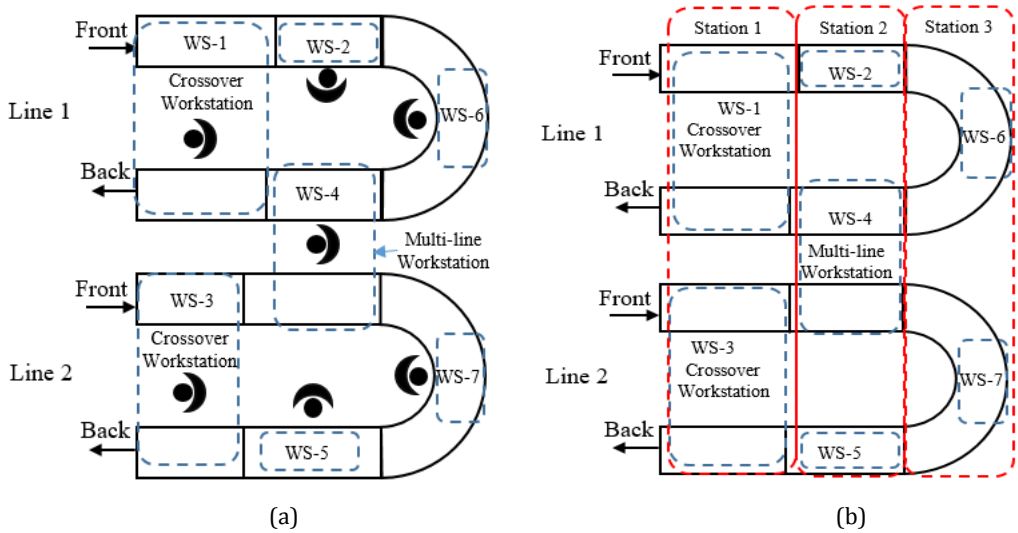

Fig. 1 PAUL configuration: (a) without station number, and (b) with station number

The remaining sections are organised as follows. The detailed description of the PAUL is presented in Section 2. The approach to solving the PAULBP is proposed in Section 3. Experimental designs, results and discussions are explained in Section 4. Finally, the conclusion and future research are discussed in Section 5.

2. Problem definition

Obviously, in a production system (e.g. electronics and electrical industry) where several U-lines are located close to each other (i.e. the walking time between adjacent U-lines of multi-line workers is negligible) could provide an opportunity for better line balancing. In this research, the layout of two U-lines laid out adjacently side-by-side is considered (Fig. 1). The entry and exit points of both lines are on the same side. By this arrangement, an additional form of workstations could be realised apart from regular and crossover workstations as typically found in traditional U-lines. This type of workstation is called a multi-line station which could occur between the Back of Line 1 and the Front of Line 2. The worker who is assigned to perform tasks in a multi-line station is cross-trained to manipulate different product families and models belonging to both U-lines of the PAUL. The assumptions used in this research are as follows: (a) both U-lines produce mixed-model products, (b) task times, cycle times and precedence diagrams of products on both U-lines are given and fixed, (c) cycle times of both U-lines could be different, (d) workers are cross-trained, and (e) walking time of the worker is negligible regardless of workstation types.

2.1 Objective functions

Five objectives related to line efficiency and workload distribution are employed in this research. The reasons for using many objectives as such is to evaluate the effectiveness of the proposed algorithm in dealing with the problems with high dimensional search space and the problem itself is a multi-objective optimisation in nature. Note that these objectives are conflicted with each other; therefore, trade-offs among them are inevitable. The followings are the formulations and descriptions of the objectives.

(1) Minimise the number of workstations (N_W): If the workloads assigned to all workstations in the PAUL are equal or nearly equal to the cycle time of the system, the efficiency of the system will be high resulting in less number of workstations required.

$$f_1 = Minimise\ N_W \tag{1}$$

(2) Minimise workload variations between workstations (B_b): This objective attempts to equalise the workload assigned to each workstation as much as possible. Highly unbalanced workload causes a bottleneck, inequality of workers and also fatigues to the worker who works in the bottleneck workstation.

$$f_2 = Minimise\ B_b = \frac{N_w}{N_w - 1}\sum_{k=1}^{N_w}\sum_{b=1}^{3}\left(\frac{S_{k,b}}{TAD} - \frac{1}{N_w}\right)^2 \tag{2}$$

(3) Minimise unbalanced workloads within the workstation (B_w): This objective is trivial in a single-model assembly line. However, it is vital for a mixed-model assembly line in which the task times of different product models could be varied. The effect of this problem is apparent while sequencing products into the line since a worker may have to work much longer than the cycle time in some cycle, but very short in another cycle. In some cases, utility workers may be called upon to ease the problem.

$$f_3 = Minimise\ B_w = \frac{M}{N_w(M-1)}\sum_{k=1}^{N_w}\sum_{m=1}^{M}\left(S_{km} - \frac{1}{M}\right)^2 \tag{3}$$

$$q_m = \frac{D_m}{\sum_{m=1}^{M} D_m};\ 0 \le q_m \le 1 \ \text{ and } \ \sum_{m=1}^{M} q_m = 1 \tag{4}$$

$$S_{km} = \begin{cases} 0, & \text{if } \sum_{m=1}^{M} q_m s_{km} \\ \dfrac{q_m s_{km}}{\sum_{m=1}^{M} q_m s_{km}}, & \text{otherwise} \end{cases} \tag{5}$$

(4) Minimise unrelatedness of tasks in the workstation (TUR): Two tasks assigned to a workstation are related to each other if both of them are directly interconnected in the precedence diagram. Their relationships are the predecessor or successor of the other. The related tasks normally require similar tools and skill of workers; hence, assigning related tasks to the same workstation facilitates skill development and expertise to a worker resulting in high system efficiency. Chutima and Chimklai [4] proposed the formulation to measure the unrelatedness of assigned tasks in the workstation as follows.

$$f_4 = Minimise\ TUR = N_w - \frac{N_w}{\sum_{k=1}^{N_w} SN_k} \tag{6}$$

where SN_k is the network of tasks that are directly related in workstation k.

(5) Minimise the number of stations (N_s): The line length of the system comprising many U-lines laid down adjacently can be measured by counting the number of stations which are compactly arranged in a longitudinal direction. Shop floor utilisation will be high if the system's line length is short. This objective can also be used to penalise the system configurations that are not an authentic PAUL which will be discussed in the next section.

$$f_5 = Minimise\ N_s \tag{7}$$

2.2 Authentic PAUL configuration

An authentic PAUL must consist of at least one crossover workstation and one multi-line workstation, possibly incorporated with or without any regular workstation. Many system configurations that claim to be the PAUL but, in reality, they are just look alike. As a result, the benefits of

the PAUL may not be realised from such unauthentic PAULs, particularly low N_w and short line length which will be illustrated in the following examples.

Fig. 1 illustrates the authentic PAUL configuration in which one crossover workstation is found in Line 1 and Line 2, one multi-line workstation is located between the adjacent legs of Line 1 and Line 2, and two regular workstations are on Line 1 and Line 2. In this case, the number of stations in the system (i.e. line length N_s) is three.

Fig. 2 depicts the two-line system which consists of four regular workstations on Line 1 and Line 2, and one multi-line workstation located in between Line 1 and Line 2. This configuration is not an authentic PAUL since no crossover workstation exists. In fact, this system is parallel lines and the line length is five.

Another example of unauthentic PAULs is shown in Fig. 3. The system consists of a U-line and a straight line working in parallel. There are two regular workstations and one crossover workstation on Line 1, four regular workstations on Line 2, and one multi-line laid between Line 1 and Line 2. The line length of the system is 5.

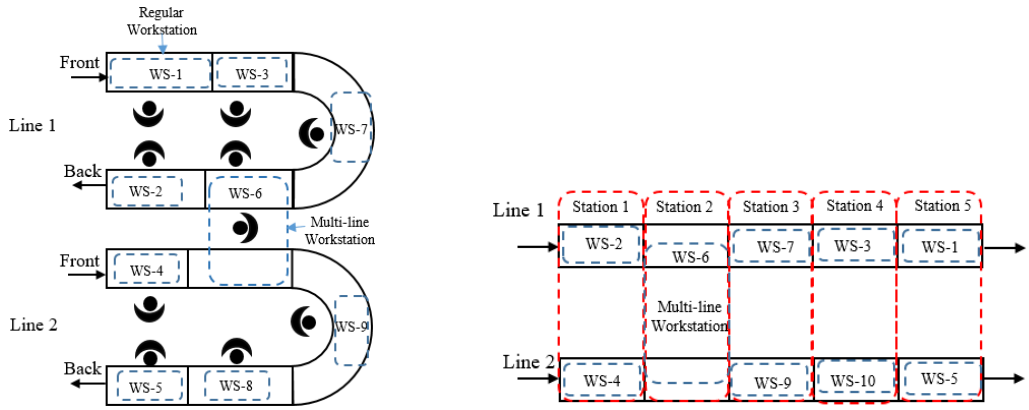

Fig. 2 Parallel lines ($N_s = 5$)

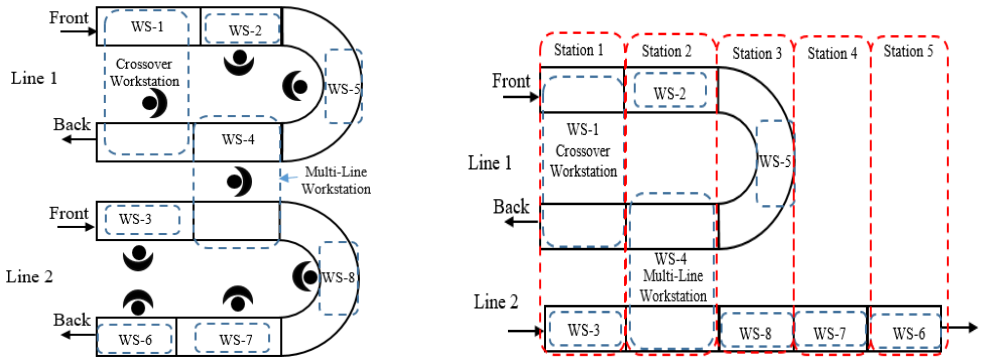

Fig. 3 One U-line and one straight line ($N_s = 5$)

3. Materials and methods

3.1 Hybridisation between MOEA/D and PSO (MOEA/D-PSO)

Much effort of the early research in the line balancing has been emphasised on a single objective optimisation. However, in practice, line balancing is a multi-objective optimisation problem (MOP) since many conflicting objectives need to be realised simultaneously as mentioned in Section 2. When solving this problem, we usually discover numerous optimal solutions which are non-dominated to each other, so-called Pareto optimal solutions (POSs). The best contour of these POSs plotted in the objective space is called the Pareto front (PF).

Various Pareto-based evolutionary multi-objective optimisation algorithms have been developed to solve MOPs. However, with these algorithms, when the number of objectives grows

more than three, known as many-objective optimisation problems (MaOPs), the dominance among solutions becomes weakened considerably resulting in worsening selection pressure towards the PF and sluggish the convergence rate of the algorithm.

Recently, the novel algorithm to effectively tackle MaOPs namely multi-objective evolutionary algorithm based on decomposition (MOEA/D) in which an original MaOP is bisected into numerous subproblems using different weight vectors which are uniformly distributed along the objective domain was developed by Zhang and Li [5]. These single objective optimisation subproblems are collaboratively optimised simultaneously in each generation. Since the fitness assignments of MOEA/D are determined by the scalar aggregation function rather than the Pareto domination as conventional, the number of objectives has a minimal effect to its selection pressure.

MOEA/D normally uses genetic operators as an offspring generating mechanism, e.g. single point crossover. However, such genetic operator has a serious drawback in computational expensive when compares with particle swarm optimisation (PSO) [6]. As a result, the genetic operator of MOEA/D is replaced with the mechanism of PSO in this research to improve the convergence rate. The hybrid algorithm is afterwards called MOEA/D-PSO.

PSO was developed by Kennedy and Eberhart [7] to mimic the collaborative social movement of the large biological swarm in searching for food such as a bird flock or fish school. PSO is a population-based meta-heuristic which stochastically manipulates its offspring generation mechanism without any evolutionary operator like appearing in GA, e.g. crossover and mutation. As a result, many relative advantages offered by PSO include fast convergence, fewer parameter settings, less memory consumption, etc.

In the context of PSO, a particle denotes an individual solution of the problem, a swarm represents the population of solutions, and the optimum solution is the food. Each particle has three key attributes, i.e. position (its current solution), velocity (magnitude and direction of the trajectory towards the optimum solution), and fitness (relative performance). The particle navigates its flight by regularly adjusting its velocity with the supervision from two sources, i.e. its own best flying experience (personal best known as *P*best) and entire population best flying experience (global best known as *G*best). The pseudo code of MOEA/D-PSO is described as follows.

Pseudo code of MOEA/D-PSO

1. Generate weight vector λ for the population size N using simplex lattice design.
2. Define the parameters of the algorithm, i.e. the neighbourhoods (T) of each weight vector, inertia weight w, and learning factors c_1 and c_2.
3. Determine particle position vector X_j for each particle $j = 1, \dots, N$ whose size equals the total number of tasks (d) in the PAUL using $R[0,1]$.
4. Determine particle velocity vector (V_j) for $j = 1, \dots, N$ whose size equals the total number of tasks (d) in the PAUL using $R[0,1]$.
5. Determine the configuration of the PAUL using the decoding algorithm (to be explained in the next section) and calculate all m objectives of each X_j.
6. Determine the minimum and maximum values of each objective, i.e. z_m^* and $f_{m(max)}$.
7. Set the initial values of Pbest (P) and Gbest (G) of each particle by $P_j = X_j$ and $G_j = X_j$.
8. Find the non-dominated solutions in the current population, add them into the external population (EP), find the non-dominated solution in EP, and trash all dominated solutions from EP (note that the initial $EP = \phi$).
9. Find the velocity vector of each particle j using $V_j(\mathrm{t}+1) = wV_j(t) + c_1 r_1\big(P_j(t) - X_j(t)\big) + c_2 r_2\big(G_j(t) - X_j(t)\big)$ and then find its new position vector using $X_j(\mathrm{t}+1) = X_j(t) + V_j(t+1)$.
10. Find the new configuration of the PAUL using the decoding algorithm and calculate all m objectives of each X_j.
11. Update z_m^* and $f_{m(max)}$.
12. Find normalised values of each objectives using $\overline{f_i} = \frac{f_i - z_i^*}{f_{i(max)} - z_i^*}$ for each X_j, P_j and G_j.

13. Update Pbest of each X_j by comparing the Tchebycheff function (minimize $g_j(\mathrm{x}) = \max_{1 \le i \le m} \{\lambda_{ij}|\overline{f}_i|\}$) between P_j and X_j. If X_j is better than P_j, set $P_j = X_j$; otherwise, maintain current P_j.
14. Update Gbest by comparing the Tchebycheff function between G_j of the randomly selected neighbourhoods and X_j. If X_j is better than G_j, set $G_j = X_j$; otherwise, maintain current G_j.
15. If the termination condition is not met, go to step 8; otherwise, stop the algorithm.

3.2 Decoding algorithm

The solution string in this paper is represented by a priority-based scheme where the number under the task indicates its assignment priority. For example, nine (A1,..., A9) and seven (B1,..., B7) tasks are produced by Line 1 and Line 2, respectively, as shown in Fig. 4. According to the arrangement of String 1, the priorities of tasks from highest to lowest are B6, B4, B7,..., A5 and A8.

String	Task															
	A1	A2	A3	A4	A5	A6	A7	A8	A9	B1	B2	B3	B4	B5	B6	B7
1	8	13	12	10	15	9	11	16	6	5	4	7	2	14	1	3

Fig. 4 An example of solution strings

The decoding algorithm to transform the solution string into the corresponding PAUL is as follows.

Decoding algorithm

1. Determine the total number of to-be-assigned tasks by adding the number of tasks in Line 1 with Line 2.
2. Determine the assignable task list which is a set of tasks that are eligible for the assignment without violating the precedence constraint. For U-line, the assignable tasks are those that locate on the left-hand side of the precedence diagram without any predecessor (assign to the Front) and on the right-hand side of the precedence diagram without any successor (assign to the Back).
3. Let S1 be the set of tasks that can be assigned to the Front of Line 1, S2 be the set of tasks that can be assigned to the Back of Line 1, S3 be the set of tasks that can be assigned to the Front of Line 2, and S4 be the set of tasks that can be assigned to the Back of Line 2. Group all assignable tasks into their appropriated sets, i.e. S1, S2, S3 and S4.
4. Open a new workstation.
5. Select the task with the highest priority from the assignable task list and assign it to the corresponding side (i.e. S1, S2, S3 and S4) of the U-line.
6. Reduce the number of to-be-assigned tasks by 1. If the number of to-be-assigned tasks is equal to 0, then the algorithm is completed; otherwise, go to (7).
7. Compute the remaining available time of the workstation.
8. Update the assignable task list by considering only those that their task times are less than the remaining available time of the current workstation without violating the precedence constraint as follows:
   a) If the assigned task is in S1 (the Front of Line 1), the assignable tasks are those that are in S1 (to form a regular workstation) and S2 (to form a crossover workstation).
   b) If the assigned task is in S2 (the Back of Line 1), the assignable tasks are those that are in S1 (to form a crossover workstation), S2 (to form a crossover workstation) and S3 (to form a multi-line workstation).
   c) If the assigned task is in S3 (the Front of Line 2), the assignable tasks are those that are in S2 (to form a multi-line workstation), S3 (to form a regular workstation) and S4 (to form a crossover workstation).
   d) If the assignable task is in S4 (the Back of Line 2), the assignable tasks are those that are in S3 (to form a multi-line workstation) and S4 (to form a regular workstation).

9. If the assignable task list is empty and the to-be-assigned tasks still exist, then go to (4); otherwise, select the task with the highest priority from the assignable task list and assign it to the classified side of the line.
10. Reduce the number of to-be-assigned tasks by 1. If the number of to-be-assigned tasks is empty, then the algorithm is completed; otherwise, go to (11).
11. Compute the remaining available time of the workstation.
12. Update the assignable task list by considering only those that their task times are less than the remaining available time of the current workstation without violating the precedence constraint as follows:
    a) If the recently assigned task still forms a regular workstation with the previously assigned tasks, the assignable tasks can be found in the same way as 8(a)-8(d).
    b) If the recently assigned task forms a crossover workstation with the previously assigned tasks, the assignable tasks are those that belong to S1 and S2, or S3 and S4, depending on the line (Line 1 or Line 2) where the crossover workstation is located.
    c) If the recently assigned task forms a multi-line workstation with the previously assigned tasks, the assignable tasks are those that belong to S2 and S3 only.
13. Repeat steps 9-12.

Assume that the precedence diagrams of the products to be assembled on Line 1 and Line 2 are shown in Fig. 5. The common cycle time of the lines is 30. The numerical example of the algorithm is demonstrated in Table 1. Fig. 6 depicts the resultant PAUL which consists of three regular workstations on Line 1, one crossover workstation on Line 1, one regular workstation on Line 2, one crossover workstations on Line 2, and one multi-line workstation.

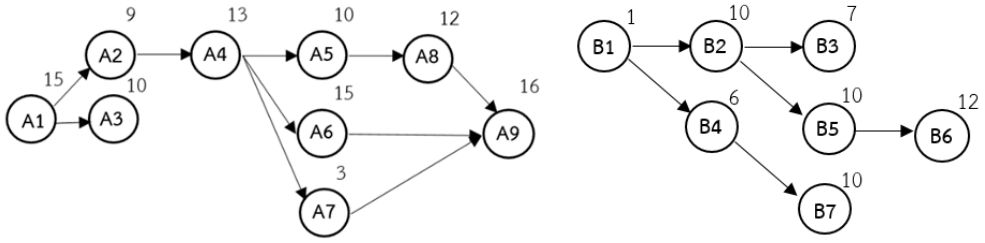

(a) Line 1 (b) Line 2

Fig. 5 An example of solution strings

Table 1 Task-to-workstation assignment (cycle time = 30)

Work-station	Assignable Task				Select	Task Time	Idle Time
	Line 1		Line 2				
	S1	S2	S3	S4			
1	A1	A9	B1	B3, B6, B7	B6	12	18
	A1	A9	B1	B3, B5, B7	B7	10	8
	A1	A9	B1	B3, B5, B4	B4	6	2
	A1	A9	B1	B3, B5	B1	1	1
2	A1	A9	B2	B3, B5	B2	10	20
	A1	A9	B3, B5	B3, B5	A9	16	4
	A1	A8, A6, A7	B3, B5	B3, B5	A7	3	1
3	A1	A8, A6	B3, B5	B3, B5	B3	7	23
	A1	A6, A8	B5	B5	B5	10	13
4	A1	A8, A6	-	-	A1	15	15
	A2, A3	A8, A6	-	-	A6	15	0
5	A2, A3	A8	-	-	A3	10	20
	A2	A8	-	-	A2	9	11
6	A4	A8	-	-	A4	13	17
	A5	A8	-	-	A5	10	7
7	A8	A8	-	-	A8	12	18

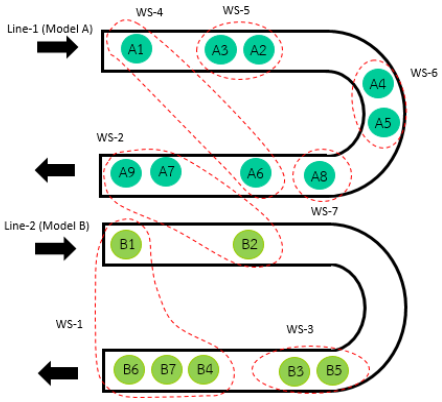

Fig. 6 The resultant PAUL

4. Results and discussion

4.1 Experimental design

Problem set

Twelve problems were used to test the performances of MOEA/D-PSO. The problems were modified from previously published research to fit in the PAUL's environment and they were classified into three sizes, i.e. small, medium and large. The number of tasks ranged from 30-50, 50-100 and 100-170 for small, medium and large, respectively. In each problem, the cycle times of the lines were assumed unequal and varied in three levels; hence, the common cycle time of the system was determined according to [2]. In addition, mixed-models of the product were produced by each U-line. Table 2 shows the detail of each problem.

Parameter settings of the algorithms

Three algorithms were tested in this research, i.e. MOEA/D, MOPSO and MOEA/D-PSO. MOPSO is the conventional PSO algorithm but applying the Pareto-based fitness scheme to guide its search trajectory. In order to provide a fair-play contest, all algorithms were carefully coded and tuned so that they could execute at their best performances. The parameter tuning of the algorithms was based on the result obtained from statistical analyses of the experimental designs, particularly the general full factorial design. All programs were coded in MathLab on a notebook computer using Intel® Core™ i7-7700HQ CPU@2.8GHz 8.00 GB RAM 64-bit operating system operated under Microsoft Windows 10 Pro.

Two parameters of MOEA/D including the number of weight vectors in the neighbourhood and the maximum number of solutions replaced by each offspring were set at 10% and 20%, respectively. The values of inertia weight, cognitive learning parameter and social learning parameter (learning) for MOPSO were set at 1, 1.5 and 1, respectively. For MOEA/D-PSO, the values of the number of weight vectors in the neighbourhood, the maximum number of solutions replaced by each offspring, inertia weight, cognitive learning parameter and social learning parameter were set at 10 %, 20 %, 1, 1.5 and 1, respectively. The number of populations in each algorithm was 133. The number of generations was 1000, 1500 and 2000 for small, medium and large problems, respectively.

Pareto-based metrics

To evaluate the relative performances of the algorithms in a Pareto sense, several metrics were employed in this research. The metrics which are related to the convergence performance of the algorithms including generational distance (GD), inverted generational distance (IGD), ratio of non-dominated solutions (self-comparison, R_{NDS1}) and ratio of non-dominated solutions (Pareto-optimum comparison, R_{NDS2}). $Spread$ is a metric to indicate the diversity of non-dominated solutions. The detailed formulations of all Pareto-based metrics were discussed by Coello Coello and Cortés [8] and Chutima and Olarnvanitchai [9].

Table 2 Problems used in the experiments

No.	Line1				Line2				Total Task	Common Cycle Time
	Problem	Models	MPS	Cycle Time	Problem	Models	MPS	Cycle Time		
1	Mitchell	3	2:1:2	15	Jackson	2	3:1	10	32	30
				18				12		36
				21				14		42
2	Jackson	3	1:2:1	9	Rozieg	2	3:1	18	36	18
				11				22		22
				13				26		26
3	Mitchell	2	2:1:2	17	Rozieg	3	1:2:1	34	46	34
				21				18		126
				21				21		21
4	Rozieg	3	1:2:1	21	Rozieg	3	2:1:2	42	50	42
				25				50		50
				16				32		32
5	Heskiaoff	3	1:1	138	Heskiaoff	2	1:1	205	56	28290
				205				216		44280
				216				324		648
6	Gunther	3	1:1	41	Sawyer	2	2:3	41	65	41
				54				54		54
				81				81		81
7	Killbridge	3	1:1	79	Heskiaoff	2	2:3	138	73	10902
				110				205		4510
				110				216		11880
8	Killbridge	2	1:1	57	Kilbridge	2	1:3	79	90	4503
				92				110		5060
				110				110		110
9	Killbridge	3	2:1:2	79	Tonge	3	1:2:1	410	115	32390
				110				468		25740
				110				527		57970
10	Tonge	3	1:1:1	320	Tonge	2	3:1	320	140	320
				207				270		6210
				293				220		64460
11	Tonge	2	3:1	220	Wee-mag	3	1:1:1	270	145	5940
				252				84		252
				303				101		303
12	Arcus1	3	1:1:2	6842	Acrus1	3	1:2:1	6842	166	6842
				7571				7571		7571
				6309				6309		6309

4.2 Experimental results

Table 3 in Appendix A shows the relative performances of all algorithms in tackling the PAULBP. As mentioned earlier, two performance aspects can be evaluated when facing MOPs, i.e. convergence and spread. The first convergence-related metric is GD which indicates the distances between the non-dominated solutions (NDSs) on the PF obtained by the algorithm and the closest NDSs on the approximated true Pareto front (ATPF). Note that ATPF is constructed by applying non-dominated sorting to the combined PFs of all algorithms obtained after the algorithm is terminated. If GD is 0 (the best value of GD), the PF of the algorithm is perfectly overlapped with the ATPF. It is obvious that GDs of MOEA/D-PSO are always lowest, followed by MOEA/D and MOPSO, regardless of the problems' sizes. In addition, GDs obtained by MOEA/D-PSO are always very close to 0 meaning that most of its obtained NDSs are on the ATPF.

IGD is similar to GD, but it measures the distances between the NDSs on the ATPF and the closest NDSs on the PF obtained by the algorithm. As a result, IGD also implies the coverage of the extreme points on ATPF by the algorithm. The algorithm with a lower IGD is the better one

(the best value of IGD is 0). It is obvious that MOEA/D-PSO always has the lowest values of IGD comparing with MOEA/D and MOPSO, regardless of problem's sizes and cycle times.

R_{NDS1} and R_{NDS2} are another important convergence-related metrics. They specify how many of the NDSs on the PF of the algorithm belongs to the ATPF. R_{NDS1} compares this number with its owned number of NDSs on the PF; whereas, R_{NDS2} compares this number with the NDSs on the ATPF. The higher the values of R_{NDS1} and R_{NDS2} are the better algorithm. The results show clearly that MOEA/D-PSO often outperforms MOEA/D and MOPSO. When the results from R_{NDS1} and R_{NDS2} are interpreted along with GD and IGD, it conveys about the PF of MOEA/D-PSO that it is located pretty close to the ATPF and all of its NDSs are almost on the ATPF. In addition, the PF of MOEA/D-PSO covers the extreme point on the ATPF.

$Spread$ is used to assess the distribution of NDSs produced by the algorithm which is related to the diversity of the solutions. This metric determines how much difference between the distance between two adjacent NDSs and the average distance. The lower $Spread$ (i.e. more uniform distribution) is the better algorithm. Although MOPSO often provides the best $Spread$, particularly in large sizes' problems, its value is marginally lower than MOEA/D and MOEA/D-PSO. This result comes with unsurprising since there is no diversity preservation mechanism embedded in any algorithm tested in this research.

Another aspect observed during the experiments, but does not present in this paper because of page limitation, is the number of workstations (N_w) and stations (N_S) created by each algorithm. It is found that the best value of N_w created by all algorithms is almost the same as the ideal number which calculates from dividing the total task time by the cycle time. MOEA/D-PSO always obtains the best N_w comparing with the other algorithms. In addition, the best value of N_S generated by each algorithm is the same. This reflects the effectiveness of the decoding method that is proposed in this research, as well as the PAUL's configuration.

In theory, the PAUL's concept is viable and could be extended to integrate more than two or even all U-lines located in close vicinity of each other to form a multi-PAUL facility. However, in practice, a number of issues that should be carefully addressed are as follows. For some factories that do not plan to utilise the PAUL in advance, it may be necessary to re-arrange their existing U-lines to be aligned with the PAUL layout.

The distance between the adjacent U-lines which will be used to form the PAUL should not be too long. In addition, multi-line workers should be more appropriate to work in a standing posture since they will have to travel back and forth between two legs of different U-lines. The need to walk while working could cause fatigue in the workplace with workers.

The features of tasks assigned to two legs of a multi-line workstation of the PAUL must not be too much diverse, e.g. soldering IC's pins (expert hands) and visual inspection (expert eyes). If possible, they should be in the same category, i.e. requiring the same skill. In fact, multi-skilled workers should not be bombarded with too many skill trainings since it could prevent them from being an expert in the field. In addition, higher wages should be paid to multi-line workers since their responsibilities are much higher than workers in regular workstations.

5. Conclusion

A novel assembly line configuration widely found in many multiple U-lines facilities but no one has ever utilised it, namely a PAUL, is proposed in this paper. This configuration is developed to increase the productivity of two or more U-lines placed adjacently and some of their workstations are underutilised (i.e. high idle time) while they are operated independently. To increase the utilisation rate of the whole system, paralleling these U-lines is done by allowing the formation of multi-line workstations located between their adjacent legs (Front of one U-line and Back of the other adjacent U-line). Multi-skilled labours are allocated such workstations to ensure the smoothness of mixed-model production flow on the PAUL. Several conflicting objectives of the PAULBP are optimised simultaneously and evaluated under a Pareto sense. Since the problem is NP-hard, the decomposition-based algorithm to generate good layouts of the PAUL is proposed namely MOEA/D-PSO which is the hybridisation between MOEA/D and PSO. The algorithm is tested against MOEA/D and MOPSO to assess their relative performances. Several prob-

lems with different sizes, number of tasks, product mixes and cycle times are employed as test-bed cases. The results reveal clearly that MOEA/D-PSO outperforms MOEA/D and MOPSO in terms of convergence-related metrics while their performances are indifferent in diversity-related metric. In addition, the decoding algorithm is quite effective in generating good PAUL layouts. The further research directions could be extended to the PAULBP Type II, considering the walking time of the worker, various skilled labour [10], asynchronous U-lines [11], or simultaneous balancing and sequencing [12].

References

[1] Cheng, C.H., Miltenburg, J., Motwani, J. (2000). The effect of straight- and U-shaped lines on quality, *IEEE Transactions on Engineering Management*, Vol. 47, No. 3, 321-334, doi: 10.1109/17.865901.

[2] Gökçen, H., Ağpak, K., Benzer, R. (2006). Balancing of parallel assembly lines, *International Journal of Production Economics*, Vol. 103, No. 2, 600-609, doi: 10.1016/j.ijpe.2005.12.001.

[3] Küçükkoç, I., Zhang, D.Z. (2015). Balancing of parallel U-shaped assembly lines, *Computers & Operations Research*, Vol. 64, 233-244, doi: 10.1016/j.cor.2015.05.014.

[4] Chutima, P., Chimklai, P. (2012). Multi-objective two-sided mixed-model assembly line balancing using particle swarm optimisation with negative knowledge, *Computers & Industrial Engineering*, Vol. 62, No. 1, 39-55, doi: 10.1016/j.cie.2011.08.015.

[5] Zhang, Q., Li, H. (2007). MOEA/D: A multiobjective evolutionary algorithm based on decomposition, *IEEE Transactions on Evolutionary Computation,* Vol. 11, No. 6, 712-731, doi: 10.1109/TEVC.2007.892759.

[6] Hassan, R., Cohanim, B., de Weck, O., Venter, G. (2005). A comparison of particle swarm optimisation and the genetic algorithm, In*: Proceedings of 46th AIAA/ASME/ASCE/AHS/ASC Structures, Structural Dynamics and Materials Conference,* Austin, Texas, USA, doi: 10.2514/6.2005-1897.

[7] Kennedy, J., Eberhart, R. (1995). Particle swarm optimization, In: *Proceedings of ICNN'95 – International Conference on Neural Networks,* Perth, WA, Australia, Vol. 4, 1942-1945, doi: 10.1109/ICNN.1995.488968.

[8] Coello, C.A.C., Cortés, N.C. (2005). Solving multiobjective optimisation problems using an artificial immune system, *Genetic Programming and Evolvable Machines,* Vol. 6, No. 2, 163-190, doi: 10.1007/s10710-005-6164-x.

[9] Chutima, P., Olarnviwatchai, S. (2016). A multi-objective car sequencing problem on two-sided assembly lines, *Journal of Intelligent Manufacturing,* Vol. 29, No. 7, 1617-1636, doi: 10.1007/s10845-016-1201-6.

[10] Corominas, A., Pastor, R., Plans, J. (2008). Balancing assembly line with skilled and unskilled workers, *Omega,* Vol. 36, No. 6, 1126-1132, doi: 10.1016/j.omega.2006.03.003.

[11] Tiacci, L. (2017). Mixed-model U-shaped assembly lines: Balancing and comparing with straight lines with buffers and parallel workstations, *Journal of Manufacturing Systems,* Vol. 45, 286-305, doi: 10.1016/j.jmsy.2017.07.005.

[12] Defersha, F.M., Mohebalizadehgashti, F. (2018). Simultaneous balancing, sequencing, and workstation planning for a mixed model manual assembly line using hybrid genetic algorithm, *Computers & Industrial Engineering,* Vol. 119, 370-387, doi: 10.1016/j.cie.2018.04.014.

Appendix A

Table 3 Experimental results

Problem	1 (S1)		2 (S2)			3 (S3)		4 (S4)		5 (M1)		6 (M2)	
No. of Tasks (Line1-Line2)	32 (21-11)		36 (11-25)			46 (21-25)		50 (25-25)		56 (28-28)		65 (35-30)	
Cycle Time	30	36	42	18	22	26	34	126	21	42	50	52	28290	44280	648	41	54	81
Generational Distance (GD)																		
MOPSO	0.0980	0.1508	0.1379	0.1349	0.1862	0.1057	0.1110	0.1079	0.1366	0.2265	0.1294	0.1565	0.1928	0.2203	0.1171	0.3239	0.1206	0.1717
MOEA/D	0.0699	0.0749	0.0648	0.0907	0.1156	0.0842	0.0498	0.0631	0.1061	0.1471	0.0616	0.1032	0.0914	0.1538	0.0793	0.1386	0.0732	0.1066
MOEA/D-PSO	**0.0412**	**0.0749**	**0.0616**	**0.0342**	**0.1027**	**0.0651**	**0.0343**	**0.0546**	**0.0180**	**0.1317**	**0.0520**	**0.0313**	**0.0877**	**0.0752**	**0.0508**	**0.0422**	**0.0510**	**0.0732**
Inverted Generational Distance (IGD)																		
MOPSO	0.1031	0.1379	0.1176	0.1467	0.1482	0.1350	0.0959	0.0935	0.1680	0.2183	0.1240	0.1683	0.1968	0.1362	0.1380	0.2882	0.1730	0.1489
MOEA/D	0.0870	0.1072	0.1105	0.1468	0.1480	0.1791	0.1764	0.0972	0.1362	0.2774	0.0714	0.0930	0.1904	0.0894	0.0982	0.1531	0.1389	0.1797
MOEA/D-PSO	**0.0621**	**0.0812**	**0.0727**	**0.1055**	**0.0730**	**0.0788**	**0.0415**	**0.0800**	**0.0892**	**0.0838**	**0.0618**	**0.0926**	**0.1901**	**0.0873**	**0.0956**	**0.1086**	**0.0864**	**0.1204**
R_{NDS1}																		
MOPSO	0.1470	0.0527	0.0689	**0.5562**	0.2514	0.1472	0.0667	0.0513	0.0426	0.1176	0.1647	0.0763	0.0959	0.0291	0.1189	0.0055	0.1480	0.0603
MOEA/D	0.3883	**0.4133**	0.4028	0.0550	0.2906	0.3504	0.4005	0.2628	0.0736	0.2414	0.2859	0.0775	0.3473	0.1923	0.3488	0.1430	0.3194	0.3571
MOEA/D-PSO	**0.4745**	0.4032	**0.4101**	0.2341	**0.3454**	**0.4116**	**0.5016**	**0.4773**	**0.7027**	**0.3095**	**0.4732**	**0.6759**	**0.4769**	**0.5253**	**0.3955**	**0.6063**	**0.3346**	**0.4567**
R_{NDS2}																		
MOPSO	0.0820	0.0283	0.0536	0.0316	0.0952	0.0727	0.0370	0.0379	0.0225	0.0476	0.0825	0.0402	0.0584	0.0227	0.0714	0.0057	0.0750	0.0443
MOEA/D	0.1914	0.2311	0.1905	0.1263	0.1619	0.1273	0.1543	0.1742	0.0449	0.1786	0.1495	0.0632	0.1948	0.1477	0.2071	0.1092	0.1375	0.2089
MOEA/D-PSO	**0.2695**	**0.2453**	**0.2857**	**0.3421**	**0.2762**	**0.3000**	**0.3148**	**0.2879**	**0.4326**	**0.2738**	**0.2732**	**0.4023**	**0.2468**	**0.3295**	**0.2214**	**0.3851**	**0.2875**	**0.2468**
Spread																		
MOPSO	**0.7448**	0.8388	**0.7758**	0.0550	0.8677	0.8937	**0.8989**	**0.8550**	0.9516	0.9487	0.8691	0.9537	**0.7304**	**0.7500**	0.8835	**0.7142**	**0.7956**	**0.8383**
MOEA/D	0.8937	0.8575	0.8745	0.2341	0.9021	0.9441	0.9871	0.9014	**0.8701**	0.8998	**0.8486**	**0.6809**	0.9766	0.7544	0.9103	0.7955	0.9608	0.9190
MOEA/D-PSO	0.8175	**0.7379**	0.8663	**0.5562**	**0.7948**	**0.8827**	0.9182	0.8836	0.9156	**0.7955**	0.8716	0.8231	0.8670	0.9083	**0.8497**	0.8920	0.8929	0.9720

Table 3 Experimental results (continuation)

Problem	7 (M3)			8 (M4)			9 (L1)			10 (L2)			11 (L3)			12 (L4)		
No. of Tasks (Line1-Line2)	73 (45-28)			90 (45-45)			115 (45-70)			140 (70-70)			145 (70-75)			166 (83-83)		
Cycle Time	10902	4510	11880	4503	5060	110	32390	25740	57970	320	6210	64460	5940	252	303	6842	7571	6309
Generational Distance (GD)																		
MOPSO	0.1953	0.1106	0.1576	0.1129	0.0756	0.1232	0.0872	0.1194	0.0977	0.3657	0.2195	0.1568	0.2382	0.2210	0.2321	0.2329	0.3424	0.1838
MOEA/D	0.1629	0.0516	0.0726	0.0633	**0.0358**	0.0817	0.0556	0.0752	0.0823	0.0630	0.1443	0.1296	0.1029	0.1541	0.1394	0.1687	0.1962	0.1239
MOEA/D-PSO	**0.0699**	**0.0455**	**0.0440**	**0.0484**	0.0389	**0.0546**	**0.0530**	**0.0751**	**0.0561**	**0.0565**	**0.0249**	**0.0245**	**0.0951**	**0.1002**	**0.0424**	**0.0758**	**0.0910**	**0.0777**
Inverted Generational Distance (IGD)																		
MOPSO	0.2113	0.1304	0.2155	0.1296	0.0922	0.1203	0.1034	0.1466	0.1862	0.2495	0.2186	0.1537	0.2324	0.1902	0.2140	0.1638	0.1386	0.1349
MOEA/D	0.2096	0.0946	0.1458	0.1944	0.0996	0.1144	0.1639	0.1375	0.1541	0.1156	0.1940	0.1535	0.1648	0.1910	0.1189	0.1297	0.1369	0.1459
MOEA/D-PSO	**0.1227**	**0.0647**	**0.0899**	**0.0888**	**0.0773**	**0.0992**	**0.1001**	**0.1070**	**0.1280**	**0.0885**	**0.1223**	**0.1056**	**0.1031**	**0.1743**	**0.1171**	**0.1220**	**0.1268**	**0.0693**
R_{NDS1}																		
MOPSO	0.0259	0.0626	0.0526	0.2068	0.1495	0.0554	0.2564	0.0250	0.0663	0.0133	0.0450	0.0328	0.1699	0.1050	0.0473	0.0756	0.0175	0.0504
MOEA/D	0.0693	0.3656	0.4114	0.2205	0.3697	0.2094	**0.4559**	0.3247	0.2107	0.4583	0.0775	0.2364	0.1632	0.1327	0.2001	0.1579	0.1134	0.2835
MOEA/D-PSO	**0.5857**	**0.4936**	**0.5781**	**0.4430**	**0.4330**	**0.3859**	0.2722	**0.5234**	**0.3968**	**0.6401**	**0.8400**	**0.6529**	**0.3818**	**0.5104**	**0.5962**	**0.5454**	**0.7155**	**0.3983**
R_{NDS2}																		
MOPSO	0.0161	0.0324	0.0174	0.1115	0.0940	0.0640	**0.1875**	0.0192	0.0739	0.0053	0.0234	0.0152	0.0427	0.0972	0.0160	0.0577	0.0159	0.0265
MOEA/D	0.0484	0.1574	0.2087	0.0808	0.1745	0.1628	0.1602	0.1154	0.1420	0.2090	0.0391	0.1091	0.1325	0.1157	0.1440	0.1538	0.0476	0.1549
MOEA/D-PSO	**0.4355**	**0.3102**	**0.2739**	**0.3077**	**0.2315**	**0.2733**	0.1523	**0.3654**	**0.2841**	**0.2857**	**0.4375**	**0.3758**	**0.3248**	**0.2870**	**0.3400**	**0.2885**	**0.4365**	**0.3186**
Spread																		
MOPSO	**0.8129**	**0.8611**	**0.7586**	**0.8241**	**0.7392**	**0.7719**	0.7754	**0.9236**	**0.8413**	**0.5435**	**0.7135**	**0.8260**	0.9029	**0.6685**	**0.7624**	**0.7755**	**1.0852**	1.0123
MOEA/D	0.9164	0.8741	0.9333	0.8840	0.8809	0.9766	0.9743	1.1529	0.9164	0.8592	0.8289	0.8856	**0.8968**	0.9949	0.8711	0.9063	1.0978	**0.9552**
MOEA/D-PSO	0.8671	0.8996	0.9009	0.9164	0.8371	0.9252	**0.7566**	1.0200	1.0618	0.9090	0.8975	0.9622	0.9378	0.8844	1.0241	0.9837	1.1209	1.0739

APEM journal
Advances in Production Engineering & Management
Volume 14 | Number 1 | March 2019 | pp 65–79
https://doi.org/10.14743/apem2019.1.312
ISSN 1854-6250
Journal home: apem-journal.org
Original scientific paper

Achieving sustainable transport through resource scheduling: A case study for electric vehicle charging stations

Gong, D.[a], Tang, M.[a,*], Liu, S.[a], Xue, G.[a], Wang, L.[a]

[a]School of Economics and Management, Beijing Jiaotong University, Beijing, P.R. China

ABSTRACT

Electric vehicles support low-carbon emissions to revitalize sustainable transportation, and more charging stations are being built to meet the daily charging demand. Charging piles and service workers are the most important resources for electric vehicle charging stations, and the scheduling of these resources is an important factor affecting the charging stations' profits and sustainable industrial development. In this paper, we simulate the charging piles and service workers in charging station resource scheduling and analyze the impacts of the number of service workers, the charging pile replacement policy and the charging pile maintenance times on an electric vehicle charging station's profits. An orthogonal test can achieve the following optimal resource scheduling results when their range is known: (1) In the lifetime of the charging pile, seven maintenance times are needed; (2) Even if the charging pile is still in normal condition, it needs to be replaced in order to achieve the maximum profits for the charging station; (3) a comprehensive analysis of service efficiency and service costs indicates that 8 service workers are needed to achieve the optimal profits for the charging station. Therefore, the scientific contribution of this research is to establish one resource scheduling simulation model that can assess the effects of the number of service workers, the charging pile replacement policy and the charging pile maintenance times on charging station revenues and to obtain the optimal results. In addition, if the model parameters change, we can still obtain the optimal results.

ARTICLE INFO

Keywords:
Sustainable transport;
Resource scheduling;
Electric vehicle;
Charging station;
Simulation;
Profit

**Corresponding author:*
mincong@bjtu.edu.cn
(Tang, M.)

Article history:
Received 8 September 2018
Revised 12 February 2019
Accepted 24 February 2019

1. Introduction

To revitalize sustainable transportation, China is vigorously developing electric vehicles (EVs). By virtue of clean energy and total emissions reductions, electric vehicles address low-carbon emissions regulations under the new requirements and new tasks in China's auto industry [1, 2]. The next decade or even decades will be a strategic opportunity for EVs. In addition to satisfying the need for sustainable transportation, more charging stations are being built to meet the daily charging demand. Charging piles and service workers are the most important resources for electric vehicle charging stations. Charging piles are distributed in different charging stations, and each pile has a certain income if it operates normally. If failure occurs, repair or replacement is necessary, and charging piles require maintenance over the lifetime of the machine; otherwise, there is a high probability of failure. Therefore, we need to allocate charging station resources to achieve optimal charging station profits and sustainable transportation.

Limited by the developmental phase of the EVs industry, resource scheduling for charging stations has not been paid adequate attention. If resource scheduling is not taken into considera-

tion, the EV industry may not develop properly, which will hinder sustainable transportation. Simulation technology is used to model the relationships and behaviors between individuals in the whole system, and computer simulations are used to establish a model that can reproduce the real system in order to obtain an optimal solution. Therefore, based on the conception model, this paper obtains a resource scheduling mathematical model of a charging station and analyzes the model based on simulation theory using the AnyLogic tool. From the simulation point of view, this paper studies the effects of the number of service workers, the equipment replacement policy (equipment refers to the charging pile, and this is the same as follows) and the equipment maintenance times on charging station profits. Reasonable resource scheduling will result in proper electric vehicle industry development and achieve sustainable transportation.

This paper is organized as follows. We first conduct a comprehensive review, which forms the theoretical foundation of this study. In section 3, an analytical model is proposed that forms the base of the research problem. In section 4, we present the mathematical materials and methods. In section 5, we verify the simulation model through a case study. Finally, conclusive remarks are presented.

2. Literature review

EVs are environmentally friendly and are becoming increasingly popular in sustainable transportation. However, factors including the mileage (battery life), charging time, charging convenience, purchase price, and vehicle performance hinder the development of the EV industry [3-6]. An adequate charging infrastructure, rational national guidance and locally targeted construction planning, that is, reasonable resource scheduling, can be an effective way to solve these problems of the EV industry.

In the actual operations of EV charging stations, personnel time and effort are necessary, thus requiring the scheduling of a larger workload [7]. Therefore, theories and methods are needed to guide resource scheduling. Scholars have made many achievements in their research, including experience summarization, mathematical programming models, and artificial intelligence algorithms.

The initial research was basically a summary. Due to the lack of scheduling experience, Miller turned to the mathematical programming model [8], and Cook viewed the scheduling problem as essentially an NP (Non-deterministic Polynomial) problem [9]. Many scholars have studied specific problems. Xi *et al*. used a linear integer program to simulate the number of L1 (level 1) and L2 (level 2) EV charging stations required at work and public locations and predicted the EV travel flows in central Ohio as well as the number, type, and location of EVs charging stations [10]. Zhang *et al*. optimized direct current, fast EV charging station allocation and temporal utilization to maximize eVMTs (electric vehicle miles traveled) through a set-cover problem. This work showed that random and late charging will increase the grid demand in the afternoon, while early, inexpensive, and reserve strategies evenly distribute charging throughout the day [11]. Chen *et al*. developed a mixed-integer optimization program considering budgetary constraints, which limit the total number of EV charging stations to be deployed. The forecasted parking demand was used as an input to the mixed-integer optimization program, which strategically locates 80 public charging stations across 900 traffic analysis zones in the Seattle, Washington region [12]. Yi and Bauer formulated an optimal energy-aware charging infrastructure placement framework. The multi-objective decision model located the EV charging stations to maximize the number of reachable households under an energy constraint while minimizing the overall transportation energy consumption of charging actions [13].

For complex production scheduling, a simple mathematical model cannot cover all the factors, and the solution process is very complex. Therefore, people have developed artificial intelligence technology to solve scheduling problems; for example, in Mehar [14], a modified GA (genetic algorithm) that considers an objective function based on investments and transportation costs was used to optimize charging station locations. By contrast, Bendiabdellah *et al*. [15] and You and Hsieh [16] employed a hybrid GA to determine the optimal number and size of public charging stations, which found the optimal location by minimizing the investments and travel

costs. Tang *et al*. [17] applied multi-phase particle swarm algorithm to solve resource scheduling problem. The main shortcomings of AI are its low precision and easy divergence, thus making AI solutions non-optimal.

By combing the literature, we find that the existing scheduling theories have a record of solving the resource scheduling problem for EV charging stations. However, EV charging stations have their own characteristics, and many specific factors can influence resource scheduling, such as different policies, policymakers, charging station planners, battery technologies and EV manufacturers [18-21]. On the other hand, some studies have discussed the layout of EV charging stations [22-26], but they paid minimal attention to the resource scheduling of EV charging stations. Based on the mathematical model and simulation method [27], this paper builds the resource scheduling agent model of the EV charging station and analyzes the effect of the number of service workers, the equipment replacement policy and the equipment maintenance times on charging station profits.

3. Problem description

The problem of resource scheduling in EV charging stations is as follows. The service workers are concentrated in a certain area. When they receive the message "equipment maintenance", "equipment repair" or "equipment replacement" sent by the message center, they go to a charging station location to complete the corresponding task. In the service process, if the equipment cannot be repaired, the worker can directly replace the equipment, and if the equipment can be repaired, the worker checks whether the equipment needs maintenance. Considering the overall profits of the charging station, the service worker can replace equipment that is in a working state.

There are three main situations related to resource scheduling in charging stations.

Single service worker and single equipment

In the model for "single service worker and single equipment", the status of the equipment determines the worker's working time (drive time) and agenda (equipment replacement, equipment repair or equipment maintenance) (Fig. 1). The worker checks whether there is demand (equipment failure) for the equipment. If there is demand, the service worker drives to the charging station location to complete the service and finally returns to the worker center.

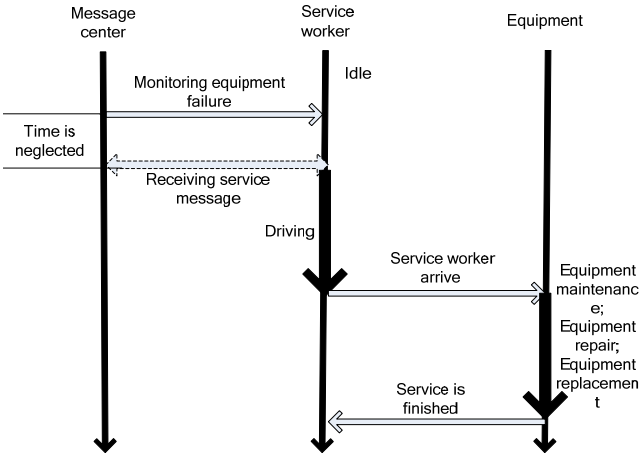

Fig 1 Situation 1

Single service worker and more equipment

In this case, there are two pieces of equipment and only one service worker (Fig. 2). When equipment 1 detects a fault and sends a service request to the message center, the message center immediately notifies the service worker, and the service worker quickly drives to the designated charging station location to finish the service. Equipment 2 also detects a fault, which also sends a service request to the message center; however, the request of equipment 2 cannot be answered until the service for equipment 1 is finished.

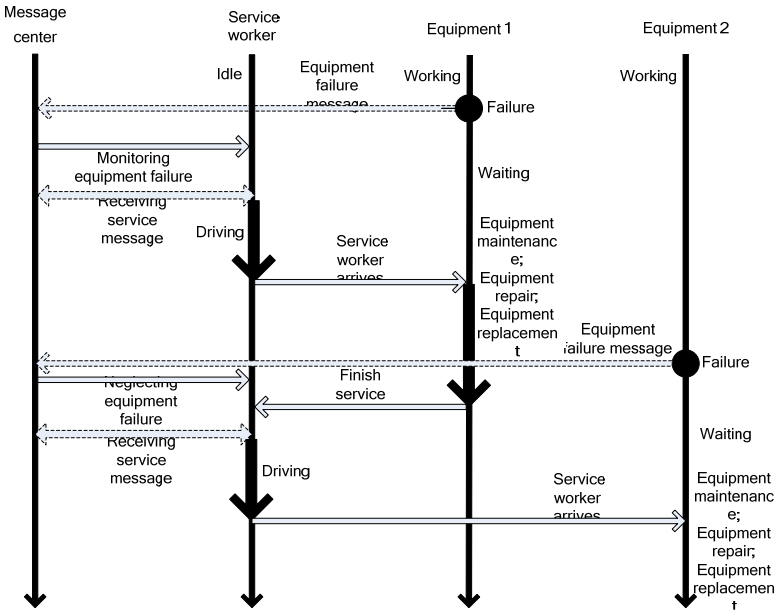

Fig 2 Situation 2

More service workers and single equipment

In this case, two workers can provide service for the same equipment (Fig. 3). The message center sends an equipment failure message to all service workers. At first, two service workers are idle, so they receive the messages and check their messages at the same time. Then, only one worker arrives at the designated charging station location to complete the service, and the other worker remains idle. In reality, it is a combination of the above three conditions.

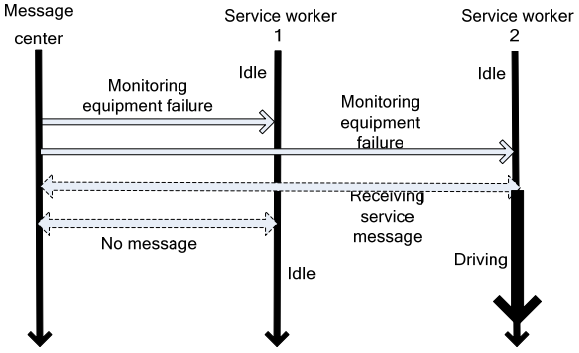

Fig. 3 Situation 3

The remainder of this paper will analyze the impacts of the number of service workers, the charging pile replacement policy and the charging pile maintenance times on the electric vehicle charging station's profits based on the mathematical model of resource scheduling and the idea of simulation modeling.

4. Materials and methods

4.1 Model definition

The assumptions in this paper are as follows:

- equipment needs maintenance, repair and replacement, and service workers can complete the above tasks,
- there are fixed costs in the process of equipment maintenance, repair and replacement,
- there is no specific running routine for the workers, and they move at a fixed rate,
- workers can provide service all day,

- workers can complete the task each time,
- workers can always arrive at the nearest charging station regardless of the running costs.

There are two types of worker-equipment constraints in the process of the worker reaching the demand point: the physical condition and the operational condition. These constraints are set as follows:

$$\begin{gathered}\sum_{i=1}^{n} v_i = V \ , \ \sum_{j=1}^{m} b_j = B \\ \text{idle}(v_i) = V_{idle} \\ \sum V_{idle} = \sum B_{type} \\ V_{idle} = B_{type} = (B_0, B_1, B_2, B_3) \Rightarrow service(v_i) = b_j\end{gathered} \tag{1}$$

where v_i is the worker, b_j is the equipment demand (maintenance, repair and replacement), V is the worker set, B is the demand set, $\text{idle}(v_i)$ is the condition of the worker, V_{idle} is the worker condition set, B_{type} is the demand type set, and $service(v_i) = b_j$ means that worker i provides service for demand j. Only if the demand type matches the worker type can service start. Therefore, the matrix of worker -equipment constraints is set as follows:

$$A = \begin{bmatrix} y_{11} & y_{12}y_{13} & \cdots & y_{1n} \\ y_{21} & \ddots & & \vdots \\ y_{31} & \ddots \ \ddots & & \vdots \\ \vdots & y_{ij} & \ddots & \vdots \\ \vdots & & \ddots & \vdots \\ y_{m1} & \cdots \cdots & \cdots & y_{mn} \end{bmatrix} \tag{2}$$

where $0 < i < n$ and $0 < j < m$.

$$y_{ij} = \begin{cases} 1 & \text{worker } v_i \text{ provides service for demand } b_j \\ 0 & \text{worker } v_i \text{ cannot provide service for demand } b_j \end{cases} \tag{3}$$

With the worker-equipment constraints, we aim to optimize the profits of the charging station and ensure the satisfaction of demand. The initial setting of the parameters is shown in Table 1.

Table 1 Initial setting of parameters

Parameter	Memo
V_n	Number of service workers
B_n	Amount of equipment
$B_0b_j, B_1b_{j'}, B_2b_{j''}, B_3b_{j'''}$	Equipment in different states (working, repair, maintenance or replacement); $j, j', j'', j''' = 1, 2,...,B_n$
t_1	Daily revenues generated by the equipment
t_2	Daily payment for the workers
t_3	Equipment repair costs
t_4	Equipment maintenance costs
t_5	Equipment replacement costs
$t_{17}(B_3)_{jm}$	Battery replacement policy
$t_{16}(B_2)$	Equipment maintenance times
X_{ijk}	Equipment j is serviced by worker i in sequence k
y_i	Equipment-worker constraints

The objective function in the model gains the maximum profits for the EV charging station. The charging station's total costs include worker costs, equipment maintenance costs, equipment repair costs and equipment replacement costs.

Total worker costs: t_2V_n

Total equipment repair costs:

$$t_3 \sum_{j'=1}^{B_n} (B_1b_{j'})$$

Total equipment maintenance costs:

$$t_4 \sum_{j''=1}^{B_n} \left(B_2 b_{j''}\right)$$

Total equipment replacement costs:

$$t_5 \sum_{j'''=1}^{B_n} \left(B_3 b_{j'''}\right)$$

Total charging station costs:

$$t_3 \sum_{j'=1}^{B_n} \left(B_1 b_{j'}\right) + t_4 \sum_{j''=1}^{B_n} \left(B_2 b_{j''}\right) + t_5 \sum_{j'''=1}^{B_n} \left(B_3 b_{j'''}\right) + t_2 V_n$$

4.2 Model construction

The total revenues of the charging station, which are generated by the normal working equipment, are as follows:

$$t_1 \sum_{j=1}^{B_n} \left(B_0 b_j\right)$$

The following maximizes the profits for the charging station when considering $t_{16}(B_2)$:

$$\begin{aligned} \underset{\substack{t_{16}(B_2)\\ V_n}}{\text{Max}}\ & t_1 \left\{ \sum_{m=1}^{t_{16}(B_2)} \sum_{j=1}^{B_n} \left(B_0 b_{m,j}\right) - \sum_{m=t_{16}(B_2)}^{\infty} \sum_{j=1}^{B_n} \left(B_2 b_{m,j''}\right) \right\} - t_3 \sum_{j'=1}^{B_n} \left(B_1 b_{j'}\right) \\ & - t_4 \sum_{m=1}^{t_{16}(B_2)} \sum_{j''=1}^{B_n} \left(B_2 b_{m,j''}\right) - t_5 \sum_{j'''=1}^{B_n} \left(B_3 b_{j'''}\right) - t_2 V_n \end{aligned} \tag{4}$$

The following maximizes the profits for the charging station when considering $t_{17}(B_3)_{jm}$:

$$\begin{aligned} \underset{\substack{t_{16}(B_2)\\ V_n\\ t_{17}(B_3)_{jm}}}{\text{Max}}\ & t_1 \left\{ \sum_{m=1}^{t_{16}(B_2)} \sum_{j=1}^{B_n} \left(B_0 b_{m,j}\right) - \sum_{m=t_{16}(B_2)}^{\infty} \sum_{j=1}^{B_n} \left(B_2 b_{m,j''}\right) \right\} \\ & - t_3 \sum_{j'=1}^{B_n} \left(B_1 b_{j'}\right) - t_4 \sum_{m=1}^{t_{16}(B_2)} \sum_{j''=1}^{B_n} \left(B_2 b_{m,j''}\right) - t_5 \sum_{j'''=1}^{B_n} \left(B_3 b_{j'''}\right) \left\{ \max\left(t_{17}(B_3)_{jm} + 1, 0\right) \right\} - t_2 V_n \end{aligned} \tag{5}$$

$$\text{if} \quad t_{17}(B_3)_{jm} = 0$$

$$\begin{aligned} \underset{\substack{t_{16}(B_2)\\ V_n\\ t_{17}(B_3)_{jm}}}{\text{Max}}\ & t_1 \left\{ \sum_{m=1}^{t_{16}(B_2)} \sum_{j=1}^{B_n} \left(B_0 b_{m,j}\right) - \sum_{m=t_{16}(B_2)}^{\infty} \sum_{j=1}^{B_n} \left(B_2 b_{m,j''}\right) - \sum_{j''=1}^{B_n} \left(B_3 b_{j''}\right) \right\} - t_3 \sum_{j'=1}^{B_n} \left(B_1 b_{j'}\right) \\ & - t_4 \sum_{m=1}^{t_{16}(B_2)} \sum_{j''=1}^{B_n} \left(B_2 b_{m,j''}\right) - t_5 \sum_{j'''=1}^{B_n} \left(B_3 b_{j'''}\right) \left\{ \max\left(t_{17}(B_3)_{jm} - 1, 0\right) \right\} - t_2 V_n \end{aligned} \tag{6}$$

$$\text{if} \quad t_{17}(B_3)_{jm} = 1$$

Considering the equipment-worker constraints, the objective function is as follows:

$$\underset{\substack{t_{16}(B_2)\\ V_n\\ t_{17}(B_3)_{jm}}}{\text{Max}} \; X_{ijk}\left[t_1\left\{\sum_{m=1}^{t_{16}(B_2)}\sum_{j=1}^{B_n}\left(B_0 b_{m,j}\right)-\sum_{m=t_{16}(B_2)}^{\infty}\sum_{j=1}^{B_n}\left(B_2 b_{m,j}\right)\right\}\right.$$
$$-t_3\sum_{j'=1}^{B_n}\left(B_1 b_{j'}\right)-t_4\sum_{m=1}^{t_{16}(B_2)}\sum_{j''=1}^{B_n}\left(B_2 b_{m,j''}\right) \tag{7}$$
$$\left.-t_5\sum_{j'''=1}^{B_n}\left(B_3 b_{j'''}\right)\left\{\max\left(t_{17}(B_3)_{jm}+1,0\right)\right\}-t_2 V_n\right]$$
$$\text{if} \quad t_{17}(B_3)_{jm}=0$$

$$\underset{\substack{t_{16}(B_2)\\ V_n\\ t_{17}(B_3)_{jm}}}{\text{Max}} \; X_{ijk}\left[t_1\left\{\sum_{m=1}^{t_{16}(B_2)}\sum_{j=1}^{B_n}(B_0 b_{m,j})-\sum_{m=t_{16}(B_2)}^{\infty}\sum_{j=1}^{B_n}\left(B_2 b_{m,j''}\right)-\sum_{j''=1}^{B_n}(B_3 b_{j''})\right\}\right.$$
$$-t_3\sum_{j'=1}^{B_n}\left(B_1 b_{j'}\right)-t_4\sum_{m=1}^{t_{16}(B_2)}\sum_{j''=1}^{B_n}\left(B_2 b_{m,j''}\right) \tag{8}$$
$$\left.-t_5\sum_{j'''=1}^{B_n}\left(B_3 b_{j'''}\right)\left\{\max\left(t_{17}(B_3)_{jm}-1,0\right)\right\}-t_2 Vn\right]$$
$$\text{if} \quad t_{17}(B_3)_{jm}=1$$

Subject to

$$\sum_{i=0}^{V_n}\sum_{j=0}^{B_n}X_{ijk}\geq 1, \qquad \text{where} \quad i=1,2\ldots V_n \tag{9}$$

Eq. 9 indicates that each instance of equipment demand can be assigned to the worker more than two times.

$$\sum_{j=0}^{B_n}X_{ijk}=1, \qquad \text{where} \quad j=1,2,\ldots,B_n \tag{10}$$

Only one equipment demand can be served by the worker at a time (Eq. 10).

$$\sum_{type=0}^{3}B_{type}=1 \tag{11}$$

Equipment failure (work, repair, maintenance or replacement) can occur only once at a time, and type = 0 means that the equipment is in normal working condition (B_0), (Eq. 11).

$$t_{16}(B_2)\in[1,M] \tag{12}$$

M is a positive number. Eq. 12 means that there is a certain limit for the equipment maintenance times according to the equipment operations and charging station profits.

$$X_{ijk}\leq y_{ij}\ , y_{ij}\in\{0,1\} \tag{13}$$

The equipment service must meet the equipment-worker constraints in Eq.13.
Matrix y_{ij} should consider the conditions below:

- whether the worker is in an idle state,
- whether the equipment is in a failure state,
- whether the equipment failure times reach the service limit.

$$\sum_{m=0}^{1} t_{17}(B_3)_{jm} = 1, j = 1,2 \ldots B_n \tag{14}$$

To increase the total profits of the charging station, even equipment in a normal working state can be replaced. Therefore, $t_{17}(B_3)_{j0} = 1$ indicates that normal equipment needs to be replaced, and $t_{17}(B_3)_{j1} = 0$ indicates that normal equipment does not need to be replaced (Eq. 14).

We can obtain the feasible solution using the Cplex model if V_n = 1 and B_n = 2, while it will be difficult to calculate the solution if more agents (equipment and workers) are included in the model. Due to the relationship complexity of the two agents and the dynamic demand of resource scheduling in the charging station, this paper develops the simulation method to model and simulate the resource scheduling for EV charging stations using the AnyLogic platform (AnyLogic platform is the leading simulation software invented by AnyLogic Company).

5. Case study

The AnyLogic simulator is developed to build equipment and worker simulation models. Our settings are shown in Table 2.

The output mainly includes the amount of equipment in operation, the amount of equipment in maintenance, and the amount of equipment in replacement or repair when changing $t_{16}(B_2)$, $t_{17}(B_3)_{jo}$, and V_n so that we can calculate the profits of charging stations. With respect to the equipment and worker simulation model, their message models are involved in the resource scheduling of the EV charging station.

Table 2 The simulation settings

Model	Item and memo
Worker model	Equipment variable
	Daily payment for worker
	Number of service workers
Equipment model	Equipment replacement time
	Equipment maintenance time
	Equipment repair time
	Equipment replacement probability
	Equipment maintenance period
	Basic equipment failure rate
	Equipment failure rate
	Workers
	Last maintenance time for equipment
	Last replacement time for equipment
	Equipment age
	Time since last maintenance
	Equipment replacement policy
	Equipment maintenance times
	Daily revenue generated by equipment
	Equipment replacement costs
	Equipment repair costs
	Equipment maintenance costs
Message	Equipment replacement or repair queue
	Equipment maintenance queue
	Equipment sent request for replacement or repair
	Equipment sent request for maintenance
	Request for replacement or repair is activated
	Request for maintenance is activated

5.1 Equipment simulation model

There are many factors that can affect the use of charging station equipment, such as the equipment failure rate, the equipment maintenance times, the equipment replacement policy, and the equipment maintenance cycle. In this model, there are four rules for each equipment agent.

Equipment failure rate

Whether a piece of equipment needs service is determined by its failure rate. The failure rate is affected by three factors: the equipment maintenance delay, the equipment age and basic failures. In this case, equipment maintenance delay = max (1, timeSinceMaintenance / MaintenancePeriod), age = max(1, ages/Flifetime), and equipment failure rate = basic failure × equipment maintenance delay × equipment age, where timeSinceMaintenance is the period since the equipment maintenance was completed, MaintenancePeriod is the maintenance period of the equipment, Flifetime is the rated life span of the equipment, and Fliftime = 3 × MaintenancePeriod.

Equipment maintenance times

After the equipment maintenance cycle, the equipment cannot work until it is serviced. However, the maintenance times K is limited by M; that is, the equipment can receive maintenance only if $K<M$, or it is directly scrapped.

Equipment replacement policy

When the equipment breaks down, the worker replaces or repairs it. Equipment replacement is also affected by the equipment replacement policy, which refers to the fact that the worker can directly replace the equipment that is still in working condition.

Equipment maintenance cycle

When the equipment repair is finished, the worker also checks whether the equipment needs maintenance. When the equipment maintenance period comes (timeSinceMaintenance > MaintenancePeriod), the worker immediately starts the maintenance service on the equipment. The operation of the equipment simulation model in AnyLogic is shown in Fig. 4.

Graphic description: The equipment is working at first. Then, it breaks down (Fails) according to the failure rate and sends the required service message to the message center. When the worker receives the request information through the message center, he or she goes to the charging station location (SCArrivaldForRepair). In this case, there are two ways of handling the issue: repair or replacement. If it is in the condition of replacement, the worker replaces the equipment (StartReplacement) after the replacement time (FinishReplacement); otherwise, the worker repairs the equipment (StartRepair) after the repair time (FinishRepair). If timeSinceMaintenance > MaintenancePeriod, the equipment needs maintenance (MaintenanceDue) after the maintenance time (FinishMaintenance); otherwise, if the maintenance cycle (MaintenanceNotDue) is not reached, the equipment can begin to run after the completion of the repairs. In addition, considering the equipment replacement policy and the overall charging station profits, we can require workers to check the working equipment (SCArrivedForMtce) even if it is still in normal condition.If it meets the equipment replacement policy, the worker should replace the working equipment (PlannedReplacement); otherwise, equipment maintenance (JustMaintenance) should be performed.

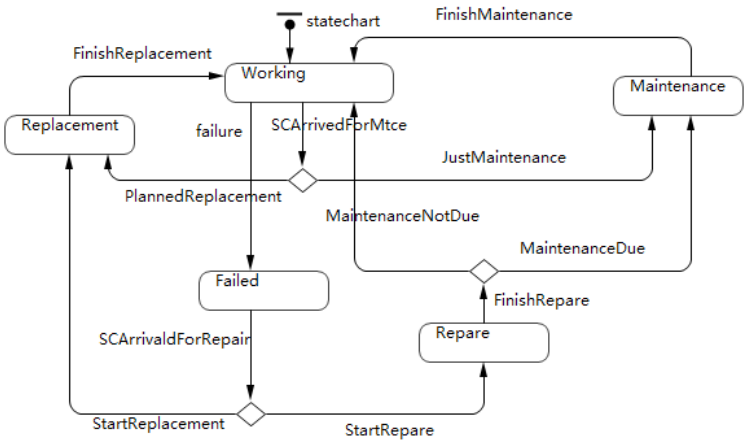

Fig. 4 Equipment agent operation

5.2 Worker simulation model

The workers will check the equipment service request from time to time. When the demand information is found and the worker is idle, the worker quickly drives to the designated charging station to complete the corresponding service. Thus, an eight-tuple is used to represent the level of worker service capability:

$$Cap\_servive(xloc, yloc, S_{number}, S_{idleornot}, S_{cost}, S_{worktime}, S_{miles}, S_{area})$$

The first two terms of the eight-tuple represent the geographical coordinates of the worker's location, S_{number} indicates the number of workers, $S_{idleornot}$ indicates the current status of the worker, $S_{idleornot} = 1$ indicates an idle state, $S_{idleornot} = 0$ indicates a busy state, S_{cost} is the payment for the worker, $S_{worktime}$ is the worker service time per day, S_{miles} is the maximum miles that a worker can drive every day, and S_{area} is the largest service area. The service process of the worker agent in AnyLogic is shown in Fig. 5.

Graphic description: At first, the worker is in the idle state $S_{idleornot} = 1$ and checks the service message from the message center (Check Request Queue). After receiving the equipment failure information (RequestsWaiting), the worker drives (DrivingtoWork) to the charging station (Arrived) and finishes the corresponding service (Working), which includes replacement, repair and maintenance. When the equipment sends out the "Finished" information, the equipment reenters the working state, and the worker is in an idle state again (IAmstillEmployed).If there are new requests for equipment service, the worker can be scheduled again, or the worker leaves the system (laidoff). If there is no equipment failure information (NoRequest), the worker returns (DrivingHome) to the original location (ArrivedHome) and assumes an idle state ($S_{idleornot} = 1$). Considering the overall profit of the charging station, we need to calculate the appropriate number of workers (checkiflaidoff).

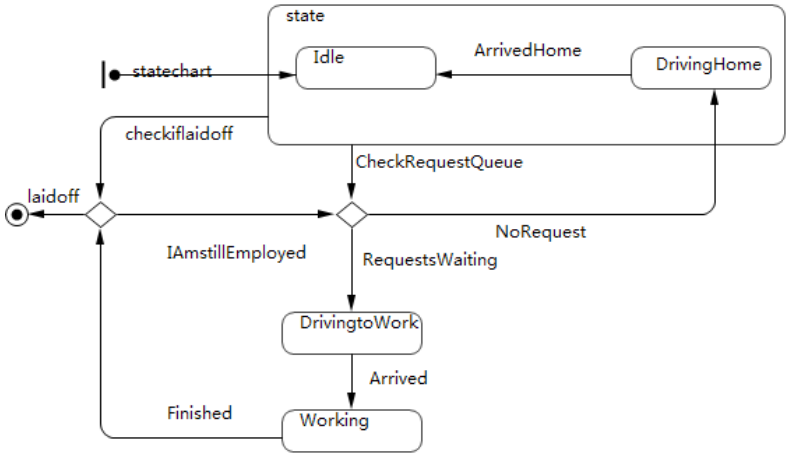

Fig 5 The service process of a worker

5.3 Message Center

Due to the "single service worker and more equipment" situation, the "first come, first service" mode is used to finish the corresponding service. The equipment failure information (replacement or repair) will be sent by the message center. The equipment failure information (maintenance) will also be sent by the message center. The worker checks the service message (replacement, repair, or maintenance) from the message center, and then the worker drives to the charging station and finishes the corresponding service.

In the simulator, we can obtain working equipment, in-service equipment, in-maintenance equipment and failed equipment.

6. Results and discussion

According to the mathematical model and simulation model, this paper can obtain the simulation results using the AnyLogic tool. The parameter setting and their values are shown in Table 3. Note: $t_{16}(B_2), t_{17}(B_3)_{j0}$ or $t_{17}(B_3)_{j1}, V_n$ are the decision variables, and the simulation time unit is years.

We need to analyze the number of service workers, the equipment replacement policy and the equipment maintenance times. When $t_{16}(B_2) = 5, t_{17}(B_3)_{j0} = 1$ and $V_n = 5$, the corresponding statistics of the worker and equipment are as shown in Fig. 6. In Fig. 6, most workers will be driving or working, and few workers are idle. In addition, most equipment are working, a few pieces are in the failed state, and a few pieces of equipment are in the maintenance state, repair state or replacement state. Based on the above statistical results, we can calculate the revenues of the charging station for years.

Table 3 Parametersettingand their values

Parameter	Memo	Distribution(value)
t_1	Daily revenues generated by equipment	U[150,250]
t_2	Daily payment for worker	U[700,800]
t_3	Equipment repair costs	U[250,450]
t_4	Equipment maintenance costs	U[100,200]
t_5	Equipment replacement costs	U[3000,4000]
t_6	Equipment repair time	$Tr_i[t_{51} \cdot 0.5, t_{51}, t_{51} \cdot 2.5], t_{51}n\ U$[0.5,1.5]
t_8	Equipment maintenance time	$Tr_i[t_7 \cdot 0.5, t_7, t_7 \cdot 1.5], t_7 \sim U$[0.3,0.7]
t_{10}	Equipment replacement time	$Tr_i[t_9 \cdot 0.5, t_9, t_9 \cdot 1.5], t_9 \sim U$[1.5,2.5]
t_{11}	Equipment replacement rate	$EXP[\lambda], \lambda = 10$
t_{12}	Equipment maintenance cycle	U[80,100]
t_{13}	Last maintenance time for equipment	U[-t_{12},0]
t_{14}	Last replacement time for equipment	U[-3t_{12},0]
t_{15}	Basic equipment failure rate	$EXP[\lambda_1], \lambda = 100/3$
$t_{16}(B_2)$	Equipment maintenance times	5
$t_{17}(B_3)_{j0} t_{17}(B_3)_{j1}$	Equipment replacement policy	$t_{17}(B_3)_{j0} = 1$ or $t_{17}(B_3)_{j1} = 0$
t_{18}	Worker driving miles per day	U[400,600]
V_n	Worker number	3
B_n	Equipment number	100
t_{21}	Service area	300000

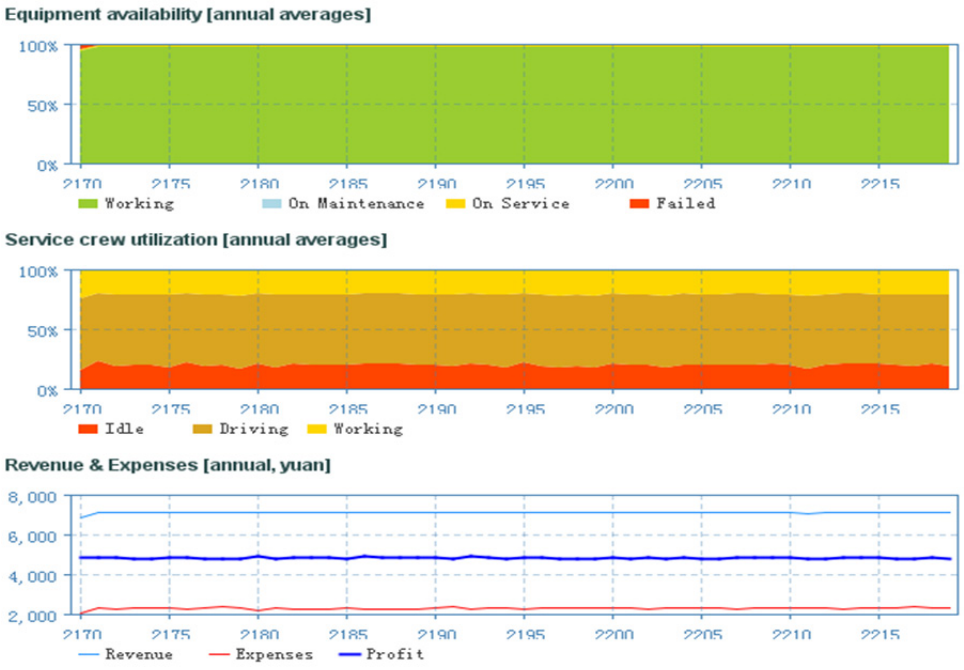

Fig. 6 Simulation results

It can be seen from Fig. 6 that the revenues, costs and profits of the charging station are held at a constant level when $t_{16}(B_2) = 5, t_{17}(B_3)_{j0} = 1$ and $V_n = 5$, and the profits are 4,800,000 yuan annually.

The goal of resource scheduling for EV charging stations is to achieve the maximum profits. Therefore, it is necessary to comprehensively consider the number of workers, equipment maintenance times and equipment replacement policy. Here, the number of workers is $V_n = 3 \in [1, \infty]$, the equipment maintenance times is $t_{16}(B_2) \in [1, \infty]$ and the equipment replacement policy is $t_{17}(B_3)_{j0} = 1$ or $t_{17}(B_3)_{j1} = 1$. Fig. 7 shows the different situations. When $t_{16}(B_2) = 6, t_{17}(B_3)_{j0} = 1$ and $V_n = 4$, the corresponding statistics of the worker and equipment can also be obtained, and the profits are 5,300,000 yuan annually (Fig. 7). When $t_{16}(B_2) = 7, t_{17}(B_3)_{j0} = 1$ and $V_n = 2$, the profits are approximately 3,200,000 yuan in one year (Fig. 8). Similarly, when $t_{16}(B_2) = 8, t_{17}(B_3)_{j0} = 1$ and $V_n = 3$, the profits are approximately 5,000,000 yuan in one year.

It is therefore impossible to calculate the optimal results through sensitivity analysis due to the infinite simulation results. An orthogonal test is developed to solve such a problem. In this paper, an orthogonal test is used to select some representative points in a nonstop way until the optimal situation is found. The parameter setting is given in Table 4.

The simulation time is 20 years, and the maximum number of iterations is 2000.The setting of the other parameters is shown in Table 2. The optimal results are obtained after 104 iterations (Table 5).

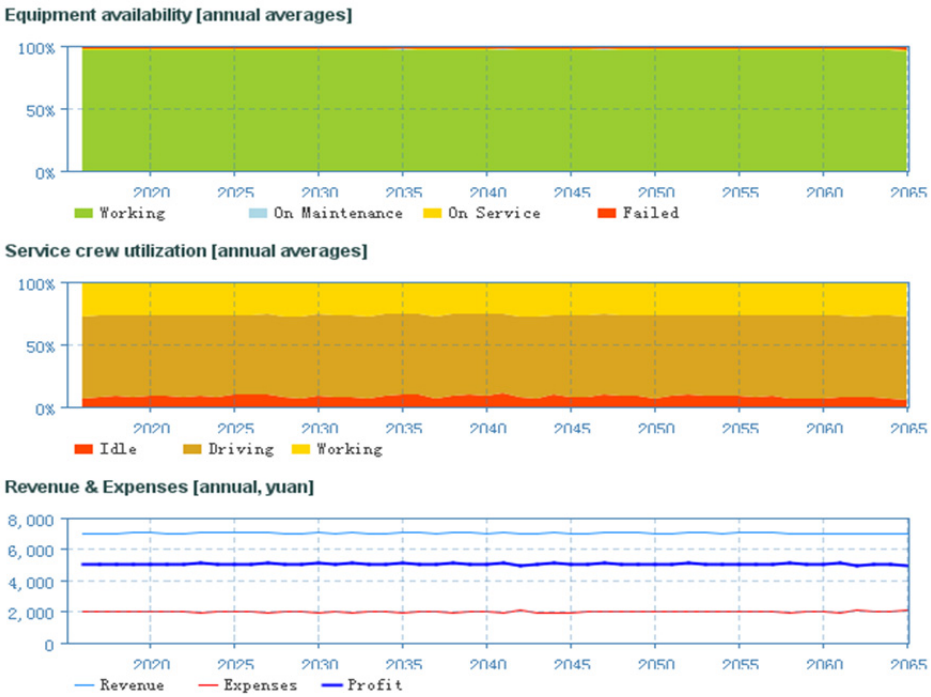

Fig. 7 Statistics of results 1

Table 4 Parameter setting in the orthogonal test

Parameter	Type	The minimum	The maximum	Step size
$t_{16}(B_2)$	Integer	2	8	1
$t_{17}(B_3)_{j0}$	Boolean	-	-	-
V_n	Integer	1	9	1

Table 5 The optimal results

Decision variables	Results
$t_{16}(B_2)$	7
$t_{17}(B_3)_{j0}$	$t_{17}(B_3)_{j0}$ = 0 or $t_{17}(B_3)_{j1}$ = 1
V_n	8

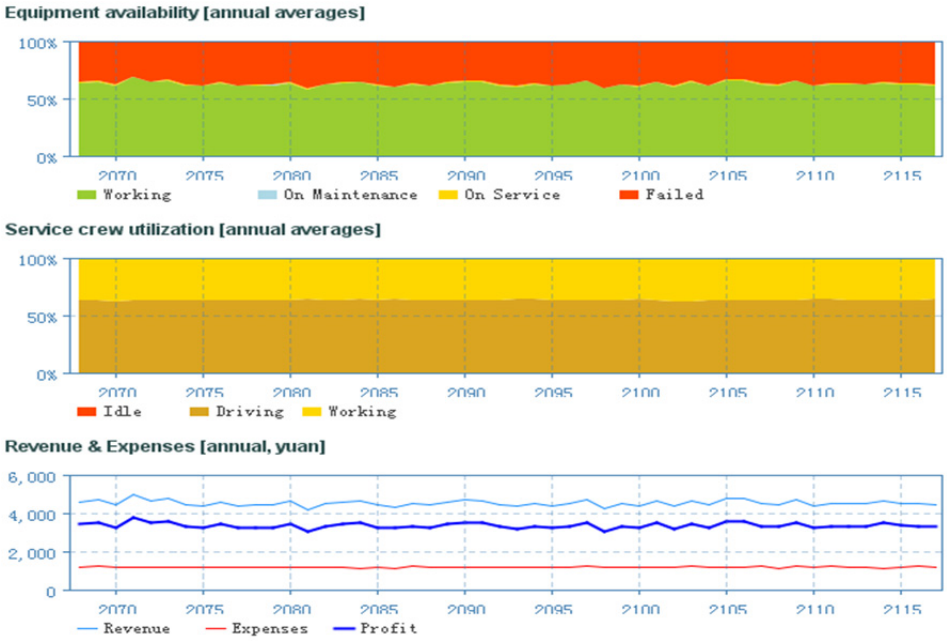

Fig 8 Statistics of results 2

Based on the results in Table 5, we can achieve additional profits of 5,928,336 yuan in one year. Therefore, we need to incorporate the following.

- Seven equipment maintenance instances. In Table 5, we known that the maximum number of maintenance instances is 8 and the minimum is 2, while it needs 7 maintenance instances for equipment during its life cycle. Therefore, it is not "the bigger, the better" for equipment maintenance. In this model, $t_{16}(B_2) = 7$.
- Replace equipment that is still in working condition. After a comprehensive analysis of labor costs, equipment maintenance costs, equipment replacement costs and equipment repair costs, equipment needs to be replaced even if it is working normally. In this model, $t_{17}(B_3)_{j0} = 0$ or $t_{17}(B_3)_{j1} = 1$.
- Eight workers are necessary for a charging station to achieve the optimal profits. Fewer workers will lead to a low service efficiency, and too many workers can create very large service costs. In the model, $V_n = 8$.

7. Conclusion

The development of EVs is an important way to improve sustainable transportation, energy security and the low-carbon economy. According to the statistics of the ISO in 2009, 25% of newly purchased vehicles (approximately 50 million) will be EVs by 2030. China has achieved a great deal in terms of the infrastructure, marketing and standardization of the EV industry. In particular, more charging stations will be built around central areas of cities. Investors or governments should optimize the resource scheduling in order to reduce investment costs due to the limited charging facilities. However, poor management, that is, unreasonable resource scheduling (including service workers and charging piles), will affect the revenues and the future development of the EV industry, thus hindering sustainable transportation; accordingly, resource scheduling for EV charging stations should be a top priority.

Therefore, this paper models and simulates the resource scheduling of an EV charging station. A mathematical resource scheduling model of a charging station is established. Due to the solution problem of the mathematical model, AnyLogic implements the communication mechanism of the multi-agent, including the worker agent, equipment agent and the message model, in order to acquire the model's results. For the simulation results, it is possible to know the effect of the number of service workers, the charging pile replacement policy and the charging pile

maintenance times on charging station revenue. Our findings are mainly the following: (1) In the lifetime of the charging pile, seven maintenance times are needed; (2) Even if the charging pile is still in normal condition, it needs to be replaced in order to achieve the maximum profits for the charging station; (3) A comprehensive analysis of service efficiency and service costs indicates that 8 service workers are needed to achieve the optimal profit for the charging station; (4) We can still obtain the optimal results if the model parameters change.

Acknowledgement

This paper is supported by the Fundamental Funds for Humanities and Social Sciences of Beijing Jiaotong University (2018RCW005,2018YJS051). We appreciate their support very much.

References

[1] Liu, S., Gong, D. (2014). Modelling and simulation on recycling of electric vehicle batteries – Using agent approach, *International Journal of Simulation Modelling*, Vol. 13, No. 1, 79-92, doi: 10.2507/IJSIMM13(1)CO1.
[2] Johanyák, Z.C. (2017). A modified particle swarm optimization algorithm for the optimization of a fuzzy classification subsystem in a series hybrid electric vehicle, *Tehnički Vjesnik – Technical Gazette*, Vol. 24, Supplement 2, 295-301, doi: 10.17559/TV-20151021202802.
[3] Webster, R. (1999). Can the electricity distribution network cope with an influx of electric vehicles?, *Journal of Power Sources,* Vol. 80, No. 1-2, 217-225, doi: 10.1016/S0378-7753(98)00262-6.
[4] Tamor, M.A., Gearhart, C., Soto, C. (2013). A statistical approach to estimating acceptance of electric vehicles and electrification of personal transportation, *Transportation Research Part C: Emerging Technologies,* Vol. 26, 125-134, doi: 10.1016/j.trc.2012.07.007.
[5] Nie, Y.(M.), Ghamami, M. (2013). A corridor-centric approach to planning electric vehicle charging infrastructure, *Transportation Research Part B: Methodological*, Vol. 57, 172-190, doi: 10.1016/j.trb.2013.08.010.
[6] Lu, X.C., Chen, Q.B., Zhang, Z.J. (2014). The electric vehicle routing optimizing algorithm and the charging stations' layout analysis in Beijing, International Journal of Simulation Modelling, Vol. 13, No. 1, 116-127, doi: 10.2507/IJSIMM13(1)CO4.
[7] Simeunović, N., Kamenko, I., Bugarski, V., Jovanović, M., Lalić, B. (2017). Improving workforce scheduling using artificial neural networks model, *Advances in Production Engineering & Management,* Vol. 12, No. 4, 337-352, doi: 10.14743/apem2017.4.262.
[8] Miller, R.E., Thatcher, J.W. Bohlinger, J.D. (eds.), (1972). *Complexity of computer computations,* Springer Verlag, Boston, USA, doi: 10.1007/978-1-4684-2001-2.
[9] Cook, S.A. (1971). The complexity of theorem-proving procedures, In: *Proceedings of the third annual ACM symposium on theory of computing STOC '71,* Ohio, USA, 151-158, doi: 10.1145/800157.805047.
[10] Xi, X., Sioshansi, R., Marano, V. (2013). Simulation–optimization model for location of a public electric vehicle charging infrastructure, *Transportation Research Part D: Transport and Environment,* Vol. 22, 60-69, doi: 10.1016/j.trd.2013.02.014.
[11] Zhang, L., Shaffer, B., Brown, T., Samuelsen, G.S. (2015). The optimization of DC fast charging deployment in California, *Applied Energy,* Vol. 157, 111-122, doi: 10.1016/j.apenergy.2015.07.057.
[12] Chen, T.D., Kockelman, K.M., Khan, M. (2013). Locating electric vehicle charging stations: Parking-based assignment method for Seattle, Washington, *Transportation Research Record: Journal of the Transportation Research Board,* Vol. 2385, No. 1, 28-36, doi: 10.3141/2385-04.
[13] Yi, Z., Bauer, P.H. (2016). Optimization models for placement of an energy-aware electric vehicle charging infrastructure, *Transportation Research Part E: Logistics and Transportation Review,* Vol. 91, 227-244, doi: 10.1016/j.tre.2016.04.013.
[14] Mehar, S., Senouci, S.M. (2013). An optimization location scheme for electric charging stations, In: *Proceedings of International Conference on Smart Communications in Network Technologies (SaCoNeT) 2013,* Paris, France, 1-5, doi: 10.1109/SaCoNeT.2013.6654565.
[15] Bendiabdellah, Z., Senouci, S.M., Feham, M. (2014). A hybrid algorithm for planning public charging stations, In: *Global Information Infrastructure and Networking Symposium (GIIS) 2014,* Montreal, Canada, 1-3, doi: 10.1109/GIIS.2014.6934262.
[16] You, P.-S., Hsieh, Y.-C. (2014). A hybrid heuristic approach to the problem of the location of vehicle charging stations, *Computers & Industrial Engineering,* Vol. 70, 195-204, doi: 10.1016/j.cie.2014.02.001.
[17] Tang, M., Gong, D., Liu, S., Zhang, H. (2016). Applying multi-phase particle swarm optimization to solve bulk cargo port scheduling problem, *Advances in Production Engineering & Management*, Vol. 11, No. 4, 299-310, doi: 10.14743/apem2016.4.228.
[18] Guo, S., Zhao, H. (2015). Optimal site selection of electric vehicle charging station by using fuzzy TOPSIS based on sustainability perspective, *Applied Energy,* Vol. 158, 390-402, doi: 10.1016/j.apenergy.2015.08.082.
[19] Wu, Y., Chen, K., Zeng, B., Yang, M., Geng, S. (2016). Cloud-based decision framework for waste-to-energy plant site selection – A case study from China, *Waste Management,* Vol. 48, 593-603, doi: 10.1016/j.wasman.2015.11.030.

[20] Shafiei, E., Thorkelsson, H., Ásgeirsson, E.I., Davidsdottir, B., Raberto, M., Stefansson, H. (2012). An agent-based modeling approach to predict the evolution of market share of electric vehicles: A case study from Iceland, *Technological Forecasting and Social Change,* Vol. 79, No. 9, 1638-1653, doi: 10.1016/j.techfore.2012.05.011.
[21] Adepetu, A., Keshav, S., Arya, V. (2016). An agent-based electric vehicle ecosystem model: San Francisco case study, *Transport Policy,* Vol. 46, 109-122, doi: 10.1016/j.tranpol.2015.11.012.
[22] Ghamami, M., Nie, Y.(M.), Zockaie, A. (2016). Planning charging infrastructure for plug-in electric vehicles in city centers, *International Journal of Sustainable Transportation*, Vol. 10, No. 4, 343-353, doi: 10.1080/15568318.2014.937840.
[23] Yıldız, B., Arslan, O., Karaşan, O.E. (2016). A branch and price approach for routing and refueling station location model, *European Journal of Operational Research,* Vol. 248, No. 3, 815-826, doi: 10.1016/j.ejor.2015.05.021.
[24] Cavadas, J., Correia, G.H.D.A., Gouveia, J. (2015). A MIP model for locating slow-charging stations for electric vehicles in urban areas accounting for driver tours, *Transportation Research Part E: Logistics and Transportation Review,* Vol. 75,188-201, doi: 10.1016/j.tre.2014.11.005.
[25] Dorling, K., Heinrichs, J., Messier, G.G., Magierowski, S. (2017). Vehicle routing problems for drone delivery, *IEEE Transactions on Systems, Man, and Cybernetics: Systems,* Vol. 47, No. 1, 70-85, doi: 10.1109/TSMC.2016.2582745.
[26] Tang, M., Gong, D., Liu, S., Lu, X. (2017). Finding key factors affecting the locations of electric vehicle charging stations: A simulation and ANOVA approach, *International Journal of Simulation Modelling,* Vol. 16, No. 3, 541-554, doi: 10.2507/IJSIMM16(3)CO15.
[27] Manley, M., Kim, Y.S., Christensen, K., Chen, A. (2016). Airport emergency evacuation planning: An agent-based simulation study of dirty bomb scenarios, *IEEE Transactions on Systems, Man, and Cybernetics: Systems,* Vol. 46, No. 10, 1390-1403, doi: 10.1109/TSMC.2015.2497213.

APEM journal
Advances in Production Engineering & Management
Volume 14 | Number 1 | March 2019 | pp 80–92
https://doi.org/10.14743/apem2019.1.313
ISSN 1854-6250
Journal home: apem-journal.org
Original scientific paper

Product quality improvement and air pollutant emission reduction in a mining metal three-stage supply chain under cap-and-trade regulation

Homaei, H.[a,b,*], **Mahdavi, I.**[c], **Tajdin, A.**[c], **Khorram, E.**[d]

[a]Mazandaran University of Science and Technology, Babol, Iran
[b]Golgohar Mining and Industrial Co., Sirjan, Iran
[c]Mazandaran University of Science and Technology, Faculty of Industrial Engineering, Babol, Iran
[d]Amirkabir University of Technology, Faculty of Mathematics and Computer Science, Tehran, Iran

ABSTRACT

In today's competitive market, all industries such as mine industries try to increase their profit and keep their customers. Product quality improvement is the miner's most important key to success in competitive market because the mining metals price depends on their quality level. On the other hand, nowadays the management of air pollutant emissions with harmful environmental and health effects is one of the most pressing problems. This paper studies the decision behaviour and coordination issue of a mining metal three-level supply chain with one supplier (extractor), one mineral processor and one manufacturer in which product quality improvement cost at the processor level is higher than the supplier level and at the level of the manufacturer is more than the processor level. We compare the decentralized and centralized systems and identify the optimal product quality level for each supply chain member by designing a revenue sharing contract for decentralized supply chain under cap-and-trade regulation. Finally, numerical example shows that the designed contract not only provides a win-win condition for all supply chain members and increases whole supply chain profit but also increases the final product quality level and reduces harmful air pollutant emissions.

ARTICLE INFO

Keywords:
Mining metals;
Supply chain;
Quality improvement;
Channel coordination;
Emissions reduction;
Cap-and-trade regulation

**Corresponding author:*
h.homaei@in.iut.ac.ir
(Homaei, H.)

Article history:
Received 16 May 2018
Revised 31 January 2019
Accepted 24 February 2019

1. Introduction

In today's globalized economy, supply chain management is one of the most useful management practices for industries to increase their profit and competitiveness. Nowadays product quality is one of the key competitive dimensions of industries. Industries are always trying to increase their profits, and mines are one of these industries whose profit depends on their product's quality level; but product quality level improvement in mine industries usually emits air pollutants that are serious threats to human health and environment. On the other hand, since rapid economic development brings huge amounts of pollutant emissions, governmental pressures such as cap-and-trade regulation are made to force companies to find new methods to reduce these emissions across all the stages of their supply chains. Under a cap-and-trade regulation, companies get predetermined free emission credits from the government [1]. They could sell/buy credits in the air pollutants trading market when they have surplus/lack credits; this emission credit price is determined by the market. There are two common practices for improv-

ing product quality in mine industries: (1) Technology changing and (2) Practical policies. Since the first method is very costly, the second method is a competitive advantage for miners; therefore, one of the most important concerns miners have is how to increase their profit through product quality level enhancement by operational approaches without increasing harmful pollutant emissions.

There are two decision making systems in a supply chain: centralized and decentralized. In the centralized system, supply chain members operate jointly as a single firm and make their decisions to maximize the total profit of the system; but in the decentralized system, supply chain members make their decisions separately to maximize their own profits. The decision making system in most supply chain models such as this study is assumed to be decentralized. To improve the overall performance of the supply chain, a coordination mechanism is needed. Different definitions and perspectives on the supply chain coordination exist in the literature (refer to [2, 3]) for the comprehensive review of supply chain coordination. A supply chain is coordinated when the members make the decisions that are optimal for the whole supply chain. For coordinating a supply chain, contracts are designed to reduce the difference between the outcome of a centralized system and a decentralized system. Different kinds of contracts such as commitment to purchase quantity, credit option, two-part tariff, revenue sharing [4, 5], buy back, sales rebate, and mail-in-rebate, have been used in supply chains as the ways improving supply chain performance. Revenue sharing is one of the widely used contracts in the supply chain that is between an upper and lower level of supply chain, where the upper level provides better selling condition to the lower level and then the lower level shares a fraction of its revenue with upper level.

There are three streams of literature related to the research in this paper. The first stream focuses on improving the quality level of products in the supply chain. Many efforts have been made to improve product quality in the supply chain. Radej *et al.* provided an overview of the quality tools and methods such as quality techniques and linked it to manufacturing process quality and manufacturing cost-effectiveness; [6]. Singer *et al.* studied a single product distribution channel and suggested a contract that simultaneously increases profit and improves quality [7]. Xiao *et al.* presented a game-theory model to show how the manufacturer coordinates the supply chain by revenue-sharing contract [8]. El Ouardighi discussed the potential coordinating power of revenue-sharing contracts in supply quality management [9]. Yan explored a joint pricing and product quality decision problem in a two level decentralized supply chain [10]. Zhu *et al.* investigated a supply chain, where the buyer has the option to invest in the supplier's quality improvement [11]. Gao *et al.* considered quality improvement effort coordination in a decentralized supply chain with a partial cost allocation contract [12].

The second part of literature explores operational decisions in the supply chain under the cap-and-trade regulation in order to reduce harmful gas emissions. The cap-and-trade regulation is a mechanism to control air pollutant emissions [13]. Many researches have studied the problems in supply chains considering the cap-and-trade regulation and it has been recommended by many senior researchers such as [14] and [15] and implemented in many parts of the world. Xu *et al.* studied the joint production and pricing problem of a manufacturer under cap-and-trade and carbon tax policies. [16]. Gong and Zhou proposed an optimal manufacturing strategy under carbon trading policy through a dynamic model [17]. Hua *et al.* explored how companies manage carbon footprints in inventory management under the carbon-trading regulation [14]. Xu *et al.* investigated the production and pricing problems in make-to-order supply chain under cap-and-trade regulation. [18]. He *et al.* considered the impact of cap-and-trade regulation on company's carbon emission decisions [19]. Zhang and Xu investigated a company's optimal manufacturing quantities under cap-and-trade regulation. [13]. Benjaafar *et al.* studied the multi-period operational decision-making of a company under cap-and-trade regulation [20].

The last subset of literature related to this research is the supply chain coordination under revenue sharing contract. Cachon provided a good survey on this contract [21]. Cachon and Lariviere proved that revenue sharing contracts for decentralized supply chains are beneficial in achieving coordination for various types of supply chains [22]. Qin and Yang used the Stackelberg game to model the revenue sharing contract problem. They showed that the party that

keeps more than half the revenue should serve as the leader of the Stackelberg game [23]. Hsueh presented a new revenue sharing contract embedding corporate social responsibility to coordinate a two level supply chain [24]. Yao *et al.* proposed a revenue sharing contract to coordinate a two stage supply chain. They illustrated that the provision of revenue sharing in the contract can increase supply chain performance more than a price-only contract [25]. Palsule-Desai proposed a game theory model for revenue-dependent revenue sharing contracts in which the supply chain revenue is shared among the members depending on the quantum of revenue generated [26]. Zhang *et al.* discussed the revenue sharing contracts for coordinating a supply chain in which demands are disrupted [27]. Hu *et al.* studied supply chain coordination via revenue sharing contracts in a three-stage supply and a two-stage supply chain [28].

However, a few researches have been done on the three level supply chain coordination with revenue sharing contract considering environmental aspects under cap-and-trade regulation; also the three-level supply chain coordination research literature mentioned above neither take the product quality improvement into account nor focuses on mining metal supply chain coordination. Therefore the main purpose of this study is to design a revenue sharing contract for a mining metal three level supply chain in order to: 1) coordinate supply chain and provide a win-win condition for all its members and decrease the difference between the outcome of a centralized system and a decentralized system, 2) reduce air pollutant emissions in the supply chain under cap-and-trade regulation, 3) improve the final product quality level of the supply chain.

The rest of this paper proceeds as follows. Section 2 presents the notations definition and the supply chain descriptions and assumptions used in this paper. We have analysed the decision behaviour the decentralized and centralized supply chain in Section 3. Section 4 develops a new revenue sharing contract for coordinating the decentralized supply chain. Section 5 provides a numerical example to illustrate the proposed contract performance. Conclusions are provided in Section 6.

2. Model description and assumptions

A decentralized mining metal three-stage supply chain in which minerals will convert to concentrate after extraction is assumed in this paper. The considered supply chain is consists of a supplier (extractor), a processor, and a manufacturer. The first level extracts processed minerals and sells them to second level who processes minerals and sells the mineral concentrate to the manufacturer, who in turn produces mineral products such as pellets and ingots and sells them to the customers. The product price of each supply chain level depends on the quality of that product. Therefore all of these supply chain members try to increase their product quality.

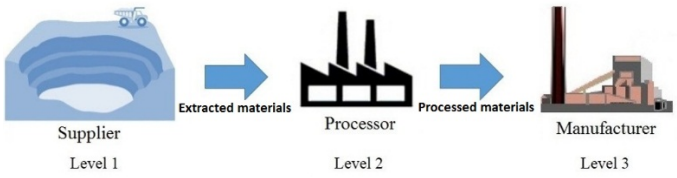

Fig. 1 Mining metal three level supply chain

The following notations are used to describe the proposed model:

i Index for supply chain levels; S for supplier, P for processor and M for manufacturer
j_0 Minimum acceptable product quality level in considered supply chain
P_{ij} selling price of unit product produced at the supply chain level i with quality level j
d_i The amount of product quality level improvement in supply chain level i
C_i Constant production cost for a unit product in supply chain level i
cd_{ij} Cost coefficient for increasing product quality level with quality level j in supply chain level i
α_i Price increasing coefficient for product produced in supply chain level i per unit product quality improvement in supply chain level i

β_i Price increasing coefficient for product produced in supply chain level i per unit product quality improvement in supply chain levels before level i
γ_i Quality improvement cost increasing coefficient in supply chain level i per unit product quality improvement in supply chain levels before level i
π_i Supply chain level i profit
ϕ_1 Processor's revenue share, $0 < \phi_1 < 1$
ϕ_2 Manufacturer's revenue share, $0 < \phi_2 < 1$
cp_i Unit air pollutant emissions trading price for supply chain level i
K_i Air pollutant emissions cap for supply chain level i
g_i Amount of air pollutant emission for a unit product quality level improvement in supply chain level i

In this paper d_i, ϕ_1 and ϕ_2 are decision variables. Product quality level improvement at the supplier level doesn't emit air pollutants because improving product quality at that level is done by some activities such as more samplings for accurate identification of underground mineral veins (Fig. 3) and performing explosive operation optimally ($cp_S = 0$). But product quality improvement in supply chain levels 2 and 3 emit air pollutants; the emitted air pollutant type at the processor level is usually dust because of the physical processes at this level and the emitted air pollutant at the manufacturer level is of the chemical type, such as SO2, due to chemical processes. That is why the parameter cp for the manufacturer is higher than the processor ($cp_M > cp_P$). The government monitors pollutant emissions of the supply chain members by online measuring equipment (Fig. 2). Product quality level improvement is not mandatory for supply chain members but supplier must supplies raw material with minimum quality level j_0. Product quality improvement for each supply chain member requires more operating costs but these cost enhancements are different for each member because of different production processes in each supply chain level and it is assumed to be a nonlinear ascending.

The product quality improvement cost increases from supplier to manufacturer due to the increasing complexity of production processes from supplier to manufacturer ($cd_{Sj} < cd_{Pj} < cd_{Mj}$). It is a mention worthy assumption that in this type of supply chain, increasing the quality of the product at each supply chain level creates an added value for both that level (with coefficient α) and the next levels (with coefficient β), but increases next levels' product quality improvement costs (with coefficient γ). For example the cost for increasing 5 quality levels from level 60 to level 65 is more than the cost for increasing 5 quality levels from level 30 to level 35.

In our study we assume that all members are in full capacity production and all their products will be sold. Therefore, the consideration of the demand parameter in the problem is neglected. Also the shipment costs are not considered in this model due to equality in centralized and decentralized system.

Fig. 2 Air pollutant online monitoring equipment in Golgohar mining & Industrial Co.

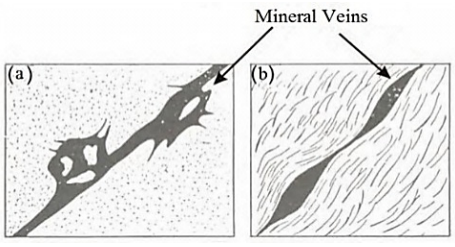

Fig. 3 Mineral Veins

3. Decision analysis

In this part, we propose the decision model for the decentralized and centralized systems. After solving both the system models, we obtain the quantitative relationships among the profits and the decision variables under the centralized and decentralized systems.

3.1 Analysis of the decentralized system

We assume that all members in the considered supply chain try to improve their products quality in order to increase their profit, but in the decentralized supply chain they try to maximize their own profit. Considering the model assumptions the supplier's profit for each unit product extraction in the decentralized system is

$$\pi_S = P_{Sj_0}(1 + \alpha_S d_S) - C_S - cd_{Sj_0} d_S^2 \tag{1}$$

where the first part denotes a unit extracted material selling price with minimum quality level plus the selling price enhancement due to product quality level improvement by the supplier (d_S). The second part is the constant extraction cost for a unit product at the supplier level. Similar to previous studies [29, 30] the third part shows the supplier's cost for increasing product quality level. As mentioned before, at this supply chain level we don't have environmental costs for product quality improvement.

The processor's profit for processing one unit product in the decentralized system is

$$\pi_P = P_{Pj_0}(1 + \beta_P d_S + \alpha_P d_P) - P_{Pj_0}(1 + \alpha_S d_S) - C_P - cd_{Pj_0} d_P^2(1 + \gamma_P d_S) - cp_P(g_P d_P - K_P) \tag{2}$$

where similar to Eq. 1, the first part shows a unit processed material selling price with minimum quality level plus the selling price enhancement due to product quality level improvement by processor (d_P) and supplier (d_S). The second part is the purchasing price of a unit extracted product from the supplier. The third part is the constant processing cost for a unit product in processor and the fourth term shows the processor's cost for increasing product quality level and the last part is the cost (income) from buying (selling) extra dust emission permits for the processor.

The manufacturer's profit for manufacturing one unit product in the decentralized system is

$$\begin{aligned}\pi_M = {} & P_{Mj_0}(1 + \beta_M(d_S + d_P) + \alpha_M d_M) - P_{Pj_0}(1 + \beta_P d_S + \alpha_P d_P) - C_M \\ & - cd_{Mj_0} cd_M^2\big(1 + \gamma_M(d_S + d_M)\big) - cp_M(g_M d_M - K_M)\end{aligned} \tag{3}$$

where the first part represents a unit manufactured product selling price with minimum quality level plus the selling price enhancement due to product quality level improvement by the manufacturer (d_M) and its previous levels ($d_S + d_P$). The second part is the purchasing price of a unit processed product from the processor. The third part is constant manufacturing cost for a unit product at the manufacturer level. The fourth part shows the manufacturer's cost for increasing product quality level and the last term is the cost (income) from buying (selling) extra chemical pollutant emission permits for the manufacturer.

As mentioned before, all members in the decentralized supply chain try to maximize their own profit so the members' optimal decision will be as follows.

Proposition 1: The optimal product quality level improvement by the supplier in considered decentralized supply chain is

$$d_S^* = \frac{\alpha_S P_{Sj_0}}{2cd_{Sj_0}} \tag{4}$$

Proposition 2: The optimal product quality level enhancement by the processor in considered decentralized supply chain is

$$d_P^* = \frac{\alpha_P P_{Pj_0} - cp_P g_P}{2cd_{Pj_0}(1 + \gamma_P d_S^*)} \tag{5}$$

Proposition 3: The optimal product quality level improvement by the manufacturer in considered decentralized supply chain is

$$d_M^* = \frac{\alpha_M P_{Mj_0} - cp_M g_M}{2cd_{Pj_0}(1 + \gamma_M(d_S^* + d_P^*))} \tag{6}$$

Therefore the optimal value of the whole decentralized supply chain profit without coordination can be written as

$$\pi_T^* = \pi_S^* + \pi_P^* + \pi_M^* \tag{7}$$

And optimal product *quality* improvement for final product without coordination can be calculated as follows

$$d_T^* = d_S^* + d_P^* + d_M^* \tag{8}$$

3.2 Analysis of the centralized system

In the centralized system, all supply chain members operate jointly as a single company and determine the optimal value of product quality level improvement to maximize the total profit of the whole supply chain. In this scenario, the total supply chain profit function can be formulated as

$$\begin{aligned}\pi_{TC} = &-cd_{Sj_0}d_S^2 - cd_{Pj_0}d_P^2(1+\gamma_P d_S) - cp_P(g_P d_P - K_P)\\ &+ P_{Mj_0}(1+\beta_M(d_S+d_P)+\alpha_M d_M) - C_M - C_S - C_P\\ &- cd_{Mj_0}d_M^2\big(1+\gamma_M(d_S+d_M)\big) - cp_M(g_M d_M - K_M)\end{aligned} \tag{9}$$

Proposition 4: The optimal product quality level enhancement by the supplier in considered centralized supply chain is

$$d_S^* = \frac{\beta_M P_{Mj_0} - cd_{Pj_0}\gamma_P d_P^2 - cd_{Mj_0}d_M^2\gamma_M}{2cd_{Sj_0}} \tag{10}$$

Proposition 5: The optimal product quality level improvement by the processor in considered centralized supply chain is

$$d_P^* = \frac{\beta_M P_{Mj_0} - cd_{Mj_0}\gamma_M d_M^2 - cp_P g_P}{2cd_{Pj_0}(1+\gamma_P d_S)} \tag{11}$$

Proposition 6: The optimal product quality level improvement by the manufacturer in considered centralized supply chain is

$$d_M^* = \frac{\alpha_M P_{Mj_0} - cp_M g_M}{2cd_{Mj_0}(1+\gamma_M(d_S+d_P)} \tag{12}$$

It is mention worthy that unlike the decentralized system, in centralized system we have to obtain optimal value of d_S, d_P and d_M by solving the systems of three equations.

4. Supply chain coordination with revenue sharing contract

Since the product quality level improvement by the supplier increases the processor and manufacturer's profit, they share a portion of this profit enhancement with the supplier. Based on the designed revenue sharing contract, whenever the supplier increases the quality of his product (d_S'), he will receive more profit from the processor. Considering this revenue sharing contract, the supplier's profit for each unit product extraction is

$$\pi_S' = \phi_1 P_{Pj_0}\beta_P d_S' + \phi_1\phi_2 P_{Mj_0}\beta_M d_S' + P_{Sj_0}(1+\alpha_S d_S') - C_S - cd_{Sj_0}d_S' \tag{13}$$

where the first and second terms show a portion of processor's profit which the supplier receives from the processor due to increasing the product quality improvement (d_S'). It is clearly understandable that if the supplier doesn't increase his product quality level he will receive no shared profit from the processor. The other parts of the Eq. 13 are similar to Eq. 1.

According to the presented revenue sharing contract, when the processor delivers product with higher quality to the manufacturer, he will share his profit more with the processor. But some percent of this product quality improvement is done by supplier and the rest of product quality improvement is done by the processor. Therefore the processor shares a portion of the profit received from the manufacturer which is related to the supplier's product quality improvement with the supplier. Hence, considering the above contract descriptions, the processor's profit for processing one unit product under the proposed revenue sharing contract is

$$\pi'_P = \phi_2 P_{Mj_0}\beta_M\big((1-\phi_1)d_S + d_P\big) + P_{Pj_0}(1 + (1-\phi_1)\beta_P d_S + \alpha_P d_P) - P_{Sj_0}(1+\alpha_S d_S) - C_P - cd_{Pj_0}d'^2_P(1+\gamma_P d_S) - cp_P(g_P d_P - K_P) \quad (14)$$

where the first part is a portion of the manufacturer's profit which the processor receives from manufacturer minus a part of it that the processor gives to supplier. The second part denotes a unit processed material selling price with minimum quality level plus the selling price enhancement due to product quality level improvement by the processor (d'_p) and the supplier (d'_S), minus a part of it that the processor gives to the supplier proportionate to (d'_S). Based on the designed contract even if the processor doesn't like to increase his product quality, it's beneficial for him to motivate the supplier to improve product quality. The other parts of Eq. 14 are similar to Eq. 2.

According to the proposed contract, the manufacturer will share a part of his profit caused by product quality improvement in previous supply chain levels with the processor, so the manufacturer's profit for manufacturing one unit product based on the presented contract can be written as

$$\pi'_M = P_{Mj_0}(1 + (1-\phi_2)\beta_M(d_S + d_P) + \alpha_M d_M) - P_{Pj_0}(1 + \beta_P d_S + \alpha_P d_P) - C_M - cd_{Mj_0}d'^2_M\big(1 + \gamma_M(d_S + d_M)\big) - cp_M(g_M d_M - K_M) \quad (15)$$

where the first term shows a unit manufactured product selling price with minimum quality level plus the selling price enhancement because of product quality level improvement by the manufacturer (d'_M) and its previous levels ($d'_S + d'_P$) minus a part of it that manufacturer gives to the processor proportionate to ($d'_S + d'_P$). The other parts of Eq. 15 are similar to Eq. 3.
After considering the proposed revenue sharing contract in the supply chain all members still try to maximize their own profit due to the decentralization of the supply chain. Therefore the members' optimal decisions can be written as follows.

Proposition 7: The optimal product quality level improvement by the supplier after considering revenue sharing contract in supply chain will be

$$d'^*_S = \frac{\phi_1\beta_P P_{Pj_0} + \phi_1\phi_2\beta_M P_{Mj_0} + \alpha_S P_{Sj_0}}{2cd_{Sj_0}} \quad (16)$$

Proposition 8: The optimal product quality level enhancement by the processor in assumed decentralized supply chain after considering revenue sharing contract is

$$d'^*_P = \frac{\phi_2\beta_M P_{Mj_0} + \alpha_P P_{Pj_0} - cd_P g_P}{2cd_{Pj_0}(1 + \gamma_P d'^*_S)} \quad (17)$$

Proposition 9: The optimal product quality level improvement by the manufacturer in considered decentralized supply chain based on designed contract is

$$d'^*_M = \frac{\alpha_M P_{Mj_0} - cp_M g_M}{2cd_{Pj_0}(1 + \gamma_M(d'^*_S + d'^*_P))} \quad (18)$$

Proposition 10: The other decision variables in considered contract are ϕ_1 and ϕ_2 ,whose optimal values can be calculated as follows

$$\phi^*_1 = \frac{2\alpha_S P_{Sj_0} + cd_{Pj_0}d'^2_P\gamma_P - \phi_2\beta_M P_{Mj_0} - \beta_P P_{Pj_0}}{-2(\phi_2\beta_M P_{Mj_0} + \beta_P P_{Pj_0})} \quad (19)$$

and

$$\phi^*_2 = \frac{1}{2} - \frac{cd_{Mj_0}d'^2_M\gamma_M}{2\beta_M P_{Mj_0}} - \frac{cd_{Pj_0}(1+\gamma_P d'_S)\big(2\phi_1\beta_P P_{Pj_0} + \alpha_S P_{Sj_0}\big) + cd_{Sj_0}(2\alpha_P P_{Pj_0} - cp_P g_P)}{2cd_{Pj_0}(1+\gamma_P d'_S)\phi_1\beta_M P_{Mj_0} + 2cd_{Sj_0}\beta_M P_{Mj_0}} \quad (20)$$

It is necessary to note that we have to obtain the optimal values of ϕ_1 and ϕ_2 by solving the systems of two equations.

Therefore, the optimal value of total supply chain profit under revenue sharing contract can be written as

$$\pi_T'^* = \pi_S'^* + \pi_P'^* + \pi_M'^* \tag{21}$$

Also, optimal product quality improvement for final product can be calculated as follows

$$d_T'^* = d_S'^* + d_P'^* + d_M'^* \tag{22}$$

The amount of air pollutant emissions depends on product quality improvement at the processor and manufacturer levels. In other words, the more product quality improvement at the processor and manufacturer levels, the greater air pollutant emissions. The *Propositions 11* and *12* obtain the upper bound and the lower bound for the decision variable ϕ_2 respectively and guarantee that processor and manufacturer's air pollutant emissions after considering proposed revenue sharing contract is less than that without the coordination case.

Proposition 11: The optimal product quality level improvement by the processor in considered decentralized supply chain without coordination is more than the coordinated with designed revenue sharing contract case ($d_P'^* < d_P^*$) if

$$\phi_2 < \frac{\phi_1\beta_P P_{Pj_0}(\alpha_P P_{Pj_0} - cp_P g_P)}{\beta_M P_{Mj_0}\left(2cd_{Sj_0} + \alpha_S P_{Sj_0}\right) - \phi_1\beta_M P_{Mj_0}(\alpha_P P_{Pj_0} - cp_P g_P)} \tag{23}$$

Proposition 12: The optimal product quality level improvement by the manufacturer in considered decentralized supply chain without coordination is more than the coordinated with proposed revenue sharing contract case ($d_M'^* < d_M^*$) if

$$\phi_2 > \frac{\left(2cd_{Sj_0} + \gamma_P\left(\phi_1\beta_P P_{Pj_0} + \phi_1\beta_M P_{Mj_0} + \alpha_S P_{Sj_0}\right)\right)\left(\frac{2cd_{Sj_0}^2(\alpha_P P_{Pj_0} - cp_P g_P)}{2cd_{Sj_0} + \gamma_P\alpha_S P_{Sj_0}} - cd_{Pj_0}\phi_1\beta_P P_{Pj_0}\right) - 2cd_{Sj_0}^2(\alpha_P P_{Pj_0} - cp_P g_P)}{\beta_M P_{Mj_0}\left(2cd_{Sj_0}^2 + \phi_1 cd_{Pj_0}\left(2cd_{Sj_0} + \gamma_P\left(\phi_1\beta_P P_{Pj_0} + \phi_1\beta_M P_{Mj_0} + \alpha_S P_{Sj_0}\right)\right)\right)} \tag{24}$$

5. Results and discussion

In this section, we provide a numerical example in order to illustrate the designed revenue sharing contract performance by using the parameters below: $C_S = 150$; $C_P = 250$; $C_M = 350$; $P_{Sj_0} = 20$; $P_{Pj_0} = 30$; $P_{Mj_0} = 40$; $\alpha_S = 3$; $\alpha_P = 5$; $\alpha_M = 7$; $\beta_P = 6$; $\beta_M = 20$; $\gamma_P = \gamma_M = 10$; $cd_{Sj_0} = 4$; $cd_{Pj_0} = 5$; $cd_{Mj_0} = 6$; $cp_P = 2$; $cp_M = 5$; $g_P = 3$; $g_M = 4$; $K_P = 50$, and $K_M = 40$.
The MATLAB software is used to solve the numerical example considering mentioned parameters and its results are presented in tables 1-3 and Figs. 4-6.

Table 1 Optimum value of key variables for centralized supply chain

Key variables	d_S^*	d_P^*	d_M^*	d_T^*	π_S^*	π_P^*	π_M^*	π_T^*
Optimum value	99.92	0.0793	0.214	100.21	-34093	11834	61908	39649

Table 1 shows the optimum value of key variables for the centralized supply chain. As it can be observed from Table 1, the highest increase in product quality level in the centralized supply chain is done by the supplier ($d_S^* \gg d_P^*, d_S^* \gg d_M^*$) and that is why that his profit is negative. It is necessary to note that the negative profit of the supplier in the centralized supply chain is not important because all members in the centralized supply chain operate jointly as a single company and achieving the win-win condition for supply chain members is not important in this case.

Table 2 Optimum value of key variables for decentralized supply chain without coordination

Key variables	d_S^*	d_P^*	d_M^*	d_T^*	π_S^*	π_P^*	π_M^*	π_T^*
Optimum value	7.5	0.1894	0.2781	7.9675	95	773	4669	5537

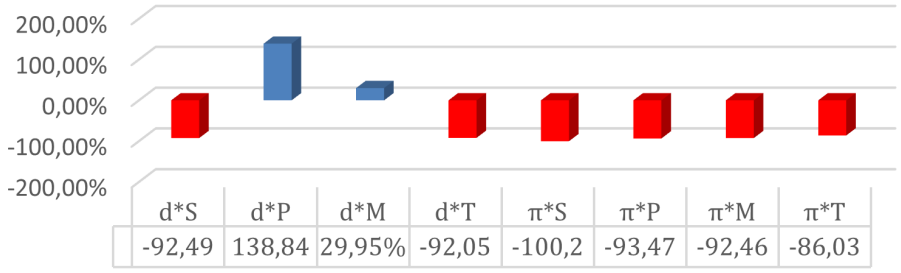

Fig. 4 Key variables change percentage of the decentralized supply chain without coordination compared to centralized supply chain

From Table 2 and Fig. 4, we observe that the profit of all supply chain members, whole supply chain profit, product quality improvement by supplier and the final product quality in decentralized supply chain without coordination are much lower than that in the centralized case; But product quality improvement by the processor and manufacturer in decentralized supply chain is higher than that in the centralized system. As mentioned before, since the air pollutant emissions depend on the product quality improvement at the processor and manufacturer level of supply chain, so increasing product quality improvement by the processor and manufacturer leads to the enhancement of air pollution emissions; therefore we can say that air pollutant emissions in the decentralized supply chain are higher than that in the centralized system.
As mentioned before, we obtain the optimal values of ϕ_1 and ϕ_2 by solving the systems of two equations using Eqs. 19 and 20. In this example, the lower bound and upper bound for the decision variable ϕ_2 are obtained -0.102 and 2.879, respectively and the conditions mentioned in *Propositions 11* and *12* are satisfied because the optimal values of ϕ_1 and ϕ_2 are obtained 0.438 and 0.190 respectively.

Table 3 Optimum value of key variables for coordinated decentralized supply chain with designed revenue sharing contract

Key variables	d_S^*	d_P^*	d_M^*	d_T^*	π_S^*	π_P^*	π_M^*	π_T^*
Optimum value	25.67	0.1148	0.0836	25.8684	2507	3127	11944	17579

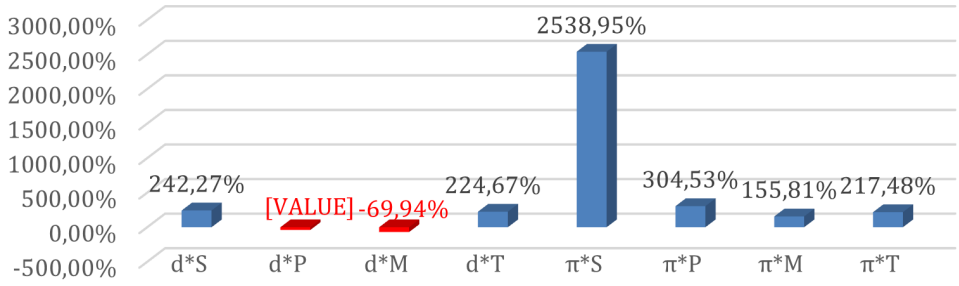

Fig. 5 Key variables change percentage of the coordinated decentralized supply chain compared to without coordination case

As it is shown in Table 3 and Fig. 5, the designed revenue sharing contract increases the whole supply chain profit and total product quality improvement by 217.48 % and 224.67 % respectively; Also the proposed revenue sharing contract increases the supplier, processor and manufacturer's profit by 2538.95 %, 304.53 % and 155.81 % respectively so we can say that this contract provides a win-win condition for all supply members. It should be mentioned that we can never increase the whole supply chain profit and the final product quality of the decentralized supply chain to its centralized case due to the necessity of the win-win condition for all members in the decentralized supply chain. Also we can say that the designed revenue sharing contract decreases air pollutant emissions 39.39 % and 69.94 % at the processor and manufacturer supply chain level respectively.

Fig. 6 shows supply chain members and the total supply chain profit for different values of ϕ_2 by fixing the decision variable ϕ_1 to its optimum value 0.438 after coordinating supply chain with the proposed revenue sharing contract. The purple line in Fig. 6 indicates the value of ϕ_2 which maximizes the manufacturer's profit. Also the numbers on intersection points of this line with the other curves can be seen in Table 3.

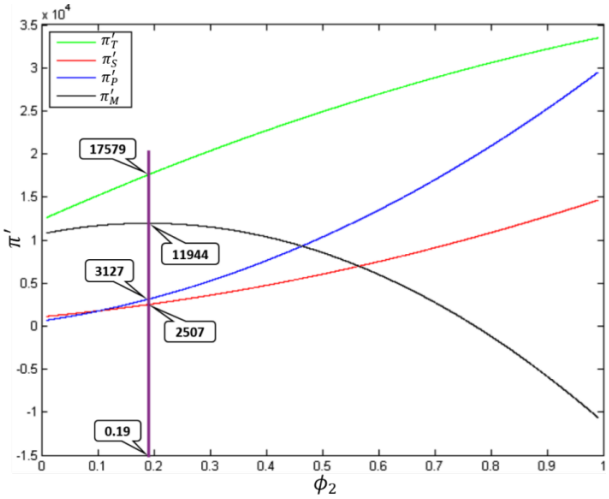

Fig. 6 Supply chain members and total supply chain profit for different values of ϕ_2 by fixing ϕ_1 to its optimum value

6. Conclusions

One of the main concerns of miners is to increase the quality level of their products because the mining metals price depends on their quality level; but increasing the quality level of these products has different costs at different levels of the supply chain. These costs usually increase after extractor level. The two main practices for increasing product quality in industries are technology changing and practical policies; the first method is rarely used by miners because it's very expensive, so miners try to increase their profit through product quality level improvement by operational approaches without increasing air pollutants emissions. This paper studied the coordination issue of a decentralized three-level mining metal supply chain with one supplier (extractor), one processor and one manufacturer under cap-and-trade regulation and compared it with the centralized system. Due to different product quality improvement costs of supply chain members, a revenue sharing contract designed and optimal product quality level for each of them was obtained. It is necessary to say that the proposed model is designed for some kinds of metals that have impurities and will be processed after extraction (such as Iron and Copper) Finally, the numerical example illustrated that the proposed revenue sharing contract can (a) increase the final product quality level, (b) provide a win-win condition for all supply chain members, (c) increase the whole supply chain profit, and (d) reduce harmful air pollutant emissions in the supply chain. The authors' suggestions for future researche is to use other coordination mechanisms and consider the quality dependent demand in the model.

References

[1] Xu, J., Chen, Y., Bai, Q. (2016). A two-echelon sustainable supply chain coordination under cap-and-trade regulation, *Journal of Cleaner Production,* Vol. 135, 42-56, doi: 10.1016/j.jclepro.2016.06.047.

[2] Arshinder; Kanda, A.; Deshmukh, S.G. (2009). A framework for evaluation of coordination by contracts: A case of two-level supply chains, *Computers & Industrial Engineering,* Vol. 56, No. 4, 1177-1191, doi: 10.1016/j.cie.2008.03.014.

[3] Arshinder; Kanda, A.; Deshmukh, S.G. (2008). Supply chain coordination: Perspectives, empirical studies and research directions, *International Journal of Production Economics,* Vol. 115, No. 2, 316-335, doi: 10.1016/j.ijpe.2008.05.011.

[4] Panda, S. (2013). Coordinating two-echelon supply chains under stock and price dependent demand rate, *Asia Pacific Journal of Operational Research,* Vol. 32, No. 2, Art. No. 1250051, doi: 10.1142/S0217595912500510.
[5] Panda, S. (2014). Coordination of a socially responsible supply chain using revenue sharing contract, *Transportation Research Part E: Logistics and Transportation Review,* Vol. 67, 92-104, doi: 10.1016/j.tre.2014. 04.002.
[6] Radej, B., Drnovšek, J., Begeš, G. (2017). An overview and evaluation of quality-improvement methods from the manufacturing and supply-chain perspective, *Advances in Production Engineering & Management,* Vol. 12, No. 4, 388-400, doi: 10.14743/apem2017.4.266.
[7] Singer, M., Donoso, P., Traverso, P. (2003). Quality strategies in supply chain alliances of disposable items, *Omega,* Vol. 31, No. 6, 499-509, doi: 10.1016/j.omega.2003.08.006.
[8] Xiao, T., Yang, D., Shen, H. (2011). Coordinating a supply chain with a quality assurance policy via a revenue-sharing contract, *International Journal of Production Research,* Vol. 49, No. 1, 99-120, doi: 10.1080/00207543. 2010.508936.
[9] El Ouardighi, F. (2014). Supply quality management with optimal wholesale price and revenue sharing contracts: A two-stage game approach, *International Journal of Production Economics,* Vol. 156, 260-268, doi: 10.1016/j.ijpe. 2014.06.006.
[10] Yan, X. (2015). Contract efficiency for a decentralized supply chain in the presence of quality improvement, *International Transactions in Operational Research,* Vol. 22, No. 4, 713-734, doi: 10.1111/itor.12106.
[11] Zhu, K., Zhang, R.Q., Tsung, F. (2007). Pushing quality improvement along supply chains, *Management Science,* Vol. 53, No. 3, 421-436, doi: 10.1287/mnsc.1060.0634.
[12] Gao, C., Cheng, T.C.E., Shen, H., Xu., L. (2016). Incentives for quality improvement efforts coordination in supply chains with partial cost allocation contract, *International Journal of Production Research,* Vol. 54, No. 20, 6216-6231, doi: 10.1080/00207543.2016.1191691.
[13] Zhang, B., Xu, L. (2013). Multi-item production planning with carbon cap and trade mechanism, *International Journal of Production Economics,* Vol. 144, No. 1, 118-127, doi: 10.1016/j.ijpe.2013.01.024.
[14] Hua, G., Cheng, T.C.E., Wang, S. (2011). Managing carbon footprints in inventory management, *International Journal of Production Economics,* Vol. 132, No. 2, 178-185, doi: 10.1016/j.ijpe.2011.03.024.
[15] Du, S., Tang, W., Song, M. (2016). Low-carbon production with low-carbon premium in cap-and-trade regulation, *Journal of Cleaner Production,* Vol. 134, Part B, 652-662, doi: 10.1016/j.jclepro.2016.01.012.
[16] Xu, X., Xu, X., He, P. (2016). Joint production and pricing decisions for multiple products with cap-and-trade and carbon tax regulations, *Journal of Cleaner Production,* Vol. 112, Part 5, 4093-4106, doi: 10.1016/j.jclepro.2015. 08.081.
[17] Gong, X., Zhou, S.X. (2013). Optimal production planning with emissions trading, *Operations Research,* Vol. 61, No. 4, 908-924, doi: 10.1287/opre.2013.1189.
[18] Xu. X., Zhang. W., He. P., Xu. X. (2017). Production and pricing problems in make-to-order supply chain with cap-and-trade regulation, *Omega,* Vol. 66, Part B, 248-257, doi: 10.1016/j.omega.2015.08.006.
[19] He, P., Zhang, W., Xu, X., Bian, Y. (2015). Production lot-sizing and carbon emissions under cap-and-trade and carbon tax regulations, *Journal of Cleaner Production,* Vol. 103, 241-248, doi: 10.1016/j.jclepro.2014.08.102.
[20] Benjaafar, S., Li, Y., Daskin, M. (2013). Carbon footprint and the management of supply chains: Insights from simple models, *IEEE Transactions on Automation Science and Engineering,* Vol. 10, No. 1, 99-116, doi: 10.1109/ TASE.2012.2203304.
[21] Cachon, G.P. (2003). Supply chain coordination with contracts, In: Graves, S., de Kok, T. (eds.), *Handbooks in Operations Research and Management Science: Supply Chain Management,* North Holland, Vol. 11, 227-339, doi: 10.1016/S0927-0507(03)11006-7.
[22] Cachon, G.P., Lariviere, M.A. (2005). Supply chain coordination with revenue-sharing contracts: Strengths and limitations, *Management Science,* Vol. 51, No. 1, 30-44, doi: 10.1287/mnsc.1040.0215.
[23] Qin, Z., Yang, J. (2008). Analysis of a revenue-sharing contract in supply chain management, *International Journal of Logistics: Research and Applications,* Vol. 11, No. 1, 17-29, doi: 10.1080/13675560701380354.
[24] Hsueh, C.-F. (2014). Improving corporate social responsibility in a supply chain through a new revenue sharing contract, *International Journal of Production Economics,* Vol. 151, 214-222, doi: 10.1016/j.ijpe.2013.10.017.
[25] Yao, Z., Leung, S.C.H., Lai, K.K. (2008). Manufacturer's revenue-sharing contract and retail competition, *European Journal of Operational Research,* Vol. 186, No. 2, 637-651, doi: 10.1016/j.ejor.2007.01.049.
[26] Palsule-Desai, O.D. (2013). Supply chain coordination using revenue-dependent revenue sharing contracts, *Omega,* Vol. 41, No. 4, 780-796, doi: 10.1016/j.omega.2012.10.001.
[27] Zhang, W.-G., Fu, J., Li, H., Xu, W. (2012). Coordination of supply chain with a revenue-sharing contract under demand disruptions when retailers compete, *International Journal of Production Economics,* Vol. 138, No. 1, 68-75, doi: 10.1016/j.ijpe.2012.03.001.
[28] Hu, B., Meng, C., Xu, D., Son, Y.-J. (2016). Three-echelon supply chain coordination with a loss-averse retailer and revenue sharing contracts, *International Journal of Production Economics,* Vol. 179, 192-202, doi: 10.1016/j.ijpe. 2016.06.001.
[29] Gavious, A., Lowengart, O. (2012). Price-quality relationship in the presence of asymmetric dynamic reference quality effects, *Marketing Letters,* Vol. 23, No. 1, 137-161, doi: 10.1007/s11002-011-9143-4.
[30] Kopalle, P.K., Winer, R.S. (1996). A dynamic model of reference price and expected quality, *Marketing Letters,* Vol. 7, No. 1, 41-52, doi: 10.1007/BF00557310.

Appendix A

Proof of Proposition 1:

Since the π_S is concave in d_S, there exists a unique optimal product quality level improvement d_S that maximizes supplier's profit because the second derivative of equation π_P is negative

$$\frac{\partial \pi_S^2}{\partial^2 d_S} = -2cd_{Sj_0} < 0$$

Therefore the optimal value of d_S can be obtained as follows

$$\frac{\partial \pi_S}{\partial d_S} = 0 \to \alpha_S P_{Sj_0} - 2cd_{Sj_0} d_S = 0 \to d_S^* = \frac{\alpha_S P_{Sj_0}}{2cd_{Sj_0}}$$

This completes the proof.

Proof of Proposition 2:

Since the π_P is concave in d_P, there exists a unique optimal product quality level improvement d_P that maximizes the processor's profit because second derivative of the function π_P is negative

$$\frac{\partial \pi_P^2}{\partial^2 d_P} = -2cd_{Pj_0}(1 + \gamma_P d_S) < 0$$

Therefore the optimal value of d_P can be obtained as follows

$$\frac{\partial \pi_P}{\partial d_P} = 0 \to \alpha_P P_{Pj_0} - 2cd_{Pj_0} d_P(1 + \gamma_P d_S) - cp_P g_P = 0 \to d_P^* = \frac{\alpha_P P_{Pj_0} - cp_P g_P}{2cd_{Pj_0}(1 + \gamma_P d_S^*)}$$

This completes the proof.

Proof of Proposition 3:

Since the π_M is concave in d_M, there exists a unique optimal product quality level improvement d_M that maximizes the manufacturer's profit because second derivative of the function π_M is negative

$$\frac{\partial \pi_M^2}{\partial^2 d_M} = -2cd_{Mj_0}(1 + \gamma_M(d_S + d_P)) < 0$$

Therefore the optimal value of d_M can be obtained as follows

$$\frac{\partial \pi_M}{\partial d_M} = 0 \to \alpha_M P_{Mj_0} - 2cd_{Mj_0} d_M(1 + \gamma_M(d_S + d_P)) - cp_M g_M = 0 \to d_M^* = \frac{\alpha_M P_{Mj_0} - cp_M g_M}{2cd_{Pj_0}(1 + \gamma_M(d_S^* + d_P^*))}$$

This completes the proof. Proof of *Propositions 4* and *7* is similar to proof of *Proposition 1*. Proof of *Propositions 5* and *8* is similar to proof of *Proposition 2*. Proof of *Propositions 6* and *9* is similar to proof of *Proposition 3*.

Proof of Proposition 10:

Since the π_P' is concave in ϕ_1 and there exists a unique optimal value for ϕ_1 that maximizes the processor's profit because second derivative of the function π_P' is negative. It should be noted that before the derivation of π_P' we should replace Eq. 16 in Eq. 14.

$$\frac{\partial \pi_P'^2}{\partial^2 \phi_1} = -2(\phi_2 \beta_M P_{Mj_0} + \beta_P P_{Pj_0}) < 0$$

Therefore, the optimal value of ϕ_1 can be obtained as follows

$$\frac{\partial \pi_P'}{\partial \phi_1} = 0 \to 2\alpha_S P_{Sj_0} + cd_{Pj_0} d_P'^2 \gamma_P - \phi_2 \beta_M P_{Mj_0} + \beta_P P_{Pj_0} + 2\phi_1(\phi_2 \beta_M P_{Mj_0} + \beta_P P_{Pj_0}) = 0 \to \phi_1^* = \frac{2\alpha_S P_{Sj_0} + cd_{Pj_0} d_P'^2 \gamma_P - \phi_2 \beta_M P_{Mj_0} - \beta_P P_{Pj_0}}{-2(\phi_2 \beta_M P_{Mj_0} + \beta_P P_{Pj_0})}$$

This proofs Eq. 19.

In the following, π'_M is concave in ϕ_2 and there exists a unique optimal value for ϕ_2 that maximizes the processor's profit because second derivative of the function π'_M is negative. It should be noted that before the derivation of π'_M we should replace Eqs. 16 and 17 in Eq. 15.

$$\frac{\partial \pi'^2_M}{\partial^2 \phi_2} = -\beta_M P_{Mj_0}\left(\frac{\phi_1 \beta_M P_{Mj_0}}{cd_{Sj_0}} + \frac{\beta_M P_{Mj_0}}{cd_{Pj_0}(1+\gamma_P d'_S)}\right) < 0$$

Therefore the optimal value of ϕ_2 can be calculated as follows

$$\frac{\partial \pi'_M}{\partial \phi_2} = 0 \rightarrow \left(\frac{\phi_1 \beta_M P_{Mj_0}}{2cd_{Sj_0}} + \frac{\beta_M P_{Mj_0}}{2cd_{Pj_0}(1+\gamma_P d'_S)}\right)\left(\beta_M P_{Mj_0} - cd_{Mj_0} d'^2_M \gamma_M\right) - \frac{\phi_1 P_{Pj_0} \beta_P \beta_M P_{Mj_0}}{2cd_{Sj_0}} -$$

$$\frac{P_{Pj_0} \alpha_P \beta_M P_{Mj_0}}{2cd_{Pj_0}(1+\gamma_P d'_S)} - 2\phi_2 \beta_M P_{Mj_0}\left(\frac{\phi_1 \beta_M P_{Mj_0}}{2cd_{Sj_0}} + \frac{\beta_M P_{Mj_0}}{2cd_{Pj_0}(1+\gamma_P d'_S)}\right) - \beta_M P_{Mj_0}\left(\frac{\phi_1 \beta_P P_{Pj_0}}{2cd_{Sj_0}} + \frac{\alpha_P P_{Pj_0} - cp_P g_P}{2cd_{Pj_0}(1+\gamma_P d'_S)}\right)$$

$$= 0 \rightarrow \phi_2^*$$

$$= \frac{1}{2} - \frac{cd_{Mj_0} d'^2_M \gamma_M}{2\beta_M P_{Mj_0}} - \frac{cd_{Pj_0}(1+\gamma_P d'_S)\left(2\phi_1 \beta_P P_{Pj_0} + \alpha_S P_{Sj_0}\right) + cd_{Sj_0}\left(2\alpha_P P_{Pj_0} - cp_P g_P\right)}{2cd_{Pj_0}(1+\gamma_P d'_S)\phi_1 \beta_M P_{Mj_0} + 2cd_{Sj_0}\beta_M P_{Mj_0}}$$

This completes the proof.

Proof of Proposition 11:

$$d'^*_P < d^*_P \rightarrow \frac{\phi_2 \beta_M P_{Mj_0} + \alpha_P P_{Pj_0} - cp_P g_P}{2cd_{Pj_0}(1+\gamma_P d'^*_S)} < \frac{\alpha_P P_{Pj_0} - cp_P g_P}{2cd_{Pj_0}(1+\gamma_P d^*_S)}$$

By replacing Eq. 16 in Eq. 17 and replacing Eq. 4 in Eq. 5 we have:

$$\frac{\phi_2 \beta_M P_{Mj_0} + \alpha_P P_{Pj_0} - cp_P g_P}{2cd_{Sj_0} + \phi_1 \beta_P P_{Pj_0} + \phi_1 \phi_2 \beta_M P_{Mj_0} + \alpha_S P_{Sj_0}} < \frac{\alpha_P P_{Pj_0} - cp_P g_P}{2cd_{Sj_0} + \alpha_S P_{Sj_0}}$$

$$\rightarrow \phi_2 < \frac{\phi_1 \beta_P P_{Pj_0}(\alpha_P P_{Pj_0} - cp_P g_P)}{\beta_M P_{Mj_0}\left(2cd_{Sj_0} + \alpha_S P_{Sj_0}\right) - \phi_1 \beta_M P_{Mj_0}(\alpha_P P_{Pj_0} - cp_P g_P)}$$

This completes the proof.

Proof of Proposition 12:

$$d'^*_M < d^*_M \rightarrow \frac{\alpha_M P_{Mj_0} - cp_M g_M}{2cd_{Pj_0}(1+\gamma_M(d'^*_S + d'^*_P))} < \frac{\alpha_M P_{Mj_0} - cp_M g_M}{2cd_{Pj_0}(1+\gamma_P(d^*_S + d^*_P))}$$

Comparing Eqs. 18 and 6 it is clear that numerator in both equations is the same so we have

$$\rightarrow 2cd_{Pj_0}\left(1+\gamma_M(d'^*_S + d'^*_P)\right) > 2cd_{Pj_0}\left(1+\gamma_P(d^*_S + d^*_P)\right) \rightarrow (d'^*_S + d'^*_P) > (d^*_S + d^*_P) \rightarrow (d'^*_S - d^*_S) > (d^*_P - d'^*_P)$$

$$\rightarrow \frac{\phi_1 \beta_P P_{Pj_0} + \phi_1 \phi_2 \beta_M P_{Mj_0} + \alpha_S P_{Sj_0}}{2cd_{Sj_0}} - \frac{\alpha_S P_{Sj_0}}{2cd_{Sj_0}} > \frac{\alpha_P P_{Pj_0} - cp_P g_P}{2cd_{Pj_0}(1+\gamma_P d^*_S)} - \frac{\phi_2 \beta_M P_{Mj_0} + \alpha_P P_{Pj_0} - cp_P g_P}{2cd_{Pj_0}(1+\gamma_P d'^*_S)} \rightarrow$$

$$\phi_2 > \frac{\left(2cd_{Sj_0} + \gamma_P\left(\phi_1 \beta_P P_{Pj_0} + \phi_1 \beta_M P_{Mj_0} + \alpha_S P_{Sj_0}\right)\right)\left(\frac{2cd^2_{Sj_0}(\alpha_P P_{Pj_0} - cp_P g_P)}{2cd_{Sj_0} + \gamma_P \alpha_S P_{Sj_0}} - cd_{Pj_0}\phi_1 \beta_P P_{Pj_0}\right) - 2cd^2_{Sj_0}(\alpha_P P_{Pj_0} - cp_P g_P)}{\beta_M P_{Mj_0}\left(2cd^2_{Sj_0} + \phi_1 cd_{Pj_0}\left(2cd_{Sj_0} + \gamma_P\left(\phi_1 \beta_P P_{Pj_0} + \phi_1 \beta_M P_{Mj_0} + \alpha_S P_{Sj_0}\right)\right)\right)}$$

This completes the proof.

APEM journal
Advances in Production Engineering & Management
Volume 14 | Number 1 | March 2019 | pp 93–111
https://doi.org/10.14743/apem2019.1.314
ISSN 1854-6250
Journal home: apem-journal.org
Original scientific paper

Inventory control model based on multi-attribute material classification: An integrated grey-rough set and probabilistic neural network approach

Zhang, Z.L.[a,b,*], **Wang, Y.F.**[c], **Li, Y.**[d,*]

[a]Northeast Forestry University, College of Economics and Management, Harbin, P.R. China
[b]Jiamusi University, College of Economics and Management, Jiamusi, P.R. China
[c]Jiamusi University, School of Clinical Medicine, Jiamusi, P.R. China
[d]Liaoning University, Business School, Shenyang, P.R. China

ABSTRACT

Efficient and reasonable inventory control can help enterprises improve inventory management efficiency, reduce inventory cost, and ensure the full utilization of resources. Considering that there are many attributes of material, different materials have different effects on enterprises. A multi-attribute material classification model based on grey rough set and probabilistic neural network is proposed, and an inventory control strategy model based on material classification is constructed according to the characteristics of different types of material. Based on the construction of the relevant models, taking the inventory materials of sample Enterprise *A* as an example, the grey rough set algorithm is used to reduce the redundant material attributes, and the sample data of normalized reduction attributes are used to classify and discriminate the materials by probabilistic neural network. The results are simulated by MATLAB to obtain the efficient and reasonable classification of the materials of enterprises. Finally, with the sample data of different types of representative materials, a matching model of inventory control strategy based on material classification is applied in practice, and the applicability and feasibility of the model are illustrated, providing a scientific basis for enterprises to make decisions on material management and inventory control.

ARTICLE INFO

Keywords:
Inventory control strategy;
Modelling;
Material classification;
Grey rough set;
Probabilistic neural network

**Corresponding author:*
jeanneettee@163.com
(Zhang, Z.L.)
lyfly68@163.com
(Li, Y.)

Article history:
Received 30 November 2018
Revised 4 February 2019
Accepted 24 February 2019

1. Introduction

Material is the premise of enterprise production. In order to ensure the production needs, enterprises should keep part of the material as a turnover inventory. However, due to a variety of reasons, enterprises generally have high inventory, resulting in inventory overstocking and waste of resources, affecting the economic efficiency of enterprises. Inventory control of enterprise materials is a hot issue in scientific management of materials as an important tactical decision-making of enterprises [1]. Its main objective is to minimize the inventory cost of materials on the premise that the needs of production and operation of enterprises are met [2].

As the premise of enterprise inventory control, material classification is the focus of enterprise procurement, production, and sales. Therefore, the basic task of inventory control is to complete the classification, storage, and safekeeping of materials through warehouses. Efficient and reasonable inventory is helpful for enterprises to expedite the flow of materials, reduce

costs, ensure the smooth progress of production, and achieve effective control and management of resources [3]. Traditional enterprise inventory control focuses on the quantity control of inventory materials to optimize the single inventory cost; it even insists that its main content is to maintain a certain quantity of materials. However, as far as the content of inventory control is concerned, quantity control constitutes only one of the important items and not the whole content of inventory control. Excessive inventory and confused classification will not only engage a large amount of operating capital of enterprises, affect the turnover of capital, increase the cost of commodity inventory, waste allocation time, but also increase the market risk of enterprises. On the contrary, extremely low inventory quantity and too fine classification will affect the smooth progress of normal production and operation activities of the enterprises and waste a substantial amount of manpower, material resources, and costs, and even make the enterprises lose market opportunities. Efficient inventory control is a prerequisite for production control and job routing decision-making in a multi-objective stochastic manufacturing system [4]. Therefore, it is necessary to adopt scientific material classification and inventory control methods to ensure that enterprises establish an efficient inventory control and classification mechanism on the basis of the normal production and business operation activities. In this way, enterprises can make full use of their limited resources, implement feasible order execution and supply plan, respond quickly to market and customer demand, minimize inventory and operating cost, and improve the economic efficiency of enterprises. It is in this context that research on inventory control based on multi-attribute material classification has become a controversial topic among scholars.

2. Literature review

In order to facilitate inventory management and control, it is necessary to classify inventory materials according to certain rules. ABC classification is a classic and widely used method. However, ABC classification has the defect of single classification index in practical application. Therefore, some scholars tried improving the method from the perspective of classification index optimization based on different scenarios. For example, Xiao *et al*. (2011) proposed a loss-based classification method to overcome the cross-selling effect in ABC classification, and the profit loss of cross-effect was considered as an important rule of classification [5]. Kabir and Hasin (2013) classified the inventory materials with the multi-criteria ABC classification integrating fuzzy analytic hierarchy process (AHP) and neural network methods [6]. Šarić *et al*. (2014) concluded that the multi-criteria classification approach combined with AHP, neural network and clustering analysis was more effective than the traditional single-criteria ABC inventory classification approach in inventory control [7]. Douissa and Jabeur (2016) took ABC classification as an assignment problem, and the multi-criteria classification method PROAFTN was used to classify the inventory materials [8]. May *et al*. (2017) proposed an improved multi-criteria weighted non-linear ABC optimization method, which offered a better multi-criteria classification method for inventory materials [9]. In addition, some scholars tried improving the classification algorithm of material classification ABC. Hu *et al*. (2015), for example, adopted K-MEANS algorithm of clustering to overcome the division error in the classification boundary of the traditional ABC classification method [10]. Chen *et al*. (2008) established a multi-factor classification matrix model, in which ABC classification was combined with the complexity of the supply market and the classification criteria was expanded from three to multiple categories [11]. The above research on multi-attribute material classification provides a scientific basis for formulating inventory control strategy.

Studies on inventory control strategies are actually concerned about the timing and manner of ordering, leading scholars to formulate corresponding inventory control strategies conducive to different conditions. Typical inventory control strategy model has been widely used. For example, Strijbosch and Moors (2006) deduced the safety factor of (*R, S*) inventory control strategy with modified normal distribution and pointed out that the safety factor of normal distribution of general standard should be increased, otherwise, the level of customer service would be reduced [12]. Rossetti *et al*. (2013) analyzed the influence of aggregation utility of demand fore-

casting time on inventory control under (Q, R) inventory control strategy. The results indicated that the longer the interval was, the more stable the data performance would be. It could be easily forecasted by a simple model, but it was also easy to ignore the problem of satisfaction rate [13]. Liu (2015) adopted (s, S) strategy for class A and B materials with a stable demand for spare parts inventory control strategy, and improved the parameter calculation. The (Q, R) strategy was adopted for class C materials [14]. Liu and Jiang (2017) studied the ordering of core materials of auto parts manufacturing enterprises with the improved (Q, R) inventory control strategy [15]. It can be seen from the above analysis that different scholars have different choices of inventory control strategies. For example, the application of (Q, R) strategies needs to be specific to the actual situation.

However, in most cases, the material demand of enterprises is not always fixed and tends to exhibit a certain degree of randomicity. Zhang (2007) put forward a quantitative inventory control model under the condition of stochastic demand, according to which the optimal ordering strategy was obtained. It used stochastic demand to obtain the expected value, and then, adopted EOQ model to solve the problem to obtain the optimal order quantity with this expected value [16]. Güler *et al*. (2015) studied a stochastic demand situation where demand was influenced by price, and pointed out that demand would be influenced by both current price and reference price. The safety inventory was used as a decision variable for modelling and solving. The results showed that the optimal level of inventory increased with the increase of reference price [17]. Zhao (2016) constructed a multi-echelon inventory control model for the supply chain under stochastic demand by the application of control theory [18]. Gocken *et al*. (2017) proposed an optimization approach to find the initial inventory, reorder point and determine the optimal value of the order in a completely stochastic supply chain environment through Optimization via Simulation (OvS) approach [19]. Moreover, demand not only exhibits stochastic, but also shows the characteristics of being non-stationary. Strijbosch *et al*. (2011) studied the interaction between forecasting and inventory control under the condition of non-stationary demand, extended the research scope to non-stationary demand by using simulation method, and analyzed the cumulative effects of the optimal estimator, optimal forecasting parameters, and correct variance [20]. Rahdar *et al*. (2018) put forward a three-tier optimization model in the case of uncertain demand and lead time. That model satisfied uncertain demand and lead time by rolling plan, so as to minimize the total order cost [21]. Li *et al*. (2011) proposed the use of confidence inference to solve the problem of non-stationary demand, and confirmed that this approach was superior to the traditional approach [22].

Based on the above literature, it can be found that, for the inventory control of multi-attribute materials, such as raw materials of manufacturing enterprises or spare parts of a certain enterprise, it is generally necessary to classify materials first and then adopt corresponding inventory control strategies for different classifications. According to the current material classification methods, the multi-criteria classification method, based on ABC classification and matrix classification, is the most widely used and studied method. If multi-criteria material classification is to be carried out, the selection of classification indicators and the determination of classification grade are keys to achieving material classification.

In view of the above analysis, the following questions are raised: (1) How to select appropriate indicators for effective classification of multi-attribute materials? (2) Which material classification method is the most suitable? (3) How to propose targeted inventory control strategies for different classifications of materials? In order to answer these three questions, this paper proposes a material classification method based on rough set probabilistic neural network. This method reduces the duplication and redundancy of material attributes of the enterprise. The attribute reduction algorithm of grey rough set is adopted to reduce the attribute index of materials. The probabilistic neural network (PNN) approach is used to build the material classification model based on the reduced attributes; the probabilistic distribution of multi-Gaussian mixture of approximate data in different material classifications is used to solve the problem of material classification. On this basis, based on the classification results, from the point of view of the demand characteristics of different types of materials, an inventory control strategy model of different types of materials is proposed. Finally, an empirical analysis is carried out using a spe-

cific example. In this paper, a material classification model based on rough set probabilistic neural network and an inventory control strategy model for different materials are proposed, which are tested by practical cases. It is helpful for enterprises to improve the intellectualization, credibility, and scientific nature in material management, and has strong practical significance for inventory control and management of enterprises.

3. Inventory model building

3.1 Evaluation index system of material attributes

The traditional ABC material classification is based on the value of material (average capital occupancy), but in reality, an indicator is obviously insufficient to show the importance of material. Therefore, a set of scientific and reasonable evaluation index system of material attributes is first needed, so as to express and realize the effective classification of multi-attribute materials by quantitative indicators, such as the importance, availability, difficulty in obtaining, cost proportion, and strategic importance of materials to enterprises. With reference to the determination of material attribute indexes in the relevant literature [23-25], this paper intends to use three first-level indicators to describe the characteristics of materials, namely procurement risk, value proportion, and strategic importance; and then determine the second-level indicators. The evaluation index system of material attributes is shown in Table 1.

Table 1 Evaluation index system of material attributes

First-level Index	Second-level Index	
	Name	Serial No.
Procurement risk	Impact of supplier interruption	C_1
	Number of suppliers	C_2
	Substitutability	C_3
	Degree of difficulty in obtaining	C_4
	Product complexity	C_5
Proportion of the value	Total amount of purchase	C_6
	Proportion of total procurement expenditure	C_7
	Proportion of total cost	C_8
	Impact of fluctuations in the price of certain materials on profits	C_9
Strategic importance	Bargaining power of suppliers	C_{10}
	Influence degree of materials on product quality	C_{11}
	Losses caused by shortage of materials	C_{12}

- Procurement risk

Procurement risk mainly refers to the unexpected situations that may occur in the procurement process. It is mainly used to describe the extent of the influence of the unexpected situations encountered in the procurement process on production. The main factors influencing the risk degree of material procurement should be fully considered in determining the second-level index of procurement risk, which mainly come from two aspects: material supplier**s** and themselves [23, 26]. For suppliers, factors such as the impact of interruption of suppliers and the number of suppliers should be taken into account. For materials themselves, the substitution of materials, the difficulty of obtaining materials and the complexity of products are the important factors influencing the risk of material procurement.

- Proportion of the value

The proportion of the value mainly represents the value of materials, that is, the contribution of materials to products. In order to better assign resources and enable enterprises to attach great importance to those materials that contribute greatly to enterprises, factors such as the total amount of purchase, the proportion of total procurement expenditure, the proportion of total cost and the influence of fluctuation in the price of certain materials on profits should be fully taken into account in the process of constructing the second-level index of value proportion [24].

- Strategic importance

From the perspective of the influence of materials on production, **s**trategic importance mainly focuses on the strategic influence on production plan, and the influencing factors mainly come from suppliers and materials themselves [27]. Therefore, the strategic importance of materials is represented by three factors in this paper, namely, the bargaining power of suppliers, the influence degree of materials on product quality, and the losses caused by shortage of materials.

3.2 Classification model of multi-attribute materials

Based on the evaluation index system of material attributes established above, a material classification model based on grey rough set and PNN is proposed in this paper. Firstly, by taking the advantage of the attribute reduction of grey rough set, the important attributes in the classification and evaluation system are extracted, and the input complexity of the evaluation index system of material attributes in the classification and decision-making system is reduced. Then, inventory classification is carried out combined with the strong classification ability of PNN. This method fully combines the advantages of grey rough set and PNN, simplifies the input complexity of material classification system, reduces the complexity of sample training and machine learning in PNN approach, improves the accuracy of material classification, and achieves the purpose of better assisting enterprises to classify materials correctly and guiding enterprises to implement different inventory control strategies according to different material classification.

Grey rough set attribute reduction algorithm

In order to solve the problem of duplication and redundancy, the attribute reduction algorithm of grey rough set is proposed in this paper. Let $S = (U,A,V)$ be a multi-attribute information system, while $U = \{1, 2, \cdots, n\}$ is a non-empty finite set of objects and $n \geq 2$; $A = \{a_1, a_2, \cdots, a_m\}$ is a non-empty finite set of attributes, including the set of efficiency indexes C and the set of cost indexes D; the larger the index attribute value of set C, the better, while the smaller the index attribute value of set D, the better. Let A_c and A_d be the subscript sets of efficiency indexes and cost indexes, respectively, where $= A_c \cup A_d$, $A_c \cap A_d = \emptyset$ and $m \geq 2$. The indexes are divided into conditional attribute C_A and decision attribute D_A, and $C_A \cup D_A = A$, $C_A \cap D_A = \emptyset$, $\forall_i \in U$, $\forall_{a_j} \in A$, V represents the set of the value of indexes, and v_{ij} represents the observed value of the object i about the indicator a_j.

In the system, each index in the indicator set has different dimensions and attributes, and the type of attribute value has two forms, namely clear number and linguistic items, and the attribute value of the same attribute has the same information form. For convenience, let A_d and A_l respectively denote the attribute subset whose attribute values are clear number and the formal information of the linguistic items. $A_d = \{A_1, A_2, \cdots, A_h\}$, $A_l = \{A_{h+1}, A_{h+2}, \cdots, A_m\}$, and $A_d \cup A_l = A$; Let S_1 and S_2 be the subscript sets of attribute subsets A_d and A_l, respectively. $S_1 = \{1, 2, \cdots, h\}, S_2 = \{h + 1, h + 2, \cdots, m\}$. For attribute values, the specific description is as follows:

- If $a_j \in A_d$, then $v_{ij} = v'_{ij}, j \in S_1, i \in U$, where v'_{ij} is a real numeric value, without losing generality, here suppose $v'_{ij} \geq 0$.
- If $a_j \in A_l$, then $v_{ij} = v''_{ij}, j \in S_2, i \in U$, where v''_{ij} is a linguistic item, $v''_{ij} \in P$. Here P is a set of linguistic items, $P = \left\{P_t \middle| t = 0, 1, \cdots, \frac{L}{2} - 1, \frac{L}{2}, \frac{L}{2} + 1, \cdots, L\right\}$, where P_t represents the $(t + 1)$-th linguistic item in P, and $(L + 1)$ represents the number of items in P. When $L = 6$, $P = \{p_0, p_1, p_2, p_3, p_4, p_5, p_6\} = \{PP(particularly\ poor), Wo(worse), P(poor), M(medium), We(well), B(better), EW(especially\ well)\}$ when $z \geq b$, P_z is better than or equal to P_b; if P_z is better than or equal to P_b, then $max\{p_z, p_b\} = P_z, min\{p_z, p_b\} = P_b$; when $b = L - z, inv(p_z) = p_b$, where inv is an inverse operator. The specific normalized calculation formulas are respectively expressed, as shown below:

  (a) If $a_j \in A_d$, then the normalized calculation formula is as follows:

$$G_{ij}^{d}=\begin{cases}\frac{v'_{ij}-v_j^N}{v_j^P-v_j^N}, i\in U, j\in S_1\cap A_c\\ \frac{v_j^P-v'_{ij}}{v_j^P-v_j^N}, i\in U, j\in S_1\cap A_d\end{cases} \tag{1}$$

where

$$v_j^P=max\left[\max_{1\le i\le n}\left(v''_{ij}\right)\right], j\in S_1 \tag{2}$$

$$v_j^N=min\left[min_{1\le i\le n}\left(v''_{ij}\right)\right], j\in S_1 \tag{3}$$

(b) If $a_j\in A_l$, then the normalized calculation formula is as follows:

$$G_{ij}^{l}=\begin{cases}v''_{ij}, i\in U, j\in S_2\cap A_c\\ inv\left(v''_{ij}\right), i\in U, j\in S_2\cap A_d\end{cases} \tag{4}$$

Linguistic item G_{ij}^{l} can be converted into corresponding triangular fuzzy number G_{ij}^{TFN} that is, $G_{ij}^{TFN}=\left(G_{ij}^{1},G_{ij}^{2},G_{ij}^{3}\right)$; the calculation formula is shown thus:

$$\varphi^{TFN}=(\varphi^1,\varphi^2,\varphi^3)=\left[\max\left(\frac{t-1}{L},0\right),\frac{t}{L},\min\left(\frac{t+1}{L},1\right)\right] \tag{5}$$

$$G_{ij}^{d}=\sqrt{\frac{1}{3}\left[\left(G_{ij}^{1}\right)^2+\left(G_{ij}^{2}\right)^2+\left(G_{ij}^{3}\right)^2\right]} \tag{6}$$

After dimensionless processing of v_{ij}, dimensionless feature values of object behaviour can be obtained. Any two objects $f,k\in U$ on the indicator $\forall_{a_j}\in A$, grey correlation coefficient ξ_{fk}^{j}, and correlation degree ξ_{fk}^{A} of indicator set A, correlation cluster analysis can be carried out for each scheme. The calculation formula to calculate the grey correlation coefficient ξ_{fk}^{j} and correlation degree ξ_{fk}^{A} of the scheme f,k on attribute a_j and attribute set A is shown as Eq. 7.

$$\xi_{fk}^{j}=\frac{\min\limits_{i}\min\limits_{j}\left|x_k^j-x_i^j\right|+\theta\max\limits_{i}\max\limits_{j}\left|x_k^j-x_i^j\right|}{\left|x_k^j-x_i^j\right|+\theta\max\limits_{i}\max\limits_{j}\left|x_k^j-x_i^j\right|} \tag{7}$$

$$\xi_{fk}^{A}=\frac{1}{m}\sum_{j=1}^{m}\xi_{fk}^{j} \tag{8}$$

On this basis, grey incidence matrix between objects can be established as follows:

$$\xi=\begin{vmatrix}\xi_{11}^{A} & \xi_{12}^{A} & \cdots & \xi_{1k}^{A} & \cdots & \xi_{1n}^{A}\\ \xi_{21}^{A} & \xi_{22}^{A} & \cdots & \xi_{2k}^{A} & \cdots & \xi_{2n}^{A}\\ \vdots & \vdots & \ddots & \vdots & \ddots & \vdots\\ \xi_{i1}^{A} & \xi_{i2}^{A} & \cdots & \xi_{ik}^{A} & \cdots & \xi_{in}^{A}\\ \vdots & \vdots & \ddots & \vdots & \ddots & \vdots\\ \xi_{n1}^{A} & \xi_{n2}^{A} & \cdots & \xi_{nk}^{A} & \cdots & \xi_{nn}^{A}\end{vmatrix}$$

According to the grey incidence matrix, ξ_{fk}^{A} is the correlation degree of the decision objects f,k on attribute set A, which represents the possibility that the object belongs to the same classification, and the best critical value can be determined by the Bayesian criterion. The specific method is as follows:

(i) C_a, C_m, and C_u respectively denote that objects f,k have a high correlation degree $AF_A^{(\alpha,\beta)}(n)$, a medium correlation degree $MB_A^{(\alpha,\beta)}(n)$, a low correlation degree $DN_A^{(\alpha,\beta)}(n)$; $E(C_{ak})$, $E(C_{mk})$ and $E(C_{uk})$ respectively denote the expected loss function, and that object f belongs to $AF_A^{(\alpha,\beta)}(n)$, $MB_A^{(\alpha,\beta)}(n)$ and $DN_A^{(\alpha,\beta)}(n)$.

The calculation formula of expected loss function is shown as Eq. 9, Eq. 10, and Eq. 11:

$$E(C_{ak}) = \delta_{aA}\xi_{fk}^{A} + \delta_{aD}\left(1 - \xi_{fk}^{A}\right) \tag{9}$$

$$E(C_{mk}) = \delta_{mA}\xi_{fk}^{A} + \delta_{mD}\left(1 - \xi_{fk}^{A}\right) \tag{10}$$

$$E(C_{uk}) = \delta_{uA}\xi_{fk}^{A} + \delta_{uD}\left(1 - \xi_{fk}^{A}\right) \tag{11}$$

where δ_{aA}, δ_{mA} and δ_{uA} respectively indicate the loss function, and that the decision makers take under a high correlation degree $AF_A^{(\alpha,\beta)}(n)$. δ_{aD}, δ_{mD} and δ_{uD} respectively indicate the loss function, and that the decision makers take under low correlation degree $DN_A^{(\alpha,\beta)}(n)$.

(ii) According to the Bayesian decision criterion, the optimal action plan needs to be selected as the action set with the minimum expected loss. The specific decision rules are as follows:

Decision rules of $AF_A^{(\alpha,\beta)}$: if both $E(C_{ak}) \le E(C_{mk})$ and $E(C_{ak}) \le E(C_{uk})$ are true, then $k \in AF_A^{(\alpha,\beta)}(n)$;
Decision rules of $MB_A^{(\alpha,\beta)}$: if both $E(C_{ak}) \ge E(C_{mk})$ and $E(C_{uk}) \ge E(C_{mk})$ are true, then $k \in MB_A^{(\alpha,\beta)}(n)$;
Decision rules of $N_A^{(\alpha,\beta)}$: if both $E(C_{uk}) \le E(C_{ak})$ and $R(O_N|k) \le R(O_U|k)$ are true, then $k \in DN_A^{(\alpha,\beta)}(n)$.

(iii) According to Bayesian reasoning, the rules for simplifying decision-making are as follows:

If $\xi_{fk}^{j} \ge \alpha$ and $\xi_{fk}^{A} \ge \alpha$, then the correlation degree of decision object f, k is high;
If $\beta < \xi_{fk}^{j} < \alpha$ and $\beta < \xi_{fk}^{A} < \alpha$, then the correlation degree of decision object f, k is medium;
If $\xi_{fk}^{j} \le \beta$ and $\xi_{fk}^{A} \le \beta$, then the correlation degree of decision object f, k is low;
where $\forall f, k \in U, \forall a_j \in A, 0 \le \beta \le \alpha \le 1$.
The correlation degree of object f about attribute set A is divided as follows:

$$AF_A^{(\alpha,\beta)}(n) = \left\{k \in U \middle| \xi_{fk}^{A} \ge \alpha\right\} \tag{12}$$

$$MB_A^{(\alpha,\beta)}(n) = \left\{k \in U \middle| \beta < \xi_{fk}^{A} < \alpha\right\} \tag{13}$$

$$DN_A^{(\alpha,\beta)}(n) = \left\{k \in U \middle| \xi_{fk}^{A} \le \beta\right\} \tag{14}$$

The calculation formulas of α and β are:

$$\alpha = \frac{(\delta_{aD} - \delta_{mD})}{(\delta_{aD} - \delta_{mD}) + (\delta_{uA} - \delta_{mA})} \tag{15}$$

$$\beta = \frac{(\delta_{mD} - \delta_{uD})}{(\delta_{mD} - \delta_{uD}) + (\delta_{uA} - \delta_{aA})} \tag{16}$$

Finally, based on the classification of critical values α and β, the attributes are reduced, and the reduction methods are as follows:

- $Q \subseteq C_A, IND(Q) = \{(e,w) \in U^2 | \forall a \in C_A, e \ne w, q(e,a) = q(w,a)\}$, and $IND(Q)$ divides the object U into z equivalence classifications, which is denoted as $U / Q = \{x_1, x_2, \cdots, x_z\}$;
- R is the equivalent relation in A and $r \in R$, if $IND(R) = IND(R - \{a\})$, then is reducible in R, otherwise, r is irreducible in R. If each r is irreducible, then r is independent;
- If $W \in R$ and W is independent, at the same time, $IND(W) = IND(Q)$, then, W is the reduction of U on attribute set Q.

To sum up, the problem to be solved in this paper is how to obtain the reduction scheme of all indexes through a multi-attribute reduction method based on multi-attribute information system S, attribute correlation coefficient ξ_{fk}^{j}, and correlation degree ξ_{fk}^{A}. The algorithm of attribute reduction based on grey rough set is as follows:

Step 1: Normalize the attribute index data with multiple information forms according to Eq. 1 to Eq. 6.

Step 2: Obtain the correlation degree between objects according to Eq. 7 to Eq. 8, and then establish the incidence matrix of characteristic variables.

Step 3: Obtain the optimal critical value of the correlation degree of each object according to Eq. 9 to Eq. 16 and categorize the objects accordingly.

Step 4: Reduce the attribute index according to the division of the correlation degree.

PNN material classification discriminate model

Probabilistic Neural Networks was proposed by Specht in 1990, it is a neural network suitable for classification [28]. According to Bayesian classification rules, it takes the mixed form of multi-Gaussian function to approximate the probability of data in each classification and select the one with the maximum probability value as the classification as the data belongs to. In essence, it is a parallel algorithm based on Bayesian minimum risk criterion. Therefore, based on the reduction results of material attributes, the PNN approach is used to build the classification and discrimination model of materials. This model applies Bayesian criterion to estimate the posterior classification probability $P(c_i / x)$, that is, the unknown vector x belongs to the probability of all possible classification c. According to Bayesian criterion, this probability is proportional to the product of prior probability π_i (the ratio of the unknown vector belongs to each classification) and the probability density function $f_i(x)$ (probability density function of each classification of vector), that is, $P(c_i / x) \propto \pi_i f_i(x)$, where the probability density function of classification i is as per Eq. 17:

$$f_i(x) = \frac{1}{(2\pi)^{\frac{v}{2}}\sigma^v}\frac{1}{k_i}\sum_{j=1}^{i} exp\left[-\frac{(x-x_{ij})^T(x-x_{ij})}{2\sigma^2}\right] \tag{17}$$

where x_{ij} is the j-th training sample belonging to classification i, k_i is the number of training samples in classification i, σ_i is the smoothing parameter, and v is the dimension of each sample. If the prior probability is unknown, it can be estimated by the occurrence frequency of each classification sample in the training set as per Eq. 18:

$$\pi_i = k_i \Big/ \sum_{j=1}^{c} k_j \tag{18}$$

If all kinds of prior probabilities are assumed to be the same and constant terms are ignored, then:

$$P(c_i / x) \propto \sum_{j=1}^{i} exp\left[-\frac{(x-x_{ij})^T(x-x_{ij})}{2\sigma^2}\right] \tag{19}$$

PNN can be obtained through three layer neural network: (a) the input layer accepts input vectors and formats them; (b) in the layer of radial basis neuron, the distance between the input vector and the training sample is first calculated and then multiplied by the threshold vector, calculated by the radial transfer function at last; (c) in the competitive layer, the calculation results of nodes in the first layer are accepted and the output belonging to the same classification is synthesized. Finally, the classification of unknown vectors is judged according to the size of each output result. It can be seen that PNN is obtained by combining radial basis function neural network with competitive neural network. It is a new classification tool, which considers both

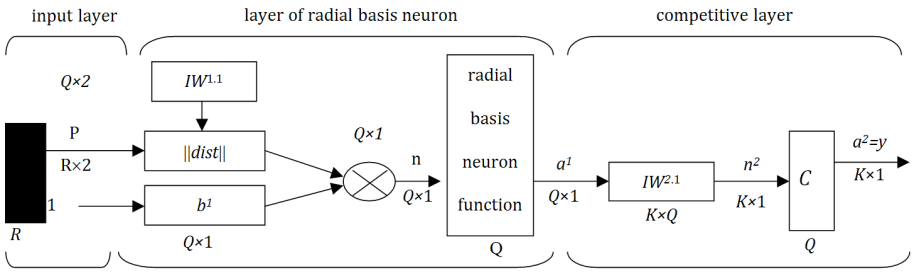

Fig. 1 The specific structure of PNN

the inhomogeneity of the input samples and the classification and pattern recognition capability of the competitive neural network. The specific structure of PNN is shown in Fig. 1.

As shown in Fig. 1, R represents the number of input vector elements; Q is the number of neurons in the second layer; P is the sample matrix of input; $\| dist \|$ represents the distance between the input vector and the weight vector; n^1 is the distance between the sample matrix of input $IW^{1.1}$ and weight matrix multiplied by the threshold b^1; a_i^1 represents the i-th element of a^1; while a^1 is the output from radial basis neuron layer, a^2 is the output from competitive layer, and $a_i^1 = radbas(\|_i\ IW^{1.1} - p\ \|\ b_i^1)$; $y = a^2 = compet(IW^{2.1} - a^2)$, where $radbas()$ is the radial basis function, $compet()$ is the competitive function; IW^1 is the weight matrix of the radial basis network layer; $IW^{1.1}$ is the i-th row vector of the weight matrix IW^1, IW^2 is the weight matrix of the competitive layer; module C represents the competitive transfer function, that is the maximum value of each element in its input vector n^2 is calculated, the output of neurons corresponding to the maximum value is set to 1, and the output of neurons of other classifications are set to 0. Specifically, the input weight of the first layer of the PNN network $IW^{1.1}$ is the transport matrix of the input sample P^T; after calculation by $\| dist \|$, the output vector of the first layer represents the approximation degree between the input vector and the sample vector, then multiplies with the threshold vector and is then calculated by the radial transfer function. When the input vector is approximate to the samples, all the elements corresponding to a^1 will be *1*s. The weight of the second layer $IW^{2.1}$ is set as the expected value vector matrix$T$; only one element in each row vector is 1, representing the corresponding classification; the remaining elements are 0, and then the product Ta^1 is calculated. Finally, n^2 is obtained through the competitive transfer function of the second layer; the larger element is 1 and the others are 0. At this point, the PNN network can complete the classification of input vectors [29, 30].

Due to the large quantity and complexity of the materials, the classification results should be simplified as far as possible. The attributes of materials are various, and the degree of influence and importance of materials are different for different equipment. The maximum and minimum values of expert evaluation classification score D are extracted, and then the value interval is divided into four equal parts; each sub-interval corresponds to a score, equal to the scores of 1, 2, 3, and 4. Here, the materials are divided into four grades, according to the range of materials: strategic materials, bottleneck materials, general materials, and leverage materials. Among them, strategic materials mainly include materials that are of vital importance to the products or industrial processes of the enterprise. These materials often have a high supply risk, mainly because of the shortage of supply or transportation difficulties. The bottleneck type is mainly characterized by the fact that the price of the material itself may be not very expensive, but it is still difficult to obtain. The main characteristics of general materials are relatively rich supply, little influence on procurement costs, and high standardization of products. Leveraged materials are relatively simplified and shared in specifications, which have a significant influence on cost and have the characteristics of a large number of suppliers and fierce market competition.

3.3 Inventory control strategy model based on material classification

Different types of materials are suitable for different inventory control strategies. In this paper, the appropriate inventory control strategy model will be selected according to the characteristics of each kind of materials (strategic materials, bottleneck materials, general materials, and leveraged materials). Therefore, it constructs a matching model based on material classification and inventory control strategy, as shown in Fig. 2.

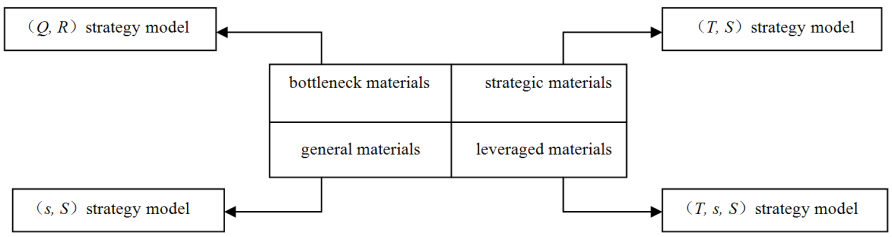

Fig. 2 Matching model of inventory control strategy based on material classification

Strategic materials – (T, S) strategy model

Strategic material has a high value, great complexity, and strong professionalism, and the supplier has great influence on it. The inventory level should be reduced as much as possible, and a good cooperative relationship should be established with the strategic material suppliers. Therefore, the (*T, S*) strategy model can be adopted. The inventory cycle interval of the *(T, S)* strategy is relatively long; it checks the inventory level through time *T* and sets the inventory to the maximum inventory level *S*. In the (*T, S*) strategy model, three parameters need to be determined: order cycle *T*, maximum inventory level *S*, and order quantity *Q*.

- Order cycle *T*

The order cycle *T* is a fixed value. Generally speaking, the order cycle *T* needs to be determined according to the consumption of materials.

- Maximum inventory level *S*

S should satisfy the consumption of order cycle *T* and the order lead time. Meanwhile, safety inventory should also be considered in order to prevent the uncertainty of demand. Assuming that the demand in order cycle and lead time is normal distribution, the mean value is μ, the standard deviation is σ, the lead time is p, the safety inventory is Iss, and the safety coefficient is k. Then, the expression of the maximum inventory level *S* is:

$$S = Iss + \mu(T + p) \tag{20}$$

$$Iss = k\sigma\sqrt{T + p} \tag{21}$$

- Order quantity *Q*

Let the inventory level at time t be It and the order quantity be Qt. From the operation process of *(T, S)* strategy model, the expression of Qt is as follows:

$$Q_t = S - I_t \tag{22}$$

However, in practice, materials are usually composed of a unit package, that is there is a minimum package unit Q_0, and the order quantity should be several times the minimum package unit. Therefore, it can be further written as follows:

$$Q_t = nQ_0 \tag{23}$$

$$n = roundup\left(\frac{S - I_t}{Q_0}\right) \tag{24}$$

where, roundup () represents the upward integer function.

Bottleneck materials – (Q, R) strategy model

Due to the low value of bottleneck materials—great complexity, strong professionalism, and high influence of suppliers on them—it is necessary to keep abreast of the inventory status of such materials, set up safe inventory, and adopt high security inventory strategy to reduce the inventory level. Therefore, the strategy model *(Q, R)* is selected in this paper. The fixed-point quantitative *(Q, R)* strategy of continuous inventory is mainly applicable to the bottleneck materials with large demand and great uncertainty, and no shortage is allowed. Once the shortage occurs, the cost of shortage is very high.

Suppose the order and purchase cost of bottleneck material *i* is C_{2i}, then:

$$C_{2i} = P_i\mu_{D_{it}} \tag{25}$$

where P_i represents unit price of material *i*; $\mu_{D_{it}}$ is the average demand of material *i* in time *t*.

The total ordering business cost C_i' within time t can be expressed as:

$$C_i' = C_i \cdot \frac{\mu_{D_{it}}}{Q_i} \tag{26}$$

where C_i is the single order cost (including storage cost, travel cost, etc.); Q_i is the order quantity of material *i.*

The total storage cost of material *i* in time *t* is C_{is}, and then:

$$C_{is} = S_i \cdot t \cdot \left(\frac{Q_i}{2} + R_i - \mu_{D_{ip}}\right) \tag{27}$$

where S_i represents the storage cost of per unit material in unit time of material *i*; R_i is the order point of material *i.*

If the demand D_{ip} of material *i* in lead time is greater than the order point R_i, there will be a shortage. The average value of shortage is:

$$\int_{R_i}^{+\infty}\left(D_{ip} - R_i\right) \cdot h \cdot (D_{ip}) \cdot d(D_{ip}) \tag{28}$$

If the shortage rate isη, the number of possible shortages in t time is $\frac{\mu_{D_{it}}}{Q_i} \cdot \eta$. If the unit cost of loss due to the shortage of material *i* is $C_{i\eta}$, then the average cost of shortage in time *t* is C_η:

$$C_\eta = C_{i\eta} \cdot \frac{\mu_{D_{it}}}{Q_i} \cdot \eta \cdot \int_{R_i}^{+\infty}\left(D_{ip} - R_i\right) \cdot h \cdot \left(D_{ip}\right) \cdot d\left(D_{ip}\right) \tag{29}$$

Therefore, the objective function namely C_{it} is the total inventory cost of material *i* in time *t*:

$$C_{it} = C_{2i} + C_i' + C_{is} + C_\eta =$$
$$P_i\mu_{D_{it}} + C_i \cdot \frac{\mu_{D_{it}}}{Q_i} + S_i \cdot t \cdot \left(\frac{Q_i}{2} + R_i - \mu_{D_{ip}}\right) + C_{i\eta} \cdot \frac{\mu_{D_{it}}}{Q_i} \cdot \eta \cdot \int_{R_i}^{+\infty}\left(D_{ip} - R_i\right) \cdot h \cdot \left(D_{ip}\right) \cdot d\left(D_{ip}\right) \tag{30}$$

The partial derivatives of the sum of Eq. 30 are respectively obtained, and the result is:

$$\begin{cases} \frac{\partial C_{it}}{\partial R_i} = S_i t - C_{i\eta} \cdot \frac{\mu_{D_{it}}}{Q_i} \cdot \eta \cdot \int_{R_i}^{+\infty}\left(D_{ip} - R_i\right) \cdot h \cdot \left(D_{ip}\right) \cdot d\left(D_{ip}\right) \\ \frac{\partial C_{it}}{\partial R_i} = \frac{S_i t}{2} - \frac{\mu_{D_{it}}\left[C_i + \eta \times C_{i\eta} \times \int_{R_i}^{+\infty}(D_{ip} - R_i) \cdot h \cdot (D_{ip}) \cdot d(D_{ip})\right]}{Q_i^2} \end{cases} \tag{31}$$

Set Eq. 31 equal to zero; then get:

$$\begin{cases} \int_{R_i}^{+\infty}\left(D_{ip} - R_i\right) \cdot h \cdot \left(D_{ip}\right) \cdot d\left(D_{ip}\right) = \frac{\eta \times C_{i\eta} \times \mu_{D_{it}} - S_i \cdot t \cdot Q_i}{\eta \times C_{i\eta} \times \mu_{D_{it}}} \\ Q_i^2 = \frac{2\mu_{D_{it}}\left[C_i + \eta \times C_{i\eta} \times \int_{R_i}^{+\infty}(D_{ip} - R_i) \cdot h \cdot (D_{ip}) \cdot d(D_{ip})\right]}{S_i t} \end{cases} \tag{32}$$

General materials – (s, S) strategy model

General materials have a low value, strong universality, and low influence from suppliers, which are suitable to adopt *(s, S)* strategy model. The *(s, S)* strategy is also known as maximum and minimum strategy. In this strategy model, four parameters need to be checked, namely inventory check time, and reorder point s, order level s, and order quantity *Q.*

- Inventory check time

The inventory level is gradually reduced with consumption, while the continuous inspection strategy does not mean to check the inventory at any time, which is not feasible in practical operation, especially for the material inventory of various manufacturers. Therefore, it is necessary to determine an inventory inspection cycle and checkpoint, which should be consistent with the production plan that is keeping in step with the material demand plan.

- Reorder point

In this strategy model, when the inventory level drops to *s* or below, the order will be issued; so the inventory of the ordering point needs to meet two consumption conditions: one is the inventory consumption in lead time, and the other is to guarantee the service level so as to avoid the shortage caused by an increase in supply or demand.

If it is subject to the normal distribution during the lead time, with a mean value of μ and standard deviation of σ, the lead time is p, and the demand of each period is independent from each other; D is the demand of lead time, and the standard deviation is σ_D. According to the nature of normal distribution, then:

$$D = \mu p \tag{33}$$

$$\sigma_D = \sqrt{p\sigma^2} \tag{34}$$

The safety factor is k, and then the expression of safety inventory *Iss* is:

$$Iss = k \cdot \sigma_D = k \cdot \sqrt{p\sigma^2} = k \cdot \sqrt{p} \cdot \sigma \tag{35}$$

Therefore, the expression of reorder point s is:

$$s = \mu p + Iss \tag{36}$$

- Determination of maximum S

Maximum S is the order level *S*. Since the strategic materials belong to the material with high value, their inventory level S should be reduced as much as possible. That is, the consumption within the lead time can be satisfied on the basis of reorder point s. The expression of S is:

$$S = s + \mu p \tag{37}$$

- Order quantity Q

The order quantity at time t is set to Q_t and according to the operation process of *(s, S)* strategy, the expression is:

$$Q_t = S - I_t \tag{38}$$

The (*s, S*) strategy also needs to consider the constraints of the minimum order unit when ordering. Therefore, it can be further written as follows:

$$Q_t = nQ_0 \tag{39}$$

$$n = roundup\left(\frac{S - I_t}{Q_0}\right) \tag{40}$$

Leveraged materials – (T, s, S) strategy model

Leveraged materials have a high value, strong universality, and low influence from suppliers. Some materials should be selected to set the inventory and reduce the times of purchase. Therefore, the (*T, s, s*) strategy model is more appropriate. (*T, s, S*) strategy is a comprehensive strategy that combines (s, S) strategy with (*T, S*) strategy, which can provide greater flexibility than the fixed-cycle, unified ordering strategy (*T, s*). Where T represents the basic order interval time, s and S respectively represent the order point and maximum inventory of materials. According to this strategy, materials are inspected periodically, and each material adopts an independent and periodic (*s, S*) strategy. Inventory is checked at intervals of T. If the inventory level of material i is below or equal to its order point, it will be replenished to the maximum inventory S. Therefore, four parameters need to be determined, namely T, s, S and Q.

- Order cycle T

Similar to (*T, S*) strategy model, the order cycle T of (*T, s, S*) strategy is a fixed value. Generally speaking, order cycle T needs to be determined according to the consumption of materials.

- Order point s

Different from the continuous inventory, the corresponding period of time to determine the demand to be met by the inventory at the ordering point is not only the lead time of order, but also an inventory cycle. Replenishment may be not replenished at the time of inventory when taking periodic inventory. If there is no replenishment, the opportunity for replenishment is at the next time of inventory. It can be seen that the service level to meet the material demand is within the time range $(T + p)$ when periodic inventory is adopted. Safety inventory and order point are

determined on the basis of total demand in time $(T+p)$, and the value is $s=\mu(T+p)+Iss$. Where $\mu(T+p)$ is the expected value of the total quantity demanded in time $(T+p)$; Iss is the safety inventory. For the given service level requirement α, the corresponding safety factor k can be obtained by referring to the standard normal distribution table. In addition to meeting the demand in lead time, the order point of each cycle also meet the demand within the inventory period, thus:

$$s=\mu(T+p)+k\sigma(T+p) \tag{41}$$

where $k\sigma(T+p)$ is the safety inventory, and $\sigma(T+p)$ is the standard deviation.

- Maximum inventory S

The determination method of maximum inventory S is the same as in (s, S) strategy, so the value of maximum S should be as small as possible, that is, the consumption in advance period can be satisfied on the basis of the order point S, which is the mean value of p in advance period, and the expression of S is:

$$S=s+\mu(T+p) \tag{42}$$

- Order quantity Q

Let the order quantity at time t is Q_t, and the expression for Q_t is:

$$Q_t=S-I_t \tag{43}$$

The constraint of the minimum order unit should also be considered when ordering. Therefore, it can be further written as:

$$Q_t=nQ_0 \tag{44}$$

$$n=roundup\left(\frac{S-I_t}{Q_0}\right) \tag{45}$$

4. Results and discussion: Inventory model application model application

In this paper, a chemical Enterprise A was selected as the research sample to apply the multi-attribute material classification model and the inventory control strategy matching model. The inventory of enterprise A mainly includes the following 60 types of materials, as shown in Table 2.

Table 2 Main material categories of Enterprise A

No.	Name	No.	Name	No.	Name
1	Metallurgical materials and cast iron pipes	21	Labour protection articles	41	Welding materials
2	Petroleum special pipes	22	Oil special equipment	42	Fasteners
3	Common steel	23	Special equipment for refining and chemical industry	43	Bearing
4	Wire and metal ropes	24	Construction machinery and equipment	44	Valves
5	Nonferrous metals and processed materials	25	Lifting and conveying equipment	45	Fire equipment
6	Building hardware	26	General machinery and equipment	46	Other mechanical equipment
7	Petroleum and products	27	Metalworking machinery and equipment	47	Special tools for petroleum
8	Coal	28	Power equipment	48	Petroleum drilling equipment accessories
9	Non-metallic building materials	29	Transportation equipment	49	Accessories for refining and chemical equipment
10	Cement and products	30	Textile equipment	50	Textile equipment and accessories
11	Wood and products	31	Electrical and electrical equipment	51	Industrial and mining accessories
12	Petroleum special chemical products	32	Electrical materials	52	Pipe fittings
13	Catalyst and additive	33	Electrical components	53	Sealing elements
14	Rubber and products	34	Daily-use electric appliances	54	Internal combustion engine parts
15	Plastic and products	35	Communication equipment	55	Heavy-duty auto parts
16	Paint and pigments	36	Electronic industrial products	56	General auto parts
17	General chemical products	37	Petroleum special instruments	57	Fittings for waterway railway equipment
18	Glass instrument	38	Universal instruments	58	Other mechanical parts
19	Pyrotechnic products	39	Small machinery	59	Packing materials
20	Textile products	40	Tools and measuring tools	60	Miscellaneous products

4.1 Application of multi-attribute material classification model

Based on the evaluation index system of material attributes, this paper adopted 12 attribute indicators (Table 1) to classify 60 kinds of material attributes of Enterprise *A*. Firstly, the evaluation index of material attributes was reduced by the grey rough set algorithm, and then, based on the reduction results, the PNN discrimination model was used to realize the effective classification of 60 types of materials.

- *Application of material attribute reduction algorithm based on grey rough sets*

Before the material classification of Enterprise *A*, attribute reduction was needed to remove duplicate and redundant indicators. This process adopted the grey rough set algorithm, which can effectively support the whole process from data pre-processing to attribute reduction analysis. Among these 12 attribute indicators, C_2, C_6, C_7 and C_8 were clear number information, and C_1, C_3, C_4, C_5, C_9, C_{10}, C_{11} and C_{12} were linguistic item information. Due to the large variety of materials, partial material sample data with multiple information forms are listed, as shown in Table 3.

In order to solve the problem of indicator reduction, the calculation process using the algorithm given above is briefly explained below.

Firstly, material classification indicator data with multiple information forms will be standardized according to Eq, 1 to Eq. 6 as shown in Table 4.

Table 3 Partial material sample data with multiple information forms

	C_1	C_2	C_3	C_4	C_5	C_6	C_7	C_8	C_9	C_{10}	C_{11}	C_{12}
Metallurgical materials and cast iron pipes	B	20	M	W_e	M	109	8	7	B	B	B	EW
Petroleum special pipes	EW	7	P	B	B	260	12	10	B	EW	B	EW
Common steel	We	26	B	M	P	100	5	3	M	B	We	We
Wire and metal ropes	B	18	EW	P	P	80	3	2	P	We	We	M

Table 4 Standardization of sample data of some materials with various forms of information

	C_1	C_2	C_3	C_4	C_5	C_6	C_7	C_8	C_9	C_{10}	C_{11}	C_{12}
Metallurgical materials and cast iron pipes	0.84	0.60	0.52	0.68	0.52	0.79	0.88	0.88	0.84	0.84	0.84	0.95
Petroleum special pipes	0.95	0.08	0.34	0.84	0.84	0.39	0.82	0.81	0.84	0.95	0.84	0.95
Common steel	0.68	0.84	0.84	0.52	0.34	0.73	0.93	0.96	0.52	0.84	0.68	0.68
Wire and metal ropes	0.84	0.52	0.95	0.34	0.34	0.93	0.96	0.98	0.34	0.68	0.68	0.52

Secondly, the grey correlation degree of attribute set among materials was calculated according to Eq. 7 and Eq. 8. Then, according to Eq. 9 to Eq. 16, considering the losses faced by Enterprise *A* in material classification and assuming loss functions, then:
$\delta_{aA} = 0.26$, $\delta_{mA} = 0.64$, $\delta_{uA} = 0.72$, $\delta_{aD} = 0.79$, $\delta_{mD} = 0.67$, $\delta_{uD} = 0.09$. The optimal critical value can be obtained as follows:

$$\alpha = \frac{(\delta_{aD} - \delta_{mD})}{(\delta_{aD} - \delta_{mD}) + (\delta_{uA} - \delta_{mA})} = 0.600$$

$$\beta = \frac{(\delta_{mD} - \delta_{uD})}{(\delta_{mD} - \delta_{uD}) + (\delta_{uA} - \delta_{aA})} = 0.558$$

According to the optimal critical value, the set of all the materials with a high correlation degree, medium correlation degree, and low correlation degree can be determined, as shown in Table 5.

Table 5 The correlation degree division of materials

U	$AF_A^{(\alpha,\beta)}(n)$	$MB_A^{(\alpha,\beta)}(n)$	$DN_A^{(\alpha,\beta)}(n)$
1	{1,2,5,7-8,12,37,47}	{3-4,6,9-11,13-36,38-46,59-60}	{48-58}
2	{1,2,5,8,12,24,31,37}	{3-4,6-7,9-11,13-23,25-30,32-36,38-48,52,56,58-60}	{49-51,53-55,57}
3	{3-4,6,9-11,13-21,32-36,38,40-45}	{1-2,5,7-8,12,37,47-60}	{22-31,39,46}
4	{4,11-19,35-44,48-52,60}	{1-3,5-10,20-23,31-34,45-47,53-59}	{24-30}

According to the division of material correlation degree shown in Table 5, the correlation degree of materials can be determined thus: {1-2,5,7-9,22-30,46}, {3-4,6,10-20,32-39,42-45,47-49,58-60}, {21,31,40-41,50-57}; that is:

$$X = U/C_A = \left\{ \begin{array}{l} \{1-2,5,7-9,22-30,46\}; \\ \{3-4,6,10-20,32-39,42-45,47-49,58-60\}; \\ \{21,31,40-41,50-57\} \end{array} \right\}$$

Finally, index reduction is carried out according to the classification of correlation degree. Conditional attribute indexes are found and deleted. By calculation, reduction is as follows:

$X_1 = U/(C - C_1)$; $X_2 = U/(C - C_2)$; $X_3 = U/(C - C_3)$; $X_4 = U/(C - C_4)$; $X_5 = U/(C - C_5)$; $X_6 = U/(C - C_6)$; $X_7 = U/(C - C_7)$; $X_8 = U/(C - C_8)$; $X_9 = U/(C - C_9)$; $X_{10} = U/(C - C_{10})$; $X_{11} = U/(C - C_{11})$; $X_{12} = U/(C - C_{12})$.

Reduction results of

$U/(C - C_2)$, $U/(C - C_2 - C_4)$, $U/(C - C_2 - C_4 - C_6)$, $U/(C - C_2 - C_4 - C_6 - C_8)$, $U/(C - C_2 - C_4 - C_6 - C_8 - C_9)$, $U/(C - C_2 - C_4 - C_6 - C_8 - C_9 - C_{10})$, and $U/(C - C_2 - C_4 - C_6 - C_8 - C_9 - C_{10} - C_{12})$

are equal, and it is found that the reduction does not influence the classification results. Therefore, the minimum set of attributes can be obtained as $\{C_1, C_3, C_5, C_7, C_{11}\}$; that is, the original 12 indicators can be reduced to 5.

- *Application of PNN material classification discriminate model*

Based on the material attribute reduction, the materials of Enterprise *A* are classified into four grades from material value, importance, complexity, and risk by experts' evaluation, according to the five attributes of material attributes reduction (each attribute of each classification is scored with a score of 0−10 points). The classification result is verified by PNN. The four grades of materials after material classification are: I (strategic material), II (bottleneck material), III (general material) and IV (leveraged material).

As can be seen from the material attribute reduction results, there are five main attributes that influence the material classification of Enterprise *A*, namely the influence of supplier interruption, substitutability, product complexity, proportion in total procurement expenditure, and the influence of materials on product quality. Therefore, the input layer of PNN has five nodes corresponding to these five characteristic parameters. In this paper, cross-validation is applied to cross-train and tests the 60 sample data in Table 2. The number of radial basis neurons is determined by the number of the training samples and the number of the neurons in the second layer of PNN is equal to the number of the classification patterns, which are I (strategic material), II (bottleneck material), III (general material), and IV (leveraged material). Therefore, the number of the neurons in the second layer of PNN is four. The transfer function of the second neuron layer is a competitive transfer function, which selects the results with the largest distance weight values as the network's output; that is, the most possible classification pattern results, corresponding to the input vectors, are taken as the output.

In this paper, Matlab is used to write the simulation program, and network training adopts the method of cross-validation [30].

Step 1: Randomly select a number of sample data (32 groups) from each category of expert evaluation for PNN training and the remaining 28 groups for testing. The training results and prediction effect of PNN are shown in Fig. 3 and Fig. 4.

Step 2: Test data in Step 1 (28 groups) are used for training, while the 32 groups training data in Step 1 are used for testing. The training results and prediction effect of PNN are shown in Fig. 5 and Fig. 6.

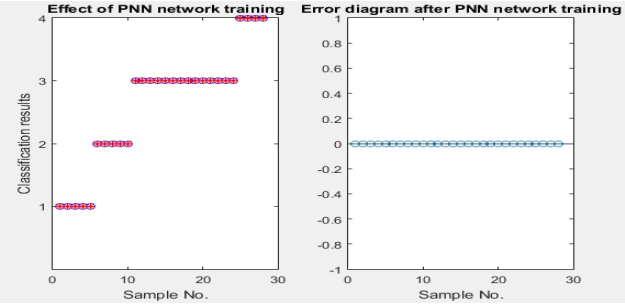

Fig. 3 Effect and error diagram of PNN network training 1

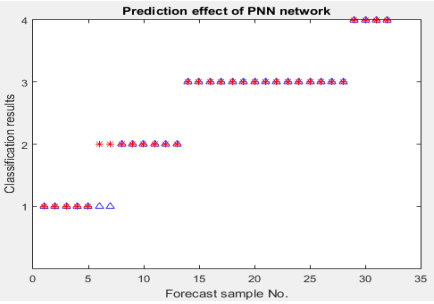

Fig. 4 Prediction effect of PNN network 1

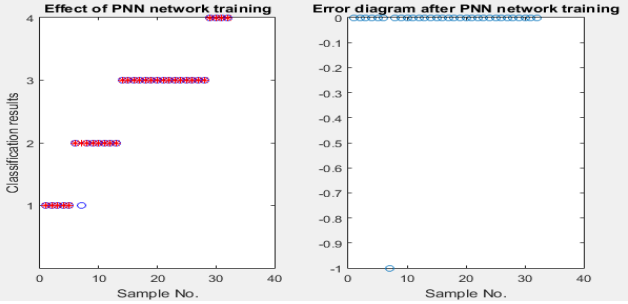

Fig. 5 Effect and error diagram of PNN network training 2

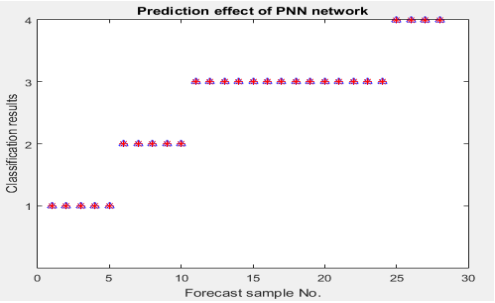

Fig. 6 Prediction effect of PNN network 2

This is equivalent to testing all the data in this way. The probability of each category is obtained by cross-validation. Finally, the classifications are given. Combining the results of the two rounds of training tests, the total accuracy of 98.3 % is obtained by calculation. From the classification results, the established PNN has the ability of accurate classification recognition.

4.2 Application of inventory control strategy matching model based on material classification

- *Application of (T, S) strategy model*

According to the inventory control strategy matching model, it can be seen that (*T, S*) strategy is suitable for the inventory control of strategic materials. This paper takes material 26 (general machinery and equipment) as an example to apply the (*T, S*) strategy model. According to the personnel experience of inventory management of material 26, the inspection cycle is generally set for 12 weeks, thus $T = 12$; the lead time of order is four weeks (i.e., $p = 4$); the service level is 95 %, and the minimum number of packages is four. According to the table of customer service level and safety factor (Table 6), the safety factor $k = 1.65$, and according to the normal distribution test results of enterprise demand prediction, $\mu = 41$ and $\sigma = 22$. Thus, there are:

Maximum inventory $S = Iss + \mu(T + p) = 1.65 \times 4 \times 22 + 41 \times 12 = 801.2$
Check that the inventory level at the beginning of the month is 779, and order quantity is $Q = roundup\,[(801.2 - 779)/4] \times 4 = 24$.

Table 6 Common customer service level and safety factor table

Service level (%)	100	99	98	97	96	95	90	85	80
Safety factor	3.09	2.33	2.05	1.88	1.75	1.65	1.28	1.04	0.84

- *Application of (Q, R) strategy model*

From the matching model of inventory control strategy, it can be seen that (*Q, R*) strategy is suitable for the inventory control of bottleneck materials. This paper takes material 48 (petroleum drilling equipment accessories) as an example to apply (*Q, R*) strategy model. According to the inventory information of material 48, its purchase price is $p = 79.19$ yuan/piece, the cost of a single order is $C_i = 24885$ yuan/time, the single shortage cost is $C_{i\eta} = 420$ yuan/piece, and the unit storage cost is $S_i = 2.5$ yuan/piece/week. According to the fitting result of material 48 demand data in time t ($t = 36$), the demand distribution of material 48 in unit time is $D_i \sim N(185, 8)$. Therefore, demand distribution in time t is $D_{it} \sim N(6660, 36^2 \times 8)$; that is: $\mu_{D_{it}} = 6660$, $\sigma_{D_{it}} = 72\sqrt{2}$; lead time $p = 8$, and the demand distribution within the lead time p is:

D_{ip}~$N(1480, 8^2 \times 8)$, that is $\mu_{D_{ip}} = 1480$, $\sigma_{D_{ip}} = 16\sqrt{2}$; the service level is 95 %, and the shortage rate $\eta = 0.05$, and set $H(R_i) = \int_{R_i}^{+\infty}(D_{ip} - R_i) \cdot h \cdot (D_{ip}) \cdot d(D_{ip})$. Eq. 32 is rewritten thus:

$$\begin{cases} H(R_i) = \frac{\eta \times C_{i\eta} \times \mu_{D_{it}} - S_i \cdot t \cdot Q_i}{\eta \times C_{i\eta} \times \mu_{D_{it}}} \\ Q_i^2 = \frac{2\mu_{D_{it}}\left\{C_i + \eta \times C_{i\eta}\left[{\sigma_{D_{ip}}}^2 \times h(R_i) - \left(R_i - \mu_{D_{ip}}\right) \times (1 - H(R_i))\right]\right\}}{S_i t} \end{cases} \quad (46)$$

$$\begin{cases} H(R_i) = \frac{0.05 \times 420 \times 6660 - 2.5 \times 36 \times Q_i}{0.05 \times 420 \times 6660} = 1 - \frac{90Q_i}{139860} \\ Q_i^2 = \frac{2 \times 6660\left\{24885 + 0.05 \times 420\left[512 \times h(R_i) - (R_i - 1480) \times \frac{90Q_i}{139860}\right]\right\}}{2.5 \times 36} \end{cases} \quad (47)$$

Take $Q_i = \sqrt{\frac{2\mu_{D_{it}} \cdot C_i}{S_i t}} = \sqrt{\frac{2 \times 6660 \times 24885}{2.5 \times 36}} = 1919.11$ and substitute $\mathrm{Q_i} = Q_1$ in Eq. 1 for Eq.47 to obtain R_1; then $R_i = R_1$ in Eq. 2 is substituted with Eq. 47 to obtain Q_2; substitute $Q_i = Q_2$ in Eq. 1 for Eq. 47 to obtain R_2; then $R_i = R_2$ in Eq. 2 is substituted with Eq. 47 to obtain Q_3; iterate over and over again until the convergence state of $Q_{k+1} = Q_k$ is reached. At this point, Q_k and R_k are solved. The final solution is:

$$\begin{cases} Q_k = 2064 \\ R_k = 1848 \end{cases}$$

- *Application of (s, S) strategy model*

From the matching model of inventory control strategy, it can be seen that (*s, S*) strategy is suitable for inventory control of general materials. This paper takes material 59 (packaging materials) as an example to apply (*s, S*) strategy model. According to the personnel experience of inventory managers, the lead time of material 59 is two weeks, the service level is 90 %, and the safety factor is 1.28, which is obtained by Table 6. The mean demand in lead time is $\mu = 7198$ and the standard deviation is σ =3288. Therefore,

Order point $s = \mu \times p + k \cdot \sqrt{p} \cdot \sigma = 7198 \times 2 + 1.28 \times \sqrt{2} \times 3288 = 20348$ pieces;

Maximum inventory level $S = s + \mu p = 20348 + 7198 \times 2 = 34744$ pieces;

Material 59 is inspected once a week. If the inventory level is 18,000 on Monday, which is less than 20,348 at the ordering point, the order should be issued. If the minimum number of packaging units for the material is 1,000, then:

Order quantity $Q = roundup\ [(34744 - 18000)/1000] \times 1000 = 17000$ pieces.

- *Application of (T, s, S) strategy model*

According to the matching model of inventory control strategy, it can be seen that (*T, s, S*) strategy is suitable for inventory control of leveraged materials. This paper takes Material 2 (petroleum special pipe) as an example to apply (*T, s, S*) strategy model. According to the personnel experience of inventory management of Material 2, the inspection cycle is generally set for eight weeks; thus, T = 8, the lead time is two weeks, that is p = 2; the service level is 95 %, and the minimum packing number is 2 tons. From the common customer service level and safety factor table (Table 6), the safety factor k = 1.65. According to the normal distribution results of enterprise demand prediction, μ = 18, σ = 7. Therefore,

Order point $s = \mu(T + p) + k\sigma(T + p) = 18 \times 10 + 1.65 \times 7 \times 10 = 295.5$ tons;

Maximum inventory level $S = s + \mu(T + p) = 295.5 + 18 \times 10 = 475.5$ tons.

If the inventory level after inspection is 280 tons, less than the order point 295.5 tons, and the minimum package quantity is 2 tons, then:

Order quantity $Q = roundup[(475.5 - 280)/2] \times 2 = 196$ tons.

5. Conclusion

Inventory control is an important issue in supply chain management. There are many attributes of inventory materials in enterprises, and the degree of influence of different materials on enterprises is also different. Faced with the new production and delivery, the manner of scientifically classifying the materials of the enterprises and making scientific inventory control strategy are of great practical significance for effectively reducing the operating costs of enterprises, improving the ability of material support, and further promoting the development, transformation and upgrading of the enterprises.

In this paper, the classification and inventory control strategies of multi-attribute materials were systematically studied. Firstly, the evaluation index system of material attributes was constructed from three aspects: procurement risk, proportion of the value and strategic importance. Then, the grey rough set algorithm was used to reduce the attribute of the material attribute index to achieve the aim of removing repetitive and redundant attributes. On this basis, the discriminate model of material classification was constructed based on the PNN approach. It is simple and practical; it has a fast training speed and a good output effect on network simulation, which can solve the material classification problem well. Then, based on the classification results, different inventory control strategy models for strategic materials, bottleneck materials, general materials and leveraged materials were proposed. That is to say, an inventory control strategy matching model based on material classification was built to provide a powerful basis for enterprises to formulate targeted inventory control strategies. Finally, taking a chemical enterprise (i.e., Enterprise *A*) as an example, using the classification approach, inventory control strategy and the corresponding model proposed in this paper, the material classification scheme of Enterprise *A* was obtained, and the order schemes under different inventory control strategies were obtained by calculation. The results strongly illustrate the feasibility and validity of the model and the method built in this paper.

The limitation of this paper is that only static inventory control strategy is considered. However, the improvement of other inventory control strategies, such as the dynamic inventory control strategy and the static-dynamic inventory control strategy need to be further studied.

Acknowledgement

This research was partially funded by the National Science Foundation of China (71373039) and the Ministry of Education's Program for New Century Excellent Talents (NCET-13-0712).

References

[1] Gholamian, M.R., Heydari, M. (2017). An inventory model with METRIC approach in location-routing-inventory problem, *Advances in Production Engineering & Management*, Vol. 12, No. 2, 115-126, doi: 10.14743/apem2017.2.244.

[2] Jin, X.-W. (1995). An inventory control model for multistage demand imbalance: comment on SM-I method, *Journal of Quantitative & Technical Economics,* No. 9, 48-51, doi: 10.13653/j.cnki.jqte.1995.09.010.

[3] Tan, Z.D. (2014). Efficient warehouse control supply and logistics "regulating valve", *Petroleum & Petrochemical Material Procurement*, Vol. 4, No. 3, 28-29.

[4] Katsios, D., Xanthopoulos, A.S., Koulouriotis, D.E., Kiatipis, A. (2018). A simulation optimisation tool and its production/inventory control application, *International Journal of Simulation Modeling,* Vol. 17, No. 2, 257-270, doi: 10.2507/IJSIMM17(2)425.

[5] Xiao, Y.-Y., Zhang, R.-Q., Kaku I. (2011). A new approach of inventory classification based on loss profit, *Expert Systems with Applications*, Vol. 38, No. 8, 9382-9391, doi: 10.1016/j.eswa.2011.01.127.

[6] Kabir, G., Hasin, M.A.A. (2013). Multi-criteria inventory classification through integration of fuzzy analytic hierarchy process and artificial neural network, *International Journal of Industrial and Systems Engineering*, Vol. 14, No. 1, 74-103, doi: 10.1504/IJISE.2013.052922.

[7] Šarić, T., Šimunović, K., Pezer, D., Šimunović, G., (2014). Inventory classification using multi-criteria ABC analysis, neural networks and cluster analysis, *Tehnički Vjesnik – Technical Gazett*e, Vol. 21, No. 5, 1109-1115.

[8] Douissa, M.R., Jabeur, K. (2016). A new model for multi-criteria ABC inventory classification: PROAFTN method, *Procedia Computer Science*, No. 96, 550-559, doi: 10.1016/j.procs.2016.08.233.

[9] May, B.I., Atkinson, M.P., Ferrer, G. (2017). Applying inventory classification to a large inventory management system, *Journal of Operations and Supply Chain Management*, Vol. 10, No. 1, 68-86, doi: 10.12660/joscmv10n1p68-86.
[10] Hu, J.-F., He, L.-L., Zhou, Q.-Y. (2015). Research on ABC inventory classification based on cluster analysis, *Industrial Control Computer*, Vol. 28, No. 3, 147-148, doi: 10.3969/j.issn.1001-182X.2015.03.062.
[11] Chen, Z., Tang, S.-H., Shan, M.-Y. (2008). Study on the strategy of inventory classified management matrix in manufacturing enterprise, *The Theory and Practice of Finance and Economics*. Vol. 29, No. 6, 105-109, doi: 10.3969/j.issn.1003-7217.2008.06.023.
[12] Strijbosch, L.W.G., Moors, J.J.A. (2006). Modified normal demand distributions in (*R, S*)-inventory control, *European Journal of Operational Research*, Vol. 172, No. 1, 201-212, doi: 10.1016/j.ejor.2004.10.002.
[13] Rossetti, M.D., Shbool, M., Varghese, V., Pohl, E. (2013). Investigating the effect of demand aggregation on the performance of an (R, Q) inventory control policy, In: *Proceedings of the 2013 Winter Simulation Conference: Simulation: Making Decisions in a Complex World,* Washington, USA, 3318-3329, doi: 10.1109/WSC.2013. 6721696.
[14] Liu, A.-Y. (2015). *Research on inventory control of service spare parts of electronic manufacturing industry company,* Master's thesis, Taiyuan University of Technology, School of economics and management, Taiyuan. China.
[15] Liu, Z.-Y., Jiang, S.-M. (2017). The ordering strategy research of core material of W auto parts manufacturing enterprise, *Logistics Engineering and Management*, Vol. 39, No. 11, 130-132.
[16] Zhang, J. (2007). Research on inventory control strategy under the condition of random requirement, *Pioneering with Science & Technology Monthly*, No. 11, 78-79, doi: 10.3969/j.issn.1672-2272.2007.11.039.
[17] Güler, M.G., Bilgiç, T., Güllü, R. (2015). Joint pricing and inventory control for additive demand models with reference effects, *Annals of Operations Research*, Vol. 226, No. 1, 255-276, doi: 10.1007/s10479-014-1706-3.
[18] Zhao, C. (2016). *Optimization and simulation of multi-echelon inventory in supply chain under stochastic demand based on control theory,* Doctoral thesis, University of International Business and Economics, School of International Trade and Economics, Beijing, P.R. China.
[19] Gocken, M., Dosdogru, A.T., Boru, A. (2017). Optimization via simulation for inventory control policies and supplier selection, *International Journal of Simulation Modeling*, Vol. 16, No. 2, 241-252, doi: 10.2507/IJSIMM16(2)5.375.
[20] Strijbosch, L.W.G., Syntetos, A.A., Boylan, J.E., Janssen, E. (2011). On the interaction between forecasting and stock control: The case of non-stationary demand, *International Journal of Production Economics*, Vol. 133, No. 1, 470-480, doi: 10.1016/j.ijpe.2009.10.032.
[21] Rahdar, M., Wang, L., Hu, G. (2018). A tri-level optimization model for inventory control with uncertain demand and lead time, *International Journal of Production Economics*, Vol. 195, 96-105, doi: 10.1016/j.ijpe.2017.10.011.
[22] Li, B., Wang, H., Yang, J., Guo, M. (2011). Belief-rule-based inference method for inventory control, *Journal of Huazhong University of Science and Technology (Natural Science Edition)*, Vol. 39, No. 7, 76-79, doi: 10.13245/j.hust.2011.07.001.
[23] Yan, X.-J., Zhang, M.-K., Chen, Z.-Y. (2016). Studies on risk control of materials purchasing using the MSPC method, *Journal of Applied Statistics and Management*, Vol. 35, No. 2, 360-368, doi: 10.13860/j.cnki.sltj.20160123-001.
[24] Li, F. (2011). *Research on material classification of wind-electric assemble plant,* Master's thesis, Chongqing University, College of Mechanical Engineering, Chongqing, P.R. China.
[25] Han, S., Lu, J., Wei, C., Liu, Z. (2014). Research of classification method of materials and equipments of coal enterprise based on probabilistic neural network, *Industry and Mine Automation*, Vol. 40, No. 4, 38-41, doi: 10.13272/j.issn.1671-251x.2014.04.009.
[26] Lee, H.L., Billington, C. (1993). Material management in decentralized supply chains, *Operations Research*, Vol. 41, No. 5, 835-847, doi: 10.1287/opre.41.5.835.
[27] Mohanty, R.P., Deshmukh, S.G. (2001). Reengineering of materials management system: A case study, *International Journal of Production Economics*, Vol. 70, No. 3, 267-278, doi: 10.1016/S0925-5273(00)00071-2.
[28] Hallikas, J., Karvonen, I., Pulkkinen, U., Virolainen, V.-M., Tuominen, M. (2004). Risk management processes in supplier networks, *International Journal of Production Economics*, Vol. 90, No. 1, 47-58, doi: 10.1016/j.ijpe.2004.02.007.
[29] Partovi, F.Y., Anandarajan, M. (2002). Classifying inventory using an artificial neural network approach, *Computers & Industrial Engineering*, Vol. 41, No. 4, 389-404, doi: 10.1016/S0360-8352(01)00064-X.
[30] Haykin, S. (2008). *Neural networks and learning machine*, 3rd edition, Pearson Education, Inc., Upper Saddle River, Pearson Prentice Hall, New Jersey.

APEM journal
Advances in Production Engineering & Management
Volume 14 | Number 1 | March 2019 | pp 112–124
https://doi.org/10.14743/apem2019.1.315
ISSN 1854-6250
Journal home: apem-journal.org
Original scientific paper

A multi-product pricing and inventory model with production rate proportional to power demand rate

Keshavarzfard, R.[a], **Makui, A.**[b], **Tavakkoli-Moghaddam, R.**[c,d,*]

[a]School of Industrial Engineering, South Tehran Branch, Islamic Azad University, Tehran, Iran
[b]School of Industrial Engineering, Iran University of Science and Technology, Tehran, Iran
[c]School of Industrial Engineering, College of Engineering, University of Tehran, Tehran, Iran
[d]Arts et Métiers ParisTech, LCFC, Metz, France

ABSTRACT

This paper deals with an economic lot size model when demand follows a power law and changes with time, owing to the fact that this kind of pattern is suitable for so many real situations. Production rate is presumed to be proportional to demand rate. Also since that demand is price sensitive in reality, we suppose that demand decreases linearly with price. With regard to these points, in this article a joint pricing and inventory model is presented where demand depends on time with a power pattern and price linearly, production rate changes pro rata with demand rate and multiple items are considered. The principal consideration of the study is to satisfy the demand and optimize the profit for all items in the system, simultaneously. Setup, holding, backlogging and production costs are involved in the inventory system. The aim is to maximize total profit function and achieve optimum values of scheduling period, reorder point and price. Employing mathematical modelling and optimization methods, the existence of the optimal solutions is proved, and then a simple heuristic algorithm is presented to maximize total inventory profit and determine the best values of variables. A numerical analysis is carried out to illustrate the applications of the proposed models.

ARTICLE INFO

Keywords:
Pricing model;
Inventory model;
Economic production quantity (EPQ);
Backordered shortages;
Power demand pattern

**Corresponding author:*
tavakoli@ut.ac.ir
(Tavakkoli-Moghaddam, R.)

Article history:
Received 14 August 2017
Revised 15 February 2019
Accepted 24 February 2019

1. Introduction

The constant demand rate is one of the presumptions of the conventional Economic Production Quantity (EPQ) model proposed by Taft [1] that is not common in practice. In the most real situations demand of consumers varies with time. Therefore, many researchers have worked on time-varying inventory models. Barbosa and Friedman [2] worked on a special type of time-varying demand to find a complete solution. Mitra *et al*. [3] used a demand pattern that increases or decreases with time in an inventory system. A multi-period inventory model is presented by Sakaguchi [4] assuming that demand varies with time. Also Khanra *et al*. [5] proposed a quadratic-time demand for an EOQ with shortages and allowable delay in payments. Sarkar *et al*. [6] studied a production system with demand depending on time and price together with considering the influence of inflation and reliability. Escuín *et al*. [7] discussed inventory models using stochastic and time varying demand for a paper manufacturer.

In this paper, we use a kind of demand pattern called power demand. It can be applied for the situations that a high percentage of requests for products happen at the beginning of the cycle, like breads, yogurt, fruits, prepared food, vegetables, fresh meat, etc., or at the end of the cycle,

like tea, coffee, sugar, oil, etc. Naddor [8] introduced an inventory system with a power demand pattern. Lee and Wu [9] presented an optimal order quantity model allowing for shortages, power demand and deteriorating items. Singh *et al*. [10] studied an EOQ model where demand has a power pattern and partial backlogging and perishable products are allowed. Sicilia *et al*. [11] analyzed systems with deterministic power demand pattern and different situations: with and without shortages, with full backordering or completely lost sales. Rajeswari and Vanjikkodi [12] worked on an inventory system considering Weibull deterioration and demand following a power law. Mishra and Singh [13] proposed an economic ordering model with demand having a power pattern, perishable units and partially backordered shortages. Sicilia *et al*. [14] offered an optimal order size model taking into account power demand along with constant deterioration rate. Sicilia *et al*. [15] presented an optimum lot size model in which demand has a power pattern, production rate changes pro rata with demand rate and backordered items are allowed. Sicilia *et al*. [16] studied lot size models where demand follows a power law and the replenishment rate is uniform. San-José *et al*. [17] analyzed an inventory system with demand following a power law and partial backordering.

Demand of consumers is price sensitive, so that pricing is one of the most important decisions in a company. Tripathi *et al*. [18] investigated inventory dependent demand with a power rate and holding cost functions for two situations. Lau *et al*. [19] worked on a joint ordering and pricing problem with deteriorating products and a two period life. Yang *et al*. [20] studied a model considering price dependent demand, deterioration and partial backordering. Banerjee and Sharma [21] investigated an inventory model in which seasonal demand varies with time and price. Soon [22] developed a review of multi-products pricing models. Maihami and Kamalabadi [23] proposed a joint inventory and pricing system with deteriorating products, price dependent demand and partial backordering. Shavandi *et al*. [24] presented a constrained inventory and pricing model with multiple items. Pal *et al*. [25] studied an economic ordering model with multiple products and price break sensitive demand. Zhu [26] worked on joint production, replenishment and pricing policies where demand is random and price sensitive and there is a supply disruption. Qin *et al*. [27] employed joint lot-sizing and pricing policies for fresh products with deterioration. Liu *et al*. [28] studied a joint investment and pricing problem for perishable products considering price and quality dependent demand. Panda *et al*. [29] presented a replenishment and pricing problem for a high tech item in a dual-channel supply chain. Alfares and Ghaithan [30] worked on a pricing and inventory system considering price dependent demand and time-varying holding cost along with quantity discounts. Chiu *et al*. [31] investigated the impact of delayed differentiation on a vendor-buyer system with rework and multiple items. Gholamian and Heydari [32] developed a mixed integer stochastic programming model by using METRIC stochastic relations in a location-routing-inventory problem.

The remainder of this paper is organized as follows. In Section 2 problem definition and mathematical model are presented. Concavity and optimal decision are proposed in section 3. A procedure for determining the optimum values can be found in section 4. Numerical analysis is presented in section 5. Finally, in section 6 some conclusions and future researches are given.

2. Problem definition and mathematical model

Consider a factory which produces N different items (where $i = 1,2,..,N$). Each item has an average demand v_i that must be satisfied. The demand varies with time with a power pattern and decreases linearly with price. Also the production rate changes pro rata with demand rate. The manager desires to satisfy the customer demand and optimize the total profit of the system, simultaneously. The inventory cycle starts with s units of net stock at time 0. At the same time $t = 0$, production begins with the production rate $P_i(t)$, at time t_{1i} reaches zero and continues until $t = \tau_i$ for each product i, consequently the replenishment quantity Q_i will be produced. Also during the interval $[0, \tau_i]$, the inventory level of product i increases at a rate $P_i(t) - D_i(t)$. After that the stock level decreases up to $t = t_{2i}$ according to demand. Finally, during the interval $[t_{2i}, T]$, demand is backlogged. Assume that $I_{1i}(t)$ and $I_{2i}(t)$ are the on-hand inventory levels of item i at time t in the intervals $[0, \tau_i]$ and $[\tau_i, T]$, respectively. The scheduling period, the

backorder size and the selling price are three decision variables of the system. In the following, an approach is presented to find the optimal values.

The following notation will be applied in the rest of the paper.

T	Scheduling period (time)
N	Number of items
Q_i	Production quantity for item i (units)
s_i	Reorder point for item i (units)
D_i	Demand quantity during the inventory cycle for item i (units)
τ_i	Production period length for item i (time)
ν_i	Average demand $\nu_i = D_i/T$ for item i (units)
Λ_i	Production setup cost for item i (\$/replenishment)
$\wp_i$	Selling price for item i, where $\wp_i > c_i$ (\$/unit)
c_i	Unit producing cost for item i (\$/unit)
$\hbar_i$	Unit carrying cost for item i (\$/unit/unit time)
ω_i	Unit backlogging cost for item i (\$/unit/unit time)
$I_{1i}(t)$	Net stock level at time t for item i ($0 \le t \le \tau_i$)
$I_{2i}(t)$	Net stock level at time t for item i ($0 \le t \le T$)
$P_i(t)$	Production rate at time t for item i ($0 \le t \le \tau_i$)
$D_i(t)$	Demand rate at time t for item i ($0 \le t \le T$)
CH_i	Cost of holding for item i (\$/unit time)
CB_i	Cost of backordering for item i (\$/unit time)
CS_i	Cost of setup for item i (\$/unit time)
CP_i	Cost of production for item i (\$/unit time)
SR_i	Sales revenue for item i (\$/unit time)
$TP_i(\wp_i, s_i, T)$	Total profit for item i (\$/unit time)
$\Pi(\vec{\wp}, \vec{s}, T)$	Total profit of the system (\$/unit time)

The following assumptions are considered:

- The planning horizon is infinite.
- Shortages are fully backordered.
- Demand rate changes with time with a power pattern and decreases linearly with price. So, the demand rate is assumed to be $D_i(t) = (a_i - b_i\wp_i)\frac{\nu_i}{\kappa_i}(\frac{t}{T})^{1/\kappa_i - 1}$, with $0 \le t \le T$, where $0 < \kappa_i < \infty$, $a_i > 0$, $b_i > 0$.
- Multiple items are assumed for the inventory system.
- The demand rate is less than the production rate for each item.
- The production rate $P_i(t)$ is proportional to demand rate $D_i(t)$ for each item i at any time $t(0 \le t \le \tau_i)$ and is defined by $P_i(t) = \alpha_i D_i\ (t)$ with $\alpha_i > 1$.

The demand over the scheduling period $[0, T]$ is defined by the following:

$$\int_0^T D_i(t)dt = \int_0^T (a_i - b_i\wp_i)\frac{\nu_i}{\kappa_i}\left(\frac{t}{T}\right)^{1/\kappa_i - 1} dt = (a_i - b_i\wp_i)\nu_i T \tag{1}$$

The differential equations governing the system are as following:

$$\frac{dI_{1i}(t)}{dt} = P_i(t) - D_i(t) = (\alpha_i - 1)D_i(t) = (\alpha_i - 1)(a_i - b_i\wp_i)\frac{\nu_i}{\kappa_i}\left(\frac{t}{T}\right)^{1/\kappa_i - 1}, \tag{2}$$

$$I_{1i}(0) = s_i, \quad 0 \le t \le \tau_i$$

$$\frac{dI_{2i}(t)}{dt} = -D_i(t) = -(a_i - b_i\wp_i)\frac{\nu_i}{\kappa_i}\left(\frac{t}{T}\right)^{1/\kappa_i - 1}, \quad I_{2i}(T) = s_i, \quad \tau_i \le t \le T \tag{3}$$

With regard to the boundary conditions, $I_{1i}(0) = I_{2i}(T) = s_i$, Eq. 1 and Eq. 2 are solved and the solutions are:

$$I_{1i}(t) = s_i + (\alpha_i - 1)(a_i - b_i\mathscr{p}_i)\nu_i T\left(\frac{t}{T}\right)^{1/\kappa_i}, \quad 0 \le t \le \tau_i \tag{4}$$

$$I_{2i}(t) = s_i + (a_i - b_i\mathscr{p}_i)\nu_i T - (a_i - b_i\mathscr{p}_i)\nu_i T\left(\frac{t}{T}\right)^{1/\kappa_i}, \quad \tau_i \le t \le T \tag{5}$$

At time τ_i the production cycle of lot size is finished and the maximum inventory level can be calculated by both Eq. 4 and Eq. 5. So that τ_i and stock level at τ_i are respectively:

$$\tau_i = \frac{T}{{\alpha_i}^{\kappa_i}} \tag{6}$$

$$I_i(\tau_i) = s_i + \frac{\alpha_i - 1}{\alpha_i}(a_i - b_i\mathscr{p}_i)\nu_i T \tag{7}$$

Also the lot size Q_i for product i is calculated by

$$Q_i = \int_0^{\tau_i} P_i(t)dt = \int_0^{\tau_i} \alpha_i(a_i - b_i\mathscr{p}_i)\frac{\nu_i}{\kappa_i}\left(\frac{t}{T}\right)^{1/\kappa_i - 1} dt = (a_i - b_i\mathscr{p}_i)\nu_i T \tag{8}$$

As it was expected, the lot quantity is equal to the demand of scheduling period. We assume that $I(\tau_i) \ge 0$ and $s_i \le 0$, So that $-(a_i - b_i\mathscr{p}_i)\frac{(\alpha_i - 1)}{\alpha_i} rT \le s_i \le 0$. Suppose that the stock level reaches zero in the production period at time t_{1i}. Since $I_{1i}(t_{1i}) = 0$, from Eq. 4 we obtain t_{1i} for item i according to decision variables s_i and T:

$$t_{1i} = \left(\frac{-s_i}{(\alpha_i - 1)(a_i - b_i\mathscr{p}_i)\nu_i T}\right)^n T \tag{9}$$

The net stock level of interval $[\tau_i, T]$ reaches zero at time t_{2i}. Solving equation $I_{2i}(t_{2i}) = 0$, t_{2i} can be obtained for item i according to decision variables s_i and T:

$$t_{2i} = \left(1 + \frac{s_i}{(a_i - b_i\mathscr{p}_i)\nu_i T}\right)^n T \tag{10}$$

We consider four various cost in the inventory system for each product i as follows. Note that the average number of production runs is $\frac{1}{T}$.

The carrying cost:

$$\begin{aligned} CH_i = \frac{\hbar_i}{T}\Bigg(&\int_{t_{1i}}^{\tau_i}\left[s_i + (\alpha_i - 1)(a_i - b_i\mathscr{p}_i)\nu_i T\left(\frac{t}{T}\right)^{1/\kappa_i}\right]dt \\ &+ \int_{\tau_i}^{t_{2i}}\left[s_i + (a_i - b_i\mathscr{p}_i)\nu_i T - (a_i - b_i\mathscr{p}_i)\nu_i T\left(\frac{t}{T}\right)^{1/\kappa_i}\right]dt\Bigg) = \\ = \Bigg(&\frac{(s_i + (a_i - b_i\mathscr{p}_i)\nu_i T)^{\kappa_i + 1}}{(\kappa_i + 1)(a_i - b_i\mathscr{p}_i)^{\kappa_i}{\nu_i}^{\kappa_i}T^{\kappa_i}} + \frac{(-s_i)^{\kappa_i + 1}}{(\kappa_i + 1)(\alpha_i - 1)^{\kappa_i}(a_i - b_i\mathscr{p}_i)^{\kappa_i}{\nu_i}^{\kappa_i}T^{\kappa_i}} \\ &- \frac{(a_i - b_i\mathscr{p}_i)\nu_i T}{(\kappa_i + 1){\alpha_i}^{\kappa_i}}\Bigg)\hbar_i \end{aligned} \tag{11}$$

The shortage cost:

$$\begin{aligned} CB_i = -\frac{\varpi_i}{T}\Bigg(&\int_0^{t_{1i}}\left[s_i + (\alpha_i - 1)(a_i - b_i\mathscr{p}_i)\nu_i T\left(\frac{t}{T}\right)^{1/\kappa_i}\right]dt \\ &+ \int_{t_{2i}}^{T}\left[s_i + (a_i - b_i\mathscr{p}_i)\nu_i T - (a_i - b_i\mathscr{p}_i)\nu_i T\left(\frac{t}{T}\right)^{1/\kappa_i}\right]dt\Bigg) = \\ = \Bigg(&\frac{(s_i + (a_i - b_i\mathscr{p}_i)\nu_i T)^{\kappa_i + 1}}{(\kappa_i + 1)(a_i - b_i\mathscr{p}_i)^{\kappa_i}{\nu_i}^{\kappa_i}T^{\kappa_i}} + \frac{(-s_i)^{\kappa_i + 1}}{(\kappa_i + 1)(\alpha_i - 1)^{\kappa_i}(a_i - b_i\mathscr{p}_i)^{\kappa_i}{\nu_i}^{\kappa_i}T^{\kappa_i}} - \frac{(a_i - b_i\mathscr{p}_i)\nu_i T}{(\kappa_i + 1)} \\ &- s_i\Bigg)\varpi_i \end{aligned} \tag{12}$$

The production cost:

$$CP_i = c_i \frac{Q_i}{T} = (a_i - b_i \wp_i) c_i \nu_i \tag{13}$$

The setup cost:

$$CS_i = \frac{\Lambda_i}{T} \tag{14}$$

The sales revenue is:

$$SR_i = \wp_i \frac{Q_i}{T} = (a_i - b_i \wp_i) \wp_i \nu_i \tag{15}$$

The total profit of product i can be calculated then as:

$$\begin{aligned} TP_i(\wp_i, s_i, T) &= SR_i - CH_i - CB_i - CP_i - CS_i = \\ &= (a_i - b_i \wp_i)\wp_i \nu_i - \frac{(s_i + (a_i - b_i \wp_i)\nu_i T)^{\kappa_i + 1}(\hbar_i + \omega_i)}{(\kappa_i + 1)(a_i - b_i \wp_i)^{\kappa_i} \nu_i{}^{\kappa_i} T^{\kappa_i}} \\ &\quad - \frac{(-s_i)^{\kappa_i + 1}(\hbar_i + \omega_i)}{(\kappa_i + 1)(\alpha_i - 1)^{\kappa_i}(a_i - b_i \wp_i)^{\kappa_i} \nu_i{}^{\kappa_i} T^{\kappa_i}} + \frac{(a_i - b_i \wp_i)\nu_i T}{(\kappa_i + 1)} \left(\frac{\hbar_i}{\alpha_i{}^{\kappa_i}} + \omega_i \right) \\ &\quad + \omega_i s_i - \frac{\Lambda_i}{T} - (a_i - b_i \wp_i) c_i \nu_i \end{aligned} \tag{16}$$

Now we define $\vec{\wp} = (\wp_1, \wp_2, \dots, \wp_N)$ and $\vec{s} = (s_1, s_2, \dots, s_N)$. So that the total profit of the system can be obtained as follows:

$$\Pi(\vec{\wp}, \vec{s}, T) = \sum_{i=1}^{N} TP_i(\wp_i, s_i, T) \tag{17}$$

3. Concavity and the optimal decision

With regard to the purpose of this paper that is finding the best production policies to maximize the total profit per unit time for the multi-product inventory system, we first prove that for any given $\vec{\wp}$, the optimum solution of $(\vec{s}, T)$ not only exists but also is unique. Because $\Pi(\vec{\wp}, \vec{s}, T)$is a function of $\vec{\wp}, \vec{s}$ and T, so for any given $\vec{\wp}$, the essential conditions to maximize the total profit per unit time is equaling partial derivatives of the $\Pi(\vec{\wp}, \vec{s}, T)$ to zero, with respect to decision variables s_i and T, simultaneously. Thus,

$$\frac{\partial \Pi(\vec{\wp}, \vec{s}, T)}{\partial s_i} = \frac{(-s_i)^{\kappa_i}(\hbar_i + \omega_i)}{(\alpha_i - 1)^{\kappa_i}(a_i - b_i \wp_i)^{\kappa_i} \nu_i{}^{\kappa_i} T^{\kappa_i}} - \frac{(s_i + (a_i - b_i \wp_i)\nu_i T)^{\kappa_i}(\hbar_i + \omega_i)}{(a_i - b_i \wp_i)^{\kappa_i} \nu_i{}^{\kappa_i} T^{\kappa_i}} + \omega_i = 0 \ \ \forall i \tag{18}$$

$$\begin{aligned} \frac{\partial \Pi(\vec{\wp}, \vec{s}, T)}{\partial T} &= \sum_{i=1}^{N} \frac{\kappa_i (-s_i)^{\kappa_i + 1}(\hbar_i + \omega_i)}{(\kappa_i + 1)(\alpha_i - 1)^{\kappa_i}(a_i - b_i \wp_i)^{\kappa_i} \nu_i{}^{\kappa_i} T^{\kappa_i + 1}} \\ &\quad - \sum_{i=1}^{N} \frac{(s_i + (a_i - b_i \wp_i)\nu_i T)^{\kappa_i}((a_i - b_i \wp_i)\nu_i T - \kappa_i s_i)(\hbar_i + \omega_i)}{(\kappa_i + 1)(a_i - b_i \wp_i)^{\kappa_i} \nu_i{}^{\kappa_i} T^{\kappa_i + 1}} \\ &\quad + \sum_{i=1}^{N} \frac{(a_i - b_i \wp_i)\nu_i}{(\kappa_i + 1)} \left(\frac{\hbar_i}{\alpha_i{}^{\kappa_i}} + \omega_i \right) + \frac{\sum_{i=1}^{N} \Lambda_i}{T^2} = 0 \end{aligned} \tag{19}$$

Theorem 1: For any given $\vec{\wp}$, The total profit function $\Pi(\vec{\wp}, \vec{s}, T)$ is concave.

Proof: Please see Appendix A.

Defining a new variable x_i by $x_i = \frac{-s_i}{(a_i - b_i p_i)\nu_i T}$, the region $-(a_i - b_i p_i)\frac{(\alpha_i - 1)}{\alpha_i} rT \le s_i \le 0$ is equivalent to $0 \le x_i \le \frac{\alpha_i - 1}{\alpha_i}$ and Eq. 18 and Eq. 19 are respectively equivalent to

$$(1 - x_i)^{\kappa_i} - \frac{{x_i}^{\kappa_i}}{(\alpha_i - 1)^{\kappa_i}} - \frac{w_i}{h_i + w_i} = 0 \tag{20}$$

$$\sum_{i=1}^{N} \frac{\kappa_i {x_i}^{\kappa_i + 1}(a_i - b_i p_i)\nu_i(h_i + w_i)}{(\kappa_i + 1)(\alpha_i - 1)^{\kappa_i}} - \sum_{i=1}^{N} \frac{(1 - x_i)^{\kappa_i}(1 + \kappa_i x_i)(a_i - b_i p_i)\nu_i(h_i + w_i)}{(\kappa_i + 1)} + \sum_{i=1}^{N} \frac{(a_i - b_i p_i)\nu_i}{(\kappa_i + 1)}\left(\frac{h_i}{{\alpha_i}^{\kappa_i}} + w_i\right) + \frac{\sum_{i=1}^{N} \Lambda_i}{T^2} = 0 \tag{21}$$

Proposition: There is a unique solution ${x_i}^*$ for the function $(1 - x_i)^{\kappa_i} - \frac{{x_i}^{\kappa_i}}{(\alpha_i - 1)^{\kappa_i}} - \frac{w_i}{h_i + w_i} = 0$, on the interval $(0, \frac{\alpha_i - 1}{\alpha_i})$.

Proof: The proof is similar to proposition 1 in [15].

The optimal solution of Eq. 20 can be obtained using any numerical method like the Newton-Raphson method (see, i.e. [33]). Also from Eq. 20 we have

$$\frac{{x_i}^{\kappa_i}}{(\alpha_i - 1)^{\kappa_i}} = (1 - x_i)^{\kappa_i} - \frac{w_i}{h_i + w_i} = 0 \tag{22}$$

Substituting Eq. 22 in Eq. 23 we obtain following equation

$$-\sum_{i=1}^{N} \frac{(a_i - b_i p_i)\nu_i(h_i + w_i)(1 - x_i)^{\kappa_i}}{(\kappa_i + 1)} - \sum_{i=1}^{N} \frac{\kappa_i (a_i - b_i p_i)\nu_i w_i x_i}{(\kappa_i + 1)} + \sum_{i=1}^{N} \frac{(a_i - b_i p_i)\nu_i}{(\kappa_i + 1)}\left(\frac{h_i}{{\alpha_i}^{\kappa_i}} + w_i\right) + \frac{\sum_{i=1}^{N} \Lambda_i}{T^2} = 0 \tag{23}$$

Then substituting the optimal solution ${x_i}^*$ obtained by Eq. 20 in Eq. 23, the best cycle length T^* for a given $\vec{p}$ is

$$T^* = \sqrt{\frac{\sum_{i=1}^{N} \Lambda_i}{\sum_{i=1}^{N}[(\frac{(a_i - b_i p_i)\nu_i}{(\kappa_i + 1)})((h_i + w_i)(1 - {x_i}^*)^{\kappa_i} + \kappa_i w_i {x_i}^* - \left(\frac{h_i}{{\alpha_i}^{\kappa_i}} + w_i\right))]}} \tag{24}$$

Also, the best reorder point and the optimal lot quantity are ${s_i}^* = -{x_i}^*(a_i - b_i p_i)\nu_i T^*$ and ${Q_i}^* = (a_i - b_i p_i)\nu_i T^*$ respectively.

Now for any ${s_1}^*, {s_2}^*, \ldots, {s_N}^*, T^*$, the first order condition to maximize the total profit function $\Pi(\vec{p}, \vec{s}^*, T^*)$ is

$$\frac{\partial \Pi(\vec{p}, \vec{s}^*, T^*)}{\partial p_i} = a_i \nu_i - 2 b_i p_i \nu_i + b_i c_i \nu_i - \frac{b_i \nu_i T^*}{(\kappa_i + 1)}\left(\frac{h_i}{{\alpha_i}^{\kappa_i}} + w_i\right) + (h_i + w_i)\frac{b_i}{(\kappa_i + 1)\nu_i{}^{\kappa_i} {T^*}^{\kappa_i}}\left[\frac{({s_i}^* + (a_i - b_i p_i)\nu_i T^*)^{\kappa_i}((a_i - b_i p_i)\nu_i T^* - \kappa_i {s_i}^*)}{(a_i - b_i p_i)^{\kappa_i + 1}} - \frac{\kappa_i(-{s_i}^*)^{\kappa_i + 1}}{(\alpha_i - 1)^{\kappa_i}(a_i - b_i p_i)^{\kappa_i + 1}}\right] = 0 \tag{25}$$

Theorem 2: The total profit function $\Pi(\vec{p}, \vec{s}^*, T^*)$ is a concave function of $\vec{p}$ for a given $(\vec{s}^*, T^*)$.

Proof: Please see Appendix B.

4. Procedure for determining the optimal values of the model

In this section, with regard to that solving Eq. 25, using numerical methods takes a noticeable time and the optimized answers are hard to achieve, a simple procedure is presented to obtain good values for $\vec{\boldsymbol{p}}, \vec{\boldsymbol{s}}, T$ and Π.

Step 1: For each product i; $p_i = c_i$, where $c_i < \frac{a_i}{b_i}$. If

$$\frac{\sum_{i=1}^{N} \Lambda_i}{\sum_{i=1}^{N}[(\frac{(a_i - b_i p_i)\nu_i}{(\kappa_i+1)})((\hbar_i + w_i)(1 - {x_i}^*)^{\kappa_i} + \kappa_i w_i {x_i}^* - \left(\frac{\hbar_i}{{\alpha_i}^{\kappa_i}} + w_i\right))]} \geq 0,$$

calculate period length T^* and find out $\vec{\boldsymbol{s}}^*$and $\Pi(\vec{\boldsymbol{p}}, \vec{\boldsymbol{s}}^*, T^*)$; otherwise, there is no feasible solution and then go to Step 5.

Step 2: For each product i $(i = 1, \ldots, N)$, do: suppose that $p_i = p_i + \varepsilon$ and $p_j = p_j,\ \forall j \neq i$. Then, calculate the best reorder vector, the economic scheduling period and total profit function, and name them $(\vec{\boldsymbol{s}}^*{}_i, {T^*}_i)$ and $\Pi_i(\vec{\boldsymbol{p}}, \vec{\boldsymbol{s}}^*{}_i, {T^*}_i)$, respectively.

Step 3: Choose the product m that has the conditions below:

- ${T^*}_m$ can be calculated.
- $p_m < \frac{a_m}{b_m}$.
- $\Pi_m(\vec{\boldsymbol{p}}, \vec{\boldsymbol{s}}^*{}_m, {T^*}_m)$ is greater than the previous $\Pi(\vec{\boldsymbol{p}}, \vec{\boldsymbol{s}}^*, T^*)$ and greater than all $\Pi_j(\vec{\boldsymbol{p}}, \vec{\boldsymbol{s}}^*{}_j, {T^*}_j), \forall j \neq m$.

If there is no product with these conditions, the best solutions are $\vec{\boldsymbol{s}}^*, T^*, \Pi(\vec{\boldsymbol{p}}, \vec{\boldsymbol{s}}^*, T^*)$ and go to Step 5.

Step 4: $p_m = p_m + \varepsilon,$ and $p_j = p_j, \forall j \neq m, T^* = {T^*}_m, \Pi(\vec{\boldsymbol{p}}, \vec{\boldsymbol{s}}^*, T^*) = \Pi_m(\vec{\boldsymbol{p}}, \vec{\boldsymbol{s}}^*{}_m, {T^*}_m)$ and go to Step 2.

Step 5: End.

5. Results and discussion

In this section a numerical example is provided in order to illustrate proposed model and then numerical analyses are presented.

Example: Consider a production system with one item and the following values for the input parameters. $\Lambda = 100$, $\hbar = 4$, $w = 5$, $\nu = 1200$, $a = 100$, $b = 2$, $c = 10$, $\alpha = 1.5$ and the index of the power demand pattern $\kappa = 3$. Now we have to solve equation $(1 - x)^3 - \frac{x^3}{0.5^3} = \frac{5}{9}$. Using Newton method, $x^* = 0.161603$. Also $T^* = 0.0735$, $Q^* = 3438.5$, $s^* = -570.1081$, $p^* = 30$ and $TP^* = 957280$. Also the graphical representation of $\Pi(\vec{\boldsymbol{p}}, \vec{\boldsymbol{s}}^*, T^*)$ is shown in Fig. 1 using input parameters of the example. Also according to the following values of parameters, Table 1 is provided: $\Lambda = 100$, $\hbar = 4$, $w = 5$, $\nu = 1200$, $a = 100$, $b = 2$ and $\kappa = 3$. Optimum policies of the inventory system considering several combinations of parameters α and c are shown in Table 1.

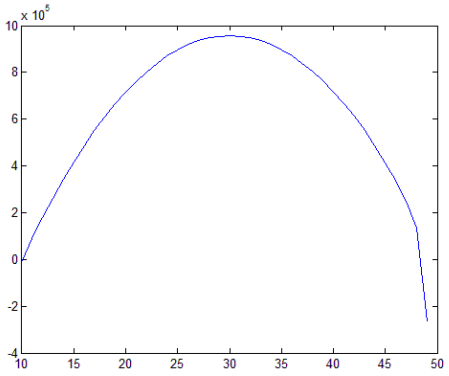

Fig. 1 Graphical representation of $\Pi(\vec{\boldsymbol{p}}, \vec{\boldsymbol{s}}^*, T^*)$

Table 1 Optimal policies for the proposed EPQ model, considering several values for α and c

$\lambda = 100$, $\hbar = 4$, $w = 5$, $\nu = 1200$, $a = 100$, $b = 2$ and $\kappa = 3$							
Production rate	Production cost	x^*	T^*	s^*	Q^*	p^*	Π^*
$\alpha = 1.1$	$c = 10$	0.064156	0.1580	-486.6977	7394.1	30	958730
	$c = 15$		0.1714	-448.7131	6785.3	33	733230
	$c = 20$		0.1825	-421.4925	6347.0	35	538900
	$c = 25$		0.2040	-376.9944	5626.0	38	373420
	$c = 30$		0.2235	-344.1472	5089.3	40	239110
$\alpha = 1.3$	$c = 10$	0.135125	0.0900	-583.7937	4211.0	30	957780
	$c = 15$		0.0976	-538.2312	3864.3	33	732350
	$c = 20$		0.1039	-505.5802	3614.7	35	538080
	$c = 25$		0.1162	-452.2047	3204.1	38	372680
	$c = 30$		0.1273	-412.8045	2898.2	40	238430
$\alpha = 1.5$	$c = 10$	0.161603	0.0735	-570.1081	3438.5	30	957280
	$c = 15$		0.0797	-525.6137	3155.4	33	731890
	$c = 20$		0.0849	-493.7281	2951.6	35	537640
	$c = 25$		0.0949	-441.6038	2616.3	38	372290
	$c = 30$		0.1039	-403.1273	2366.5	40	238080
$\alpha = 1.7$	$c = 10$	0.170823	0.0666	-546.0560	3115.7	30	957000
	$c = 15$		0.0722	-503.4388	2859.1	33	731630
	$c = 20$		0.0769	-472.8984	2674.5	35	537400
	$c = 25$		0.0860	-422.9732	2370.7	38	372070
	$c = 30$		0.0942	-3861199	2144.4	40	237880
$\alpha = 1.9$	$c = 10$	0.174358	0.0630	-527.5052	2948.8	30	956830
	$c = 15$		0.0684	-486.3358	2706.0	33	731470
	$c = 20$		0.0728	-456.8329	2531.2	35	537250
	$c = 25$		0.0814	-408.6038	2243.7	38	371940
	$c = 30$		0.0891	-373.0025	2029.5	40	237760

Table 2 shows the optimal policies of the system considering combinations of parameters κ and c using following parameters: $\lambda = 100$, $\hbar = 4$, $w = 5$, $\nu = 1200$, $a = 100$, $b = 2$ and $\alpha = 1.5$.

Table 3 shows the optimal policies of the system considering different values of a using following parameters: $\lambda = 100$, $\hbar = 4$, $w = 5$, $\nu = 1200$, $b = 2$, $c = 10$, $\kappa = 4$ and $\alpha = 1.7$.

Table 2 Optimal policies for the proposed EPQ model, considering several values for κ and c

$\lambda = 100$, $\hbar = 4$, $w = 5$, $\nu = 1200$, $a = 100$, $b = 2$ and $\alpha = 1.5$							
Production rate	Production cost	x^*	T^*	s^*	Q^*	p^*	Π^*
$\kappa = 0.5$	$c = 10$	0.081199	0.0744	-290.1504	3482.8	30	957310
	$c = 20$		0.0860	-251.2777	2989.7	35	537670
$\kappa = 1$	$c = 10$	0.148148	0.0750	-533.3328	3508.8	30	957330
	$c = 20$		0.0866	-461.8791	3012.0	35	537690
$\kappa = 2$	$c = 10$	0.175842	0.0756	-638.0297	3536.6	30	957350
	$c = 20$		0.0873	-522.5499	3035.8	35	537710
$\kappa = 3$	$c = 10$	0.161603	0.0735	-570.1081	3438.5	30	957280
	$c = 20$		0.0849	-493.7281	2951.6	35	537640

Table 3 Optimal policies for the proposed EPQ model, considering different values of a

$\lambda = 100$, $\hbar = 4$, $w = 5$, $\nu = 1200$, $b = 2$, $c = 10$, $\kappa = 4$ and $\alpha = 1.7$						
a	x^*	T^*	s^*	Q^*	p^*	Π^*
$a = 100$	0.170823	0.0666	-546.0560	3115.7	30	957000
$a = 200$		0.0444	-819.0840	4741.4	30	4855500
$a = 300$		0.0356	-1021.6	5937.5	30	11754000

Table 4 Optimal policies for the proposed EPQ model, considering different values of b

	$\lambda = 100, \hbar = 4, w = 5, \nu = 1200, a = 100, c = 10, \kappa = 4$ and $\alpha = 1.7$					
b	x^*	T^*	s^*	Q^*	p^*	Π^*
$b = 1$	0.170823	0.0628	-579.1799	3352.6	55	2426800
$b = 2$		0.0666	-546.0560	3115.7	30	957000
$b = 3$		0.0722	-503.4388	2814.1	22	486130

Table 4 shows the optimal policies of the system considering different values of b using following parameters: $\lambda = 100, \hbar = 4, w = 5, \nu = 1200, a = 100, c = 10, \kappa = 4$ and $\alpha = 1.7$.

Figs. 2 and 3 show the cycle length and the total profit as functions of unit production cost, when input parameters are used from Table 1. In each figure different values of α are considered ($\alpha = 1.1, 1.3, 1.5, 1.9$).

Figs. 4 and 5 show changes of the lot size and total profit respect to the changes of the index of demand pattern using Table 2. In each figure two values of production cost c are considered ($c = 10, 20$).

Figs. 6 and 7 show changes of the price respect to the changes of the parameters a and b using Table 3 and 4, respectively.

Some managerial insights can be expressed as follows.

In Table 1, by fixing the replenishment rate parameter α, if the unit production cost c increases then the total profit function Π^*, the best lot size Q^* and the value of s^* decrease. However, the optimal cycle length T^* and the optimum price p^* increase in the same situation.

In the same Table 1, fixed the unit production cost c, the total profit function Π^*, slightly, the best scheduling period T^* and the economic lot quantity Q^* decrease as the production rate α increases. However, In the same conditions the optimal price p^* does not change.

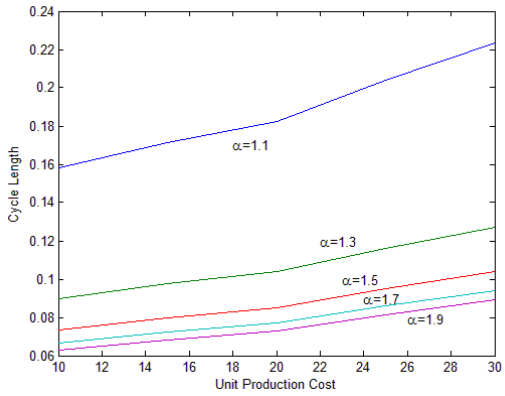

Fig. 2 Changes of cycle length respect to the changes of unit production cost using Table 1

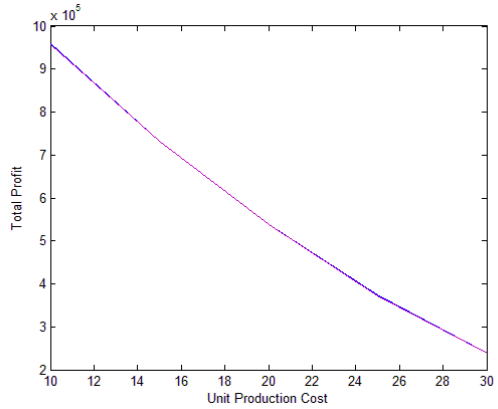

Fig. 3 Changes of total profit respect to the changes of unit production cost using Table 1

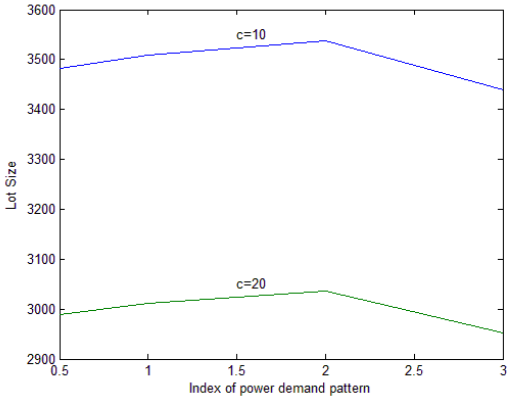

Fig. 4 Changes of lot size respect to the changes of κ using Table 2

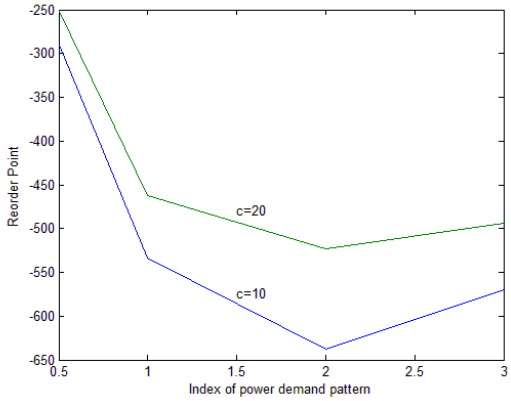

Fig. 5 Changes of reorder point respect to the changes of κ using Table 2

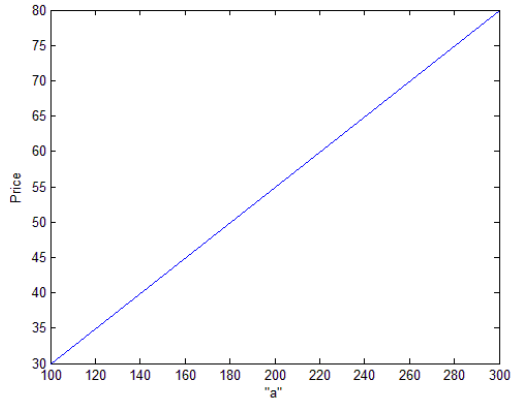

Fig. 6 Changes of price respect to the changes of parameter a using Table 3

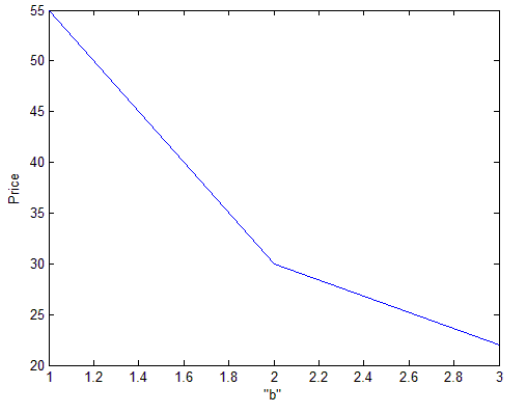

Fig. 7 Changes of price respect to the changes of parameter b using Table 4

Using Table 2, by fixing the index of power demand κ unit production cost c, if the unit production cost c increases then the total profit function Π^*, the economic lot quantity Q^* and the value of s^*decrease. In the same conditions the best price $\wp^*$ and the optimum cycle length T^* increase.

In Table 3, fixing c, α, κ and b, if parameter a increases then the total profit function Π^*, the price $\wp^*$ and the economic lot quantity Q^* increase. However the optimal scheduling period T^* decreases in the same conditions.

In Table 4, fixing c, α, κ and a, if parameter b increases then the total profit function Π^*, the best price $\wp^*$ and the economic lot quantity Q^* decrease. However the optimum scheduling period T^* increases in the same conditions.

6. Conclusions and future research

In this paper, an economic production model has been presented using kind of demand rate named power demand. Also it is supposed that demand of customers dependes on price linearly and production rate changes pro rata with demand rate. Multiple products are assumed to be in the inventory system and shortages are allowed and fully backlogged. Mathematical modeling and optimization methods are used to find optimal solutions for both single-product and multiple-products situations. Also since that achieving optimum inventory policies for second situation is hard a simple heuristic procedure is proposed to obtain the near-optimal solutions for multi-items form. Several examples are presented to illustrate the applications of the model using various values of parameters. The outcomes reveal that fixing the production rate parameter, if the unit production cost increases then the total profit function and the economic lot size decrease, while the best cycle length and the optimum price increase. The total profit function slightly, the best scheduling period and the optimal lot quantity decrease as the production rate increases. By fixing the index of power demand, if the unit production cost increases, the total profit function and the economic lot quantity decrease while the best price and the optimal cycle length increase. In the end, the following suggestions for further research are made:

- The proposed model can be extended using deterioration in the inventory system.
- Allowing for shortages that are lost sales or partially backorderd could be considered.
- Imperfect items are produced in many production systems as well as perfect items. So it could be considered in the inventory system.
- Since that different price functions may be possible in the real world situations, they could be considered in the inventory system.
- The proposed model can be considered with manufacturing disruption costs.
- Taking sustainability concerns into account could be another interesting recommendation.

References

[1] Taft, E.W. (1918). The most economical production lot, *The Iron Age,* Vol. 101, 1410-1412.
[2] Barbosa, L.C., Friedman, M. (1978). Deterministic inventory lot size models – A general root law, *Management* Science, Vol. 24, No. 8, 819-826, doi: 10.1287/mnsc.24.8.819.
[3] Mitra, A., Cox, J.F., Jesse Jr, R.R. (1984). A note on determining order quantities with a linear trend in demand, *The Journal of the Operational Research Society,* Vol. 35, No. 2, 141-144, doi: 10.2307/2581442.
[4] Sakaguchi, M. (2009). Inventory model for an inventory system with time-varying demand rate, *International Journal of Production Economics*, Vol. 122, No. 1, 269-275, doi: 10.1016/j.ijpe.2009.06.003.
[5] Khanra, S., Mandal, B., Sarkar, B. (2013). An inventory model with time dependent demand and shortages under trade credit policy, *Economic Modelling*, Vol. 35, 349-355, doi: 10.1016/j.econmod.2013.07.031.
[6] Sarkar, B., Mandal, P., Sarkar, S. (2014). An EMQ model with price and time dependent demand under the effect of reliability and inflation, *Applied Mathematics and Computation*, Vol. 231, 414-421, doi: 10.1016/j.amc.2014.01.004.
[7] Escuín, D., Polo, L., Ciprés, D. (2017). On the comparison of inventory replenishment policies with time-varying stochastic demand for the paper industry, *Journal of Computational and Applied Mathematics*, Vol. 309, 424-434, doi: 10.1016/j.cam.2016.03.027.
[8] Naddor, E. (1966). *Inventory Systems*, John Wiley and Sons, New York, USA.
[9] Lee, W.-C., Wu, J.-W. (2002). An EOQ model for items with Weibull distributed deterioration, shortages and power demand pattern, *International Journal of Information and Management Sciences*, Vol. 13, No. 2, 19-34.
[10] Singh, T.J., Singh, S.R., Dutt, R. (2009). An EOQ model for perishable items with power demand and partial backlogging, *International Journal of Production Economics*, Vol. 15, No. 1, 65-72.
[11] Sicilia, J., Febles-Acosta, J., González-De La Rosa, M. (2012). Deterministic inventory systems with power demand pattern, *Asia-Pacific Journal of Operational Research*, Vol. 29, No. 05, Art. No. 1250025, doi: 10.1142/S02175959125002 5X.
[12] Rajeswari, N., Vanjikkodi, T. (2012). An inventory model for items with two parameter Weibull distribution deterioration and backlogging, *American Journal of Operations Research*, Vol. 2, No. 2, 247-252, doi: 10.4236/ajor.2012.22029.
[13] Mishra, S.S., Singh, P.K. (2013). Partial backlogging EOQ model for queued customers with power demand and quadratic deterioration: computational approach, *American Journal of Operational Research*, Vol. 3, No. 2, 13-27.
[14] Sicilia, J., González-De-la-Rosa, M., Febles-Acosta, J., Alcaide-López-de-Pablo, D. (2014). An inventory model for deteriorating items with shortages and time-varying demand, *International Journal of Production Economics,* Vol. 155, 155-162, doi: 10.1016/j.ijpe.2014.01.024.
[15] Sicilia, J., González-De-la-Rosa, M., Febles-Acosta, J., Alcaide-López-de-Pablo, D. (2014). Optimal policy for an inventory system with power demand, backlogged shortages and production rate proportional to demand rate, *International Journal of Production Economics,* Vol. 155, 163-171, doi: 10.1016/j.ijpe.2013.11.020.
[16] Sicilia, J., González-De-la-Rosa, M., Febles-Acosta, J., Alcaide-López-de-Pablo, D. (2015). Optimal inventory policies for uniform replenishment systems with time-dependent demand, *International Journal of Production Research*, Vol. 53, No. 12, 3603-3622, doi: 10.1080/00207543.2014.983618.
[17] San-José, L.A., Sicilia, J., González-De-la-Rosa, M., Febles-Acosta, J. (2017). Optimal inventory policy under power demand pattern and partial backlogging, *Applied Mathematical Modelling*, Vol. 46, 618-630, doi: 10.1016/j.apm.2017.01.082.
[18] Tripathi, R.P., Pareek, S., Kaur, M. (2017). Inventory models with power demand and inventory-induced demand with holding cost functions, *American Journal of Applied Sciences*, Vol. 14, No. 6, 607-613, doi: 10.3844/ajassp.2017.607.613.
[19] Lau, H.-S., Lau, A.H.-L., Kottas, J.F. (2001). Pricing/inventory decisions and profit shares in a non-integrated marketing channel for a single-period product, *Journal of the Operational Research Society*, Vol. 52, No. 6, 682-690, doi: 10.1057/palgrave.jors.2601131.
[20] Yang, C.-T., Ouyang, L.-Y., Wu, H.-H. (2009). Retailer's optimal pricing and ordering policies for non-instantaneous deteriorating items with price-dependent demand and partial backlogging, *Mathematical Problems in Engineering*, Vol. 2009, Article ID 198305, doi: 10.1155/2009/198305.
[21] Banerjee, S., Sharma, A. (2010). Optimal procurement and pricing policies for inventory models with price and time dependent seasonal demand, *Mathematical and Computer Modelling*, Vol. 51, No. 5-6, 700-714, doi: 10.1016/j.mcm.2009.10.022.
[22] Soon, W. (2011). A review of multi-product pricing models, *Applied Mathematics and Computation*, Vol. 217, No. 21, 8149-8165, doi: 10.1016/j.amc.2011.03.042.
[23] Maihami, R., Kamalabadi, I.N. (2012). Joint pricing and inventory control for non-instantaneous deteriorating items with partial backlogging and time and price dependent demand, *International Journal of Production Economics*, Vol. 136, No. 1, 116-122, doi: 10.1016/j.ijpe.2011.09.020.
[24] Shavandi, H., Mahlooji, H., Nosratian, N.E. (2012). A constrained multi-product pricing and inventory control problem, *Applied Soft Computing*, Vol. 12, No. 8, 2454-2461, doi: 10.1016/j.asoc.2012.03.036.
[25] Pal, B., Sana, S.S., Chaudhuri, K. (2012). Multi-item EOQ model while demand is sales price and price break sensitive, *Economic Modelling*, Vol. 29, No. 6, 2283-2288, doi: 10.1016/j.econmod.2012.06.039.
[26] Zhu, S.X. (2013). Dynamic replenishment, production, and pricing decisions, in the face of supply disruption and random price-sensitive demand, *International Journal of Production Economics*, Vol. 146, No. 2, 612-619, doi: 10.1016/j.ijpe.2013.08.009.

[27] Qin, Y., Wang, J., Wei, C. (2014). Joint pricing and inventory control for fresh produce and foods with quality and physical quantity deteriorating simultaneously, *International Journal of Production Economics*, Vol. 152, 42-48, doi: 10.1016/j.ijpe.2014.01.005.
[28] Liu, G., Zhang, J., Tang, W. (2015). Joint dynamic pricing and investment strategy for perishable foods with price-quality dependent demand, *Annals of Operations Research,* Vol. 226, No. 1, 397-416, doi: 10.1007/s10479-014-1671-x.
[29] Panda, S., Modak, N.M., Sana, S.S., Basu, M. (2015). Pricing and replenishment policies in dual-channel supply chain under continuous unit cost decrease, *Applied Mathematics and Computation*, Vol. 256, 913-929, doi: 10.1016/j.amc.2015.01.081.
[30] Alfares, H.K., Ghaithan, A.M. (2016). Inventory and pricing model with price-dependent demand, time-varying holding cost, and quantity discounts, *Computers & Industrial Engineering*, Vol. 94, 170-177, doi: 10.1016/j.cie.2016.02.009.
[31] Chiu, Y.-S.P., Kuo, J.-S., Chiu, S.W., Hsieh, Y.-T. (2016). Effect of delayed differentiation on a multiproduct vendor-buyer integrated inventory system with rework, *Advances in Production Engineering & Management*, Vol. 11, No. 4, 333-344, doi: 10.14743/apem2016.4.231.
[32] Gholamian, M.R., Heydari, M. (2017). An inventory model with METRIC approach in location-routing-inventory problem, *Advances in Production Engineering & Management*, Vol. 12, No. 2, 115-126, doi: 10.14743/apem2017.2.244.
[33] Stoer, J., Bulirsch, R. (2013). *Introduction to numerical analysis*, Springer Science & Business Media, New York, USA.

Appendix A

For any given $\vec{\boldsymbol{p}}$, The total profit function $\Pi(\vec{\boldsymbol{p}}, \vec{\boldsymbol{s}}, T)$ is concave.

Proof: The Hessian matrix can be used to prove the concavity of $\Pi(\vec{\boldsymbol{p}}, \vec{\boldsymbol{s}}, T)$.

$$\begin{aligned}\Pi(\vec{\boldsymbol{p}}, \vec{\boldsymbol{s}}, T) = \sum_{i=1}^{N} TP_i(p_i, s_i, T) = \sum_{i=1}^{N} [(a_i - b_i p_i) p_i v_i - \frac{(s_i + (a_i - b_i p_i) v_i T)^{\kappa_i + 1} (h_i + w_i)}{(\kappa_i + 1)(a_i - b_i p_i)^{\kappa_i} v_i^{\kappa_i} T^{\kappa_i}} \\ - \frac{(-s_i)^{\kappa_i + 1} (h_i + w_i)}{(\kappa_i + 1)(\alpha_i - 1)^{\kappa_i} (a_i - b_i p_i)^{\kappa_i} v_i^{\kappa_i} T^{\kappa_i}} + \frac{(a_i - b_i p_i) v_i T}{(\kappa_i + 1)} \left(\frac{h_i}{\alpha_i^{\kappa_i}} + w_i \right) + w_i s_i - \frac{\Lambda_i}{T} \\ - (a_i - b_i p_i) c_i v_i]\end{aligned} \tag{A1}$$

$$\frac{\partial \Pi(\vec{\boldsymbol{p}}, \vec{\boldsymbol{s}}, T)}{\partial s_i} = \frac{(-s_i)^{\kappa_i} (h_i + w_i)}{(\alpha_i - 1)^{\kappa_i} (a_i - b_i p_i)^{\kappa_i} v_i^{\kappa_i} T^{\kappa_i}} - \frac{(s_i + (a_i - b_i p_i) v_i T)^{\kappa_i} (h_i + w_i)}{(a_i - b_i p_i)^{\kappa_i} v_i^{\kappa_i} T^{\kappa_i}} + w_i, \quad \forall i \tag{A2}$$

$$\begin{aligned}\frac{\partial \Pi(\vec{\boldsymbol{p}}, \vec{\boldsymbol{s}}, T)}{\partial T} = \sum_{i=1}^{N} \frac{\kappa_i (-s_i)^{\kappa_i + 1} (h_i + w_i)}{(\kappa_i + 1)(\alpha_i - 1)^{\kappa_i} (a_i - b_i p_i)^{\kappa_i} v_i^{\kappa_i} T^{\kappa_i + 1}} \\ - \sum_{i=1}^{N} \frac{(s_i + (a_i - b_i p_i) v_i T)^{\kappa_i} ((a_i - b_i p_i) v_i T - \kappa_i s_i) (h_i + w_i)}{(\kappa_i + 1)(a_i - b_i p_i)^{\kappa_i} v_i^{\kappa_i} T^{\kappa_i + 1}} \\ + \sum_{i=1}^{N} \frac{(a_i - b_i p_i) v_i}{(\kappa_i + 1)} \left(\frac{h_i}{\alpha_i^{\kappa_i}} + w_i \right) + \frac{\sum_{i=1}^{N} \Lambda_i}{T^2}\end{aligned} \tag{A3}$$

$$\frac{\partial^2 \Pi(\vec{\boldsymbol{p}}, \vec{\boldsymbol{s}}, T)}{\partial {s_i}^2} = - \frac{\kappa_i (-s_i)^{\kappa_i - 1} (h_i + w_i)}{(\alpha_i - 1)^{\kappa_i} (a_i - b_i p_i)^{\kappa_i} v_i^{\kappa_i} T^{\kappa_i}} - \frac{\kappa_i (s_i + (a_i - b_i p_i) v_i T)^{\kappa_i - 1} (h_i + w_i)}{(a_i - b_i p_i)^{\kappa_i} v_i^{\kappa_i} T^{\kappa_i}} < 0, \quad \forall i \tag{A4}$$

$$\begin{aligned}\frac{\partial^2 \Pi(\vec{\boldsymbol{p}}, \vec{\boldsymbol{s}}, T)}{\partial T^2} = - \sum_{i=1}^{N} \frac{\kappa_i (-s_i)^{\kappa_i + 1} (h_i + w_i)}{(\alpha_i - 1)^{\kappa_i} (a_i - b_i p_i)^{\kappa_i} v_i^{\kappa_i} T^{\kappa_i + 2}} \\ - \sum_{i=1}^{N} \frac{\kappa_i {s_i}^2 (s_i + (a_i - b_i p_i) v_i T)^{\kappa_i - 1} (h_i + w_i)}{(a_i - b_i p_i)^{\kappa_i} v_i^{\kappa_i} T^{\kappa_i + 2}} - \frac{2 \sum_{i=1}^{N} \Lambda_i}{T^3} < 0\end{aligned} \tag{A5}$$

$$\frac{\partial^2 \Pi(\vec{\boldsymbol{p}}, \vec{\boldsymbol{s}}, T)}{\partial s_i \partial T} = - \frac{\kappa_i (-s_i)^{\kappa_i} (h_i + w_i)}{(\alpha_i - 1)^{\kappa_i} (a_i - b_i p_i)^{\kappa_i} v_i^{\kappa_i} T^{\kappa_i + 1}} + \frac{\kappa_i s_i (s_i + (a_i - b_i p_i) v_i T)^{\kappa_i - 1} (h_i + w_i)}{(a_i - b_i p_i)^{\kappa_i} v_i^{\kappa_i} T^{\kappa_i + 1}}, \quad \forall i \tag{A6}$$

$$\frac{\partial^2 \Pi(\vec{\mathcal{p}}, \vec{s}, T)}{\partial s_i \partial s_j} = 0, \quad \forall i, j \tag{A7}$$

We suppose that $s_i + (a_i - b_i \mathcal{p}_i) v_i T \geq 0$.

$$[T, s_1, s_2, \dots, s_N] \begin{bmatrix} \frac{\partial^2 \Pi}{\partial T^2} & \frac{\partial^2 \Pi}{\partial T \partial s_1} & \cdots & \frac{\partial^2 \Pi}{\partial T \partial s_N} \\ \frac{\partial^2 \Pi}{\partial s_1 \partial T} & \frac{\partial^2 \Pi}{\partial {s_1}^2} & \cdots & \frac{\partial^2 \Pi}{\partial s_1 \partial s_N} \\ \vdots & \vdots & \vdots & \vdots \\ \frac{\partial^2 \Pi}{\partial s_N \partial T} & \frac{\partial^2 \Pi}{\partial s_N \partial s_1} & \cdots & \frac{\partial^2 \Pi}{\partial {s_N}^2} \end{bmatrix} \begin{bmatrix} T \\ s_1 \\ s_2 \\ \vdots \\ s_N \end{bmatrix} = \tag{A8}$$

$$= T^2 \frac{\partial^2 \Pi}{\partial T^2} + {s_1}^2 \frac{\partial^2 \Pi}{\partial {s_1}^2} + \cdots + {s_N}^2 \frac{\partial^2 \Pi}{\partial {s_N}^2} + 2T \left(s_1 \frac{\partial^2 \Pi}{\partial s_1 \partial T} + \cdots + s_N \frac{\partial^2 \Pi}{\partial s_N \partial T} \right) = \frac{2 \sum_{i=1}^{N} \Lambda_i}{T^3} < 0$$

Appendix B

The total profit function $\Pi(\vec{\mathcal{p}}, \vec{s}^*, T^*)$ is a concave function of $\vec{\mathcal{p}}$ for a given $(\vec{s}^*, T^*)$.

Proof: We have

$$\frac{\partial \Pi(\vec{\mathcal{p}}, \vec{s}^*, T^*)}{\partial \mathcal{p}_i} = a_i v_i - 2 b_i \mathcal{p}_i v_i + b_i c_i v_i - \frac{b_i v_i T^*}{(\kappa_i + 1)} \left(\frac{\hbar_i}{{\alpha_i}^{\kappa_i}} + \omega_i \right) + \frac{b_i (\hbar_i + \omega_i)}{(\kappa_i + 1) {v_i}^{\kappa_i} {T^*}^{\kappa_i}} \left[\frac{({s_i}^* + (a_i - b_i \mathcal{p}_i) v_i T^*)^{\kappa_i} ((a_i - b_i \mathcal{p}_i) v_i T^* - \kappa_i {s_i}^*)}{(a_i - b_i \mathcal{p}_i)^{\kappa_i + 1}} - \frac{\kappa_i (-{s_i}^*)^{\kappa_i + 1}}{(\alpha_i - 1)^{\kappa_i} (a_i - b_i \mathcal{p}_i)^{\kappa_i + 1}} \right] \tag{B1}$$

$$\frac{\partial^2 \Pi(\vec{\mathcal{p}}, \vec{s}^*, T^*)}{\partial {\mathcal{p}_i}^2} = -2 b_i v_i - \frac{\kappa_i {b_i}^2 (-{s_i}^*)^{\kappa_i + 1} (\hbar_i + \omega_i)}{(\alpha_i - 1)^{\kappa_i} {v_i}^{\kappa_i} {T^*}^{\kappa_i} (a_i - b_i \mathcal{p}_i)^{\kappa_i + 2}} - \frac{\kappa_i {b_i}^2 {s_i}^{*2} ({s_i}^* + (a_i - b_i \mathcal{p}_i) v_i T^*)^{\kappa_i - 1} (\hbar_i + \omega_i)}{{v_i}^{\kappa_i} {T^*}^{\kappa_i} (a_i - b_i \mathcal{p}_i)^{\kappa_i + 2}} < 0 \tag{B2}$$

$$\frac{\partial^2 \Pi(\vec{\mathcal{p}}, \vec{s}^*, T^*)}{\partial \mathcal{p}_i \partial \mathcal{p}_j} = 0 \tag{B3}$$

And so that

$$[\mathcal{p}_1, \mathcal{p}_2, \dots, \mathcal{p}_N] \begin{bmatrix} \frac{\partial^2 \Pi}{\partial {\mathcal{p}_1}^2} & \frac{\partial^2 \Pi}{\partial \mathcal{p}_1 \partial \mathcal{p}_2} & \cdots & \frac{\partial^2 \Pi}{\partial \mathcal{p}_1 \partial \mathcal{p}_N} \\ \frac{\partial^2 \Pi}{\partial \mathcal{p}_2 \partial \mathcal{p}_1} & \frac{\partial^2 \Pi}{\partial {\mathcal{p}_2}^2} & \cdots & \frac{\partial^2 \Pi}{\partial \mathcal{p}_2 \partial \mathcal{p}_N} \\ \vdots & \vdots & \vdots & \vdots \\ \frac{\partial^2 \Pi}{\partial \mathcal{p}_N \partial \mathcal{p}_1} & \frac{\partial^2 \Pi}{\partial \mathcal{p}_N \partial \mathcal{p}_2} & \cdots & \frac{\partial^2 \Pi}{\partial {\mathcal{p}_N}^2} \end{bmatrix} \begin{bmatrix} \mathcal{p}_1 \\ \mathcal{p}_2 \\ \vdots \\ \mathcal{p}_N \end{bmatrix} = \sum_{i=1}^{N} {\mathcal{p}_i}^2 \frac{\partial^2 \Pi(\vec{\mathcal{p}}, \vec{s}^*, T^*)}{\partial {\mathcal{p}_i}^2} < 0 \tag{B4}$$

APEM journal
Advances in Production Engineering & Management
Volume 14 | Number 1 | March 2019 | pp 125–135
https://doi.org/10.14743/apem2019.1.316
ISSN 1854-6250
Journal home: apem-journal.org
Original scientific paper

Maximum-minimum distance clustering method for split-delivery vehicle-routing problem: Case studies and performance comparisons

Min, J.N.[a], **Jin, C.**[a,*], **Lu, L.J.**[a,b]

[a]Taihu University of Wuxi, School of Economics and Management, Jiangsu, P.R. China
[b]Nanjing University, School of Management, Nanjing, Jiangsu, P.R. China

ABSTRACT

The split-delivery vehicle-routing problem in which delivery to a demand point can be served by any number of vehicles is an important branch of classic VRP. Objective function is used to minimise travel distance while using the lowest number of vehicles. According to the maximum-minimum distance clustering method, a three-stage algorithm is proposed. First, the maximum-minimum distance method is employed to cluster customer points into the lowest number of groups. Second, according to the maximum vehicle capacity, the load demand in each group is adjusted to create suitable customer points in each clustering group by adopting 'push-out' and 'pull-in' operations. Third, a tabu search is used and an optimised route for each group is generated to minimise the total travel distance. Numerical experiments, some on the benchmark data set, are presented to verify the feasibility and effectiveness of the proposed algorithm. The computational results show that the performance of the proposed algorithm is better in terms of both optimised travel distance and less computation time when the problem size is less than 75. The results also show that when the customer points are in a cluster distribution around the depot, the algorithm achieves better performance.

ARTICLE INFO

Keywords:
Split-delivery vehicle-routing problem;
Maximum-minimum distance method;
Load-demand adjustment;
Route optimisation;
Tabu search;
Clustering first and routing later

**Corresponding author:*
mjn3862@126.com
(Jin, C.)

Article history:
Received 5 December 2018
Revised 12 February 2019
Accepted 25 February 2019

1. Introduction

The split-delivery vehicle-routing problem (SDVRP) was formally introduced by Dror and Trudeau [1] in 1989. In SDVRP, the constraint in which each customer is visited only once, which is imposed in the classic VRP, is relaxed [2]. In other words, in SDVRP, delivery to a demand point can be split among any number of vehicles [1-3]. This relaxation can further optimise the VRP in terms of the number of vehicles used, travel distance, and carbon emissions, which have recently become a significant environmental protection problem. The fractional capacity of a vehicle can be better utilised. When the remaining capacity of the vehicle is insufficient to provide complete service to a customer, that vehicle can still provide service to the customer that is equal to the residual capacity, and the remaining customer demand can be served by other vehicles. The transportation cost can be reduced because of the following reasons. (1) The optimal solution of the number of vehicles used in SDVRP might be lower than that used in the VRP. (2) Largest savings are obtained when the average customer demand is only more than half of the vehicle capacity, and the variance in the customer demands is low [4, 5]. Therefore, the SDVRP has quickly

become an important branch of VRP since it has been introduced and has received increasing attention over time [2].

Studies have mainly focused on attempting to solve the problem in designing heuristic and meta-heuristic solution approaches [2]. Dror and Trudeau [1] proposed a first heuristic algorithm for the SDVRP. Two types of methods were introduced: the first method is the *k*-split interchange, i.e. a customer demand is split into different routes in which the remaining capacity is sufficient for the split customer. The second method is route addition, i.e. a split customer is removed from all the routes where the customer lies and a new route is created, which is composed of that customer only. The computational results showed that main savings are achieved for large values of customer demands. Archetti *et al.* [4] proposed the first tabu search algorithm (TSA) called SPLITABU. At each iteration, a neighbour solution is obtained by removing a customer from a set of routes in which the customer is currently visited and inserting the customer into either a new route or an existing route with sufficient residual capacity. A numerical experiment proved that this is much more effective than the algorithm of Dror and Trudeau [1] even though it is obviously much slower. Chen *et al.* [5] proposed the first hybrid heuristic algorithm. In this algorithm, the initial solution is obtained using the Clarke-Wright saving algorithm for the VRP. Then, an endpoint mixed-integer program (EMIP) is applied to this initial solution to optimally reallocate the endpoints of each route. The solution obtained from EMIP is then improved using a variable-length record-to-record travel algorithm. The computational results showed that the performance of this approach is better than that of the TSA in [4] under the same set of instances even if the CPU time tends to be quite high in large instances. Archetti *et al.* [6] proposed an improved three-stage algorithm based on the TSA proposed in [4]. First, the SDVRP is solved by applying the TSA in [4]. Then, the solutions are analysed to ascertain particular information, namely, (1) if an edge is often traversed in these solutions, then this edge is included in high-quality solutions with a high probability, and (2) if a customer is never or rarely split in the TSA solution, then that customer is probably not split in high-quality solutions. Once the TS ends, the information from (1) is used to reduce the original graph by discarding those edges that are never or rarely traversed by the TSA. All possible routes are constructed based on this reduced graph. The information from (2) is used to construct a route-based formulation to identify the best routes among the set of generated routes. Finally, the mixed-integer linear programming (MILP) model is repeatedly applied on small subsets of routes in the ascending order, which is sorted according to the 'desirable' parameter. The computational results of this algorithm improved those produced under the same set of instances presented by the TSA in [4] in many cases. Gulczynski *et al.* [7] allowed split deliveries only if a minimum fraction of a customer demand was serviced by a vehicle and developed an EMIP with an enhanced record-to-record travel algorithm to solve this problem. Wilck IV and Cavalier [8] developed a construction heuristic algorithm to solve the SDVRP, and their computational results showed that its performance is better than the two-phase method under the same data set in terms of travel distance and computation speed. Liu *et al.* [9] proposed the *k*-means clustering algorithm and designed two different algorithmic approaches: one was the grouping first and routing later; the other was the routing first and grouping later. A comparison of these two approaches indicated that the approach of grouping first and routing later exhibited better performance. Lu *et al*. [10] proposed a routing optimisation algorithm for different electric-vehicle-movement situations. A multi-agent simulation model was run using city real data. Wang *et al.* [11] proposed a bee-colony optimisation model for the SDVRP based on the reaction threshold and stimulatory value. The experimental results indicated the feasibility of the algorithm. Zhu *et al.* [12] addressed a multi-depot capacitated VRP where the client demand is composed of two-dimensional weighted items. A quantum-behaved particle swarm optimisation and an exploration heuristic local search algorithm were proposed, and computational experiments on the benchmark instances were effectively carried out. Wen [13] proposed a multi-re-start iteration local search (MRSILS) algorithm. First, a large travelling salesman problem (TSP), which includes all customer points, is solved by adopting GENIUS. The solution is partitioned into groups according to the vehicle capacity in order for each group to meet the load-demand limitations. Then, for each point, a greedy point re-insertion algorithm is used to delete a point from its current group and

re-insert it into an optimal position in the current solution by considering the delivery-split tactics. This re-insertion is iterated until no further improvement occurs. Finally, the 'perturbation' and solution pool are adopted to repeat the re-insertion in order to obtain the optimisation result. The experimental results on the benchmark data set showed that the MRSILS is competitive. Wu *et al.* [14] introduced a multi-objective algorithm to solve VRPs using time windows. The algorithm combines a discrete particle swarm optimisation based on a set-decoding scheme and variable neighbourhood searches to find the Pareto optimal routing solutions. Tang *et al.* [15] developed a model and the corresponding multi-phase particle swarm optimisation algorithm for bulk-cargo port scheduling. Xiang *et al.* [16] proposed a clustering algorithm of 'routing after grouping'. The grouping is based on the 'nearest' principle. A split threshold is set to limit the vehicle load to within a certain range, and the ant-colony optimisation algorithm is used to arrange the routes. Cao *et al.* [17] proposed an improved wolf-pack algorithm to solve the VRP using multiple fuzzy-time windows. Johanyák *et al.* [18] proposed a modified particle swarm optimisation algorithm, which was combined with a local-search technique, to solve large-scale nonlinear optimisation problems. Wang *et al.* [19] adopted a hybrid fruit-fly optimisation algorithm integrated with three local search methods (two-opt, swap, and insert) to solve the multi-compartment VRP.

Research in the SDVRP solution also extends to exact algorithms [2]. Belenguer *et al.* [20] proposed a cutting-plane approach wherein a polyhedron model was built. Some facet-inducing and other valid inequalities were embedded in the cutting-plane algorithm. They solved a relatively smaller problem and achieved satisfactory results. Lee *et al.* [21] proposed the shortest-path approach in which the SDVRP is formulated as a dynamic programming model, where the routes are sequentially constructed using a labelling algorithm. The solution space and corresponding states were reduced according to the *k*-split-cycle property. They tested their approach on instances with up to seven customers. Jin *et al.* [22] proposed a two-stage algorithm with valid inequalities (TSVI). The first stage divided the customers into clusters and established a lower bound. The objective function minimised the clustering cost in which the cost of each cluster was initially set to zero. The second stage calculated the minimum travel distance in each cluster by solving the corresponding TSP. The sum of the minimum distance travelled over all clusters yielded an upper bound. The minimum distance of each TSP was used to update the objective function in the first stage, and the procedure was iterated. Valid inequalities were developed and added to strengthen the MILP model. The approach was able to solve instances with up to 22 vertices but with a large computational effort. Archetti *et al.* [23] implemented a branch-price-cut algorithm based on the principle of problem decomposition. Each column generated by the sub-problem represented a route with delivery quantities. The generated columns were used to find an optimal heuristic solution to the problem. Both cases where the fleet of vehicles was unlimited and limited to the minimum possible number of vehicles were considered. The computational results showed that the algorithm reduced the optimality gap in most of the benchmark instances. Archetti *et al.* [24] proposed a branch-price-cut algorithm for a commodity-constrained SDVRP. They solved up to 40 customers with three commodities per customer. Luo *et al.* [25] proposed branch, price, and cut for the SDVRP with time windows and linear weight-related cost. Ozbaygin *et al.* [26] proposed an exact flow-based formulation using vehicle indexes. The size of this vehicle-indexed formulation was reduced via a relaxation procedure by aggregating the decision variables over all vehicles. The optimal solutions could be obtained either by locally extending the formulation using the vehicle-indexed variables or by node splitting.

Most techniques used in this research field are heuristic and meta-heuristic methods. These are time-consuming methods because multiple iterations or comparisons of many results are necessary to find the optimal solution. Meanwhile, most of the exact algorithms provided in the literature can only solve small-size SDVRPs. To solve these time-consuming and large-scale problems, we propose an algorithm of 'clustering first and routing later' [27]. It consists of firstly clustering the domain of the customer points according to the 'nearest' principle, adjusting the load demands for each sub-domain according to the maximum vehicle-load capacity, and finally routing each sub-domain to minimise the travel distance. In this manner, a near-optimal solution can be obtained in less time. To obtain more optimised results, the modified version of the first

two stages are provided, and TS is used in the third stage in this study. More case studies on the benchmark data set are used, and the computational results are compared to verify the feasibility and effectiveness of the algorithm proposed in this study. The proposed algorithm can be of practical value for both reducing the time consumption and shortening the travel distance.

The remainder of this paper is organised as follows. In Section 2, the SDVRP is described. In Section 3, a three-stage algorithm based on the 'clustering first and routing later' strategy plus TS (CRTS) for the SDVRP is presented. In Section 4, the computational results are shown and discussed. Finally, the conclusion is presented in Section 5.

2. Problem description

SDVRP is undigraph $G = (V, E)$, where V is the vertex set, i.e. $V = \{0,1, \dots, m\}$. 0 stands for the depot, and the other vertices stand for the customer points. E is the edge set. c_{ij} is the length of edge (i, j) $(c_{ij} \in E)$; it is non-negative and satisfies the triangle inequality. d_i stands for the demand of customer point i, where $i \in V - \{0\}$. The vehicles in the fleet are homogenous, and the maximum load capacity of a vehicle is Q. The lowest vehicle number is $\lceil \sum_{i=1}^{n} d_i / Q \rceil$ [2]. Each vehicle starts from and ends at the depot. The customer demands should be completely satisfied. The carrying weight of a vehicle in each route cannot be larger than Q. The following notations are used.

x_{ij}^v is equal to one when vehicle v directly moves from i to j; otherwise, $x_{ij}^v = 0$. y_{iv} is the quantity of the demand of i delivered by vehicle v.

The objective function is to minimise the total travel distances of the vehicles and is formulated as follows:

$$\min \sum_{i=0}^{n} \sum_{j=0}^{n} \sum_{v=1}^{m} c_{ij}\, x_{ij}^v \tag{1}$$

s. t.

$$\sum_{i=0}^{n} \sum_{v=1}^{m} x_{ij}^v \geq 1, j = 0,1, \dots, n \tag{2}$$

$$\sum_{i=0}^{n} x_{ip}^v - \sum_{j=0}^{n} x_{pj}^v = 0, p = 0,1,2, \dots, n; v = 1,2, \dots, m \tag{3}$$

$$\sum_{i \in S} \sum_{j \in S} x_{ij}^v \leq |S| - 1, v = 1,2, \dots, m; S \subseteq V\text{-}\{0\} \tag{4}$$

$$y_{iv} \leq d_i \sum_{j=0}^{n} x_{ij}^v, i = 1,2, \dots, n; v = 1,2, \dots, m \tag{5}$$

$$\sum_{v=1}^{m} y_{iv} = d_i, i = 1,2, \dots, n \tag{6}$$

$$\sum_{i=1}^{n} y_{iv} \leq Q, v = 1,2, \dots, m \tag{7}$$

$$x_{ij}^v \in \{0,1\}, i, j = 0,1, \dots, n; v = 1,2, \dots, m \tag{8}$$

$$y_{iv} \geq 0, i = 1,2, \dots, n; v = 1,2, \dots m. \tag{9}$$

Eq. 2 states that each customer point can be visited at least once. Eq. 3 is the flow-conservation constraint. Eq. 4 is the sub-route elimination constraint. Eq. 5 states that customer point i is served by vehicle v only if vehicle v visits customer point i. Eq. 6 ensures that all customer demands are met. Eq. 7 ensures that each vehicle does not exceed its maximum load capacity.

3. Used methods: Proposed algorithm

The proposed algorithm is a three-stage algorithm based on the CRTS. The first stage clusters the customers. The maximum-minimum distance method (Max-Min dis) is adopted to cluster the customer points according to their geographic locations. The second stage adjusts the load weight for each cluster. The 'push out' and 'pull in' operations are used to adjust the load weight to collect all possible points in each cluster according to the load demand. The 'push out' operation directs the extra weight away from a cluster, and the 'pull in' operation directs some demands from the nearest customer points of neighbour clusters into clusters whose weights are less than Q. The third stage optimises the route, which uses the TSA. The details of the proposed algorithm are described in the next sections.

3.1 Pre-processing

Load demand of each customer point $d_i > Q$ should be handled before the CRTS. Weight Q can be transported by one vehicle, and remaining weight $d_i = d_i - Q$ at this point is handled using the following procedures.

3.2 Clustering the customers

Basic idea of the maximum-minimum distance

Max-Min dis is a type of pattern recognition method, which can improve the efficiency of dividing the initial data set [28].

Procedure of the Max-Min dis

Step 1: Take x_1 (normally x_1 is the depot) as first clustering centre z_1.
Step 2: Calculate distances D_{i1} at each point i to z_1, $i = 1,2, \dots, n$.
Step 3: Take x_k as second clustering centre z_2 if $D_{k1} = max\{D_{i1}\}$.
Step 4: Calculate distances D_{i1} and D_{i2} at each point i to z_1 and z_2.
Step 5: Take x_l as third clustering centre z_3; if $D_l = \max\{\min(D_{i1}, D_{i2})\}$ and $D_l > \theta \cdot D_{12}$, D_{12} is the distance of z_1 and z_2, where θ is in [0,1], a selectable parameter to meet the requirement of $[\sum_{i=1}^{n} d_i/Q]$.
Step 6: Calculate $D_j = \max\{\min(D_{i1}, D_{i2}, D_{i3})\}$ and $D_j > \theta \cdot D_{12}$; if z_3 exists, x_j is taken as fourth clustering centre z_4 and so on until $D_j \leq \theta \cdot D_{12}$; finally, end the procedure.
Step 7: Classify all points into the nearest clusters according to the principle of minimum distance.

3.3 Adjusting the load weight for each cluster

After clustering the customer points, the calculation and adjustment of the load weight for each cluster is performed as follows.

'Push out' procedure

Step 1: If load weight w_g of a cluster is in $[\alpha \cdot Q, Q]$ and the number of points in this cluster is two, then these two points form a route. If μ_1 clusters similar to this exist, then μ_1 routes are created.
Step 2: If load weight w_g of a cluster is in $[Q, 2 \cdot Q]$ and the number of points in this cluster is two, then these two points form an inner route, and load $w_g - Q$ is pushed out. If μ_2 clusters similar to this exist, then μ_2 routes are created.
Step 3: If load weight w_g of a cluster is larger than $\eta \cdot Q (\eta > 2)$, then $(\eta - 1)$ inner routes are formed in this cluster, and the remaining demand $w_g - (\eta - 1) \cdot Q$ is pushed out. If μ_3 clusters similar to this exist, then $\sum_{i=1}^{\mu_3}(\eta_i - 1)$ routes are created. After the abovementioned three steps are completed, clustering of the remaining customer points in these clusters proceeds to Step 4.
Step 4: The remaining customer points are re-clustered to form $[\sum_{i=1}^{n} d_i/Q] - \mu$, $\mu = \mu_1 + \mu_2 + \mu_3 * (\eta - 1)$ clustering groups, where α is in $[\sum_{i=1}^{n} d_i/([\sum_{i=1}^{n} d_i/Q] * Q)$, 1].

'Pull in' procedure

Step 1: The clusters with less than Q are visited according to the cluster number sequence, e.g. the first one is group $A(w_{gA} < Q)$.
Step 2: Among the neighbours, nearest point t to centre i of cluster A is searched, e.g. cluster B.
Step 3: If point t has load weight $d_t > (Q - w_{gA})$ and the load weight of cluster B w_{gB} is larger than Q, then point t is split into t and t', $d_{t'} = Q - w_{gA}$ is moved to cluster A, and $d_t = d_t - (Q - w_{gA})$ is maintained.
Step 4: If point t has demand $d_t = (Q - w_{gA})$ and the load weight of cluster B w_{gB} is larger than Q, then point t is moved (merged) into cluster A.
Step 5: If point t does not have sufficient load demand $d_t < (Q - w_{gA})$, then point t is first moved (merged) into cluster A. Second, point t', which is nearest to t in cluster B, is searched if w_{gB} is sufficient; otherwise, point t' is searched in cluster C of the next nearest neighbour from cluster A. Third, Step 3 is performed.
Step 6: If the load weight of group A is in $[\alpha \cdot Q, Q]$, then handling for cluster A is terminated. If the load weight of group A $w_{gA} < \alpha \cdot Q$, then Step 2 is performed.
Step 7: If all groups are visited, the procedure is terminated; otherwise, Step 1 is performed.

3.4 Optimising the routes

The problem domain has been divided into several smaller-sized clusters after the abovementioned three operations. Thus, many algorithms can be used to optimise the solution. We adopt the TSA to optimise the route in each cluster. The detailed procedure for the TS is described as follows.

Step 1: Initialising the variables
Set: *tL* (tabu length) = T, *MIs* (terminal condition maximum iterations) = NG,
cN (customerNum) = N
Create *tabu* [*tL*];
Generate randomly *serialNum* [*cN*] (initial route solution)
Step 2: Calculate the objective function value *serialNum* [*cN*] and deposit it into the variable *bestValue*
Step 3: If iteration = NG, terminate the program and output the optimal results; otherwise, continuously iterate and execute the following steps in each loop.
Step 4: Generate *rr* neighbourhood of the current solution by adopting suitable selection functions (e.g. two-opts).
Step 5: Sort it according to a non-descending order and store it into variable *tempDist* [*rr*].
Step 6: If *tempDist* [0] < *bestValue*, let (assumed at the m^{th} iteration):
bestValue = *tempDist* [0]; *currentBestValue* = *tempDist* [0]
bestQueue = the corresponding objects of *tempDist*[0]
currentBestQueue of NG_m = the corresponding objects of *tempDist*[0]
tabu = corresponding objects of *tempDist*[0].
Go to Step3
Otherwise, execute the following steps:
Step 7: Analyse the tabu attributes of the corresponding objects of *tempDist* [*rr*]
currentBestValue = the best value of *tempDist* [*i*] (assume the i^{th} one)
currentBestQueue of NG_m = the corresponding objects of *tempDist*[*i*]
Step 8: Go to Step3.

4. Case studies

To verify the feasibility and effectiveness of the proposed algorithm, three case studies were adopted. Case study 1 was from [22] and was compared with its TSVI algorithm. Case study 2 was from [16] and was compared with its clustering algorithm with a splitting threshold and the *k*-means clustering algorithm in [9], which are all based on the 'routing after grouping' strate-

gy. Case study 3 involved the benchmark data set from the Capacitated Vehicle Routing Problem library (CVRPLIB) and was compared with the SPLITABU algorithm in [4] and MRSILS in [13]. The numerical experiments were implemented on *C* in a Windows 7 64-bit machine with an Intel (R) Core processor and 8 GB of memory.

4.1 Case study 1

Case study 1 contains three instances (N7L1-N7L3). The number of clients in each instance is $N = 7$, the maximum load of the vehicle is one, and the coordinates of the depot are (0, 0). In Table 1, the columns indicate the total travel distance (*Dis.*), consumed computational (CPU) time (*T*) of the TSVI (the data come from [22]) and CRTS, and the relative deviation percentage (*RDP*) of the distance between the CRTS and TSVI. *RDP* (*Dis.*) is equal to $((Distance_{CRTS} - Distance_{algorithm})/Distance_{algorithm})\cdot 100\,\%$, and *RDP* (*T*) is equal to $((Time_{CRTS} - Time_{algorithm})/Time_{algorithm})\cdot 100\,\%$.

The executions in which *RDP* was equal to or less than 1.0 % comprised 48.49 % of the total 66 executions. The executions in which *RDP* was larger than 5.0 % were 12.12 % of the total 66 executions.

The CPU time (*T*) of CRTS listed in Table 1 is equal to 100 times the actual value (to save display space), which indicates that the consumed CPU time of the CRTS is much lower than that of the TVSI.

The results of the total travel distance obtained by the CRTS and TSVI in the three instances in case study 1 are shown in Fig. 1. The good consistency of the curves of the two different algorithms indicates that the CRTS algorithm is feasible and effective.

Table 1 Comparisons of the results between the CRTS and TSVI

No.	N7L1 execution results					N7L2 execution results					N7L3 execution results				
	TSVI		CRTS		RDP	TSVI		CRTS		RDP	TSVI		CRTS		RDP
	Dis.	T	Dis.	T	%	Dis.	T	Dis.	T	%	Dis.	T	Dis.	T	%
Q1	52.33	<1	55.34	0.2	5.75	65.48	<1	66.04	0.2	0.86	38.35	<1	41.22	0.2	7.48
Q2	54.47	<1	55.34	0.2	1.6	66.70	<1	66.70	1.2	0	39.21	<1	41.22	0.2	5.13
Q3	64.67	<1	64.16	1.2	-0.79	73.02	<1	73.02	1.2	0	42.60	<1	42.6	1.4	0
Q4	77.27	2	79.75	1.1	3.21	81.14	<1	81.70	1.2	0.69	48.89	<1	51.18	1.1	4.68
Q5	71.86	<1	71.87	1.3	0.01	77.34	<1	76.44	1.2	-1.16	45.95	<1	47.66	1.1	3.72
Q6	88.67	1	90.34	0.2	1.88	90.11	<1	91.01	0.2	1.0	53.14	<1	55.62	1.1	4.67
Q7	85.80	<1	87.33	1.1	1.78	99.76	1	110.61	1.1	10.88	55.62	<1	55.62	1.1	0
Q8	96.76	1	98.79	1.4	2.1	111.74	1	122.37	1.4	9.51	62.45	<1	63.31	1.7	1.38
Q9	93.46	<1	96.35	1.1	3.09	112.52	<1	120.34	1.3	6.95	69.24	<1	71.97	1.2	3.94
Q10	107.60	2	112.76	1.3	4.8	116.85	<1	116.91	1.6	0.05	71.39	2	72.63	1.4	1.74
Q11	101.79	<1	101.79	0.2	0	136.10	<1	136.10	0.2	0	83.52	<1	85.18	1.2	1.99
Q12	120.26	2	124.86	1.2	3.83	120.04	<1	120.04	1.1	0	78.59	<1	78.59	1.2	0
Q13	128.50	23	129.54	1.3	0.81	114.39	1	119.56	1.3	4.52	61.92	<1	63.14	1.3	1.97
Q14	128.15	<1	129.38	1.4	0.96	158.24	<1	158.55	1.4	0.2	91.37	<1	94.78	1.2	3.73
Q15	133.13	2	133.18	1.3	0.04	161.42	1	162.69	1.2	0.79	86.84	1	86.84	1.2	0
Q16	149.70	3	150.53	0.2	0.55	161.46	1	166.79	1.1	3.3	90.37	3	91.82	1.2	1.6
Q17	144.97	<1	145.80	0.2	0.57	161.91	1	163.85	1.2	1.2	93.89	1	95.24	1.0	1.44
Q18	164.07	2	166.12	1.4	1.25	154.89	1	156.32	1.2	0.92	95.13	<1	97.97	13	2.99
Q19	153.07	1	165.20	1.2	7.92	193.60	3	192.71	1.5	-0.46	99.02	5	99.90	1.2	0.89
Q20	159.19	7	169.07	1.2	6.21	164.49	10	164.81	1.1	0.19	105.11	5	105.11	1.2	0
Q21	180.87	1	185.27	1.2	2.43	188.13	8	189.16	1.8	0.55	125.13	1	125.12	1.1	0
Q22	175.68	8	176.48	1.3	0.46	196.13	2	195.83	1.1	-0.15	116.02	2	118.20	1.1	1.88

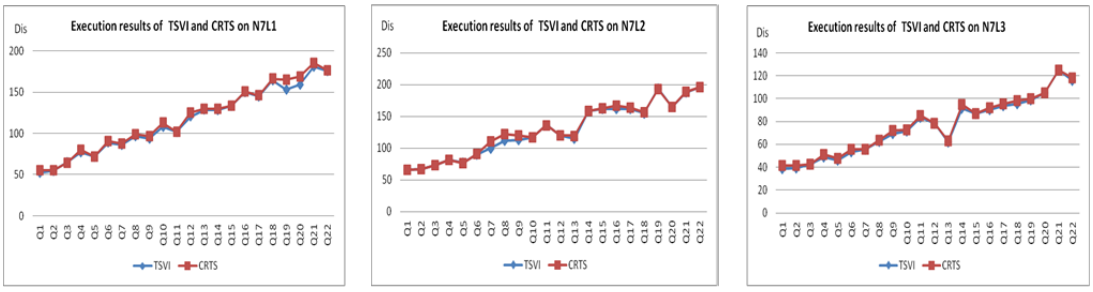

N7L1 N7L2 N7L3

Fig. 1 Computational results of the three instances in case study 1

4.2 Case study 2

Case study 2 contains three instances. The basic information of the customer number, total customer demand, capacity of vehicles, and vehicle number required in each instance are listed in Table 2.

In Table 3, the columns indicate the total travel distance (*Dis.*), consumed CPU time (*T*) of the *k*-means clustering algorithm, the clustering algorithm with splitting threshold and the CRTS (the former two data come respectively from [9] and [16]), and *RDP* of the distance and time between the CRTS and each of the above-described algorithms. A positive *RDP* value indicates that the CRTS value is large, whereas a negative *RDP* value indicates that the CRTS value is small.

Table 3 lists the following. (1) From the perspective of the total travel distance, the clustering algorithm with a split threshold is the lowest in the two instances of $N = 15$ and $N = 20$, and the *RDP* (*Dis.*) values are 0.815 % and 4.067 % lower than those of the CRTS, respectively. Meanwhile, the CRTS at $N = 36$ is the lowest, and the *RDP* (*Dis.*) values are 0.805 % and 1.25 % lower than the resolutions of the other two algorithms, respectively. (2) From the perspective of the consumed CPU time, the CRTS consumes the lowest CPU time.

Fig. 2 clearly shows that the CRTS is feasible and effective. The curves in Fig. 2(a) show that the gap in the total travel distances of the three algorithms in each of the three instances, namely, $N = 15$, $N = 20$, and $N = 36$, is relatively small. The CRTS obtains better results. Fig. 2(b) shows that the CRTS performance is between that of the *k*-means and split-threshold approaches in terms of the total travel distance.

Table 2 Basic information of each instance in case study 2

Instance	Customer number	Total demand	Capacity of vehicles	Vehicle number
2-1	15	4,881	500	10
2-2	20	40	5	8
2-3	36	15.29	1	16

Table 3 Computational results of the three algorithms

N	*k*-means				Split threshold				CRTS	
	Dis.	*T*	*RDP*(*Dis.*)%	*RDP*(*T*)%	*Dis.*	*T*	*RDP*(*Dis.*)%	*RDP*(*T*)%	*Dis.*	*T*
15	1,800.27	5.276	-3.18	-81.8	1,728.9	1.33	0.815	-27.82	1,742.99	0.96
20	182.712	5.15	-0.90	-81.8	173.99	1.35	4.067	-30.37	181.07	0.94
36	354.7	4.26	-1.25	-44.1	353.1	2.99	-0.805	-20.40	350.26	2.38

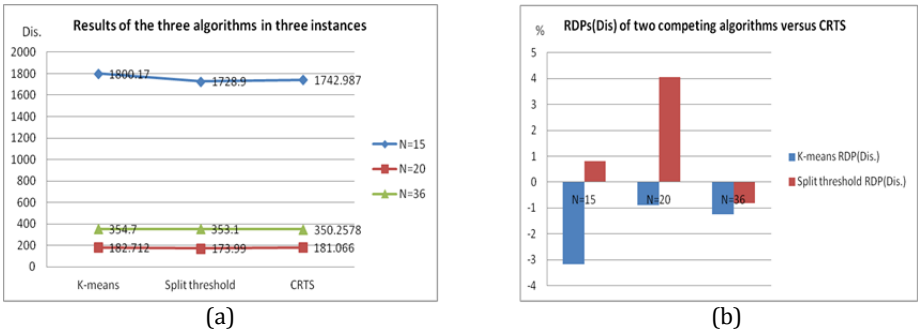

(a) (b)

Fig. 2 Computational results of the three instances in case study 2

4.3 Case study 3

To evaluate the CRTS performance on larger sized instances, we adopted six instances in case study 3 from CVRPLIB and compared the results obtained by SPLITABU in [4] and MRSILS in [13]. The basic information of customer number, total customer demand, capacity of vehicles, and vehicle number required in each instance is listed in Table 4.

In Table 5, the columns indicate the total travel distance (*Dis.*), consumed CPU time (*T*) by each of the three algorithms (the former two data come respectively from [4] and [13]), and *RDP* of the CRTS distance compared with those of the other two algorithms.

Table 4 Basic information in each instance in case study 3

Instance	Name	Customer number	Total demand	Capacity of vehicles	Vehicle number
3-1	vrpnc1	50	777	160	5
3-2	vrpnc2	75	1,364	140	10
3-3	vrpnc3	100	1,458	200	8
3-4	vrpnc4	150	2,235	200	12
3-5	vrpnc5	199	3,186	200	16
3-6	vrpnc11	120	1,375	200	7

Table 5 Computational results of the three algorithms

N	SPLITABU			MRSILS			CRTS	
	Dis.	*T*	*RDP*(*Dis.*)%	*Dis.*	*T*	*RDP*(*Dis.*)%	*Dis.*	*T*
50	527.66	17	5.69	531.03	24	5.02	557.71	2.18
75	853.61	64	7.91	831.85	24	10.74	921.16	5.94
100	840.12	60	12.61	834.52	24	13.37	946.06	6.26
150	1,055.08	440	14.45	1,066.04	24	13.28	1207.57	10.42
199	1,338.36	1,900	16.06	1,343.67	24	15.60	1553.32	13.38
120	1,056.96	39	2.04	1,048.00	24	2.91	1,078.47	8.34

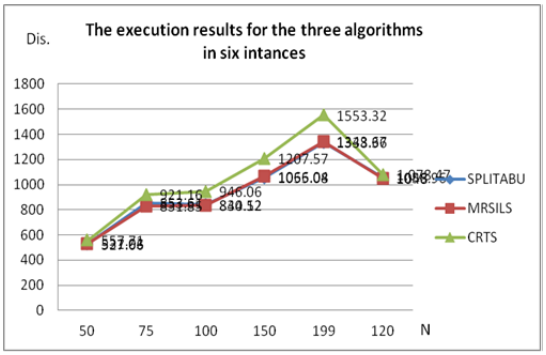

Fig. 3 Computational results for six instances in case study 3

Table 5 indicates the following. (1) The total travel distance of the CRTS is the highest among the three algorithms, and *RDPs* (*Dis.*) of SPLITABU and MRSILS are all positive. (2) When $N = 50$ and $N = 75$, the *RDP* (*Dis.*) values of SPLITABU and MRSILS are lower than or very close to 10 %. (3) When $N = 120$ in which all customer points are in a cluster distribution around the depot, the *RDP* (*Dis.*) values of SPLITABU and MRSILS are lower than 3 %. (4) The consumed CPU time by the CRTS is much lower than those by the other two algorithms.

Fig. 3 clearly shows that the CRTS is feasible and effective. Fig. 3 shows the curves of the total travel distances of the three algorithms in each of the three instances, namely, $N = 50$, $N = 75$, and $N = 120$. It also shows that the gap in the total travel distances between SPLITABU and the CRTS in each of the three instances, namely, $N = 50$, $N = 75$, and $N = 120$, is relatively small. The CRTS achieves near-optimal results even though no iteration is performed in the first two stages.

5. Conclusion

In this study, a mathematical model for SDVRP was described. On the basis of the CRTS, a three-stage algorithm was proposed. In the first stage, clustering was employed to partition the domain of customer points into sub-domains. In the second stage, 'push-out' and 'pull-in' operations were adopted to adjust the load demand in each sub-domain according to vehicle capacity Q. In the third stage, a proven TSA for TSP was used to optimise the total travel distance. Numerical experiments for the three cases were performed, and the computational results showed that the proposed CRTS algorithm provides feasible and effective solutions to the SDVRP in most parts of the test data set. The CRTS obtained approximate optimal solutions in 75 % of the instances. Three competing algorithms, namely, TSVI, *k*-means clustering method, and clustering method with a split threshold, were evaluated alongside the proposed method. These algorithms

were based on a 'routing after grouping' strategy. The CRTS performance in cases 1 and 2 was very close to that of the other three evaluated algorithms in finding the total travel distance. Comparison was also conducted for the computational results in case 3, which is a benchmark data set. When N = 50 and N = 75 in which the customer points were uniformly distributed around the depot, the *RDP* (*Dis.*) values were 5.69 % and 7.91 %, respectively. When N = 120, i.e. where the customer points were in a cluster distribution around the depot, *RDP* (*Dis*) was less than 3 %. Interestingly, the consumed CPU time by the proposed algorithm was much lower than that of any of the other algorithms evaluated in this study.

Acknowledgement

This work was financed by the National Natural Science Foundation of China (Grant No. 61872077), the Natural Science Fund of Jiangsu Province Education Commission (Grant No. 17KJB520040), the Humanities and Social Sciences Research Base Fund of Jiangsu Province Education Commission (Grant No. 2017ZSJD020), and the Jiangsu Key Construction Laboratory of IoT Application Technology, Taihu University of Wuxi.

References

[1] Dror, M., Trudeau, P. (1989). Savings by split delivery routing, *Transportation Science*, Vol. 23, No. 2, 141-149, doi: 10.1287/trsc.23.2.141.
[2] Archetti, C., Speranza, M.G. (2012). Vehicle routing problems with split deliveries, *International Transactions in Operational Research*, Vol. 19, No. 1-2, 3-22, doi: 10.1111/j.1475-3995.2011.00811.x.
[3] Dror, M., Laporte, G., Trudeau, P. (1994). Vehicle routing with split deliveries, *Discrete Applied Mathematics,* Vol. 50, No. 3, 239-254, doi: 10.1016/0166-218X(92)00172-I.
[4] Archetti, C., Speranza, M.G., Hertz, A. (2006). A tabu search algorithm for the split delivery vehicle routing problem, *Transportation Science*, Vol. 40, No. 1, 64-73, doi: 10.1287/trsc.1040.0103.
[5] Chen, S., Golden, B., Wasil, E. (2007). The split delivery vehicle routing problem: Applications, algorithms, test problems, and computational results, *Networks*, Vol. 49, No. 4, 318-329, doi: 10.1002/net.20181.
[6] Archetti, C., Speranza, M.G., Savelsbergh, M.W.P. (2008). An optimization-based heuristic for the split delivery vehicle routing problem, *Transportation Science*, Vol. 42, No. 1, 22-31, doi: 10.1287/trsc.1070.0204.
[7] Gulczynski, D., Golden, B., Wasil, E. (2010). The split delivery vehicle routing problem with minimum delivery amount, *Transportation Research Part E: Logistics and Transportation Review,* Vol. 46, No. 5, 612-626, doi: 10.1016/j.tre.2009.12.007.
[8] Wilck IV, J.H., Cavalier, T.M. (2012). A construction heuristic for the split delivery vehicle routing problem, *American Journal of Operations Research*, Vol. 2, No. 2, 153-162, doi: 10.4236/ajor.2012.22018.
[9] Liu, W.-S., Yang, F., Li, M.-Q., Chen, P.-Z. (2012). Clustering algorithm for split delivery vehicle routing problem, *Control and Decision*, Vol. 27, No. 4, 535-541, doi: 10.13195/j.cd.2012.04.57.liuwsh.017.
[10] Lu, X.C., Chen, Q.B., Zhang, Z.J. (2014). The electric vehicle routing optimizing algorithm and the charging stations' layout analysis in Beijing, *International Journal of Simulation Modelling*, Vol. 13, No. 1, 116-127, doi: 10.2507/IJSIMM13(1)CO4.
[11] Wang, T.-T., Ni, Y.-D., He, W.-L. (2014). Bee colony optimization algorithm for split delivery vehicle routing problem, *Journal of Hefei University of Technology*, Vol. 37, No. 8, 1015-1019, doi: 10.3969/j.issn.1003-5060.2014.08.024.
[12] Zhu, X.N., Yan, R., Zhang, Q. (2015). A promoted hybrid heuristic algorithm for two-dimensional multi-depots vehicle routing problem, *International Journal of Simulation Modelling*, Vol. 14, No. 3, 499-510, doi: 10.2507/IJSIMM14(3)CO11.
[13] Wen, Z.Z. (2015). *Researches on iterated local search for the split delivery vehicle routing problem*, Beijing Transportation University, Beijing, P.R. China.
[14] Wu, D.Q., Dong, M., Li, H.Y., Li, F. (2016). Vehicle routing problem with time windows using multi-objective co-evolutionary approach, *International Journal of Simulation Modellin*g, Vol. 15, No. 4, 742-753, doi: 10.2507/IJSIMM15(4)CO19.
[15] Tang, M., Gong, D., Liu, S., Zhang, H. (2016). Applying multi-phase particle swarm optimization to solve bulk cargo port scheduling problem, *Advances in Production Engineering & Management*, Vol. 11, No. 4, 299-310, doi: 10.14743/apem2016.4.228.
[16] Xiang, T., Pan, D. (2016). Clustering algorithm for split delivery vehicle routing problem, *Journal of Computer Applications*, Vol. 36, No. 11, 3141-3145, doi: 10.11772/j.issn.1001-9081.2016.11.3141.
[17] Cao, Q.K., Yang, K.W., Ren, X.Y. (2017). Vehicle routing optimization with multiple fuzzy time windows based on improved wolf pack algorithm, *Advances in Production Engineering & Management*, Vol. 12, No. 4, 401-411, doi: 10.14743/apem017.4.267.
[18] Johanyák, Z.C. (2017). A modified particle swarm optimization algorithm for the optimization of a fuzzy classification subsystem in a series hybrid electric vehicle, *Tehnički Vjesnik – Technical Gazette*, Vol. 24, Supplement 2, 295-301, doi: 10.17559/TV-20151021202802.

[19] Wang, C.L., Li, S.W. (2018). Hybrid fruit fly optimization algorithm for solving multi-compartment vehicle routing problem in intelligent logistics, *Advances in Production Engineering & Management*, Vol. 13, No. 4, 466-478, doi: 10.14743/apem2018.4.304.
[20] Belenguer, J.M., Martinez, M.C., Mota, E. (2000). A lower bound for the split delivery vehicle routing problem, *Operations Research*, Vol. 48, No. 5, 801-810, doi: 10.1287/opre.48.5.801.12407.
[21] Lee, C.-G., Epelman, M.A, White III, C.C., Bozer, Y.A. (2006). A shortest path approach to the multiple-vehicle routing problem with split pick-ups, *Transportation Research B: Methodological*, Vol. 40, No. 4, 265-284, doi: 10.1016/j.trb.2004.11.004.
[22] Jin, M., Liu, K., Bowden, R.O. (2007). A two-stage algorithm with valid inequalities for the split delivery vehicle routing problem, *International Journal of Production Economics*, Vol. 105, No. 1, 228-242, doi: 10.1016/j.ijpe.2006.04.014.
[23] Archetti, C., Bianchessi, N., Speranza, M.G. (2011). A column generation approach for the split delivery vehicle routing problem, *Networks*, Vol. 58, No. 4, 241-254, doi: 10.1002/net.20467.
[24] Archetti, C., Bianchessi, N., Speranza, M.G. (2015). A branch-price-and-cut algorithm for the commodity constrained split delivery vehicle routing problem, *Computers & Operations Research*, Vol. 64, 1-10, doi: 10.1016/j.cor.2015.04.023.
[25] Luo, Z., Qin, H., Zhu, W., Lim, A. (2017). Branch and price and cut for the split-delivery vehicle routing problem with time windows and linear weight-related cost, *Transportation Science*, Vol. 51, No. 2, 668-687, doi: 10.1287/trsc.2015.0666.
[26] Ozbaygin, G., Karasan, O., Yaman, H. (2018). New exact solution approaches for the split delivery vehicle routing problem, *EURO Journal on Computational Optimization*, Vol. 6, No. 1, 85-115, doi: 10.1007/s13675-017-0089-z.
[27] Min, J., Jin, C., Lu, L. (2018). A three-stage approach for split delivery vehicle routing problem solving, In: *Proceedings of 8th International Conference on Logistics, Informatics and Service Sciences* (LISS), Toronto, Canada, 1-6, doi: 10.1109/LISS.2018.8593226.
[28] Zhou, J., Xiong Z.Y., Zhang Y.F., Ren, F. (2006). Multiseed clustering algorithm based on max-min distance algorithm, *Journal of Computer Applications*, Vol. 26, No. 6, 1425-1427.

Calendar of events

- International Conference on Industrial Engineering and Engineering Management, December 16-19, 2018, Bangkok, Thailand.
- 11th International Conference on Computer Modeling and Simulation, January 16-19, 2019, Melbourne, Australia.
- International Conference on Green Manufacturing and Production Engineering, January 17-18, 2019, Rome, Italy.
- 16th Annual Congress on Materials Research and Technology, February 18-20, 2019, Amsterdam, Netherlands.
- 3rd International Conference on 3D Printing Technology and Innovations, March 25-26, 2019, Rome, Italy.
- International Conference on Intelligent Manufacturing and Intelligent Materials, May 9-11, 2019, Sanya, China.
- International Conference on Agile and Flexible Manufacturing Systems, May 21-22, 2019, Berlin, Germany.
- International Conference on Advanced Manufacturing Technologies and Intelligent Machining, May 29-30, 2019, Osaka, Japan.
- 17th Annual Industrial Simulation Conference, June 5-7, 2019, Lisbon, Portugal.
- International Conference on Design and Implementation of Intelligent Manufacturing Systems, June 10-11, 2019, Tokyo, Japan.
- 6th International Conference and Exhibition on Automobile & Mechanical Engineering, July 8-9, 2019, Zurich, Switzerland.
- 23rd International Conference on Advanced Materials & Nanotechnology, August 19-20, 2019, Tokyo, Japan.
- AI Manufacturing 2019: Machine Learning and Artificial Intelligence, The Fourth Industrial Revolution, August 28-29, 2019, Westin O'Hare, Rosemont, Illinois, USA.
- 9th IFAC Conference on Manufacturing Modeling, Management, and Control, August 28-30, 2019, Berlin, Germany.
- 30th DAAAM International Symposium, October 23-26, 2019, Zadar, Croatia.

Notes for contributors

General

Articles submitted to the *APEM journal* should be original and unpublished contributions and should not be under consideration for any other publication at the same time. Manuscript should be written in English. Responsibility for the contents of the paper rests upon the authors and not upon the editors or the publisher. Authors of submitted papers automatically accept a copyright transfer to *Chair of Production Engineering*, *University of Maribor*. For most up-to-date information on publishing procedure please see the *APEM journal* homepage *apem-journal.org*.

Submission of papers

A submission must include the corresponding author's complete name, affiliation, address, phone and fax numbers, and e-mail address. All papers for consideration by *Advances in Production Engineering & Management* should be submitted by e-mail to the journal Editor-in-Chief:

Miran Brezocnik, Editor-in-Chief
UNIVERSITY OF MARIBOR
Faculty of Mechanical Engineering
Chair of Production Engineering
Smetanova ulica 17, SI – 2000 Maribor
Slovenia, European Union
E-mail: editor@apem-journal.org

Manuscript preparation

Manuscript should be prepared in *Microsoft Word 2010* (or higher version) word processor. *Word .docx* format is required. Papers on A4 format, single-spaced, typed in one column, using body text font size of 11 pt, should not exceed 12 pages, including abstract, keywords, body text, figures, tables, acknowledgements (if any), references, and appendices (if any). The title of the paper, authors' names, affiliations and headings of the body text should be in *Calibri* font. Body text, figures and tables captions have to be written in *Cambria* font. Mathematical equations and expressions must be set in *Microsoft Word Equation Editor* and written in *Cambria Math* font. For detail instructions on manuscript preparation please see instruction for authors in the *APEM journal* homepage *apem-journal.org*.

The review process

Every manuscript submitted for possible publication in the *APEM journal* is first briefly reviewed by the editor for general suitability for the journal. Notification of successful submission is sent. After initial screening, and checking by a special plagiarism detection tool, the manuscript is passed on to at least two referees. A double-blind peer review process ensures the content's validity and relevance. Optionally, authors are invited to suggest up to three well-respected experts in the field discussed in the article who might act as reviewers. The review process can take up to eight weeks on average. Based on the comments of the referees, the editor will take a decision about the paper. The following decisions can be made: accepting the paper, reconsidering the paper after changes, or rejecting the paper. Accepted papers may not be offered elsewhere for publication. The editor may, in some circumstances, vary this process at his discretion.

Proofs

Proofs will be sent to the corresponding author and should be returned within 3 days of receipt. Corrections should be restricted to typesetting errors and minor changes.

Offprints

An e-offprint, i.e., a PDF version of the published article, will be sent by e-mail to the corresponding author. Additionally, one complete copy of the journal will be sent free of charge to the corresponding author of the published article.

APEM journal

Advances in Production Engineering & Management

Chair of Production Engineering (CPE)
University of Maribor
APEM homepage: apem-journal.org

Volume 14 | Number 1 | March 2019 | pp 1-138

Contents

ISSN 1854-6250
9 771854 625008

apem-journal.org